Alma Mater Studiorum – Università di Bologna

DOTTORATO DI RICERCA IN

INGEGNERIA CIVILE, AMBIENTALE E DEI MATERIALI

Ciclo XXVIII

Settore Concorsuale di afferenza: 08/A3

Settore Scientifico disciplinare: ICAR/04

DEVELOPMENT OF NEW METHODOLOGIES FOR PREDICTION OF PERFORMANCES OF ASPHALT MIXTURES

Candidato: Dott. Ing. RICCARDO LAMPERTI

Coordinatore Dottorato

Prof. Ing. Alberto Lamberti

Relatori

Prof. Ing. Andrea Simone

Dott. Ing. Valeria Vignali

Esame finale anno 2016

Abstract

This thesis proposes the use of new methodologies for prediction of performances of asphalt mixtures.

Recent improvements in technology make it possible to adopt new methods of investigation with the dual objective of improving the performance in the survey of the parameters and investigate new properties so far not analyzed. In particular, the image analysis and the tyre/surface interaction belong to an innovative framework, which is next to flank, if not replace, the classic measurements so far employed.

The thesis deals with the use of these technologies for the analysis of three rubberized stone mastic asphalts, which were laid on a stretch of road close to Bologna, Italy.

Three different surveys were carried out on site during the first year of service. The surveys included the change in texture and skid resistance due to the traffic, along with the acoustic properties of the pavement. Local as well as dynamic continuous measurements were carried out, involving the use of a profilometer and a skiddometer.

A second phase involved the prediction of the surface parameters with simulated trafficking on Road Test Machine. At each stage of simulated trafficking, change in macrotexture, skid resistance, adhesion between bitumen and aggregates and finally contact pressures and areas were assessed.

The image analysis is used for the assessment of the adhesion between the bitumen and the aggregate. The proposed procedure overcomes the shortcomings of the current evaluation, offering great reliability and accuracy.
The images are then processed in order to create 3D models of the asphalt specimens and investigate the surface and volume properties.
The tyre/pavement interaction is another fundamental phenomena that received little considerations from the research, given its importance.

A final discussion summarizes these investigations by separately review three different simulated periods, i.e. the early life, the in-service equilibrium and the end of life. In order to accelerate the distress, one slab was subjected to Immersion Wheel Track test, the results of which were interpreted through the same methodologies.

Abstract

Questa tesi propone l'utilizzo di nuove metodologie per predire le prestazioni di conglomerati bituminosi.

I recenti progressi nella tecnologia rendono possibile adottare nuovi metodi di indagine con il duplice obiettivo di migliorare il rendimento del rilievo dei parametri e approfondire nuove caratteristiche ancora non studiate. In particolare, l'analisi delle immagini e l'interazione ruota/pavimentazione appartengono ad un contesto innovativo destinato ad affiancare, se non a sostituire, i metodi classici di indagine finora impiegati.

La tesi tratta l'impiego di queste tecnologie per l'analisi di tre miscele di stone mastic asphalt contenenti polverino di gomma, le quali sono state stese in un tratto stradale vicino a Bologna.

Nell'arco temporale di un anno dopo la stesa sono stati effettuati tre differenti rilievi. Essi hanno permesso di indagare l'evoluzione dei parametri di tessitura, attrito e riduzione del rumore di rotolamento. Sono state effettuate misure puntuali e dinamiche in continuo mediante l'utilizzo di un profilometro e dello skiddometer.

Una seconda fase ha previsto la stima dei parametri superficiali a seguito di trafficamento simulato in laboratorio. Ad ogni livello sono stati determinati i cambiamenti di macrotessitura, attrito, adesione bitume inerte, nonché le pressioni e l'area di contatto.

L'analisi delle immagini è usata per determinare l'adesione tra inerte e bitume. La procedura proposta supera le limitazioni della valutazione visiva, offrendo grande affidabilità e precisione.

Le immagini sono seguentemente combinate per creare modelli 3D dei campioni di conglomerato e studiare i parametri superficiali e volumetrici.

L'interazione ruota pavimentazione è un altro fenomeno fondamentale che, nonostante la sua importanza, ha ricevuto poca considerazione dalla ricerca.

La discussione finale sintetizza i vari aspetti esaminati raggruppando tre diverse "età" della pavimentazione, ovvero inizio vita, equilibrio e fine vita o ammaloramento. Al fine di accelerare il processo di ammaloramento, un campione è stato sottoposto a wheel track ad immersione, interpretando i risultati con le stesse metodologie.

TABLE OF CONTENTS

List of Figures

List of Tables

Table 8.1: Settings for the sparse point cloud computation

Introduction

The pavement engineering industry is facing a continuous change nowadays. The concept of sustainability is becoming of paramount importance in any field of research and has become one of the main goal of the researchers, favoured by the recent legislative measures and the public opinions. By way of example, the last International Conference on Transportation Infrastructures, held in Pisa in 2014, dealt with the "*Sustainability, Eco-Efficiency, and Conservation in Transportation Infrastructure Asset Management*".

Efforts are made throughout the world in identifying suitable recycled materials for the use in road pavements. Among them, one of the most reused material is the crumb rubber, which was the subject of numerous studies.

Moreover, recent improvements in technology make it possible to adopt new methods of investigation with the dual objective of improving the performance in the survey of the parameters and investigate new properties so far not analysed.
For instance, the use of non-contact methods based on the image analysis and processing for 3D reconstruction, has potential for highway monitoring and maintenance.
The tyre/pavement interaction is another fundamental phenomena that received little considerations from the research, given its importance.
These techniques can be very useful for a better understanding of pavement surface texture properties such as skid resistance, road surface noise and rolling resistance.

This thesis proposes the use of new technologies for the analysis of surface characteristics of road pavements. In particular, the study was carried out on three mixtures of rubberized Stone Mastic Asphalts, which have been laid on a stretch of road close to Bologna (Italy). It is shown that the technologies adopted and the proposed parameters can be used to describe and predict the texture change over time. How surface texture changes over time will indicate how performance properties change over time, therefore indicating the condition of a pavement surface, i.e. its level of distress.

The thesis is organized in ten Chapters.

Chapter 1 introduces the concepts of texture and its relationship with other important factors such as skid resistance. The measurement techniques of texture and skid resistance are presented.

Chapter 2 is a literature review of the research that was carried out on the topic of this thesis. The reviewed papers are divided in different sections, i.e. texture, skid resistance, tyre/surface interaction, recycling and sustainability, acoustic properties of pavements. The papers that are more linked to this thesis are discussed in details.

Chapter 3 reports the results of the mechanical characterization of the mixture under investigation.

Chapter 4 presents the adopted trial site and reports the results of the survey for monitoring the health of workers during the laying of the mixtures.

Chapter 5 deals with the results of the in-situ surveys for the measurement of the tyre rolling noise emissions and of the texture and skid resistance.

Chapter 6 introduces the simulated traffic machines and presents the results of the classic measurements made in laboratory.

Chapter 7 presents the analysis of the adhesion between bitumen and aggregate of the mixtures through an innovative 2D images technique.

Chapter 8 deals with the investigation of the texture change during simulated trafficking with the close range photogrammetry. In particular, the investigations considered surface and volume parameters, the study through slices, the differences between two machines for the traffic simulation, the use of vinyl cast to replicate the pavement macrotexture.

Chapter 9 deals with the tyre surface interaction. After a comparison between different gradations of SMA, the rubberized surfaces under investigation were characterized in terms of peak pressures beneath the tyre, contact areas and frequency distribution.

Finally, Chapter 10 presents a discussion of the results presented in the previous Chapter, with special regard to the use of the laboratory parameters to predict the condition of the pavement surfaces.

Chapter 1

Texture and skid resistance

1.1 Texture of road pavement

Surface texture is an important road surface characteristic and relates to performance requirements including skid resistance, road surface noise, rolling resistance, surface water drainage and surface spray. The pavement texture is defined as the deviation of a pavement surface from a true planar surface, within the wavelength ranges. The wavelength is the minimum distance between periodically repeated parts of the curve.

Term	Wavelength
Microtexture	$\lambda < 0.5$ mm
Macrotexture	0.5 mm $< \lambda <$ 50 mm
Megatexture	50 mm $< \lambda <$ 500 mm
Roughness	0.5 m $< \lambda <$ 50 m

Table 1.1: Texture wavelengths

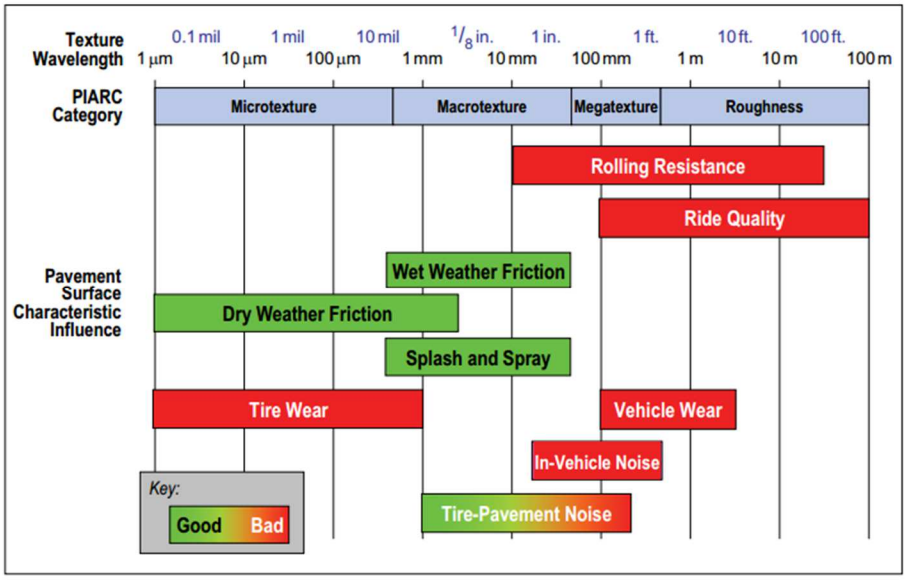

Figure 1.1: Texture wavelengths and relationship with pavement surface characteristics

Road surface texture is classified as microtexture, macrotexture, megatexture and roughness. The texture characterization and their corresponding wavelengths are shown in Table 1.1. The definitions and terms presented in this section refer to the ISO 13473-1:1997 and 13473-2:2002 standards.

Figure 1.1 illustrates how the different scales of texture influence surface performance properties at the tyre-pavement interface.

1.1.1 Microtexture

Microtexture is the deviation of a pavement surface from a true planar surface with the characteristic dimensions along the surface of less than 0.5 mm (corresponding to texture wavelengths with third-octave bands with up to 0.4 mm of centre wavelengths). Peak-to-peak amplitudes normally vary in the range 0.001 mm to 0.5 mm. This type of texture is the texture which makes the surface feel more or less harsh but which is usually too small to be observed by the eye. It represents typically the surface texture of aggregate particles, which come in direct contact with the tyres.

Microtexture is therefore influenced by aggregate type and its properties. Figure 1.1 shows microtexture to influence tyre / road friction and tyre wear. Microtexture is important to ensure adequate skid resistance at low speed, whereas a combination of microtexture and macrotexture is required at higher speeds.

Microtexture is required to break through films of water that form between the surface of the aggregate particle and the tyre (DMRB, 2006). This improves tyre-pavement contact and reduces the risk of aquaplaning. Poor microtexture will increase the risk of insufficient friction leading to reduction of vehicle control and road user safety. There is no method currently available as a harmonised European Standard for the measurement of road surface in-situ microtexture (EN ISO 13473-5:2009).

However, the measurement of wet skid resistance using a device such as SCRIM or GripTester is assumed to offer an indication of microtexture. The only methods currently available in Europe of measuring microtexture are the laboratory polished stone value (EN1097-8:2009) and Friction after polishing (EN 12697-49:2014) test methods (McQuaid, 2015).

1.1.2 Macrotexture

Macrotexture is the deviation of a pavement surface from a true planar surface with the characteristic dimensions along the surface of 0.5 mm to 50 mm (corresponding to texture wavelengths with third-octave bands including the range 0.5 mm to 50 mm of centre wavelengths). Peak-to-peak amplitudes may normally vary in the range 0.l mm to 20 mm. This type of texture is the texture, which has wavelengths in the same order of size as tyre tread elements in the tyre/road interface.

Figure 1.1 shows macrotexture to influence tyre / road friction, exterior tyre / road noise, rolling resistance, tyre wear and road surface noise in vehicles.

The macrotexture is obtained by suitable proportioning of the aggregate and mortar of the surface or by certain surface finishing techniques. Surfaces are normally designed with a certain macrotexture in order to obtain a suitable water drainage in the tyre/road interface. Indeed, Macrotexture enables drainage of water from the tyre footprint, especially at higher speeds and volumes of surface water.

According to the Design Manual for Roads and Bridges (DMRB, 2006), an important difference between surfaces, which has a strong effect on noise generation, is the degree to which the surface aggregate particles protrude above the plane of the tyre contact patch. Positive texture describes a series of aggregate peaks protruding from the surface that can be formed, for instance, by rolling aggregate chippings into the soft surface of an underlying matrix during construction. Negative texture describes a relatively flat compacted surface that has a drainage network below the plane of the contact patch. For the same texture depth, the latter generate much less tyre noise.

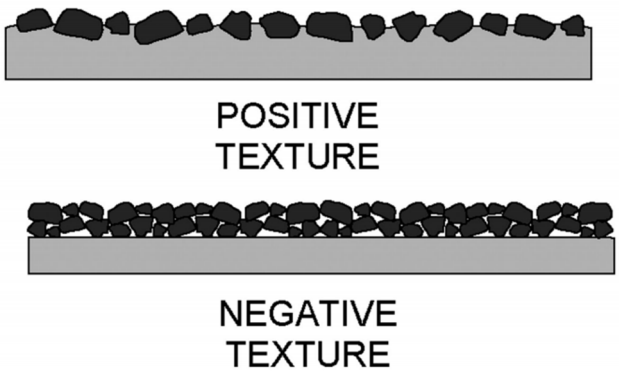

Figure 1.2: Positive and negative texture

Positive and negative texture types are shown in Figure 1.2. Hot rolled asphalt, surface dressing and brushed concrete surfaces are generally considered to be positively textured whereas porous asphalt, Stone Mastic Asphalt, thin surfacing and exposed aggregate concrete surfaces are generally considered to be negatively textured.

1.1.3 Megatexture

Surface deviations from a true planar surface within the wavelength range 50 mm – 500 mm are known as megatexture. Figure 1.1 shows megatexture to influence rolling resistance, discomfort, tyre / road friction and noise in vehicles. It is usually an unwanted characteristic resulting from defects or deterioration of the pavement surface e.g. potholes or waviness.

The measurement of megatexture issues such as potholes can be carried out using profiles obtained from a profilometer device (EN ISO 13473-5:2009).

1.2 Measurement of pavement surface texture

There are two basic types of pavement surface texture measurement i.e. contact and non-contact. The methods may be sub-divided into those that are used to assess road surfaces and those that have been used in laboratory based investigations.

1.2.1 Contact

The sand patch or volumetric patch technique is used throughout the world to assess pavement surface macrotexture (EN 13036-1:2010). The method is used as the definitive assessment, or control value of a pavement surface materials macrotexture against which other measurement methods are compared. Despite this, it has limited use in research. The method relies on the spreading of a material, usually sand or glass spheres, in a patch. The material is distributed with a rubber pad to form an approximately circular patch, the average diameter of which is measured. By dividing the volume of material by the area covered, a value is obtained which represents the average depth of the layer, i.e. a 'mean texture depth'. The test gives a mean texture depth (MTD) value. Material properties such as aggregate size and shape are not indicated (EN 13036-1:2010) limiting its ability to fully assess surface texture.

EN 13036-3 (2002) details a method to determine the horizontal drainability of pavement surface texture. It is recommended for use only on smooth, low macrotexture non-porous surfaces. The method uses an outflow meter device and time as a measure of surface macrotexture. However the outflow meter provides minimum insight into the complexity of macrotexture. It gives little indication of any deterioration present in the surface, which may contribute to quicker outflow times than would be representative of the surface. The method has poor correlation with both MPD and MTD reflecting the different characteristics being assessed (McQuaid, 2015).

1.2.2 Non-contact

Laser based dynamic profilometers have been used for many years to measure pavement surface texture. These are typically vehicle mounted and use high-speed lasers. The measurements are either 2D profiles measured in the wheel path or 3D measurements of a lane width. The profiles produced by these devices can be used to compute various profile statistics, such as the Mean Profile Depth (MPD) and the Sensor Measured Texture Depth (SMTD).

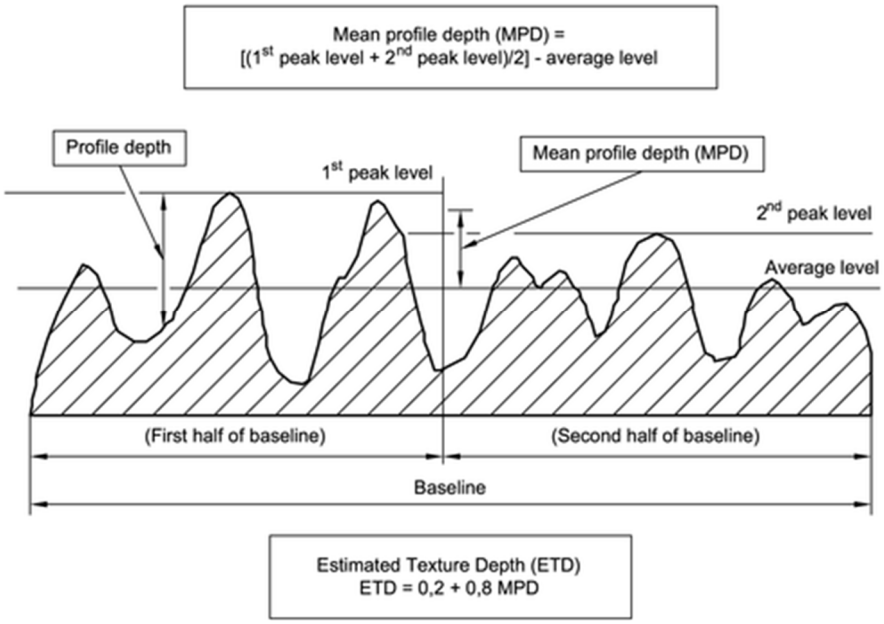

Figure 1.3: Mean Profile Depth calculation

According to ISO 13473-1:1997, the MPD is calculated by dividing the measured profile into segments of 100 mm length (recommended base line). The slope of each segment is suppressed by subtracting a linear regression of the segment, providing a zero mean

profile. The MTD may be estimated through a conversion equation. In this case, the MTD is indicated as Estimated Texture Depth (ETD). Their relationship is:

$$ETD = 0{,}2 + 0{,}8\,MPD$$

An example of 2D wheel path measurement is the SCRIMTEX device. This is a WDM Sideway-force Coefficient Routine Investigation Machine (SCRIM) that measures both wet skid resistance and macrotexture in the same wheel path at either 30 or 60 mph.

Development of technology and data processing has resulted in devices such as the Traffic Speed Condition Survey device (TRACS). This uses an array of lasers to measures macrotexture along with other data at highway speeds up to 60 miles per hour. This allows measurement of fretting, rut depth, estimates of surface type, cracking and sensor measured texture depth (SMTD).

The Pavemetrics Laser Crack Measuring System (LCMS) can produce transverse profiles of a road whilst travelling at speed. The LCMS consists of laser line projectors, filters and cameras. The device can scan a width of 4 m at a resolution of 1 mm. Identity data is used to allow interpretation of location. Features on the pavement surface such as rutting, cracks and line markings can be identified with a 95% certainty claimed (McQuaid, 2015).

The Siteco Road-Scanner is a vehicle to carry out a rapid survey of a road infrastructure and combines the following technologies: GPS and Inertial Positioning System, medium-to-high resolution 5/8 front-mounted colour TV cameras and a rear-mounted vertical TV camera, a Dynatest RSPIV profilometer, a 2 GHz IDS georadar, an odometer and a Faro Photon 120 helical laser scanner. The latter acquires a cloud of laser points distributed on a helicoid at a step of 20-40 cm and lastly, the rear TV camera provides a continuous plane view of the road surface of around 4 m in width. Photogrammetric measurements are precise to 10 cm, while the relative accuracy obtained by the laser scanner (distance between 2 points) is of 2 mm (Lantieri et al., 2015).

The Circular Track Meter (CT meter) is an example of a static laser based non-contact method of road surface texture measurement (ASTM E2157, 2009). The CT meter is used in USA as a reference method of macrotexture measurement. The CT Meter uses a laser to measure the profile of a circle 284 mm in diameter or 892 mm in circumference. The profile is divided into eight segments of 111.5 mm and the average mean profile depth

(MPD) is determined for each of the segments of the circle. The reported MPD is the average of all eight segments depths. Several studies reported excellent correlations between the volumetric patch technique MTD and the CT Meter MPD. Among them Flintsch et al. (2003) regarded MPD as a two dimensional estimate of the three dimensional MTD.

1.3 Surface metrology on road pavements

Surface metrology is the science that deals with the characterization of a surface by the amplitude, spacing and shape of its features. One of the goal of this thesis is to understand the behaviour of asphalt mixtures that undergo simulated trafficking in terms of change of texture. This section will introduce key concepts that are at the base of the analysis presented in Chapter 8.

Figure 1.4 shows an example of a reconstructed 3D surface of an asphalt mixture. Even if it could appear a perfect representation of the real surface, it is not. In fact, it can be affected by roughness and waviness. Thus, two filters are defined: the S-filter and the L-filter- The first is defined as a filter that removes unwanted small-scale lateral components of the measured surface such as measurement noise or functionally irrelevant small features. The second is used to remove unwanted large-scale lateral components of the surface, and the F-operator removes the nominal form (by default using a least square method. The scale at which the filters operate is controlled by the nesting index, which is the extension of the notion of the original cut-off wavelength and is suitable for all types of filters. For example, for a Gaussian filter, the nesting index is equivalent to the cut-off wavelength. These filters are used in combination to create SF and SL surfaces. An SF surface results from using an S-filter and an F-operator in combination on a surface, and an SL surface by using an L-filter on an SF surface. Both are called scale-limited surface (Leach, 2010).

The scale-limited surface depends on the filters and operators used, with the scale being controlled by the nesting indices of those filters. The reference standard for the analysis of 3D areal surface texture is the ISO 25178. While defining all the parameters that will be presented hereafter, it always refers to the concept of scale-limited surface.

However scale-limited surfaces may display “fractal-type behaviours” over a range of scales.

A concept, which is essential and linked to any analysis, is the *material ratio*. The Material Ratio, *mr*, is the ratio of an intersecting area, parallel to the mean plane, passing through the surface at a given height to the cross sectional area of the evaluation region. The material ratio, according to Figure 1.5, is given by:

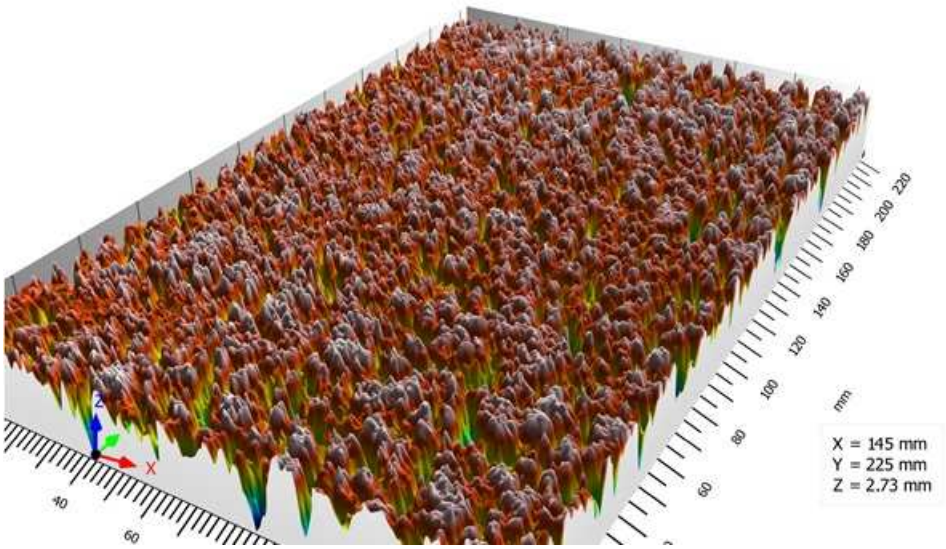

Figure 1.4: Reconstructed 3D surface of an asphalt sample

$$Material\ ratio = \frac{(A + B + C + D)}{L} \cdot 100$$

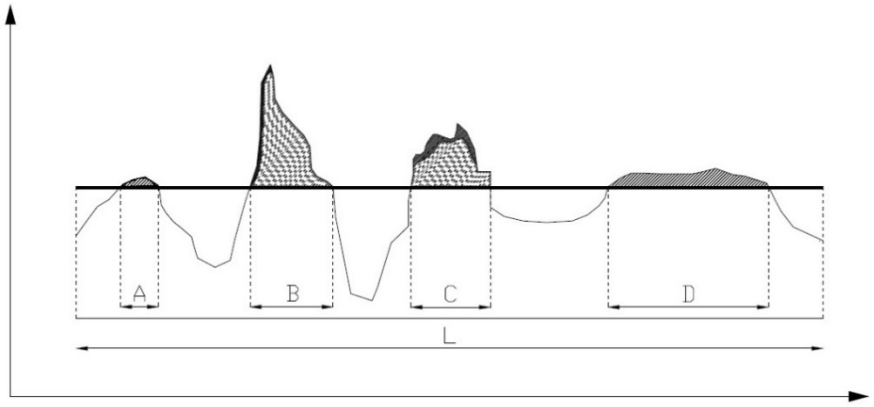

Figure 1.5: Concept of Material Ratio

The Areal Material Ratio Curve, referred to as the *Abbot Firestone Curve*, is established by evaluating *mr* at various levels from the highest peak to the lowest valley. Mathematically it represents the cumulative probability density function of the surface profile's height. An example of the AFC is shown in Figure 1.7. Using the Abbott curve,

a graphical study can be performed in order to retrieve functional parameters characterizing the profile, the surface or the volume intersected by a line or a plane.

The equivalent straight line, calculated according to ISO 25178-2, intersects the 0 % and 100 % lines on the *mr* axis. From these points, two lines are plotted parallel to the x-axis; these determine the core surface by separating the protruding hills and dales. The vertical distance between these intersection lines is the material core. Their intersections with the areal material ratio curve define the material ratios Smr1 and Smr2. They are usually set at 10% and 80% respectively.

For one profile it is possible to extrapolate the parameters Rk, Rpk, and Rvk. They represent respectively the core roughness profile excluding the protruding peaks and the deep valleys, the average height of the protruding peaks above the core profile, and the average depth of the profile valleys projecting through the core profile. The parameters Rpk and Rvk are each calculated as the height of the right-angle triangle, which is constructed to have the same area as the "peak area" (A1) or "valley area" (A2), respectively.

Taking the previous concepts from one profile to one surface, the Abbott curve for the surface can be calculated. The reduced peak height, Spk, is a measure of the peak height above the core roughness. The core roughness Depth, Sk, is a measure of the "core" roughness (peak-to-valley) of the surface with the predominant peaks and valleys removed, according to the set thresholds. The reduced valley depth, Svk, is a measure of the valley depth below the core roughness.

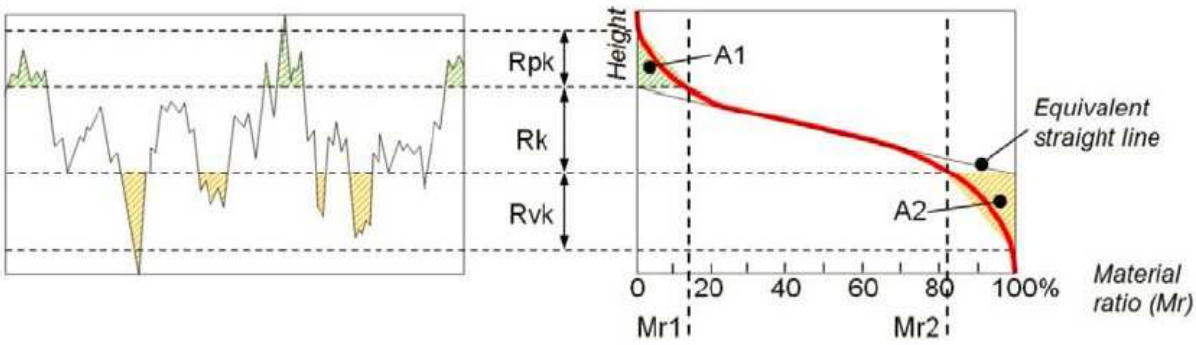

Figure 1.6: Abbott curve for a single profile and parameters Rk, Rpk and Rvk (Bitelli et al., 2012)

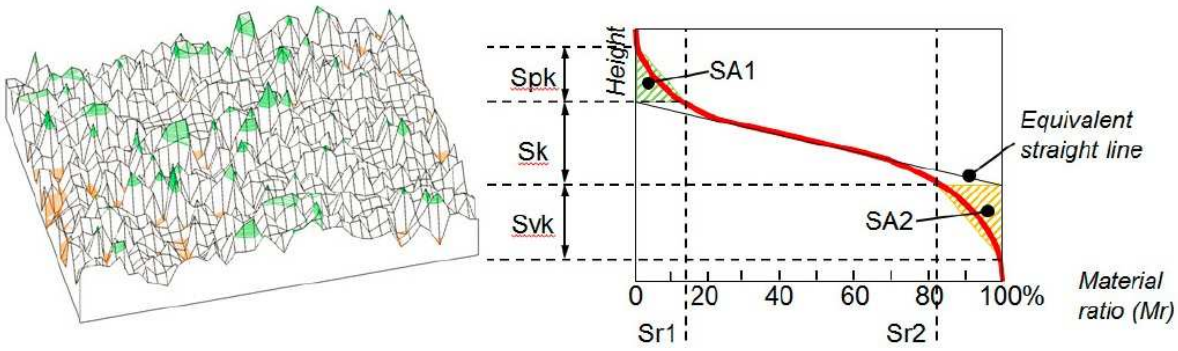

Figure 1.7: Abbott curve for a surface and parameters Sk, Spk, Svk (Bitelli et al., 2012)

Following the identical procedure, the AFC can be calculated for the 3D surface, obtaining volume parameters:

- Vv(mr), the Void Volume, is the volume of space bounded by the surface texture from a plane at a height corresponding to a chosen "mr" value to the lowest valley. "mr" may be set to any value from 0% to 100%.
- Vvv(p), the Dale Void Volume, is the volume of space bounded by the surface texture from a plane at a height corresponding to a material ratio (mr) level, "p" to the lowest valley. The default value for "p" is 80% but may be changed as needed.
- Vvc(p,q), The Core Void Volume, is the volume of space bounded by the texture at heights corresponding to the material ratio values of "p" and "q". The default value for "p" is 10% and the default value for "q" is 80%.

Vv(mr), Vvv(p) and Vvc(p,q) all indicate a measure of the void volume provided by the surface between various heights as established by the chosen material ratio(s) values. The volume parameters represents the more reliable way to study the change of surface texture. In this case, the y-axis is usually in terms of ml/m^2.

1.4 Skid resistance

Friction between the tyre and road surface consists of two main components, both of which are related to speed:

a) adhesion between tyre and surface, which is a function of the microtexture, and depends on the nature of the materials in contact;
b) hysteresis, i.e. the loss of energy caused by tyre deformation, which is a function of the macrotexture.

Therefore, during a single braking operation the friction available to the vehicle is not constant.
In dry conditions all clean, surfaced roads have a high skidding resistance. In fact, when in a dry and clean state, roads generally provide insignificant differences in friction levels, regardless the type of pavement and surface configuration. On the other hand, the water acts as a lubrificant between the surface and the tyre, reducing friction.

The fine scale microtexture of the surface aggregate is the main contributor to sliding resistance and is the dominant factor in determining wet skidding resistance at lower speeds. Coarse Macrotexture, which provides rapid drainage routes between the tyre and road surface, and tyre resilience are important factors in determining wet skidding resistance at high speeds. Megatexture relates to the roughness of the road and has no effect on skidding resistance but affects noise (DMRB, 2006).

1.5 Measurement of skid resistance

Laboratory methods are used for evaluating the friction characteristics of core samples or laboratory-prepared samples. The two devices currently in use are the British Portable Tester (BPT), and the Japanese Dynamic Friction Tester (DFTester). The BPT will be discussed in a next Chapter as it was used for this thesis.
The Dynamic Friction Tester (DF Tester) is a portable instrument for measuring pavement surface friction as a function of speed and under various conditions. The instrument is comprised of a measuring unit and a control unit; an x-y plotter or laptop can be used to record data. The measuring unit consists of a disc made to rotate horizontally at a specified velocity before being lowered onto a wetted test surface for measurement of friction. The torque-generated by the resistance between the test surface and spring-loaded rubber "sliders" attached to the underside of the rotating disc is continuously monitored and converted to a measurement of friction.

Device	% Slip (yaw angle)	Speed [km/h]	Country
British Portable Tester	100	10	United Kingdom
DFTester	100	0÷90	Japan

Table 1.2: Slider friction measurement devices (NCHRP, 2000)

A summary of the devices for the friction measurement currently in use is presented in Table 1.3-1.6. There are four basic types of full-scale friction measuring devices depending on the slip condition of the measuring wheel: locked wheel, side force, fixed slip, and variable slip (NCHRP, 2000).

Locked wheel systems produce a 100 percent slip condition. The relative velocity between the surface of the tire and the pavement surface (the slip speed) is equal to the vehicle speed. The brake is applied and the force is measured and averaged for 1 second after the test wheel is fully locked. Because the force measurement is continuous during the braking process, these systems usually can detect the peak friction. The locked wheel testers are usually fitted with a self-watering system for wet testing, and a nominal water film of 0.5 mm is commonly used. When the measurement is made in accordance with ASTM Standard Test Method E-274 the result is reported as the skid number SN that is the measured value of friction times 100.

Device	% Slip (yaw angle)	Speed [km/h]	Country
ASTM E-274 Trailer	100	30÷90	United States
Dagonal Braked Vehicle (DBV)		65	United States
Japanese Skid Tester		30÷90	Japan
LCPC Adhera		40÷90	France
Polish SRT-3		30÷90	Japan
Skidclometer BV-8		30÷90	Sweden
Stuttgarter Reibungsmesser (SRM)	100, 20	30÷90	Germany

Table 1.3: Locked Wheel friction measurement devices (NCHRP, 2000)

Side force systems maintain the test wheel in a plane at an angle (the yaw angle) to the direction of motion, otherwise the wheel is allowed to roll freely. The side force is measured perpendicular to the plane of rotation. An advantage of this method is that these devices can measure continuously through the test section, whereas locked wheel devices usually sample the friction over the distance corresponding to 1 second of the vehicle travel, after the brake is released.

These systems produce a low-speed measurement even though the vehicle velocity is high. Because these devices are low slip speed systems, they are sensitive to microtexture. For this reason, they are usually used in conjunction with a macrotexture measure. The most frequently used side force devices are the MuMeter and the SidewayForce Coefficient Routine lnvestigation Machine (SCRIM). Because they are relatively insensitive to variations in macrotexture most SCRIMs are now fitted with a laser macrotexture measurement system mounted on the front of the vehicle and are called SCRIMTEX.

Device	% Slip (yaw angle)	Speed [km/h]	Country
MuMeter	13 (7.5°)	20÷90	United Kingdom
Odoliograph	34 (20°)	30÷90	Belgium
SCRIM	34 (20°)	30÷90	United Kingdom
Stradograph	21 (12°)	30÷90	Denmark

Table 1.4: Side Force friction measurement devices (NCHRP, 2000)

Fixed Slip devices operate at a constant slip, usually between 10 and 20 percent. The test wheel is driven at a lower angular velocity than its free rolling velocity. This is usually accomplished by incorporating a gear reduction or chain drive of the test wheel drive shaft from the drive shaft of the host vehicle. In some cases, it is accomplished by hydraulic retardation of the test wheel. These devices also measure low-speed friction as the slip speed is V (% slip/100).

Device	% Slip (yaw angle)	Speed [km/h]	Country
DWW Trailer	86	30÷90	Netherlands
Griptester	14.5	30÷90	United Kingdom
Runway Frïction tester	15	30÷90	United States
Saab Friction Tester	15	30÷90	Sweden
Skiddometer BV-l I	20	30÷90	Sweden

Table 1.5: Fixed slip friction measurement devices (NCHRP, 2000)

Like the side force method, the fixed slip method can also be operated continuously over the test section without excessive wear of the test tyre.
An example of a fixed slip tester is the Griptester. Most fixed slip devices are designed to operate at only one slip ratio; however the slip ratio can be varied on some fixed slip devices, referred to as variable fixed slip devices.

Variable slip devices sweep through a predetermined set of slip ratios. This is usually accomplished by driving the test wheel through a programmed slip ratio using a hydraulic motor. Some locked wheel testers can be operated in a mode that captures the friction as the test tire proceeds from free rolling to the fully locked wheel condition (0 to 100 percent slip). Locked wheel testers can also be programmed to operate in acccordance with ASTM E1337, in which the brake is released just after the peak is reached (NCHRP, 2000).

Device	% Slip (yaw angle)	Speed [km/h]	Country
IMAG	0÷100	30÷90	France
Komatsu Skid Tester	10÷30	30÷60	Japan
Norsemeter Oscar	0÷90	30÷90	Norway
Norsemetel ROAR	0÷90	30÷90	Norway
Norsemeter SAUIAR	0÷90	30÷90	Norway

Table 1.6: Variable - Fixed slip friction measurement devices (NCHRP, 2000)

1.6 PIARC harmonization – IFI index

Due to the great variety of measurement devices, the World Road Association - PIARC carried out an International experiment to compare and harmonize texture and skid resistance measurements in the fall of 1992. There were 51 different friction and texture measurements made by participants from 14 countries. The measurements were conducted on 54 sites as follows: 28 sites in Belgium (22 on public roads, 2 at airports, and 4 at racetracks) and 26 sites in Spain (18 on public roads and 8 at airports). Texture measurements, and friction measurements. Each friction tester was operated at three speeds: 30, 60 and 90 km/h, and each tester made two repeated runs at each speed. All texture measurements were made on dry surfaces before any water was applied to the roadway. As a control, a microtexture measurement was made before and after the skid

testers made their tests. These data were used to show that there were no statistically significant changes occurring during the testing.

Since the aim of the Technical Committee of the Surface characteristics AIRPC was to harmonize the different measurement methods used for the evaluation of friction and texture of road surfaces, a single index was proposed. The IFI index (International Friction Index) is calculated using relationships obtained from regressions of friction and textural data detected with different types of equipment.

$$IFI = (F_{60}\ ;\ S_p)$$

Where:

S_p is the speed constant in km/h. It does not depend on the adopted equipment for the friction measurement and it is function of the Mean Profile Depth only. It is calculated as follows.

$$S_p = a + b\ \cdot MPD$$

The coefficients a and b depend on the equipment adopted for the measure of macrotexture.

F_{60} is the parameter that represents the friction at the reference speed of 60 km/h and it is calculated as follows.

$$F_{60} = A + B\ \cdot FR_{60} + C \cdot MPD$$

The coefficients A, B and C depend on the type of instrument used for the measurement of the friction, while FR_{60} is the friction coefficient measured by the adopted instrument at the sliding speed of 60 km/h, which is calculated as follows.

$$F_{60} = FR_s \cdot \exp\left[\frac{S - 60}{S_p}\right]$$

FR_s is the friction coefficient measured at the sliding speed S of the adopted equipment, which is calculated as follows.

$$S = \frac{V \cdot s}{100}$$

In this case, V is the measurement cart speed in km/h while s is the sliding of the measurement wheel.

A, B, and C were determined were tabulated in the ASTM Standard Practice E-1960. The value of C is always zero when the friction is measured with a smooth tread tire. However, the term $C \cdot MPD$ was found to be necessary for ribbed or patterned test tires because they are relatively insensitive to macrotexture.

The two parameters that make up the IFI $(F_{60}\ ;\ S_p)$ are sufficient to describe the friction as a function of slip speed. Note that a texture measurement is required to apply the IFI.

Another advantage of the IFI is that the value of F_{60} for a pavement will be the same regardless of the slip speed. That permits the test vehicle to operate at any safe speed that could be at higher speeds on high-speed highways and lower speeds in urban situations.

Chapter 2

Literature review

2.1 Texture

The texture of laboratory test specimens has traditionally been measured using the volumetric patch technique as used for pavement surfacing. This allows direct comparison of road and laboratory data. However, research has considered complimentary non-contact alternatives to better understand the role of texture at different scales (McQuaid, 2015).

Among them Millar (2013) compared the use of a 3D hand held laser and close range photogrammetry (CRP) techniques and analyzed the models using functional volume parameters.

Flintsch et al. (2003) discussed different techniques for measuring pavement surface macrotexture and its application in pavement management and investigated a series of correlations between different measuring devices through the survey of many wearing surfaces.

Sangiorgi et al (2013) used a laser laboratory device to collect point cloud data for a section of road surfaces and used a combination of roughness parameters, MPD and Abbott-Firestone Curve analysis techniques.

Friel (2013), Mitchell (2014) and McQuaid (2015) used the Close Range Photogrammetry method and a hand held 3D laser respectively to assess surface texture changes with time for asphalt test specimens subject to accelerated simulated trafficking with the Road Test Machine.

Losa et al. (2010) looked for a reliable pavement profile data processing procedure for evaluation of pavement macrotexture, according to the definition of the ISO 13473-1, and for the verification of the assumption of equivalence between the profilometric and volumetric methods.

2.1.1 A comparison of techniques to determine surface texture data

This paper investigates the 3D capture of specimen surface texture using both Close Range Photogrammetry and High Resolution Scanner (HRS) methodologies. A vinyl cast with vinamold was made and assessed. The vinyl cast technique results in a permanent record of the asphalt surface texture and allows for time based studies showing its evolution. The 3D meshes were analysed for a 2D and 3D areal parameters using Digital Surf MountainsMap 6. Analysis of the findings show how sand patch, 3D photogrammetry and laser techniques data may be used to better understand road surface textures.

The analysis was made on a laboratory compacted hot rolled asphalt (HRA) test specimen. This was 305 x 305 x 50 mm in size and had Silurian greywacke 20 mm chippings at a spread rate 12 kg/m² applied during compaction to create macrotexture. The test specimen underwent 10,000 wheel passes of accelerated wet trafficking on the University of Ulster Road Test Machine (RTM).

The CRP procedure used a Canon EOS 400D SLR camera, with a 10Mp CCD array and a calibrated 60 mm macro lens. All images were captured normal to the surface under natural lighting conditions. The camera was mounted on a tripod and a remote shutter release used to minimize camera shake. A framework of control points was used to allow the recovery of surface elevation and orientation. It was calibrated using a digital micrometer forming a control calibration file. The control points were cross matched with additional tie points to reduce the level of redundancy. The stereo image pair, control calibration file and camera calibration files were imported into Topcon ImageMaster photogrammetric software. A TIN was created at a mesh resolution of 0.5 mm. No filtering was applied to the TIN in case it removed surface roughness. The resultant Cartesian coordinates of the TIN were exported in a comma separated value (CSV) file format into Digital Surf MountainsMap Version 6 surface analysis software.

The HRS procedure used a ZScanner 800 high resolution 3D laser scanner (HRS) with a stated resolution of 50 μm. A combination of scan resolutions was used to maximize the point cloud for the test specimen surface. This involved an initial coarse scan at 2 mm resolution followed by a fine resolution scan of 0.5 mm. Figure 2 shows the reference framework of control points used during laser scanning. After scanning and prior to export, the point cloud facets were edited to remove redundant data points. The facet resolution was set to 0.5 mm, allowing a comparable 3D model with that produced though

the CRP procedure. The point cloud was exported as a TXT file into Digital Surf MountainsMap Version6 surface analysis software. Digital Surf MountainsMap software allowed 2D and 3D parameters to be measured in accordance with BS EN ISO 25178-2.

The Study concluded that:

• The height parameters, Sq, Sa, Sp and Sv showed consistently higher values for the use of the cast compared to the slab. The same relationship occurs when the CRP method is compared with the HRS. The Ssk and Sku values correlated well with each other for all four 3D models. This suggests that the use of the cast for 3D capture of surface texture recovered to a greater depth into the surface when compared with the slab 3D models

• The AFC and percentage depth distribution data was able to confirm the presence of surface noise in CRP derived 3D models. As with previous SMA analysis this had negligible effect on the volumetric analysis (AFC) but did influence the height parameters.

• The removal of 1% AMBR to the peaks and valleys (AMBR 1% - 99%) can be used to remove outlier data due.

2.1.2 A study on texture and acoustic properties of cold laid microsurfacings

This study aim was to develop a slurry seal microsurfacings, which, in addition to skid resistance and roughness characteristics, would provide rolling noise reduction and eco-compatibility characteristics with the use of recycled crumb rubber. A 3D laser scanner device has been used to evaluate the surface texture and analyze the roughness parameters. Goals are similar to those reached by this PhD thesis.

Various bituminous mixtures for cold microsurfacings have been tested in laboratory conditions: they contained porphyry and basalt aggregates and a fraction of crumb rubber equal to 1.5 % on the mixture weight. Then, they were mixed with Portland cement, water and 60% bitumen emulsion modified with latex.

After the definition of the gradation curves by determining the best dosage of the compounds, four mixtures have been selected for the in-situ application: one with only basaltic aggregates (KmodBB), one with basaltic sand and porphyritic aggregate (KmodBP) and the same two mixtures, where a part of the sand fraction has been replaced by crumb rubber (KmodBBp and KmodBPp).

After the microsurfacings have been laid, a series of in situ surveys was carried out to characterize the road surface texture by means of a high-precision laser scanner device. The system used in this work is produced by the NextEngine and is based on the Multi-stripe Laser Triangulation (MLT) technology (Desktop 3D), capable of recording the three-dimensional representation of the surface texture of a portion of pavement.

The BPN and HS tests were performed in 10 longitudinally-equidistant road sections for both directions, in order to cover the whole road stretch, while two road areas per lane close to the Sound Level Meter have been laser scanned.

According to ISO 13473-2, 2D and 3D parameters were calculated for two of the three analyzed sites. An interesting study was represented by the correlation between the emerged area and water volume retention. The same study will be presented later for the rubberized 8 mm SMA in the 3D Image analysis Chapter. Sangiorgi et al. found a higher percentage of emerged areas in basaltic mixtures, instead of the basaltic and porphyritic ones, stating that this results is linked to the greater roughness of the surface. According to the ISO 25178 other indicators were calculated, i.e. areal and volumetric parameters, for a better classification of the pavement texture components (peaks, valleys and the core roughness profile) through the construction of the Abbott curves. Bearing ratio thresholds were set by default to 10% and 80%. Volume of material peak was found to be around 30 ml/m^2 and volume of void ranged between 66.30 and 84.30 ml/m^2.

As for the acoustic measurements, the Statistical Pass-By Method (UNI EN ISO 11819-1) was chosen, for its reliability and representativeness of the actual perception of road noise by receptors located close to the transportation infrastructure and it was applied on a statistically significant sample of passing-by road vehicles. Results highlighted a reduction equal to 2.2 dB(A) in the first site for the KmodBBp surface, compared to the previous asphalt pavement, while for the KmodBB one the reduction was equal to 0.7 dB(A).

In the second site the tests returned more similar results for both KmodBP and KmodBPp mixtures, with a reduction respectively equal to 1.5 dB(A) and 1.6 dB(A). In the third site, the A-weighted sound pressure levels related to one of the vehicle categories, did not undergone significant modifications and, therefore, the SPBI indexes remain substantially unaltered.

The paper concludes with the announce of new experimental and trial sites with the aim of the study the relationship between geometric and statistical indicators of a road surface texture and its noise performances: this PhD thesis confirms this statement.

2.1.3 Changes of surface dressing texture as related to time and chipping size

This paper reports the findings of a research project to study surface dressing performance in terms of its aggregate embedment due to trafficking and of the skid resistance and texture depth change with time. The influence of chipping size is also discussed. The reference materials are a range of smaller chipping sizes embedded into three types of underlying surfaces i.e. soft sand asphalt, 14mm Stone Mastic Asphalt (SMA) and concrete. The test specimens were compacted using a 17kg hand roller compacter with a minimum of 10 passes until the chippings were laid on their least dimension. Each test specimen was kept in an oven at 200°C for 24 hours to remove the water present in the emulsion. The rate of spread of binder and chippings was in accordance to Road Note 39. The wheel-tracker equipment was used to simulate trafficking of a small scale pavement structure and test for chipping embedment into the underlying material. Testing was periodically stopped and changes in texture depth and dry skid resistance determined. The authors divided the data into three stages. The first stage lasted for approximately 1960 passes of wheel tracking, followed by a second stage of between 1950 to 6240 passes. After 6240 passes, the test specimen was considered as belonging to a third stage where the rate of chipping embedment becomes minimal. The discussion of results is divided into three parts, dealing with texture depth, skid resistance and both of them respectively.

As for the texture depth, results showed that as the tracking time increased texture depth decreased at a gradually rate. Embedment was rapid during the initial stages after which the rate slows down which is expected as the chippings become interlocked.

The development of early life dry skid resistance was not as predictable as the decay in texture depth. This was attributed to complex interactions linked to the aggregate particles re-orientation, the embedding and polishing during prolonged tracking. This appeared to cause an initial increase in skid resistance followed by a gradual reduction. Skid resistance attains a maximum value soon after construction, when all the asphalt film on the surface has been worn away and the fresh gritty surface of the aggregate is exposed. With time,

skid resistance reduces under the action of traffic and environmental factors. The same behavior was found by the Author of this thesis and will be presented in Chapter 7.

The rate of texture depth change was quite similar for all types of specimens in stage 2 and stage 3, but not in stage 1. In stage 1, bigger chippings such as 10mm and 6mm show a slightly higher rate of texture reduction compared to 3mm chippings especially on the soft sand asphalt underlying surfaces. The average least dimension of the 10mm and 6mm chippings are higher than the 3mm chippings resulting in higher texture. Therefore, the soft sand asphalt has more room to move flow around the 10mm and 6mm chippings and results in increased embedment. In stage two, the effect of chippings size is less important as texture reduction is more dependents on hardness of the underlying surface. In stage three, the texture changes became constant with only major differences in texture depth value due to the differences in chipping size.

In contrast with the texture depth, the smaller aggregate sizes provide higher levels of dry skid resistance. Results shows that the 3mm chippings maintain 70 to 90 dry PTV throughout the whole time of testing. However, a bigger variation occurred for the 6mm and 10mm chippings, especially after 180 minutes of tracking time. The differences were probably due to the larger chippings size that was more sensitive to the different types of underlying surface.

The results indicate similar findings to the surface dressing performance in the field. This study was able to show the texture depth decreased but at a gradually decreasing rate. This change can be distinctively identified at 3 stages namely as stage 1 which is rapid linear decay of texture, stage 2, slow linear decay of texture and stage 3, period of erratic behavior.

This behavior is confirmed by the tests that will be presented later in Chapter 8 of this thesis. In term of chipping size, smaller chippings gave better skid resistance. The data tends to suggest a new emphasis towards smaller aggregate sized surface dressings. The skid resistance was also found to be high after construction and it started to drop due to the polishing of the gritty surface of the aggregate.

2.2 Skid resistance

Skid resistance is of paramount importance for the safety of road users. Different devices are available among highways agencies in order to assess the skid resistance on pavements, as described in Chapter 1.

Researchers of every country of the world attempted to study the phenomena that govern friction and their relationship with other parameters like texture.

Ueckermann et al. (2015) underlined that the skid resistance measurement is depending on factors like water film thickness, temperature, measurement speed, rubber aging, rubber wear, road evenness and curviness, which are difficult to control.

Ahammed & Tighe (2011) undertook a study to re-examine some of the pavement surface texture and skid resistance related issues and aid the highway agencies in this area through the analysis of data collected from nine asphalt concrete surfaces. Essentially they underline the existence of a correlation between skid resistance and macrotexture.

Leandri et al. (2015) made a reliable estimation of peak friction values experienced by Skiddometer BV11 at a certain speed on several types of dense asphalt concrete surface layers in order to propose a new model for predicting the speed gradient of peak friction values on asphalt pavements based on surface characteristics.

Kane et al. (2013) proposed an aggregate hardness parameter based on the mineralogical composition of the aggregates and the hardness of the individual mineral grains, which resulted to gives a good indication of the ability of an aggregate to retain its microtexture and consequently its friction properties.

This section first report an interesting paper that lists the important studies made on the relationship between road friction and road safety. It follows a series of papers dealing with the determination of skid resistance both on site and in laboratory, which are in some way connected with the topic of this thesis.

2.2.1 An assessment of the skid resistance effect on traffic safety under wet - pavement conditions

The relationship between road friction and road safety has been the object of numerous studies. In general, they are based on data from a specific road network of the country where the study is performed, but since the nature of the problem is common, the results have been used for international reference. For this purpose, most published research results refer to the two most common skid resistance measurements: SN and SCRIM. Giles and Sabey (1959) conducted a study on the relationship between skid resistance measured with SN40 and accident rates. SN40 values in 120 sites where crashes had occurred due to skidding were compared with 100 randomly selected control sites of similar characteristics and traffic volumes.

The study concluded that the risk of skidding crashes is extremely low when the SN40 value is greater than 65 and that it increases rapidly for SN40 values below 50. In a US study, Blackburn et al. (1978) analyzed the effect of SN40 skid resistance values on wet-pavement crash rates in 6 highway classes. They found that the variation of wet-pavement crash rates per 1 unit SN40 skid resistance value was −.0286 wet-pavement crashes/106 vehicle km. In Germany, Kamplade (1990) studied 464 1-km long freeway segments to determine the relationship between crash rates on dry and wet pavement and the SCRIM skid resistance.

They found a relationship between wet-pavement crash rates and SCRIM values. In a study conducted in France, Yerpez and Ferrández (1986) showed that crashes related to lack of friction on wet pavement are not always concentrated at sites where the skid resistance is low. Instead, they accumulate in sections where friction demand is high. Nevertheless, Gothié (1990, 2000) conducted three studies with data from different types of roads in France and observed a tight relationship between the skid resistance measured with SCRIM and crash rates. He found sharp increases in slopes of the crash-rate–skid-resistance relationships at cut-off values that range between 52 and 55 for the different samples that he analyzed.

In the UK, Roe et al. (1991) concluded that the absolute value of skid resistance was not the most important factor influencing crash rates but that these depended instead on the relative risk of skidding at each particular site. Nevertheless, the UK adopted a comprehensive standard for the desired minimum SCRIM values at 50 km/h for different

road classes (motorway, dual carriageway, and single carriageway), sections (curve, approach to junctions, roundabout, etc.), and road gradients. These desired minimum values are referred to as investigatory levels and range from a minimum of 0.35 for a motorway mainline to a maximum of .55 for an approach to a traffic signal (Rogers and Gargett, 1991). At the Pennsylvania Transportation Institute, Xiao et al. (2000) found that the safety condition, measured by the percent reduction in wet-pavement accidents, could be improved nearly 60% if the skid number increased from 33.4 to 48. Lindenmann (2004), using data from the entire Swiss national highway network, surveyed nearly 6,000 km of roadway with the SCRIM. Attempts to correlate the friction data with accident data from 5 years were unsuccessful.

Kuttesch (2004) used accident and skid resistance data from the Virginia wet-accident reduction program as well as from sections without pre-identified accident or skid problems. He found a statistically significant effect of skid resistance on wet-accident rates indicating that wet-accident rates increase with decreasing skid numbers. He concluded that a target skid number SN64 of 25–30 could be justified in general and that a target number of 40 could have a positive effect on reducing the wet-accident rates on interstate highways. Caliendo et al. (2007) calibrated crash-prediction models for a four-lane median-divided Italian motorway. They found that wet pavement significantly increases the number of crashes. Although they considered the side friction coefficient, (SFC) measured by means of a SCRIM device as a potential explanatory variable, it was not found to be significant in the analysis, and it was therefore not included in the models.

Milton et al. (2008) used highway-injury data from Washington State to calibrate a mixed (random parameters) logit model to estimate the injury-severity distributions of accidents on highway segments. They considered three severity categories: property damage only, possible injury, and injury accidents. The pavement friction number was found to be significant in the possible-injury distribution. According to their results, increasing pavement friction results in a decrease in the likelihood of possible injury and, simultaneously, in an increase in the probability of property damage only and injury accidents. The authors suggest that this data may reflect the behavior of some drivers who overcompensate and drive too aggressively (thus negating the additional friction benefits) while other drivers do not.

2.2.2 Mobile laser scanning system for assessment of the rainwater runoff and drainage conditions on road pavements

The Authors used the data collected from a Mobile mapping system, named "Road-Scanner" to develop a methodology for the analysis of rainwater runoff on road pavements, providing possible solutions that are impossible with traditional tools. Mobile Laser Scanning technology, together with data processed by the operator, is an effective tool to establish reliable maintenance operations specific to the problems encountered in the field.

The vehicle used is equipped with a wide range of state-of-the-art sensors and devices to carry out a rapid survey of a road infrastructure with all its appurtenances, by automatically acquiring large amounts of data. It combines the following technologies: GPS and Inertial Positioning System, medium-to-high resolution 5/8 front-mounted colour TV cameras (1400×1000 or 1024×768) and a rear-mounted vertical TV camera, a Dynatest RSPIV profilometer, a 2 GHz IDS georadar, an odometer and a Faro Photon 120 helical laser scanner.

The proposed approach was applied to a 15 km stretch of highway located in a mountainous area and subjected to dangerous water build up and ponding. The data analysis is based on the digital model of the road surface generated from the point cloud obtained by the laser scanner. The methodology is as follows.

The points are aligned on a regular grid with rectangular step. The amount of points returned from the laser scanner is too high to be handled in a Digital Terrain Model (DTM), as well as being superfluous for identifying water runoff problems. For these reasons, the first phase involves re-sampling the laser points, i.e., modifying the original survey to reduce the number of points in the scan, through a filtering operation to eliminate all the points not belonging to the road surface. The filter automatically eliminates all the points over 15 cm above the road surface, therefore leaving aside any car that overtakes the Road-Scanner vehicle during survey operations. The pitch of the mesh model is fixed at 20 cm. The reference altitude is derived from a statistical average of all the points within the range. The color scale used to represent the points is based on the difference in altitude between each point and the interpolating plane previously defined.

Based on this grid, a DTM is created for each carriageway. The single DTM, consisting of approximately 2,300,000 points, is used to rebuild the road alignment of the section under study, and this fundamental data will serve as a support for the whole subsequent processing. The laser scans the road sections with an angular extension of 320° and a depth of 150 m. The scan line, i.e. the number of points measured for each rotation of the mirror of the laser scanner, has a variable acquisition step of 20 to 30 cm, depending on the speed of travel. Around 2,000 points, including 700 on the road, are acquired for each scan line, giving an accuracy of 2 mm. Accordingly, sections are defined and all their geometrical parameters are well know, in particular that of the slope. For its calculation is chosen a baseline, representative of the width of the roadway, avoiding comprise edges that could affect the result obtained; the point cloud is then interpolated by a linear regression law, based on the method of least squares. The digital model of road surface is an essential tool for the hydraulic analysis of the highway.

The contour curves of the road, spaced 2 cm apart, are determined and are based on the altitude of the individual cells of the DTM. The frequency and direction of these curves provide information on the slope and on the flow direction of the runoff as well as water depth. Based on the DTM, the authors developed a module for graphical display of the runoff and of the water depth that is formed on the pavement road surface. After evaluating the absolute value of each cell and establishing the direction of flow, an iteration algorithm assigns the amount of water for each cell to the next, for a specified storm return period.

The flow path iteration algorithm selects among adjacent cells the one with the highest vertical drop, up to the side of the road. If it does not find the path that leads to an accumulated area, it repeats the iteration to another adjacent cell taking into account the new water level reached. A low drainage gradient leads to standing water forming on the road surface, which can undermine user safety by introducing the well-known effects of spray and aquaplaning. The developed module can help identifying the runoff type on the pavement with chromatic scale indicating the amount of water depth that is formed on the road surface during a defined rainfall event. Authors choose the model developed by Ross and Russam for predicting the water depth and applied it to the DTM by way of ArcGIS.

The intensity of rain was determined from the intensity duration frequency curve which correlates the rainfall intensity to the duration of the event that occurs at every assigned

return time. This is constructed by analyzing years of rainfall records registered by the weather station closest to the road.

In the software the stream line, i.e. the length of the runoff, is identified by the sequence of the individual cells to which the longitudinal and transverse slopes are associated. The exact knowledge of the horizontal and vertical alignment of the road means that it is possible to introduce several theories for designing drainage systems. Among these, the theory of Wooding, under certain conditions, is used to study the runoff process from a flat surface by means of an approximation of the De Saint Venant equations. The rain duration that causes the critical condition of maximum runoff, a function of the road alignment and the IDF curve, is first calculated. The maximum flow rate flowing out in the generic section can therefore be obtained.

Once the geometry of the receiving elements such as water channels (and hence their capacity Q) is known and a flow width on the carriageway is fixed, the maximum spacing between the outflow elements (road gullies and batter drains) is calculated as the ratio between Q and q0. Using the data obtained by the MLSS, it is possible to analyze the effectiveness of the drainage system for both the runoff towards the kerb shoulder and the runoff towards the median shoulder. This analysis is carried out for all possible horizontal and vertical alignment configurations, which are identified by the average slope values measured for each horizontal alignment and its gradient. It is then possible to compare the current spacing of road gullies and batter drains, determined from the geo-referenced videos, with the maximum allowable spacing for the system to function correctly in its current state. In the case of negative feedback, it is then possible to identify the alignment configurations on which to work.

The longitudinal evenness is examined using the Dynatest class I profilometer, which provides three values for IRI with a measurement interval of 10 m. These values are displayed directly on the geo-referenced images or tabulated as a function of the distance.

The Authors present an application of the defined procedure, first analyzing the data and secondly proposing a maintenance solution to restore the safety and compliance with the Standards of the road.

Different plots are show, which easily help identifying the sections to be restored. Among them:

- current runoff situation;
- comparison between current and maximum allowable spacing of batter drains;
- batter drain spacing design and comparison between current situation and design solution;
- water depth: current situation vs design solution;
- medium expected water depth versus road alignment configuration;

At the end, an interesting investigation correlates the medium expected water depth, WD, versus the sideway force coefficient, SFC, measured separately with SCRIM apparatus. This was made in order to understand which configurations are at a greater risk of aquaplaning. Thresholds were set both for water depth, 5 mm, and sideway force coefficient, 55, according to ANAS Italian technical standard. Therefore four different zones were identified (A, B, C, D). A includes road stretches with high WD and low SFC, consequently with high risk of aquaplaning; on the other hand, D includes those configurations having the highest safety rate. B and C areas should be carefully analyzed, as the effects of WD and SFC are opposite on the sliding risk.

Concluding, this paper validate MLS as a survey tool used for resolving water related issues on roads and consequently choosing specific maintenance work. As a large amount of data can be collected and subsequently processed, the road surface condition in the presence of water can be determined, comparing significant parameters. The following remarks summarized the work done:

- by detecting the slopes, the actual geometry of the roadway can be reconstructed and a comparison can be made with standard requirements;
- by applying a specific model to the DTM, it is possible to reconstruct the actual runoff water on the road surface, highlighting the critical cases. The weakest areas are the same as found by case histories of the road;
- the calculation of the water depth and the comparison between current and design situation allows the reduction of aquaplaning risk to be quantified;
- sections characterized by a greater risk of accident can be identified by combining friction measurements with calculated water depth;
- based on horizontal and vertical alignments, it is possible to define the efficiency of the existing drainage system and to quantify the effect of possible maintenance work, providing simple batter drain spacing graphs.

2.2.3 Geometric texture indicators for safety on AC pavements with 1 mm 3D laser texture data

In this paper pavement friction prediction model is developed based on the investigation of several texture indicators that are widely used in pavement engineering but also in other fields. The developed approach may be used as a cost-effective and promising method for the network level pavement safety survey. To achieve the objective, 1 mm 3D texture data with full lane coverage are collected using proprietary hardware: Digital Highway Data Vehicle (DHDV) equipped with PaveVision3D Ultra.

The first is a system for conducting full lane data collection on roadways at highway speed up to 100 km/h. The second is an imaging sensor technology that is able to acquire both 2D and 3D laser imaging data from pavement surface through two separate left and right sensors. The collected texture data has the resolutions of 0.3 mm in vertical direction and 1mm in the longitudinal direction. With the high power line laser projection system and custom optic filters, DHDV can work at highway speed during daytime and night time and maintain image quality and consistency. By illuminating pavement surface using a line laser and acquiring 2D and 3D images using the 3D cameras, the surface intensity variation and range variation in the vertical direction are captured based on the laser imaging triangulation principle, through which the distance from the camera to the pavement is determined for each point on pavement surface.

A Chinese road of approximately 393 m length was chosen as trial section for this study. The route consists of two surface types: High Friction Surface Treatment (HFST) and the regular AC pavement surface type. HFST is located in the middle of the test section. The regular surface is located at the lead-in and lead-out segments.

The friction data are acquired with Dynatest 6875 Highway friction tester, and 1 mm 3D texture data are collected using DHDV with Pavesion3D Ultra. The test section is sampled into 84 segments, and each segment has length of 4.57 m (two 3D image long). To validate the reliability of the collected friction data, three repetitive measurements are conducted, obtaining correlation coefficients of 0.95, 0.98, and 0.95, respectively. The mean friction numbers (FNs) from the three measurements are used for model development and validation.

Six texture indicators, namely MPD, Skewness, Kurtosis, TAR, SAR, and SBI are selected for pavement friction model development. Based on the multivariate regression analysis, pavement friction (FNp) can be estimated with the six texture indicators by a mathematical function.

The correlation between the predicted and measured FNs based on the multivariate regression analysis, shows an R-squared value of 0.868. A good agreement appears at the lead-in and HFST segments, but a large difference exists at the lead-out segment. In addition, the sensitivity analyses of the predicted FNs to the six texture indicators indicate that Kurtosis and SAR have no significant influences on the predicted FNs based on the p-values (e.g. $p > 0.05$). The p-value for the remaining four variables is less than 0.05, indicating the developed model is statistically significant for pavement friction prediction. Accordingly, pavement friction enables to be estimated with MPD, Skewness, TAR, and SBI.

In this model the effects of each independent variables (e.g. MPD) on dependent variables (e.g. FN) are assumed to be linear. If the effects of the independent variables on the dependent variables appear to be non-linear, this model may not be the appropriate fit for the data. In this study the residual plots is used to investigate the linear effects of independent variable on the dependent variable.

The findings from the presented research can be used to predict pavement friction based on various texture indicators including amplitude (MPD, Skewness), spacing (TAR), and functional (SBI) parameters. This study would be beneficial in the continuous measurement and evaluation of pavement safety for the project- and network-level pavement surveys.

2.2.4 Measuring skid resistance without contact

This interesting report investigates whether detailed imaging of the road surface has potential to be applied to the determination of microtexture and then to the measurement of skid resistance. The ultimate objective of this work is the development of a method suitable for implementation on a traffic-speed survey vehicle.

In this work Authors used a great number of aggregates that are very typical of those used in the construction of UK roads. These were photographed using a line scan camera

system, which has been developed separately for Highways Agency. The high-speed colour line scan camera collects a single pixel wide image 2048 pixels long at a scan rate of 11kHz. The distance of the camera from the surface allows a width of approximately 55mm to be photographed, giving a transverse resolution of approximately 54μm. Distance is measured, and the camera is triggered to capture, using a shaft encoder mounted on a small wheel in contact with the road surface. The line scan camera can be triggered to record a line of image once every 25μm. Artificial polishing and friction testing was carried out using the Wehner Schulze polishing machine so that the change in surface texture could be examined.

The specimens were made using seven aggregate sources. Aggregate particles are bound together into discs using epoxy resin and sand, which are green in colour. For each aggregate source, the discs were made in duplicate with a range of aggregate sizes 6 mm, 10 mm, 14mm and 20mm.
Photographs were taken of every sample before and after each stage of concentrated polishing. Following image collection the images required processing to characterise the microtexture. This was achieved by analysing and masking the image to isolate chippings from the remaining surface, followed by processing of the image of isolated chippings.

A critical part of this project has been the automatic pre-processing of images in order to isolate the chippings. In a previous work of the Authors, this was done manually to obtain small ‘windows’ of each full image for analysis, which was very slow, and considerably reduced the amount of image actually used. It was found that many small areas were required for analysis before a stable result could be achieved. By automatically masking everything but the upper stone surfaces in the image it is now possible to use the images to their full extent. During this experiment the use of green sand and green resin in the specimens made this process quicker and more accurate, but the algorithms developed do also work on standard asphalt samples.

The second stage of the image processing is that of assessing the microtexture, and therefore the friction, on the regions of the image segmented by the mask.
A characteristic parameter was developed in the previous stage of this work to assess the microtexture, called “CMT1”. This parameter utilises the intensity of each pixel and considers the density of pixel intensities within the image. The parameter was found to correlate successfully with the measured coefficient of friction, although the relationship

depended on the material being examined. Authors tried to improve the results using "CMT1", again using intensity, but attempting to achieve a material-independent relationship. A new parameter "CMT2", developed using an initial set of the polished specimens, uses a comparison of the intensity of each pixel with the intensities of adjacent pixels, rather than with a predefined threshold, as in CMT1. The relationship between μ and CMT2 was successful for two types of aggregates only and did not hold after analysis of further aggregate types. Therefore, the CMT2 parameter was altered to use the distribution of values calculated during analysis as well as the values themselves, and the parameter "CMT2A" was created.

Results show that CMT2A predicts the friction well for all but one sample, which has been treated as an outlier. The report conclude with a remark on the importance of determining the likelihood and impact of erroneous measurements. Furthermore, it will be necessary to investigate changes to the image analysis that will improve performance, such as collection of many more images to gain a more stable average parameter value.
A 2D image analysis is proposed in Chapter 7 of this thesis for the analysis of adhesion between bitumen and aggregates.

2.3 Tyre/surface interaction

Compared to other aspects of asphalt research this is an area that has received relatively little research given its importance. The prominent studies are presented in the next paragraphs.

2.3.1 Measuring grip and the contact patch

This paper combines two investigations i.e. the laboratory measurement of static contact patch properties with the dynamic measurement of wet grip on-site, to better understand the role of the tire in the measurement of tyre / asphalt interface properties of wet grip. Both investigations were carried out at a range of tire inflation pressures using a new and worn tire. In laboratory, although the British Standard for GripTester testing specifies a tire inflation pressure of 20psi (137.9 kPa), the inflation pressures assessed ranged from 2 to 41psi (13.8 to 282.7kPa) while measuring the contact patch. The comparison of a new

and a partially worn tires showed that at high inflation pressures their contact areas are similar; however they start to diverge with decreasing inflation pressure.

The measured load from the pressure pad was plot against tire inflation pressure for the two tires. Both plots were similar showing greatest measured load at lowest inflation pressure. In theory the measure load should remain constant as the test condition was static. The highest values of measured load from the pressure pad relate to the lower inflation pressures. The Authors suggests that the distribution of pressure within the contact patch may be having an influence i.e. concentrated under the sidewalls of the tire at the lower inflation pressures. The lower values for the new tire possibly reflect the stiffening effect of the unworn tyre.

The relationship between the load and the contact area from the pressure pad is shown. The data plots different to what would be expected reflecting the distribution of pressure within the contact patch. Within the tyre inflation pressure range of 20 +/- 10psi the plots show measured load to be relatively unaffected by tyre inflation pressure. The variation in pressure distribution measured within the contact patch may be affecting the data. The Authors highlight that with respect to any attempt to model tyre/asphalt surface interaction, this aspect of pressure distribution within the contact patch is critical.

The second part of the investigation aimed to determine whether lower inflation pressure of the tyre equals greater contact area; and the way it could affect the measurement of wet grip. The two tires used in the pressure mapping experiment were used. Test speed and water application rate was kept constant for all test measurement runs i.e. 50 km/h and 10.5 l/min respectively, according to the standard test conditions for GripTesting. The road surfacing assessed was Hot Rolled Asphalt (HRA) with 20mm chippings and a short section of 3mm high friction surfacing (HFS). Similar trends between measured wet grip and inflation pressure were found for the two surfaces and the two tires. However, there were small but significant differences relating to how interaction occurred.

The effect of inflation pressure is greater for the 3mm HFS surfacing, whereas the lower grip HRA appeared to be less affected by inflation pressure. Most effect occurred at the lower inflation pressures used in the investigation. The plots show measured wet grip to increase with increasing inflation pressure for both tires and surfaces. For the new tire, the amount of increase was greatest for the lowest inflation pressures thereafter remaining almost constant. The worn tire took longer to reach this condition.

Data of the static contact area were combined with the dynamic wet grip data for different new tire inflation pressures. The Authors underline the effect of tire wear and loading under the sidewalls of the tire. Any attempt to model tyre / asphalt surface interaction, even for this simple smooth tire needs to consider this aspect of pressure distribution within the contact patch. The measurement of wet grip is simply not related to contact area but also to the distribution of contact pressure within the patch and helps to explain the relationships presented in this paper.
The worn of the tyre can be analysed and the detected, as will be discussed in the Chapter 10 of this thesis.

2.3.2 The wear of Stone Mastic Asphalt due to slow speed high stress simulated laboratory trafficking

This paper has summarized a laboratory investigation into the wear Stone Mastic Asphalt road surfacing material. Two types of hot mixture asphalt surface course were used in this laboratory investigation i.e. 14 mm SMA and 10 mm SMA made in accordance with EN 13108-5. The coarse and fine aggregate used in both asphalt mixtures was a Silurian greywacke, with a declared PSV of 65 determined in accordance with EN 1097-8. Five test specimens of each SMA were selected for wear testing using the RTM. It is proposed that the RTM Wear Test gives better prediction of performance and durability as it uses full-size pneumatic tires and subjects asphalt test specimens to the worst conditions i.e. slow speed high stress.

The contact patch area between a ASTM friction measuring tire and the test specimen surface was assessed using a methodology developed at Ulster University, that will be discussed in a dedicated Chapter of this PhD thesis. Relationships between macrotexture and PTV against simulated trafficking are proposed. Emphasis is given to the tyre pavement interaction with the presentation of the development of contact area with the simulated trafficking and its relationship with macrotexture.
Contact area decreased over the first 500 wheel passes for all test specimens. Thereafter it continues to decrease at a lower rate for most of the test specimens. Little relationship between texture depth and contact area was found. The data shows that despite there being a significant range in texture depth the amount of measured contact between the tire and

asphalt remained the same. Author suggest that the greater measured values of macrotexture relate to greater depth of texture into the poorer compacted test specimen.

Conclusion summarize that 14 mm SMA and 10 mm SMA behave in similar ways. The main difference being 14 mm SMA has greater possible macrotexture. The gyratory data found good relationships between the amount of compaction and macrotexture. For negatively textured SMA, increasing macrotexture, reflects poorer levels of compaction creating texture and interconnected voids within the test specimen. This will lead to future durability problems for a material that is not designed to be porous. Relationships between variables relating to newly compacted test specimens were found to quickly change with the onset of simulated trafficking.

This raises issues with laboratory investigations that do not involve some aspect of tire/test specimen wear at their interface. Contact area would appear to be a better property to measure than macrotexture given issues with SMA negative texture. A poor relationship between contact area and pendulum tester suggests that either something additional at the contact interface has to be measured or there are limitations with the pendulum tester. It is concluded that more research is required to better understand wear at the tire/asphalt interface and the prediction / measurement / monitoring / modelling of properties such as skid resistance, rolling resistance and noise generation.

2.3.3 Durable laboratory rubber friction test countersurfaces that replicate the roughness of asphalt pavements

This paper is the resulted of a project founded by the European Community under the Marie Curie Industry–Academia Partnership and Pathways as well as the Fonds National de la Recherche Luxembourg. It deals with the development of a method for manufacturing durable countersurfaces for testing the friction of rubber samples in a laboratory.

Four different types of samples were manufactured and tested: two bitumen bound stone mastic asphalt samples, one concrete bound sample, and one epoxy bound sample. All of them replicated the surface roughness characteristics of a 8 mm SMA. In order to avoid changes in the friction levels due to binder removal the binder was pre-emptively removed from the fresh sample surface by sandblasting with and without water for bitumen samples

and cement or epoxy samples respectively. After the binder removal was completed, the initial friction and roughness levels of the test sample surfaces were measured.

Understanding tire–pavement interaction and especially tire friction is very important for tire manufacturers to develop tires with continuously increasing performance and safety. The authors used a laboratory rubber friction tester for comparing the friction performance of various rubber samples. However they ascertained that performing meaningful friction tests with rubber samples even in laboratory conditions is challenging due to the effect of the pavement surface roughness. On one hand, the surface roughness of the laboratory road sample should match that of the intended tire–road application. On the other hand, the roughness should also remain as constant as possible throughout test programs to provide comparable results for the different rubber samples and to reduce test variability. The latter is difficult to obtain since the rubber–road friction evolves during the lifetime of the pavement as a result of many different causes.

Therefore, the aim of the research is developing a test surface for laboratory tests that minimizes these changes during the targeted life span of the surface, allowing more repeatable and meaningful results from laboratory rubber friction tests. In order to reach the goals of both surface roughness characteristics and durability, the countersurface samples were prepared using three alternative binders: bitumen, epoxy and cement. The mixtures were compacted to small slabs and the applicability of each surface type was assessed using 3D surface topography scans and repeated laboratory rubber friction measurements. The purpose was to attain similar surface roughness as in a target stone mastic asphalt 8 mm SMA road surface. Granite from Koskenkylä quarry, located in southern Finland, was used in the surface samples due to its high resistance to wear by studded tires.

The friction on each surface sample was measured on two lanes 20 mm wide and 85 mm long. The wear cycles using a 20 by 20 mm^2 rectangular sliding rubber block made out of a rubber compound of a modern passenger car summer tire were applied on one of the two lane and the other one was used as a reference. The friction tests were performed using a high-precision linear laboratory friction tester. During the test the rubber block is loaded on to the asphalt sample with a specified load, and then slid for a given distance at a given speed while the longitudinal and vertical forces as well as the rubber block temperature are being measured. The test parameters were set so that the nominal contact pressure was

0.3 MPa and the sliding speed was 7 mm/s. The asphalt surface was dry during the tests. The test parameters were chosen to support fundamental research on rubber friction, and not necessarily to replicate typical road conditions.

The surface scans were performed with a MicroCADlite fringe-projection type optical 3D scanner manufactured by GFMesstechnik GmbH. The field-of-view of the device was 30 by 40 mm^2 and spatial resolution 55 μm while the height resolution was 3 μm. The test lanes were captured by performing four scans on each.

The performance of each asphalt sample was evaluated using four criteria: initial state and evolution of surface topography, durability based on visual observations, and evolution of friction results.
Both friction and surface characterization measurements showed that no significant changes took place in the surface roughness of the epoxy or concrete lanes during the test sessions.
The maximum number of wear test sweeps used in this study was set to 1000 based on the target application and were not comparable to the number of polishing cycles used for example in studies with the Wehner– Schultze machine, which are normally 105-106 cycles. In fact the polishing cycles in the Wehner–Schultze studies typically refer to the number of passes with a rolling rubbercone in the presence of water and abrasive particles and the number of dry rubber sliding friction test adopted in this study is expected to be more severe, especially in terms of raveling.

Results showed that the bitumen bound samples exhibited early deterioration, probably caused by the sandblasting. The authors suggest the use of different ageing methods in place of sandblasting for the bitumen samples. The interlocking between the larger stones on the surface is reduced with the removal of bitumen and smaller sand particles. This is similar with the ravelling caused by the drag of the wheel on the Immersion Wheel Track, which results will be presented in Chapter 9. Epoxy creates stronger bonds between the stones and is therefore able to withstand the stresses exerted on it during the testing much better and perhaps retain more sand particles during the sandblasting.

As for the replication of the surface topography only the bitumen and epoxy samples matched the target surface in terms of roughness power spectrum to a reasonable extent while the concrete sample had an overall too low roughness. As for the durability, the samples bound by bitumen were removed from the friction tests at an early stage due to

detachment of stones. The only sample that was both able to replicate the target surface roughness and endured the repeated friction tests was the epoxy sample.

2.4 Recycling and sustainability of road pavements

2.4.1 Stone Mastic Asphalts

Stone mastic asphalt (SMA) is a hot mix asphalt, developed in Germany during the 1960s consisting of a gap graded coarse aggregate skeleton with high percentages of void filled with a high binder content mortar. Because of the excellent performances of SMA in terms of rut resistance, high skid resistance, high durability, improved resistance to reflective cracking, SMA has been widely adopted in Europe, Australia, USA, Canada, Japan, China and many other countries worldwide, as a surface course for heavily trafficked roads. Its disadvantages are only related to the need of stabilization in order to inhibit drain-down of the high content of asphalt and to the higher primary costs.

2.4.1.1 Evaluation of SBS modified stone mastic asphalt pavement performance

The purpose of this Turkish study is the investigation of SBS polymer modified stone mastic asphalt performance. The tests were carried out by comparing a standard SMA with a SBS SMA. Optimal bitumen contents were calculated with experimental stages. The SBS modified SMA and reference SMA mixtures were evaluated with Marshall Quotient (MQ) approach, repeated creep test (RCT), indirect tensile strength test (ITST), Laboratoire Central des Ponts et Chaussees (LCPC) Wheel tracking tests. Results can be summarized as follows:

- according to the MQ results SBS modified samples gives higher values than conventional control mixtures. Flow values were obtained with similar values but higher stability. Higher MQ can be thought as more resistance to the plastic deformation. Controversial results can be obtained with MQ approach for some types of asphalt mixture gradations. Because of structural integrity and stone on stone contact gradation for SMA MQ approach gives more harmonious results.
- as for ITS, both unconditioned control mixtures and conditioned control mixtures have lower strength values with respect to SBS mixtures for 25 °C and 40 °C. It was understood that SBS polymer modified mixtures have higher load spreading

capacity. This result indicates higher resistance to rutting. As regard with the ITSR values SBS mixtures have higher moisture damage resistance according to the conventional control mixtures. Modified samples gave higher indirect tensile strength than control ones.

- SBS modified mixtures was particularly found as a superior additive for rutting. The repeated creep tests, based on Nottingham Asphalt Tester, show that SBS modified asphalt mixtures have higher permanent deformation resistance than the control mixtures for both 25 °C and 40 °C test temperatures. At moderate temperature, 25 °C SBS mixtures shows utmost performance and it is said that fatigue performance of SBS modified mixtures was increased.
- SBS mixtures reveal highest performance according to the control mixtures. SBS polymer modified asphalt mixtures gives at least double rutting resistance for 50,000 cycles with LCPC test results.

2.4.1.2 Comparison of performance of stone matrix asphalt mixtures using basalt and limestone aggregates

The main objective of this study was to compare the performance of three kinds of stone matrix asphalt mixtures, using basalt coarse and fine aggregates, named B-SMA, limestone coarse and fine aggregates, named L-SMA and basalt coarse aggregates and limestone fine aggregates, named BL-SMA.

According to the specifications for construction of highway asphalt pavements of China, a nominal maximum size 13.2 mm SMA mixture was used for the mix design in this study. To achieve the comparability of performance evaluation of three kinds of SMA mixtures, the principle of the same coarse skeleton structure, the same asphalt content, and the similar volumetric parameters of compacted mixtures was applied in mix design.

Crushed stones of basalt and limestone were used for coarse aggregate and fine aggregate respectively. Three particle sizes of coarse aggregates (13.2–16 mm, 9.5–13.2 mm, and 4.75–9.5 mm) of two kinds of stones were chosen. Six particle sizes of fine aggregates (2.36–4.75 mm, 1.18–2.36 mm, 0.6–1.18 mm, 0.3–0.6 mm, 0.15–0.3 mm, and 0.075–0.15 mm) of two kinds of stones were used. SBS modified asphalt binder supplied by a commercial petroleum company was used in laboratory. The mineral filler used was limestone powder, which was passed through the #200 sieve. Wood fibre as a drainage

inhibitor for asphalt binder was applied in SMA mixtures. The Authors adopted four performance tests in the laboratory: wheel tracking, low temperature beam bending, moisture susceptibility, and dynamic modulus tests.

Statistical analysis was performed using the Statistical Product and Service Solutions (SPSS) program to conduct analysis of variance (ANOVA) and Fisher's least significant difference (LSD) comparison. On the basis of the results and analyses of this laboratory test on the performance of SMA mixtures using basalt and limestone aggregates, the main findings and conclusions are summarized as follows:

- according to the wheel tracking test, B-SMA indicates the best rutting resistance, followed by BL-SMA and L-SMA comes in last. Differences of dynamic stability, which could be expressed by the number of times of wheel passing the sample per rut depth on a time interval between 45 and 60 min, between B-SMA and L-SMA and between BL-SMA and L-SMA are statistically significant, while the differences between B-SMA and BL-SMA are insignificant.
- as a result of the beam bending test, L-SMA shows the largest failure strain, while B-SMA shows the smallest failure strain, and BL-SMA is between the two. However, the difference of failure strain values between each SMA mixture is not significant and this means the insignificant differences in terms of low temperature cracking susceptibility.
- the moisture susceptibility of three kinds of SMA mixtures meet the requirement of specifications, and aggregate type has no significant effect on the moisture susceptibility at the 5% level.
- the dynamic modulus increases as loading frequency increases under a constant testing temperature, while decreases as temperature increases under a constant frequency. B-SMA shows the greatest dynamic modulus, followed by BL-SMA and L-SMA comes in last. Also, master curves of dynamic modulus of SMA mixtures were constructed.

Authors concluded the paper suggesting further investigations concerning the fatigue cracking properties and the need to repeat the tests with other asphalt binders to confirm these findings.

2.4.2 The art of recycling into road mixtures

The use of sustainable solutions in construction industry is increasingly becoming a need of the Society. In the last years, lots of research has been made with the goal to find new solutions for waste valorisation and to increase the amount of wastes reused. Historically, the first waste to be analysed and used in the pavement engineering has been the reclaimed asphalt.

The waste materials are being used in asphalt mixtures as additives, asphalt modifiers, fillers or in partly substitution to aggregates. Published papers do not always show successful results, so that not all materials can be re-used effectively in asphalt mixtures. Abreu et al. (2015) studied recycled mixtures containing 50% of reclaimed asphalt (RA), used motor oil (UMO) and waste high-density polyethylene (HDPE). It was concluded that up to 7.5% of UMO and 4.0% of HDPE can be used in a new modified binder for asphalt mixtures with 50% of RA, which have excellent properties concerning the rutting, the fatigue resistance and the water sensitivity.

Pasandín et al. (2015) investigated the feasibility of using green liquor dregs and biomass fly ash from the paper industry as filler in hot-mix asphalt (HMA) for road pavement. It is concluded that they lead to hot-mix asphalt with a poor water resistance (significantly worse in the case of mixtures made with dregs as filler) despite displaying adequate mechanical properties (stiffness and permanent deformation).

Sangiorgi et al. (2014, 2016) investigated the using of waste bleaching clays from the food industry as a substitute of common limestone filler traditionally used in the production of ACs for binder layers and open graded mixtures. Physical and mechanical characteristics were assessed, with promising results in terms of increasing of Indirect Tensile Strength, stiffness, and resistance to permanent deformation.

Mohd Hasan et al. (2016) evaluated the performance of e-waste modified asphalt binders made with Acrylonitrile Butadiene Styrene (ABS), Acrylonitrile Butadiene Styrene-Polycarbonate (ABS-PC) and High Impact Polystyrene (HIPS) passing through a #50 sieve. The e-wastes were blended with the control binder as untreated and chemically treated modified binders. Results showed that the treatment with cumene hydroperoxide increases significantly the stiffness and the elastic behaviour compared to the control binder, as well as the resistance to rutting of asphalt binders.

Anwar Parvez et al. (2014) explored the asphalt modification with Oil Fly Ash (OFA), testing the rheological properties of pure and modified asphalt binders. OFA were used at 2–8% by weight of asphalt binder. An ARES rheometer was used for temperature sweep, dynamic shear and steady shear rheological measurements. OFA - carboxylic group modification reduced temperature susceptibility of modified asphalt binder and increased the upper grading temperature. The rutting parameter G* / sinδ increased linearly with OFAACOOH content of asphalt binder.

Morova et al. (2016) In this study, utility of polyparaphenylene terephtalamide (PT) was investigated in hot mix asphalt as a fiber. Results showed that the best fiber rate was 0.25% and determined optimum bitumen content remain constant with the fiber additive for the reference samples. Besides, some sample groups which prepared using different PTF rates proved the specification limits and it was said that PTF can be used in asphalt concrete as a fiber additive.

Baghaee Moghaddam et al. (2012) investigated the effects of adding different percentages of waste polyethylene terephthalate (PET) with maximum size of 2.36 mm on stiffness and fatigue properties of SMA mixtures at optimum asphalt contents. The results showed that stiffness modulus of mixture increased at lower amount of PET content but adding higher amount of PET made mixture less stiff. In addition, PET reinforced mixtures exhibit significantly higher fatigue lives compared to the mixtures without PET.

K. Yan et al. (2015) analysed the compound modification effect of waste tire rubber (WTR) and reclaimed low density polyethylene (RPE) on the asphalt binders' rheological properties. Results indicated a decreased penetration and phase angle, increased softening point, rotational viscosity and complex modulus, indicating that intermediate and high temperature rheological properties of the asphalts have been improved by the modification of WTR and RPE. However, the modification effect of WTR and RPE on the low temperature rheological properties of asphalts is controversial, as the addition of WTR and RPE introduces decrease both in creep stiffness and m-value.

Gómez-Meijide et al. (2015) investigated the stiffness of cold asphalt mixtures (CAM) with 100% recycled construction and demolition waste aggregates (CDWA) through the indirect tensile stiffness modulus (ITSM), the dynamic modulus at different temperatures and frequencies and the correlation between them. They found that CAM with CDWA frequently achieved higher stiffness than control mixes using natural aggregate (NA), but

that they required significantly higher bitumen and water contents. They were less temperature susceptible, therefore, potentially more fatigue resistant, but more complicated to design.

2.4.3 Use of crumb-rubber into road mixtures

2.4.3.1 Evaluating the effects of the wet and dry processes for including crumb rubber modifier in hot mix asphalt

This dissertation was discussed in Alabama in the 1995 and discusses the properties of blends containing crumb rubber, CRM, modified in hot mix asphalts, both in wet and dry process.
The Author refers to "react" ground CRM particles when they are blended in the bitumen prior to mixing with the aggregate, i.e. 'wet process. The dry process takes place when CRM is added directly to the aggregate, rubberizing the aggregate and lessens modification costs.

The primary objective of this study was to compare the performance effects of adding the same ground CRM to HMA by the wet versus the dry process. Secondary objectives were to use the SUPERPAVE binder tests to determine the effects of ground CRM in both a reacted and unreacted state and determine how the gradation of ground CRM affects binder and mix properties in both processes.

Phase I utilized all the SUPERPAVE performance related binder tests. Four blends tested involved fully reacted CRM (nominal maximum sizes of 16, 40, 50 and 120 mesh) in a compatible AC-10 grade, while four other blends incorporated unreacted CRM (same sizes) in the same AC-10. The CRM/AC-10 weight ratio was held constant at 15%. The AC-10 and an AC-30 from the same source were also tested as controls. The reacted blends were prepared by blending the CRM into the AC-10 at 177° C until viscosity reached a maximum level and stabilized. They were then aged according to SUPERPAVE and tested. The unreacted blends were prepared by quickly mixing the CRM into the AC-10, which was already aged according to SUPERPAVE, and immediately poured into test samples. The reacted samples simulated wet process binders, while dry process binders likely act between the reacted and unreacted samples.

Test results indicated the fully reacted CRM improved all SUPERPAVE performance modes, while the unreacted CRM did the same but to a lesser degree. CRM size had very little effect relative to the overall effect of the presence of CRM.

Phase I demonstrated the addition of both fully reacted and unreacted CRM improves predicted binder performance using the SUPERPAVE tests and criteria. Since the unreacted blends establish the "worst case" binder modification by the dry process while the reacted blends establish the "best case", one can assume the true binder modification associated by adding the CRM dry is somewhere between the unreacted and the reacted blends. Generally, the reacted blends outperformed the unreacted blends, while both outperformed the control blends. The SUPERPAVE grading system uses increments of 6° C to distinguish between grades, both on the high and low temperature ends. This 6 °C incrementing of grades is used in the following statements to summarize the effects of both reacted and unreacted CRM:

- for tenderness and rutting, the reacted blends (with an AC-10 base) were approximately one SUPERPAVE grade better than the AC-30 and two grades better than the AC-10. The unreacted blends (also with an AC-10 base) were approximately half grade better than the AC-30 and one and a half grades better than the AC-10;
- for fatigue, the reacted blends were approximately one grade better than the AC-10 and two grades better than the AC-30. The unreacted blends were approximately half grade better than the AC-10 and one and a half grades better than the AC-30;
- For cold-temperature cracking with the S parameter, the reacted blends were approximately one grade better than the AC-10 and two grades better than the AC-30. The unreacted blends were approximately half grade better than the AC-10 and one and a half grades better than the AC-30;
- for cold-temperature cracking with the m parameter, the reacted blends were approximately half grade better than the AC-10 and one and a half grades better than the AC-30. The unreacted blends were approximately the same grade as the AC-10 and one grade better than the AC-30;
- all reacted and unreacted blends had better "relative elasticity" (lower phase angle for the same stiffness) than the control blends at both high and low temperatures.

This was demonstrated by plotting delta versus G" for all blends. The two control blends (from the same source) had identical delta versus G" relationships;

- CRM size between 16M and 120M nominal maximum size had little influence on binder properties relative to the overall large effect from the presence of CRM;
- The reacted blends aged slower in the TFO than the controls, suggesting the addition of CRM slows the binder aging process.

Phase II involved testing five mixes with a 100% limestone gap-gradation: 16M wet, 16M dry, 80M wet, 80M dry, and an AC-30 control. The CRM/ AC-10 ratio was again held constant at 15 %, even in the design of the dry mixes. Prior to compaction, all the loose mixes were short-term aged at 152 °C for four hours to simulate construction conditions. The optimum binder contents to achieve 4% voids were identical between the wet and dry mixes, for both CRM sizes. Resilient modulus at three temperatures, indirect tension, and dynamic creep results all showed no significant difference between the wet and dry mixes. They also showed the control mix was more temperature susceptible and had significantly higher resilient moduli and tensile strengths than the CRM mixes.

The five mixes tested in Phase II were: 16M wet, 16M dry, 80M wet, 80M dry and a control. All mixes had the same limestone aggregate, gap-gradation and compatible AC source. The four CRM mixes had a constant CRM/AC-10 ratio of 0.15 while the control mix's binder was an AC-30 with no CRM. All mixes were short-term aged for 4 hours at 152 °C before compacting into samples. Comparisons were made between mixes of the wet versus dry process, 16M versus 80M CRM, and CRM versus no CRM.
The author did not found substantial differences between mixes when the CRM was added wet rather than being added dry. This is supported by the following results:

- from the independent mix designs performed on each mix, the 16M wet and 16M dry mixes each had identical optimum binder contents selected at 5.0% to achieve 4% VTM. The 80M wet and 80M dry each had identical optimums of 4.4%. The control mix had an optimum of 4.1 %. These identical optimums indicate the wet and dry mixes are compacting identically. Since the same amount of CRM and AC-10 was in each of the wet and dry samples which had the same CRM size, the only difference between the wet and dry samples was how the CRM was added;
- none of the measured lab properties, (RM at 5, 25 and 40 °C, ITS and ε_f from the indirect tensile test, and permanent ε from the dynamic creep test) were

significantly different between the wet and dry mixes. Some significant differences were found between the 16M and 80M CRM mixes and between the control and CRM mixes.

Furthermore there was no significant difference between the 16M and 80M CRM mixes for RM (at 5, 25 and 40 °C) and for permanent creep ε. The 16M CRM mixes did have significantly higher ε_f and significantly lower ITS compared to the 80M CRM mixes.

Concluding, the control mix had significantly higher RM (at 5, 25, and 40 °C), ITS and ε_f values compared to the four CRM mixes, but the permanent creep ε values were not significantly different.

2.4.3.2 Improvement of Pavement Sustainability by the Use of Crumb Rubber Modified Asphalt Concrete for Wearing Courses

This paper reports on a research project performed to evaluate the advantages of using crumb rubber in the production of low noise gap-graded asphalt concrete surfaces, by using both the wet (W) and the dry (D) processes, specifically designed to reduce rolling noise by optimizing surface texture.

The study also compared the mechanical and functional performances of the mixes obtained by using the two technologies in order to assess their respective potentials for use as viable alternatives to other low noise asphalt surfaces that improve pavement sustainability. The two laid mixtures are both 0/8 gap graded (GG), 3 cm thick, mixed with asphalt rubber (AR) and polymer modified bitumen (PMB) respectively, and containing similar percentages of crumb rubber: 1.8% and 2.0% for the GGW and the GGD respectively.

The in-situ measurement were made with the same equipment adopted in the Zola Predosa trial site, which is object of this PhD thesis. The results of laboratory and in situ tests showed that:

- The two mixtures showed similar ITS values, which are higher than the minimum values required by the national standards for gap graded asphalt mixes to be used as wearing courses. No problems pertaining to moisture susceptibility arose for the two mixes.

- The AR shows a fatigue attitude similar to that of the PMA blended with the CRM.
- The GGW mix shows macrotexture values higher than those of the GGD mix, depending on the greater nominal diameter of the aggregate gradation. Over time, the macrotexture of the two mixes increases, and this tendency is more pronounced for the GGW mix.
- The friction levels recorded for both mixes highlight the increased level of safety for traffic that can be obtained by using CRM in the production of asphalt concretes. Over time, the friction level of the GGW mix shows a slight increase, whereas the GGD mix shows a slight reduction. This is due to the greater adhesion of the AR to the aggregate compared to the GGD mix, in which the CRM acts as an aggregate.
- Acoustic absorption coefficient measurements show no meaningful absorption may be found for both the mixtures.
- The differences between the global CPXL level measured on each experimental wearing course and that measured on a traditional dense asphalt course 0/12 surface are about 4.5 dB(A) for the GGW mix and 5.5 dB(A) for the GGD mix.

The study concludes highlighting the benefits in terms of tire/road noise reduction that can be obtained by using crumb rubber in the production of low noise asphalt surfaces and the mechanical and frictional performances of the crumb rubber modified asphalt concretes that the Authors suggest classifying as a construction material that can enhance the three dimensions of sustainability.

2.4.3.3 The mechanical performance of dry-process crumb rubber modified hot bituminous mixes: The influence of digestion time and crumb rubber percentage

This paper describes an in-depth study of the dry process of adding crumb rubber to asphalt mixes, which was the second phase of a previous study which analysed the influence of the digestion time and crumb rubber content in the design phase of the mixes. This research study involved the analysis of these variables and their impact on the mechanical performance of dry process bituminous mixes.

The mix had a discontinuous grain size (from which the 4–2 mm fraction was eliminated). It had a larger percentage of coarse aggregate, which gave it bearing capacity

(approximately 65–80% of the total with a maximum size of 8–12 mm). The rest of the mix was composed of fine aggregate 20–35% of the total), which along with the bitumen and the filler (7–10%) were the elements in mortar that made the mix cohesive and provided it with resistance to tangential stresses. The mixes used were spread in thin layers (2–3.5 mm), and had an excellent surface macrotexture and good skid resistance. The aggregates selected for the mix design were ophite for the coarse fraction and limestone for the fine fraction.

The mixes studied had an identical mineral skeleton, except for the finest aggregate fraction of the same size as the crumb rubber, which, depending on the amount of crumb rubber added, was modified so that it could be accommodated in the skeleton without causing anomalies. The mixes only varied in their percentage of crumb rubber (0%, 0.5%, 1%, and 1.5% of the total weight); the digestion time used before compaction (45, 90, and 120 min); and the type of bitumen used (BM3c and B 50/70). The bitumen content of the mixes had specified optimal amounts of bitumen, according to the Marshall test results. During the manufacture of the CRM mixes, the temperature of the mix was increased to 180 °C (10 °C more than that of the reference mix) so as to facilitate the interaction between the rubber and the bitumen, thus improving the cohesion of the mastic.

The manufacturing process first involved a 10 seconds agitation of the natural aggregates in the mineral skeleton in order to better homogenize them. In order to ensure a homogeneous dispersion of the particles throughout the mix, the crumb rubber was added to the aggregates and then mixed with them for a period of 20 seconds. When the bitumen was added, there was a 2 minutes agitation period until it was thoroughly blended with the aggregates and crumb rubber. The last ingredient added was the filler. This was followed by a final agitation lasting 3 minutes, which allowed the formation of the mastic to provide cohesion. The digestion process of the mix occurred in an oven at a compaction temperature of 160-165 °C. The response of the mixes to moisture was tested by the moisture sensitivity test (EN 12697-12), and their response to rutting (plastic deformations) was tested by the wheel tracking test (EN 12697-22).

The main conclusions of this study were the following:

- both the digestion time as well as the amount of crumb rubber added to dry process bituminous mixes had a significant influence on the mechanical performance of the mixes. Nevertheless, the amount of crumb rubber in the mixes had a greater

impact on their mechanical performance, as reflected in the mix response to water sensitivity and plastic deformation;

- increasing the crumb rubber content over 1.0% caused a considerable reduction in the density of the mixes, an increase in their air void content, and a substantial loss of cohesion. This signified that the mix had a less satisfactory performance as reflected in its indirect traction and retained strength in response to moisture action (due to the de-compaction produced by the rebound effect, associated with the resilient properties of rubber).

  Moreover, the addition of crumb rubber in percentages of 0.5% and 1% of the total weight of the mix made it possible to obtain values for indirect traction resistance and retained strength after immersion in water that were similar to those of the reference mix with high-performance bitumen. In fact, these values were even high for certain digestion times. Results showed that optimal mix values were a digestion time of 45 min and a crumb rubber content of 1%;
- the amount of crumb rubber is once again a determining factor on the mixes' resistance to plastic deformations (resistance to rutting). In fact, results showed that the addition of large quantities of crumb rubber to the mix (1.5%) greatly improved its response to plastic deformations. Its performance in this respect was much better than that of the reference mix. Even for lower crumb rubber contents (0.5% and 1.0%), the deformation values were similar to those obtained with the high-performance bitumen. In this case, the digestion time did not have as much influence as in the case of the moisture sensitivity test;
- despite the fact that the greater part of the mixes analysed complied with the Spanish regulations, the optimal values for the variables studied were a digestion time of 45 min and crumb rubber percentages of 0.5% and 1.0% of the total weight of the mix.

2.5 Acoustic properties of pavements

2.5.1 A modified Close Proximity method to evaluate the time trends of road pavements acoustical performances

A new adapted measurement methodology based on CPX method has been presented to improve the evaluation of road surface acoustical performances, in terms of stability, in time and space, and its effectiveness for a mitigation action. Concerning the requirements of the ISO/DIS 11819-2, the procedure here proposed uses a finer spatial resolution, defining the segment 5.76 m long. Moreover, it takes into account the measurement uncertainty related to the single segment to calculate the spatial weighted mean levels.

Data are used to determine the parameters for the relationship between speed and levels, estimating levels at the reference speed and avoiding the blind speed correction used in the original method. Thus, the knowledge about pavement performances within the whole typical road speed range is acquired and the reliability of the levels estimation at reference speed is improved. The use of special road surfaces with low acoustical emission profiles is one of the most applied solution to mitigate noise levels at dwellings in urban situations, where other actions, such as noise barrier, are difficult.

Anyway, time stability of these surfaces must be monitored in order to verify the mitigation effects at dwellings. So acoustical labelling for special pavements could be done also over time.

Furthermore, the proposed methodology has been applied, within the LEOPOLDO project, to survey three different pavement types, laid as experimental mitigation action other than those performed on the reference surface:

- ISO 10844 optimized texture dense graded;
- monogranular open graded (0/10);
- SMA gap graded with optimized texture (0/8).

According to ISO/CD 11819-2 and taking into account previous studies available in literature a self-powered vehicle has been developed, mounting the two mandatory free field microphones located close the rear right side pneumatic, far from the exhaust pipe. In particular this set-up was tested in other studies against the influence of internal and external noise sources (exhaust, engine, other aerodynamic sources).

The tyre used is a Michelin XSE 185/65 R15 88T, according to the reference ones identified by the ISO/CD 11819-2 with a tread pattern similar to the B type. It ran less than 5000 km and it worked only during every measurement session. Before starting each measurement session the pneumatic was driven some minutes to be brought to the normal operating temperature. As recommended by the ISO/DIS 11819-2, measurements are conducted only on perfectly dry surfaces. Measurement sessions are carried out when measured air temperature is within the range representative for the climatic zone and wind speed not exceeding 5 m/s.

To minimize the influence of the variability on the results, the proposed procedure prescribes that during the same measurement session in which a new surface is surveyed, run repetitions have to be extended over a second road surface close to the test one as much as possible and chosen as reference. In particular, in case the aim of the measurements is to evaluate time trends, it is suggested to choose as reference a long aged surface presumably acoustically stable in time, as in many cases the closest surface as much similar to the ante-operam one as possible. Using this technique (here called differential criterion), acoustical characteristics of different pavement types can be compared.

Besides the acoustical uniformity of each single surface can be evaluated in order to label or verify the installation of special pavements mainly prepared for environmental noise reduction. This technique can also be used to assess the acoustical performances of a road surface over time.

2.5.2 Noise Abatement of Rubberized Hot Mix Asphalt: A Brief Review

This paper, published in 2015, is a short review of the various experiences about the noise abatement properties of the rubberized asphalts.
Among them, a six-year study showed that rubberized asphalt reduces the traffic noise level by 4 dB more than conventional non-rubberized asphalt even though, the noise abatement declined with age for both materials. Similarly, a similar study concluded from a ten-year experience that rubberized overlays reduce the noise by 3 to 7 dB, where conventional asphalt would reduce the noise by 1 to 2 dB only, but the noise abatement after ten years was measured to be between 0 to 3 dB only. Thus, the difference between

rubberized and non-rubberized overlays diminishes with time. A more recent study obtained field measurements from 23 test sections in multiple locations across California, verified that rubberized mixes had lower sound intensity level. Results also revealed a potential correlation between the noise level and the thickness of the section, as well as the air-void content of the mix. The effect of thickness on noise abatement was analytically confirmed by another study, which deals with a finite-element based model to evaluate the vibration attenuation of various materials, including rubberized asphalt. Presence of rubber can also alter the noise frequencies to lower frequencies, where human ears feel less discomfort; it is reported that most noise reduction in rubberized asphalt sections falls within 500 to 4,000 Hz, which is consistent with the natural frequency of tire noise. Field studies have also included the effect of traffic speed on noise abatement, showing higher noise abatement for faster traffic flow. RHMA is less effective on reducing the noise generated by medium and large trucks, which their engines and exhausts are responsible for larger portion of the traffic noise. On the average, RHMA reduces the noise by nearly 2 to 3 dB more than conventional hot mix asphalt (HMA) and 4.5 to 6 dB more than Portland cement concrete (PCC). Open graded asphalt reduces the noise up to 1.5 to 3 dB more than dense graded and gap graded asphalts due to higher void ratio.

The paper states that the effect of RHMA on noise abatement decreases through the life of the pavement. Long term studies have shown that RHMA might still be effective on noise reduction after six to ten years. At the same time, HMA overlay might reduce the noise for up to 4 years only. Open-graded friction course (OGFC) has shorter effective life span for noise reduction than dense-graded hot mix asphalt.

Application of rubber tends to shift the frequency of noise to lower frequencies, which is basically closer to natural frequency of tire noise. In the other word, rubber does not resonate at high-frequency, and therefore, does not amplify the high frequency content of the sound. Therefore, resulted noise would be more tolerable and less uncomfortable for human ears. The frequency content might also shift back to higher frequencies as RHMA becomes more compact and rubber becomes stiffer through aging.

It is concluded that RHMA effect on noise abatement is challenging. Testing methods, prediction models, and long-term experimental results are current challenges in evaluating the impact of RHMA on noise reduction.

2.5.3 The effects of pavement surface characteristics on tire/pavement noise

The objective of this paper is to evaluate the effects of single and multiple pavement surface characteristics on tire/pavement noise levels. During the period from August 2009 to August 2011, noise levels and pavement surface characteristics are measured quarterly on many different asphalt pavements at 2009 NCAT test track.
Among the forty-six asphalt pavement sections included in the 2009 NCAT oval-shaped test track, 10 fine-graded and eight coarse graded Superpave pavement sections (all constructed in 2009 except for E4 section in 2000), five SMA and five OGFC pavement sections are selected and analyzed in this paper.

Tire/pavement noise was measured by On-board Sound Intensity (OBSI) method (AASHTO TP 76-08). Two sound intensity probes were used in OBSI measurements, one at the leading edge and another at the trailing edge of the tire/pavement contact patch. All measurements were conducted at 72 km/h using a Chevrolet Uplander minivan with SRTTs (Uniroyal tires). Three consecutive runs were taken for each measurement. During the period from August 2009 to August 2011, noise was measured nine times. The results of OBSI measurements are called as Sound Intensity Levels (SILs) and given in terms of spectral contents in one-third octave bands from 315 Hz through 4000 Hz. In this paper, the frequencies of interest only include lower frequencies (315, 500, 1000 Hz) and higher frequencies (1600, 2000 and 2500 Hz).

In addition to noise measurements, pavement surface characteristics, which have been reported to affect tire/pavement noise, were collected during the same period. Surface texture was measured by circular texture meter (CTM) and recorded in terms of Mean Profile Depth (MPD). Pavement roughness was measured with inertial laser profiler (mounted on a NCAT ARAN van) and reported as International Roughness Index (IRI). Stiffness (reported as Dynamic Elasticity, E*) was obtained according to the master curve of E* of surface asphalt mixtures at different temperatures. Porosity and aggregate size were determined using Quality Control (QC) documents during the initial constructions and recorded as air void (VA) and nominal maximum aggregate size (NMAS), respectively.

The linear regression analysis method is used to evaluate the effects of single pavement characteristic on noise levels. Furthermore Multiple surface characteristic analyses was

adopted to understand which pavement surface characteristic is the paramount important contributor to noise levels at different frequencies. The relative significance of pavement surface characteristics is determined using the dominance analysis methods. This method can identify the inter-dependent problem in which one characteristic may highly correlate with other characteristic. The general dominance weights are used to evaluate relative significance of multiple pavement surface characteristics on noise levels. The range of dominance weights varies from 0 to 100. Dominance weight 100 means that noise level is fully governed by this characteristic (that is, other characteristics have no effects on this noise level). Conversely, weight 0 means that this characteristic has no effect on noise level. General dominance weights of all characteristics sum up to 100.

The final discussion of the paper summarizes the findings between impervious and open-graded asphalt pavements.

For the first, the surface texture increase noise levels at lower frequencies (below 1600 Hz, especially at 500 Hz). So, in order to reduce noise levels efficiently it is suggested reducing the Mean Profile Depth as far as possible. But this may sacrifice driving safety on these pavements because friction between a tire and a pavement may decrease as texture wavelength decreases. This implies that a balance between noise and driving safety should be maintained. To meet this balance, texture wavelength should fall into a reasonable range. To design the future low-noise asphalt pavement, developing a surface texture which can balance noise and safety will be a crucial step.

Regarding Open-graded asphalt pavement, porosity within asphalt pavement decrease noise levels at every frequency (except at some frequency). To reduce noise levels more efficiently, the factors such as pore distribution, inter-connected pore content, pore shape and pore size, should be further taken into consideration. Unfortunately, how these factors affects noise generation is still unknown. From current research, noise levels decrease with the increasing of porosity. So, a balance between noise and pavement durability should be carefully maintained.

2.5.4 Road pavement rehabilitation using a binder with a high content of crumb rubber: Influence on noise reduction

This paper presents the laboratory characterization and the evaluation of field performances of a gap-graded mix with 20% of crumb rubber by weight of bitumen, added by a wet process. Acoustical field characterization were performed by determining, at different speeds, sound levels and noise spectra measured in close proximity. Road profiles along the test sections and sound absorption of compacted sample cores also were studied to analyze their relationship with the noise emitted.
A gap-graded bituminous mix, BBTM 11 A, according to EN-13108-2, with a maximum aggregate size of 11.2 mm was used for the rehabilitation of the existing deteriorated surface: a 15 year-old asphalt concrete type AC 16 surf S, according to EN-13108-1.

With the aim of studying the influence of the crumb rubber on the acoustical properties, two mixes were prepared with the same type of aggregates and gradation but different type of bitumen. The first one is high viscosity modified bitumen manufactured with crumb rubber, made with base 35/50 penetration-grade bitumen. The amount of crumb rubber added by wet process (CRMB) was 20% of the weight of the base bitumen. The crumb rubber particles used in the mix had a maximum size of 1 mm and was added gradually into the asphalt binder at a reaction temperature of 175–180 °C, and mixed mechanically. The optimal bitumen percentage used to manufacture the mix was 8.3% of the total mix weight. The bitumen used for the reference test section, which did not contain crumb rubber, is conventional 50/70 penetration grade bitumen, with a content of 5.2% of the total mix weight. In both cases, the optimal binder content was determined according to the Marshall mix design.

Materials characteristics in term of volumetric properties and water sensitivity were performed on cylindrical specimens manufactured with 101 mm in diameter and 60 mm in height. These test specimens were compacted according to the standard EN 12697-30.
To evaluate the acoustic characteristics of compacted core samples, a 4206 Bruel&Kjaer (B&K) impedance tube was employed. The impedance tube consists of a 100 mm inner diameter with a loudspeaker mounted at one end. The B&K impedance tube allowed measurements between 50 Hz and 1600 Hz.
The mean values of the close proximity tire/pavement noise levels at reference speeds of 80 km/h and 50 km/h, associated teach test sections, were analyzed. Averaged values were

calculated from measurements along eight stretches of at least 100 m, before and after the reference section, using different runs.

The main conclusions that can be derived from the laboratory and field measurements at this stage are as follows:

- the choice of binders, B 50/70 or high content of CR incorporated by wet process, for example, apart from texture and air void content (very similar for the mixtures of this research), may be of great importance on the acoustic behavior of asphalt mixtures;
- acoustical monitoring with a semi-anechoic chamber (CPX methodology) shows a significant noise reduction (around 2.5 dB(A) for 80 km/h) attributed to the incorporation of CR in a high content to the gap-graded mixture;
- surface rehabilitation or new construction with gap-graded bituminous mixes with a high content of CR appears to be a good environmental measure to significantly mitigate noise pollution in urban areas; a variation of 2.5 dB(A) attributed to the high content of CR is substantial as it corresponds, in terms of equivalent traffic, to approximately halving the traffic volume;
- from an environmental point of view, a surface rehabilitation of a deteriorated AC 16 surf S pavement with a CRMB gap-graded mix may improve tyre/pavement noise reduction in around 4 dB(A);
- the noise reduction due to the incorporation of CRMB takes place at frequency domains between approximately 630 Hz and 2 kHz, coinciding with the peak of the typical frequency spectrum generated by traffic noise;
- the tire impact/vibrations and air-flow related mechanisms show different dependencies on rolling speed: coefficients B of 26 dB(A) and 36 dB(A) are found, respectively. This behavior has also appeared in another bituminous mixture without crumb rubber;
- according to variability of the acoustical monitoring of the road surface and pavement texture from surface profiles it can be concluded that the production of mixtures, paving operations and/or service conditions, in addition to the inherent properties of the mixtures, can strongly affect the in-service performance of the mixtures.

2.5.5 Durability and variability of the acoustical performance of rubberized road surfaces

This paper describes results obtained by monitoring four rubberized surfaces one year after the laying and by evaluating the time stability of LEOPOLDO one by means of the Close Proximity method (CPX). All surfaces here analyzed are laid in real scenarios, so the actual efficacy of this action is evaluated. The results on the LEOPOLDO surface show spatial homogeneity, a good time stability and a significant noise emission reduction. Instead, analysis of the four rubberized surfaces shows variability in the results, probably due to the pavement installation quality, as supported by the data. Thus, the rubberized road surface looks to be a very efficient mitigation technology, providing the installation have been carried out with care and proficiency.

The procedure applied by ARPAT within the LEOPOLDO project combines the technical international standard with the guidelines provided by HARMONOISE project. HARMONOISE introduces a second measurement position, at 3.0 m height and at 7.5 m far from the central line of the measured lane, to improve the evaluation of the influence of local context, because the ground just outside the road carriage can change with the location and it influences significantly the sound pressure level at the 1.2 m height position. Moreover, the applied procedure is based on measuring the acoustical energy of the various isolated vehicles passing by at different speeds, using the sound exposure level. During the measurement session, pass-by sound pressure signal and related speed are registered.

The first rubberized surface analyzed is one of the experimental pavements laid within the LEOPOLDO project. This experimental surface is a gap graded 0/8 with a bitumen mixture modified by the addition of rubber crumb recycled from scrap tires, through the wet process. The reference surface is a part of the pre-existing pavement, a long aged DAC 0/12. Furthermore, after one month a DAC 0/12 surface was laid next to the rubber surface, allowing the evaluation of their different time evolution.
The CPX and SPB methods were applied in six measurement sessions, carrying out a four year long monitoring of the acoustical performances of road surfaces. All LCPX values are calculated at the reference speed of 50 km/h. The rubberized surface installation shows a good spatial homogeneity and the LCPX differential values between rubberized and reference surfaces are significantly constant in time.

On the contrary, the coeval DAC installation does not show a spatial homogeneity and the LCPX value increases significantly in time, reducing the difference with the reference surface. In terms of emission spectrum, no significant shape differences can be highlighted among the three surfaces analyzed. The experimental rubberized installation shows a good stability in time, better than the coeval DAC one, and its efficacy is significantly remarkable.

Beyond the research activity in the LEOPOLDO project, ARPAT within this activity of verifying the respect of noise limits provided by regulations has monitored three rubber surfaces with the CPX method. The four surfaces were laid on urban or extra-urban roads and every one was exposed at high traffic density, but within different kind of Italian weather conditions and climatic areas.
All the surfaces depths here analyzed are between 3 and 5 cm. The first is the previously analyzed, the second is a wet technique 0/12.5 surface, the third is a dry technique 0/6 and the fourth is a 0/12.5 wet. Results are obtained as arithmetic mean of both lanes and are corrected for air temperature.

In terms of absolute values, surface 1 and 4 have the same value of nearly 91.5 dB(A), whereas surface 2 and 3 report different levels, respectively 2.5 dB(A) lower and about 1.0 dB(A) higher. Anyway, in terms of differential values, surface 1 and 2 have a lower sound emission estimated in respectively about .7 and 6.2 dB(A). These results are clearly better than those obtained for the other surfaces, showing differential values lower than 3 dB(A). It needs to be emphasized that a 3 dB(A) value is often the minimum gain expected from a surface used as mitigation action. Same conclusions can be drawn from the results obtained at 80 km/h. The analysis of differential values is determined by the choice of the reference surfaces during the measurement planning.

The frequency analysis is the last way to compare the four surfaces here used. This type of spectrum, also seen in the ISO 1793 series for normalizing the acoustic response of barriers, has the total energy sum always equal to 0 dB. It allows to compare different emission energy spectra (here in 1/3 octave bands) in order to identify the specific frequency behaviors. All surfaces show a spectral peak at 1000 Hz, with the same relative intensity. The only shape details noteworthy are the secondary spectral peak at 2000 Hz shown by surfaces 1 and 2, and the low frequency levels (500–630 Hz) of surface 2 being higher than other surfaces. The secondary spectral peak for surface 1 and 2 have no

remarkable effect on the LCPX values because levels at 2000 Hz are 4 dB(A) lower than the 1000 Hz ones and slightly influences the overall level.

On the contrary, a shifting energy towards low frequencies produces a significantly lower overall level, through to the A-weighing. Surely, this is one of the reasons for the good performance of surface 2. Anyway the frequency analysis is not able to justify the differences among the surfaces.

The paper ends with a remark on the fact that the rubberized surface solution can represent a very efficient and well adaptable mitigation action, especially in an urban context where other solutions cannot be applied (i.e. barriers, flow control or open-graded surfaces).

Chapter 3

Materials characterization

3.1 Mixtures characterization

The aim of this preliminary characterization was to determine the mechanical properties of the mixtures. Different physical ad mechanical tests were carried out. A proper mix design of the mixtures did not take place.

The mixtures composition in terms of grading curve, bitumen content and rubber content was in fact decided a priori following an agreement between the different parts involved, i.e. bitumen producer, University of Bologna, asphalt mixture producer and paver and finally rubber supplier. The composition was also based on a literature review and previous experiences.

Three different mixtures were established for the analysis and subsequent laying at the Zola Predosa site. They are composed as follows:

- SMA 0/8 mm FF: 6.6% by weight of aggregates modified bitumen + 0.3% fibres, referred as SMA or SMA 0;
- SMA 0/8 mm 0.75 CR: bit.mod. 7.5% by weight of aggregates modified bitumen + 0.75% by weight of aggregates of < 420 µm crumb rubber, referred as SMA 0.75;
- SMA 0/8 mm 0.75 CR: bit.mod. 8.5% by weight of aggregates modified bitumen + 1.20% by weight of aggregates of < 420 µm crumb rubber, referred as SMA 1.20.

Figure 3.1 shows the grading curves of the three mixtures.

Table 3.1 resumes the composition of the blends under investigation.

The adding of bitumen and rubber leads to a reduction in the bulk density of the specimens, which passed from 2.387 for the SMA 0, to 2.349 for the SMA 0.75 and to 2.316 for the SMA 1.20.

The mixtures were compacted following the Marshall procedures with 25, 50 and 75 blows each side. Residual voids and bulk densities are shown in Table 3.2. The residual voids of standard and rubberized SMA are clearly different, especially at few blows of compaction.

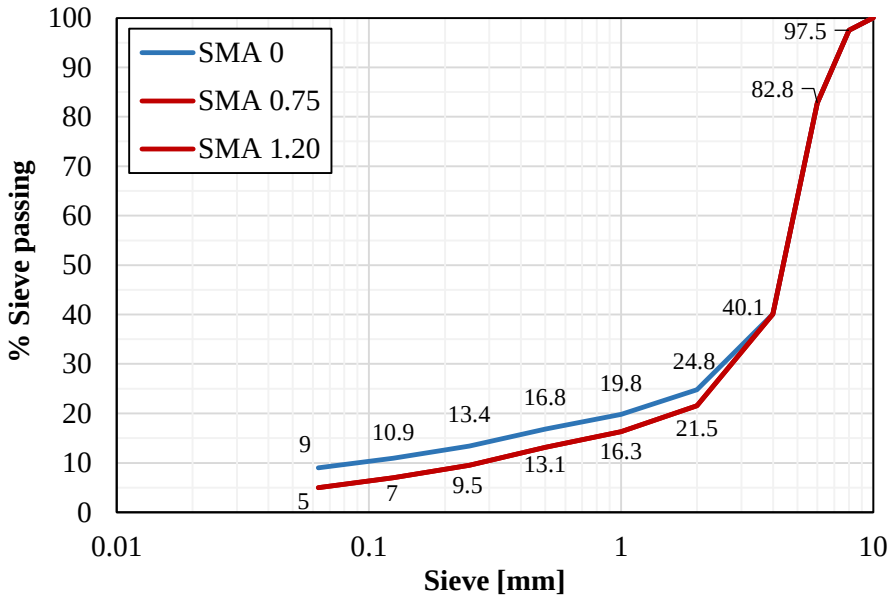

Figure 3.1: Grading curves of the mixtures

Following tests were conducted on samples compacted at 50 blows each side.

Physical characteristics	EN Standard	U.M.	SMA 0	SMA 0.75	SMA 1.20
Bitumen by aggregate weight		%	6.6	7.5	8.5
Rubber by aggregate weight		%	0	0.75	1.20
Fibers by aggregate weight		%	0.3	\	\
bulk density of aggregates and rubber	1097-6	kg/dm^3	2.614	2.599	2.591
bulk density of asphalt concrete	12697-5	kg/dm^3	2.387	2.349	2.316

Table 3.1: Physical characteristics of asphalt mixtures

Table 3.3 summarizes the results of water damage and cantabro tests. The SMA 0.75 exhibits the greater water damage while the SMA 0 shows the best resistance with a 93.4% according to 12697-12.

Volumetric properties	U.M.	SMA 0	SMA 0.75	SMA 1.20
Blow each side		50	50	50
Bulk density of the compacted sample	kg/dm^3	2.227	2.207	2.231
Residual voids	%	3.4	6.1	5.0
Voids in the mineral aggregate VMA	%	18.8	21.0	20.1
Voids filled with bitumen VFB	%	81.7	71.2	75.0
Blow each side		75	75	75
Residual voids	%	2.0	4.9	4.4
Blow each side		25	25	25
Residual voids	%	5.1	6.3	5.9

Table 3.2: Volumetric properties after Marshall compaction

Physical characteristics	EN Standard	U.M.	SMA 0	SMA 0.75	SMA 1.20
Water damage	12697-12	%	93.4	85.7	89.2
Cantabro after water damage	12697-17	%	4.3	5.1	3.4

Table 3.3: Water damage and Cantabro tests

Results of Marshall tests are reported in Table 3.4. Also here, SMA 0.75 shows the lower stability compared to the similar value of SMA 0 and SMA 1.20. The same applies for flow and stability.

Marshall test	U.M.	SMA	SMA 0.75	SMA 1.20
Stability	kN	11.16	9.51	11.07
Flow	mm	3.90	3.65	3.99
Marshall Quotient	kN/mm	2.86	2.60	2.78

Table 3.4: Marshall properties after 50 blows

Results of Indirect tension test according to EN 12697-23 are shown in Table 3.5. SMA 0 exhibits the higher IT strength as well as IT coefficient. While SMA 1.20 IT strength is similar to that of SMA 0, its IT coefficient is closer to that of SMA 0.75.

Mechanical characteristics	**U.M.**	**SMA**	**SMA 0.75**	**SMA 1.20**
Indirect Tensile Strength	MPa	1.32	1.14	1.25
Indirect Tensile coefficient	MPa	106.8	92.2	89.1
Compression strain		0.0194	0.0194	0.0220
Tensile strain		0.0027	0.0029	0.0036

Table 3.5: Indirect tensile results on Marshall specimens at 60°C

Results of Indirect tensile stiffness modulus test according to EN 12697-26 are shown in Table 3.6. Tests were carried out at 5, 20 and 35 °C on three specimens each mixture. The average value is reported in Table 4.7. SMA 0 exhibits the higher ITSM over the three temperatures. A lower ITSM of the rubberized mixtures is in line with the expectations. Notwithstanding, ITSM are always greater than 4,000 MPa at 20 °C. Conversely, it is not the SMA 1.20 but the SMA 0.75 having the smallest ITSM, with an exception at the 5°C.

ITSM (MPa)	SMA 0			SMA 0.75			SMA 1.20		
Sample no.	*1*	*2*	*3*	*1*	*2*	*3*	*1*	*2*	*3*
5°C	13133	13305	13975	11306	12794	12267	11757	11647	11405
20°C	5626	5279	5909	4104	4184	3721	4879	4245	4473
35C°	1365	1162	1354	991	938	787	1122	1099	1046

Table 3.6: ITSM results on Marshall specimens at different temperatures

ITSM (MPa)	**5°C**	**20°C**	**35°C**
SMA 0	13471	5605	1294
SMA 0.75	12122	4003	905
SMA 1.20	11603	4532	1089

Table 3.7: ITSM results on Marshall specimens at different temperatures

3.2 Quality acceptance controls: mechanical characterization

While the mixtures were being laid at the Zola Predosa trial site, which will be explained in Chapter 5, tins of asphalts were sampled for the quality acceptance controls, as shown in Figure 3.2.

Figure 3.2: Sampling of material during the laying

The laboratories of Valli Zabban, i.e. the bitumen supplier, and of the University of Bologna carried out the mechanical characterization on the sampled asphalts.

Figure 3.3 shows the comparison between the designed and the sampled grading curves, according to EN 12697-1. The sampled grading curves were found to be in line with the design.

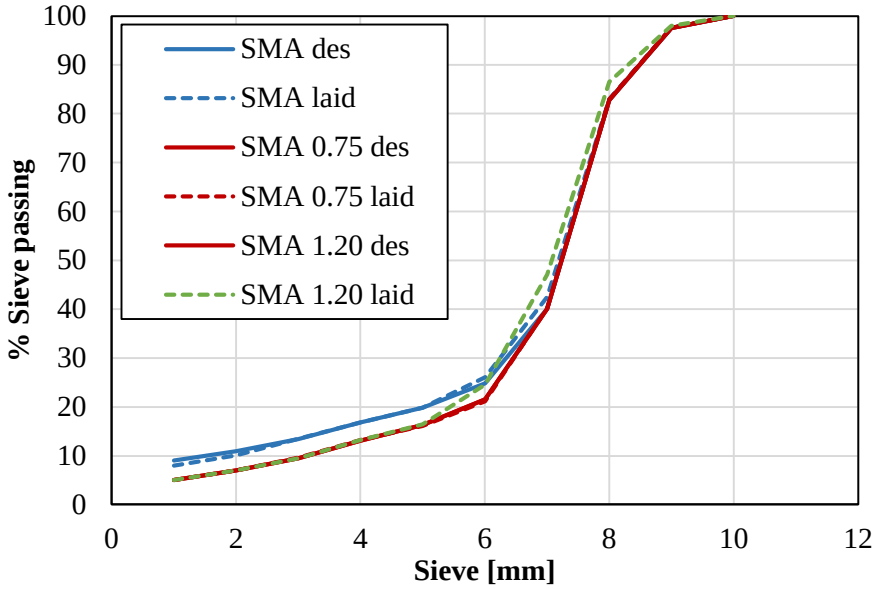

Figure 3.3: Designed and sampled grading curves

Table 3.8 shows the physical properties of the sampled asphalts.

Table 3.9 reports the results of the Marshall compaction on the sampled mixtures, according to EN 12697-30.

Physical characteristics	EN Standard	U.M.	SMA 0	SMA 0.75	SMA 1.20
Bitumen by aggregate weight		%	6.55	7.51	8.53
Rubber by aggregate weight		%	0	0.75	1.20
bulk density of aggregates	1097-6	kg/dm^3	2.617	2.599	2.575
bulk density of asphalt concrete	12697-5	kg/dm^3	2.394	2.353	2.308

Table 3.8: Physical characteristics of asphalt mixtures

Volumetric properties	U.M.	SMA 0	SMA 0.75	SMA 1.20
Compaction temperature	°C	145	160	150
Blow each side		50	50	50
bulk density of the compacted sample	kg/dm^3	2.231	2.157	2.183
Residual voids	%	6.8	8.3	5.4
Voids in the mineral aggregate VMA	%	20.0	22.8	21.9
Voids filled with bitumen VFB	%	66.0	63.6	75.4

Table 3.9: Volumetric properties after Marshall compaction

The comparison of these results with those of the design described in the 3.1 paragraph highlights a substantial consistence of the data.

Table 3.10 shows the results of the Marshall test, according to EN 12697-34, on the samples compacted with 50 blows.

Table 3.11 shows the results of the Indirect tensile results on Marshall specimens at 60°C compacted with 50 blows each face.

Terms in brackets refer to the difference with the design values; positive signs indicate a greater value compared to the preliminary analysis.

Marshall test	U.M.	SMA	SMA 0.75	SMA 1.20
Stability	kN	11.50 *(+0.34)*	9.94 *(+0.43)*	10.74 *(-0.33)*
Flow	mm	3.84 *(-0.06)*	3.31 *(-0.34)*	3.69 *(-0.30)*
Marshall Quotient	kN/mm	3.00 *(+0.14)*	3.00 *(+0.40)*	2.92 *(+0.14)*

Table 3.10: Marshall test after 50 blows of compaction

Mechanical characteristics	U.M.	SMA	SMA 0.75	SMA 1.20
Indirect Tensile Strength	MPa	1.38 *(+0.06)*	1.14 *(-)*	1.42 *(+0.17)*
Indirect Tensile coefficient	MPa	106.3 *(-0.5)*	91.0 *(-1.2)*	117.3 *(+28.2)*
Compression strain		0.0204	0.0197	0.0191
Tensile strain		0.0033	0.0020	0.0028
Water sensitivity ITSR	%	93.4	90.7	90.1

Table 3.11: Indirect tensile results on Marshall specimens at 60°C

Differences are negligible for the SMA 0 and the SMA 0.75, while the SMA 1.20 exhibits higher indirect tensile strength and coefficient.

Volumetric properties	U.M.	SMA 0	SMA 0.75	SMA 1.20
Compaction temperature		145	160	150
Number of gyrations		10	10	10
Residual voids	%	15.2	16.2	13.8
Number of gyrations		50	50	50
Residual voids	%	8.0	9.6	7.0
Number of gyrations		130	130	130
Residual voids	%	4.5	6.5	4.1

Table 3.12: Volumetric properties after different compaction gyrations

Besides the Marshall study, the sampled asphalts were compacted through a gyratory compactor for a volumetric investigation, in accordance with EN 12697-31. The mixtures were compacted at 10, 50 and 130 gyrations and the results are shown in Table 3.13.

Table 3.13 shows the Indirect tensile results on these samples compacted at 130 gyrations.

Mechanical characteristics	U.M.	SMA	SMA 0.75	SMA 1.20
Indirect Tensile Strength Rt	MPa	1.41	1.27	1.41
Indirect Tensile coefficient CTI	MPa	100.9	83.2	91.7
Compression strain		0.0219	0.0239	0.0241
Tensile strain		0.0034	0.0032	0.0029

Table 3.13: Indirect tensile test on gyratory compacted samples at 25°C

Results show an essential uniformity between the Marshall and the gyratory compacted samples, in terms of ITS. The gaps are 0.03, 0.13 and 0.01 MPa for SMA, SMA 0.75 and SMA 1.20 respectively.

Finally, indirect tensile stiffness modulus ITSM, in accordance with EN 12697-26, was determined. Results are shown in Table 3.14. Results demonstrates that the laid mixtures exhibit greater ITSM values compared to those of the preliminary study. Remarkable is that the ITSM of the rubberized mixtures appear to be less sensitive to the temperature change, especially the SMA 1.20.

ITSM [MPa]	Temperature test		
	5°	20°	35°
SMA	20011	10860	3121
SMA 0.75	16108	7091	1842
SMA 1.20	14462	6890	2013

Table 3.14: Average ITSM

Chapter 4

The trial site

4.1 Trial site description

The experimental laying of the three SMA mixtures was carried out on a 300 m in a city centre road stretch of the Zola Predosa city council, province of Bologna. A single carriageway in two-way traffic composes the road, which adjoins the railway on a side and the block on the other. The maintenance intervention of the surface course was carried out on both lanes with the laying of 4 cm of SMAs. The classic SMA mixture was laid on the lane in the direction of Bologna, while the rubberized mixtures were laid on the opposite lane in the direction of Modena, for a length of 150 m each. The laying took place in the 31th of July 2014. The paving operations lasted for around 2 hours for each stretch.

Figure 4.1: Aerial view and location of the trial site in Zola Predosa

The air temperature ranged from 23.2 °C to 26.3 °C during the paving with standard asphalt, with a maximum wind speed of 4.8 km/h, and from 27.7°C to 29.5°C degree during the placement of rubberized asphalt, with a maximum wind speed of 9.7 km/h.

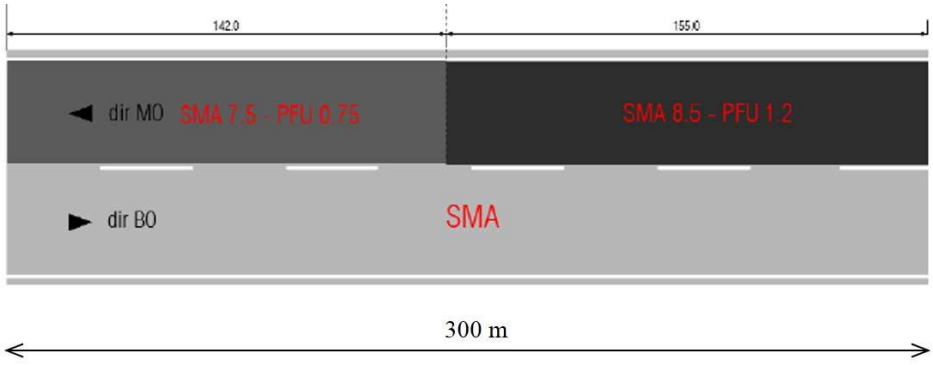

Figure 4.2: Plant of the experimental site

Figure 4.3: Laying and compaction phases of the SMA

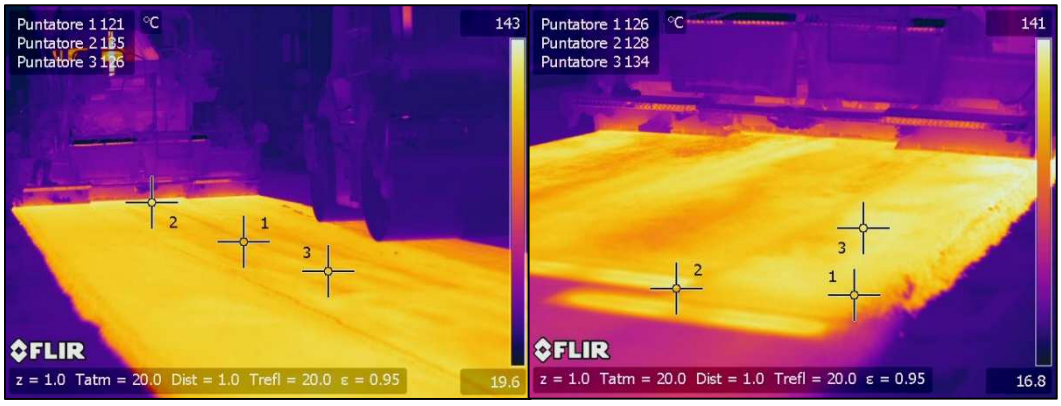

Figure 4.4: Temperature verification during laying: no rubber on the left, with rubber on the right

The laying took place following traditional technologies for Hot Mix Asphalt and the mixtures were wax-modified in order to reduce the working temperatures. An infrared camera FLIR was used to monitor the temperatures during this phase, as shown in Figure

5.4 in which it is possible to observe that just before compaction a maximum of 135°C was registered close to the paver screed. The monitored laying temperatures were very similar and nearly around 125÷130°C, which is ideal for Warm Mix Asphalts.

4.2 Environmental surveys

4.2.1 Polycyclic aromatic hydrocarbons (PAHs)

According to the Agency for Toxic Substances and Disease Registry (ATSDR), PAHs are a group of chemicals that are formed during the incomplete burning of coal, oil, gas, wood, garbage, or other organic substances, such as tobacco and charbroiled meat. There are more than 100 different PAHs. PAHs generally occur as complex mixtures (for example, as part of combustion products such as soot), not as single compounds.

To learn more about the significance of PAHs in the environment, enormous efforts have been devoted to quantifying the level of emissions, assessing ambient concentrations, characterizing speciation, and determining temporal/spatial trends. Currently, there is broad agreement on the main emission sources but harmonization of emission estimation and reporting is still at an early stage of development. Data from a number of occupational health studies suggest that there is an association between lung cancer and exposure to PAH compounds.
The most important exposure route for lung cancer would appear to be via inhalation. Several PAHs have been acknowledged as probable or possible human carcinogens, most of which are known to be associated with airborne particles. BaP, a probable human carcinogen found in appreciable concentrations in the atmosphere, can be used as a marker of the carcinogenic risk of airborne PAH (K.-H. Kim et al., 2013).

Concise International Chemical Assessment Documents (CICADs) are similar to Environmental Health Criteria (EHC) documents in providing internationally accepted reviews on the effects on human health and the environment of chemicals or combinations of chemicals. They aim to characterize the hazard and dose-response of exposure to chemicals and to provide examples of exposure estimation and risk characterisations for application at the national or local level. Among them, the document no. 59 deals with the asphalt, in other words the bitumen. It was published under the joint sponsorship of the United Nations Environment Programme, the International Labour Organization, and

the World Health Organization, and produced within the framework of the Inter-Organization Programme for the Sound Management of Chemicals. This section is a short summarize of this work, in order to introduce the analysis carried out at the Zola Predosa site.

The following can be found in this report:

"Asphalt (CAS No. 8052-42-4), more commonly referred to as bitumen in Europe, is a dark brown to black, cement-like semisolid or solid or viscous liquid produced by the non-destructive distillation of crude oil during petroleum refining. Oxidized asphalt (CAS No. 64742-93-4), also called air-blown or air-refined asphalt, is asphalt (CAS No. 8052-42-4) that has been treated by blowing air through it at elevated temperatures to produce physical properties required for the industrial use of the final product. Performance specifications (e.g., paving asphalts and roofing asphalts), not chemical composition, direct asphalt production.

The exact chemical composition of asphalt is dependent on the chemical complexity of the original crude petroleum and the manufacturing process. Crude petroleum consists mainly of aliphatic compounds, cyclic alkanes, aromatic hydrocarbons, polycyclic aromatic compounds (PACs), and metals (e.g., iron, nickel, and vanadium). The proportions of these chemicals can vary greatly because of significant differences in crude petroleum from oil field to oil field or even at different locations in the same oil field.

While the manufacturing process may change the physical properties of asphalt dramatically, the chemical nature of the asphalt does not change unless thermal cracking occurs. Raising the temperature will increase the likelihood of cracking and cause more volatiles and even higher-boiling components to be released from the residuum.

Although no two asphalts are chemically identical and chemical analysis cannot be used to define the exact chemical structure or chemical composition of asphalt, elemental analyses indicate that most asphalts contain 79÷88% by weight carbon, 7÷13% hydrogen, traces to 8% sulphur, 2÷8% oxygen, and traces to 3% nitrogen.

When asphalts are heated, vapours are released; as these vapours cool, they condense. As such, these vapours are enriched in the more volatile components present in the asphalt and would be expected to be chemically and potentially toxicologically distinct from the

parent material. Asphalt fumes are the cloud of small particles created by condensation from the gaseous state after volatilization of asphalt.

However, because the components in the vapour do not condense all at once, workers are exposed not only to asphalt fumes but also to vapours. The physical nature of the fumes and vapours has not been well characterized. Nevertheless, a chemical analysis of oxidized roofing asphalt and non-oxidized paving asphalt fumes identified many of the same chemical classes. In addition, differences in the way in which asphalts are handled during paving and roofing operations probably influence the composition of asphalt fumes and vapours.

Since the compositions of asphalts and asphalt fumes and vapours vary depending on temperature, manufacturing process, presence of additives and modifiers, and work practices, it should be no surprise to learn that laboratory-generated asphalt fumes that mimic asphalt fumes in the environment are difficult to produce. Researchers have concluded that temperature, rate of stirring, and pulling versus pushing the collection air all affect the chemical composition of the fumes."

Section 6.2 of the same report deals with the human exposure.

"Data collected between 1994 and 1997 during seven paving surveys conducted in the USA by NIOSH (2000) indicated that, in general, most time weighted average (TWA) personal breathing zone (PBZ) air concentrations for both total particulates (TP) and benzene soluble particles (BSP) were below 0.5 mg/m^3. Geometric mean (GM) full-shift PBZ samples for TP and 0.073 to 0.12 mg/m^3, respectively. However, GM data collected during paving operations in a tunnel in Boston, Massachusetts, USA (Sylvain & Miller, 1996), indicated that PBZ exposures to TP and BSP were about 3 times higher than exposures measured during the seven NIOSH surveys at open-air roadway paving sites (NIOSH, 2000). Personal exposures to TP and BSP ranged from 1.09 to 2.17 mg/m^3 and from 0.30 to 1.26 mg/m^3, respectively (Sylvain & Miller, 1996).

Other studies examined exposures to asphalt not only at road paving sites, but also at hot-mix plants, refineries and terminals, roofing manufacturing plants, and roofing application sites in the USA (Hicks, 1995; Exxon, 1997; Gamble et al., 1999). GM exposures for TP and BSP varied across all industry types: TP ranged from 0.18 to 1.40 mg/m^3 and BSP ranged from 0.05 to 0.27 mg/m^3. Heikkilä et al. (2002) reported GM

exposures for TP from asphalt (described by the author as bitumen fume) of 0.4, 0.5, and 4.1 mg/m^3 for paving operator, screed operator, and manual mastic paver, respectively. Similarly, Burstyn et al. (2000) reported higher GM asphalt fume exposures (described by the author as bitumen) during mastic laying operations (2.29 mg/m^3) compared with exposures during paving operations (0.28 mg/m^3). These values indicate that exposures may be higher in situations such as mastic laying.

Several investigators have attempted to assess asphalt exposure by the dermal route. Wolff et al. (1989) collected dermal wipe samples by wiping a 3 × 3 cm area of the forehead of workers exposed to asphalt during the application of hot asphalt to roofs in order to evaluate the extent to which dermal absorption of polycyclic aromatic hydrocarbons (PAHs) may contribute to the total body burden. These dermal wipe samples were analysed for specific PAHs. In the Wolff et al. (1989) study, PAH residues per square centimetre of skin were higher in postshift samples (6.1–31 ng/cm^2) than in preshift samples (0.44–2.2 ng/cm^2). However, workers monitored during the entire roofing application were potentially exposed to PAHs during both the removal of the old coal tar pitch roof and the application of hot asphalt for the new roof. Hicks (1995) collected dermal wipe samples by wiping a 4 × 8 cm area from the back of the hand or forehead of workers at various asphalt sectors.. The PAH concentrations determined from these postshift samples ranged from 2.2 to 520 ng/cm^2.

Workers in paving operations produced the largest number of PAHs detected (12 of 16), while refinery and roofing workers had the fewest (2 of 16). However, the HPLC/fluorescence technique used by these authors cannot reliably identify and quantify components of asphalt; their results are presented for completeness only. Toraason et al. (2001, 2002) examined urinary 1- OHP concentrations at the beginning and end of the same work week (4 days later) in seven roofers who applied hot asphalt products but had no coal tar exposure during the preceding 3 months. All seven workers were smokers at the time of the study. Urinary 1-OHP concentrations were statistically significantly increased ($P < 0.05$) at the end of the work week (start of work week 0.26 ± 0.13 µmol/mol creatinine; end of work week 0.58 ± 0.29 µmol/mol creatinine). The average weekly TWA exposure for TP and BSP for a crew of six asphalt-only roofers was 0.24 ± 0.10 mg/m3 and 0.08 ± 0.02 mg/m3 ,respectively. The TWA exposures for TP and BSP for a seventh roofer in another crew were 0.31 mg/m3 and 0.18 mg/m3 , respectively.

Heikkilä et al. (2002) measured preshift and postshift urinary 1-OHP concentrations in 32 road pavers participating in a study to evaluate asphalt fume exposures of workers employed at 13 paving sites where 11 different asphalt mixtures were applied. The mean TP exposure for the 11 asphalt mixtures ranged from 0.2 to 4.2 mg/m3 (AM [arithmetic mean] = 0.6 mg/m3 ; GM = 0.5 mg/m3). The mean TP exposure for all mixtures was below 0.5 mg/m3 , with the exception of manual mastic (2.0 mg/m3). The control group consisted of 78 smoking and non-smoking unexposed office workers obtained from a national reference group for 1-OHP in Finland. The authors reported that mean 1-OHP concentrations were statistically significantly higher (P < 0.05) among pavers (AM = 6.6 nmol/litre, standard deviation [SD] =9.8) than in controls (AM = 1.6 nmol/litre, SD = 2.6) and twice as high among pavers who were smokers (preshift: AM = 8.5 nmol/litre, SD = 10.5) as among pavers who were non-smokers (preshift: AM = 4.0 nmol/litre, SD = 8.0) (P < 0.05) (P. Heikkilä, personal communication, Finnish Institute of Occupational Health, Helsinki, 2003). A similar trend was observed in postshift data. There was no difference between non-smoking road pavers or non-smoking referents, suggesting that smoking strongly influences urinary 1-OHP concentrations and may not be a sensitive measure of occupational asphalt fume exposure."

4.2.2 Site survey and results

With the aim of understanding the side effects of the use of crumb rubber into road mixtures and ensure a safe and healthy environment for the workers, emanated emissions and gas were strictly monitored during laying phase.

The monitoring was committed to the company Waste and Chemicals. The data presented in this section is the result of their work, which was published in the report "Worker exposure to pollutants contained in rubberized and non-rubberized asphalt mixtures – survey at the work environment".

The goal of this investigation is the evaluation of the risks associated to the use of the crumb rubber derived from scrap tires in asphalt mixtures, with special regard to the fumes emitted during the laying phase.

The environmental and cutaneous survey presented in this section defines the exposition levels to polycyclic aromatic hydrocarbons (PAH) and dust for the workers of the laying

team having different tasks. Results are reported in terms of pollutants mass (ng) for cubic meter of breathed air (from both high-volume pump for air sampling and personal air sampling pumps) and of pollutants mass (ng) for centimetre square of exposed area (on dermal patch for the cutaneous sampling).

Figure 4.5: Environmental and cutaneous surveys

During the laying of the rubberized and non-rubberized mixtures the same workers were monitored. This allowed to make a reliable comparison of the exposition to emissions generated from the two types of asphalt mixtures under study. A summary of the monitored parameters and workers is made in Table 4.1.

Worker task	Monitored parameter	Road dimension	Asphalt type	Surveying time (hh:min)
Roller	PAH inhalational exposure	4.25m x 300m	Standard SMA	02:00
Screed operator	PAH inhalational exposure			
Paver operator	PAH inhalational exposure dermal exposure	4.25m x 300m	Rubberized SMA	02:15
Paver operator	PAH inhalational exposure dermal exposure			

Table 4.1: Analysed parameters and monitored workers

The laying of the two asphalts type took place the same day one after the other. The laying time of the standard SMA took the same time compared to the laying of the two rubberized

mixtures. In order to ensure a sufficient monitoring time, the rubberized surfaces were monitored as they were one and refers to an average dosage of bitumen and rubber between the two.

Figures 4.6, 4.7, 4.8 and 4.9 report the survey of the concentration of the 11 PAHs regulated by the EU or Italian regulation. The environmental concentration of PAHs resulted in all cases compliant with the Italian regulatory limit of 1ng/n3 of Benzo[a]Pyrene (B(a)P).

The measured environmental concentrations were not different from the background concentrations of PAHs usually observed in other Italian urban areas. The environmental concentration of PAHs resulted, on the average, lower during the paving with rubberized asphalt in comparison with the paving with standard asphalts.

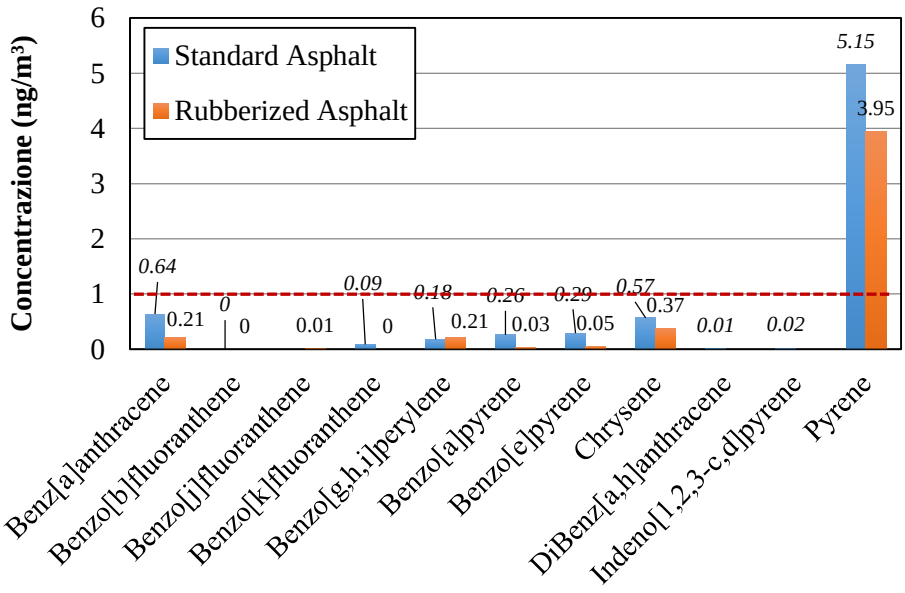

Figure 4.6: Environmental survey – PAHs

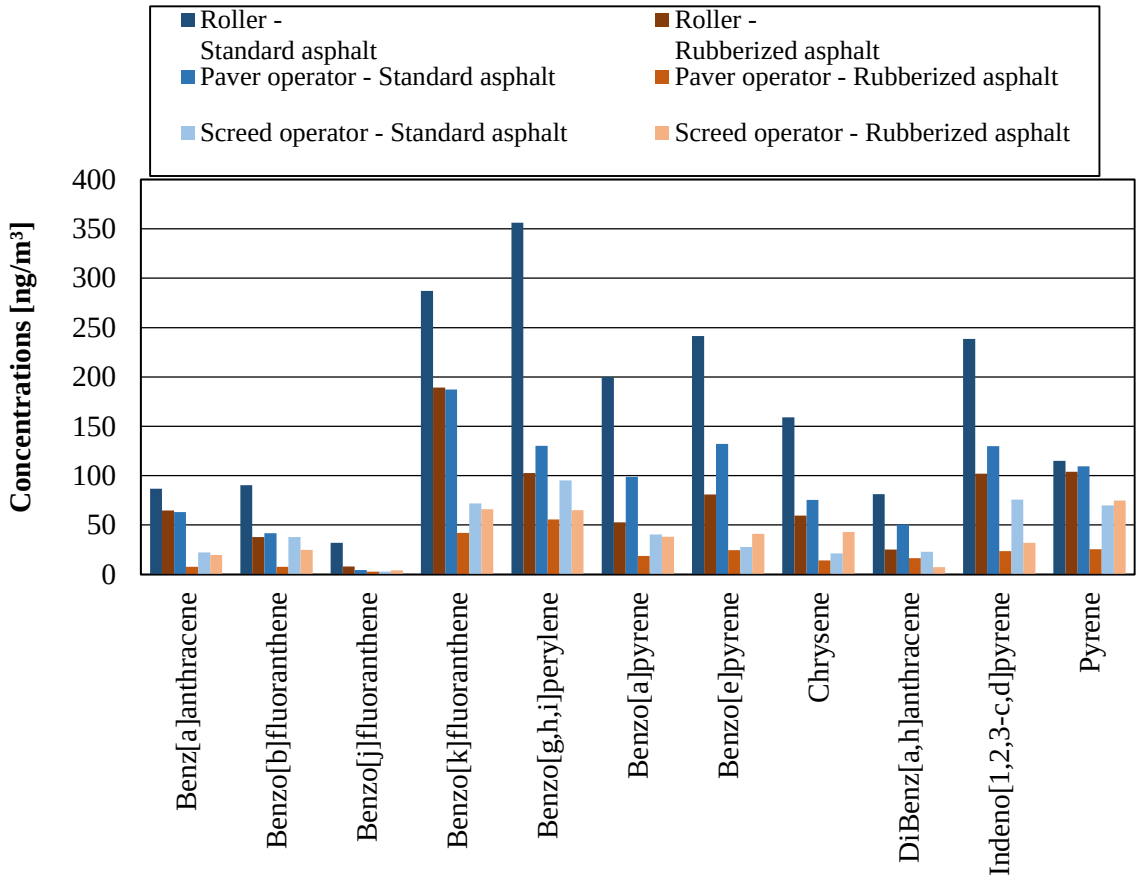

Figure 4.7: PAHs concentration survey for workers

Figure 4.7 shows the exposure to PAHs inhalation for the workers.

Pavers are exposed to higher concentration of PAHs when standard asphalt is placed, in comparison with rubberized asphalt. In this case the difference is not significant.

Screedmen are exposed to significantly higher concentration of PAHs when standard asphalt is placed, in comparison with rubberized asphalt.

Rollers are exposed to significantly higher concentration of PAHs when standard asphalt is placed, in comparison with rubberized asphalt.

Regardless to the type of asphalt placed rollers and screedmen resulted exposed to higher concentration of PAHs compared to the pavers.

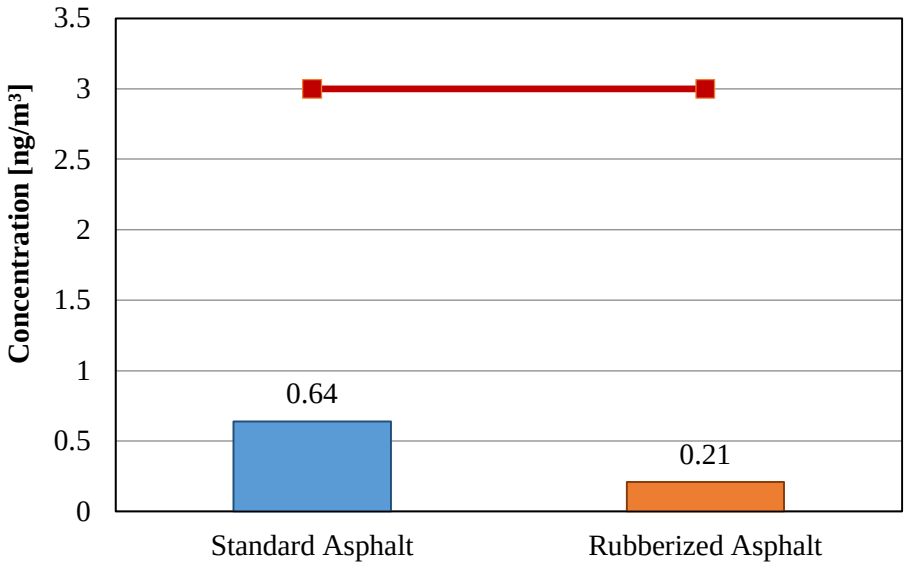

Figure 4.8: Breathable dust survey for workers

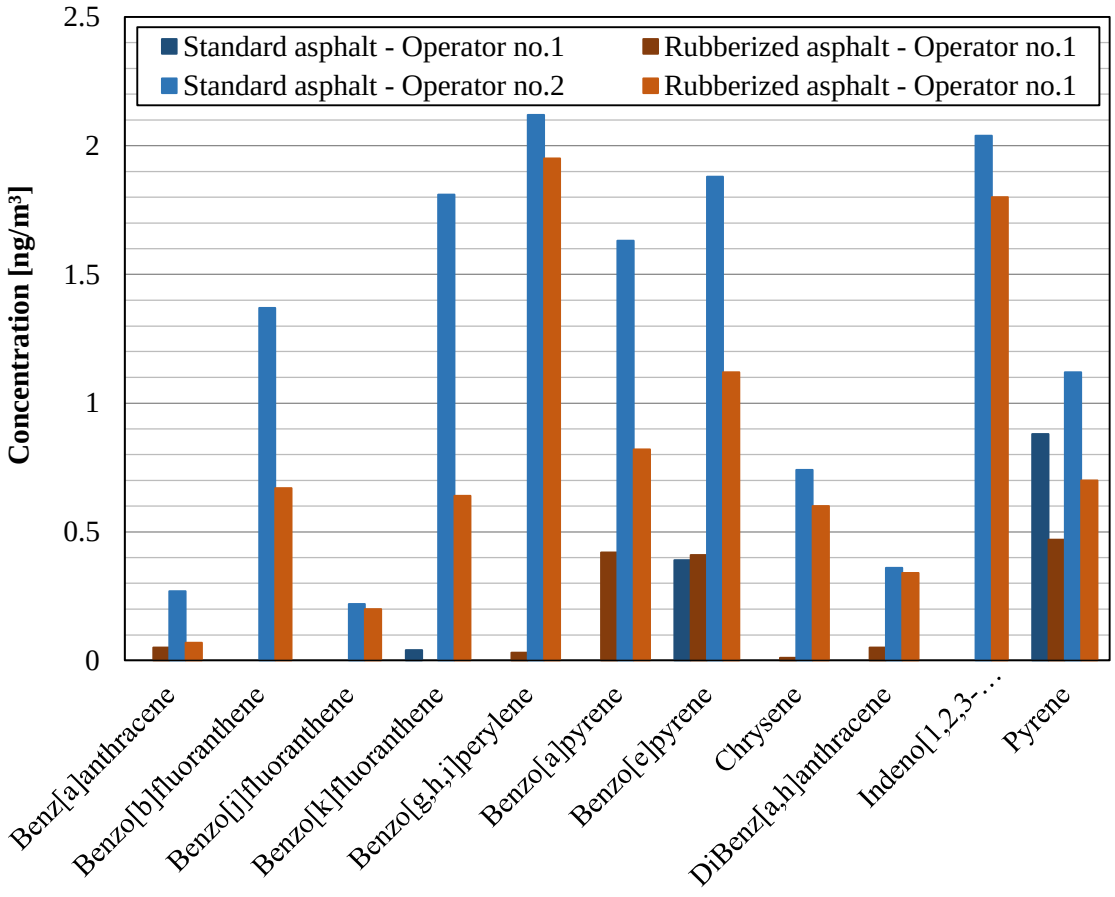

Figure 4.9: PAHs measured with dermal patch applied on workers

With regard to the dermal pads data the highest exposed worker the screedmen undergo to a significantly higher dermal exposure to PAHs when standard asphalt is placed, in comparison with rubberized asphalt.

Based on the outcome of the monitoring activities, the use of rubberized asphalt resulted in a significant, though slight reduction of the incremental carcinogenic risk for workers. Given the single trial site, is not possible to prove that the observed benefit has to be associated to site-specific conditions rather than to an actual reduction of the release of PAHs from rubberized asphalts. It is necessary to underline that these benefits could derive from the use of warm mix asphalts that lowered the laying temperatures.

Chapter 5

Site surveys

5.1 Noise measurements

5.1.1 Test method

This section presents the test methods for noise measurements derived from tyre / pavement interaction. The adopted method is based on the Close Proximity Index, stadardized in CPX ISO / DIS 11819-2.
The sound pressure signal is acquired by the use of two microphones mounted in the vicinity of the right rear tyre (185 R15 / 60), driving the vehicle at various constant speeds on the pavement under investigation. The particular position of the microphones is sufficient condition for considering the noise coming from the tyre / pavement interaction as dominant, and considering negligible other vehicle's noise sources like engine, mechanical system and the exhaust pipe. A particular encoder applied to the left rear wheel allows to acquire the space travelled and therefore the instantaneous speed.

During data processing, the space signal path is analysed so as to divide the signals acquired according to a spatial basis equal to about 5.90 m (section defined as a length equal to 3 times the circumference of the measuring tyre). The sound pressure signals are then processed in order to be associated with each section of the spectrum in third octave bands in the range 315 - 5000 Hz. The broadband level weighted A, LCPX is finally obtained as appropriately weighted sum of energy levels of the spectrum in third octave bands.

Therefore, each measure is associated to the speed values, the spectrum in terms of third octave bands and LCPX, to each section of the covered pavement.
In order to increase the statistical robustness of the results, different acquisitions were made by altering the traveling speed. Data are used to calculate a linear regression with the minimum chi-square method, based on the known relationship, which links the sound levels to the traveling speed (logarithmic relationship). Linear regression of the data returns as a result the values of LCPX and spectrum in third octave bands calculated for

the reference speed 50 km / h and 80 km / h provided by the standard , with their associated uncertainties, for each section.

In order to characterize the investigated pavements the average values on the entire measured sections of LCPX and of the band levels in the third octave are calculated. The statistical uncertainty associated component is equal to the variance of the levels and thus appears to be a measure of the homogeneity of the audited stretched.

The measurement technique is influenced by the measuring conditions, with special regard to the temperature and humidity of the air and of the pavement, in addition to the instrumental uncertainties of calibration and acquisition. For these reasons, it is preferable to apply a differential criterion and evaluate the acoustic performance of pavements in relative terms to a reference pavement, measured on the same campaign. This method allows making comparisons between the results obtained in different time sessions, in order to evaluate the evolution of the performances, reducing the influence of the boundary conditions.

5.1.2 Results

This section discusses the results of the noise measurements based on the Close Proximity Index (CPX ISO/DIS 11819-2), carried out during three different surveys, i.e. October 2014, April 2015 and October 2015. The goal is to determine the acoustic properties of the rubberized pavements compared to the standard one. I-POOL, a spin-off company of the Italian National Research Council (CNR) was appointed to perform the measurements and examine the data that will be shown hereafter.

Results are shown in Figure 5.1, 5.2 and 5.3 in terms of absolute LCPX values at 50 km/h for the reference SMA 0, SMA 0.75 and SMA 1.20 respectively. All data were adjusted to take into account the temperature, as prescribed by the ISO standard.

Figures 5.4, 5.5 and 5.6 plot the emission spectra obtained at 50 km/h for the reference SMA 0, SMA 0.75 and SMA 1.20 respectively.

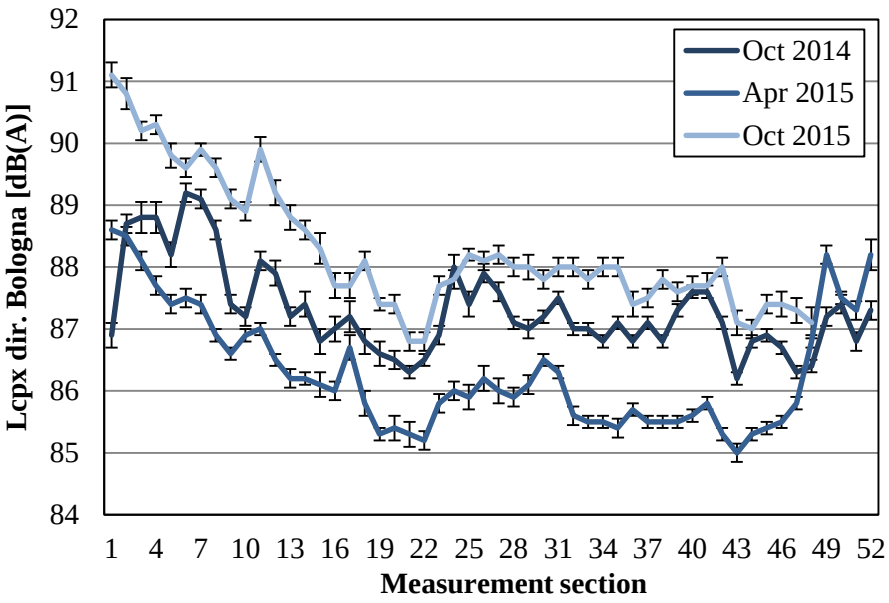

Figure 5.1: Lcpx dir. Bologna measured at 50 Km/h for SMA 0

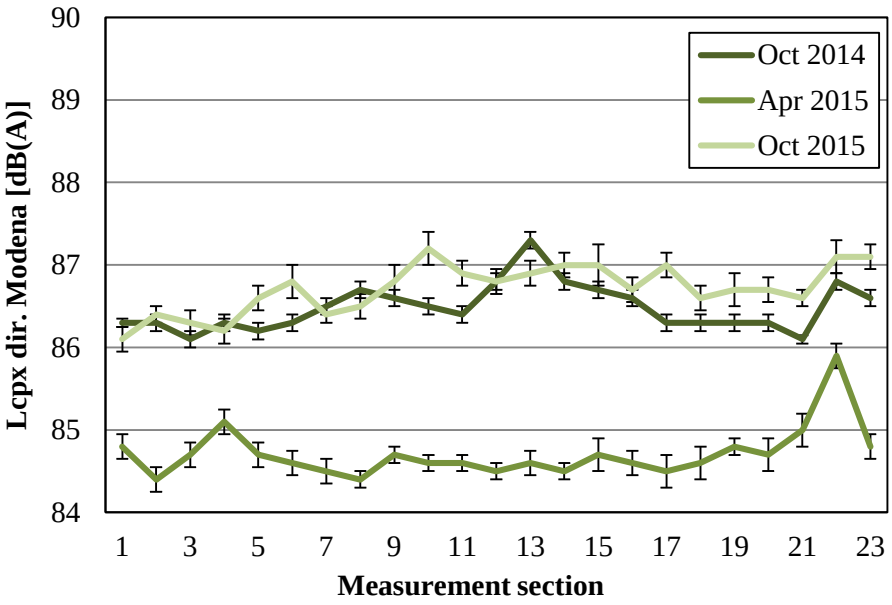

Figure 5.2: Lcpx dir. Modena measured at 50 Km/h for SMA 0.75

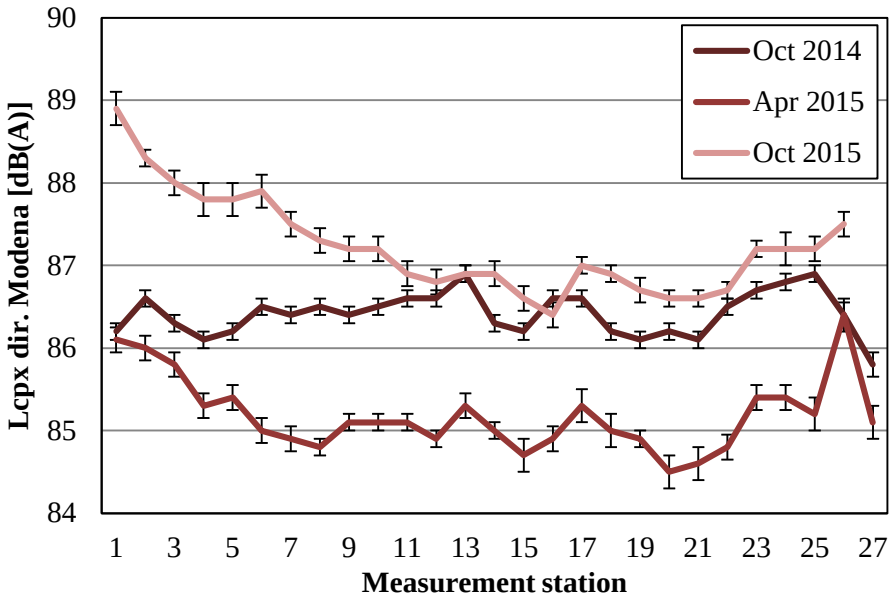

Figure 5.3: Lcpx dir. Modena measured at 50 Km/h for SMA 1.20

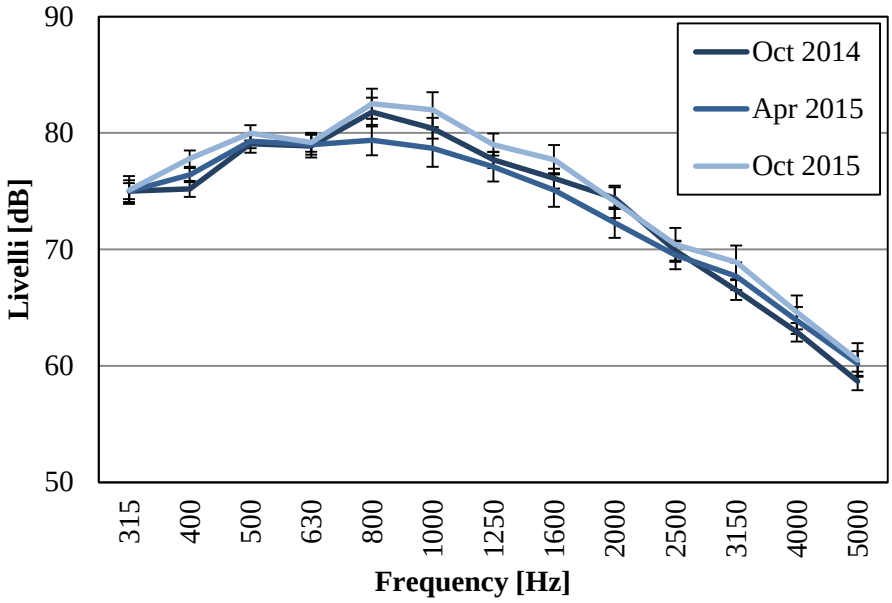

Figure 5.4: Emission spectra for SMA 0.00

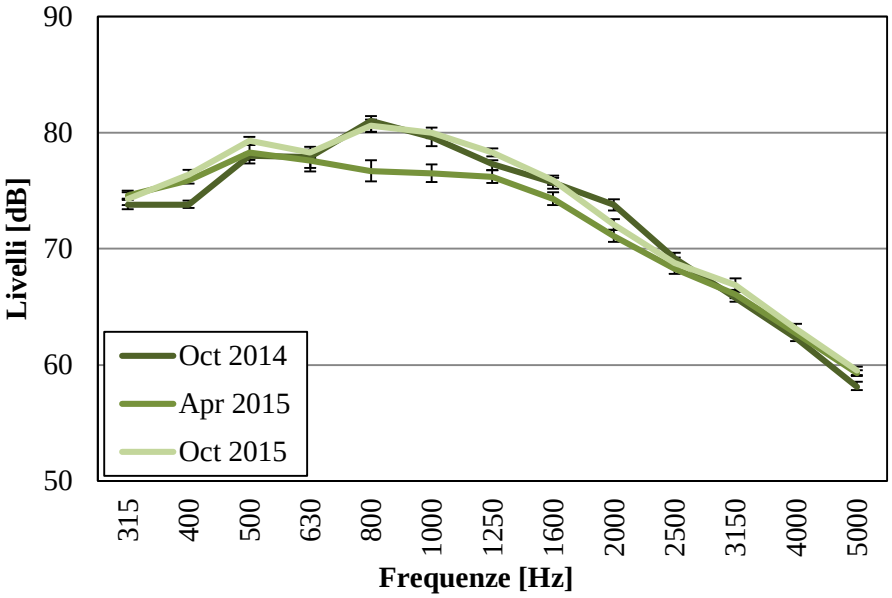

Figure 5.5: Emission spectra for SMA 0.75

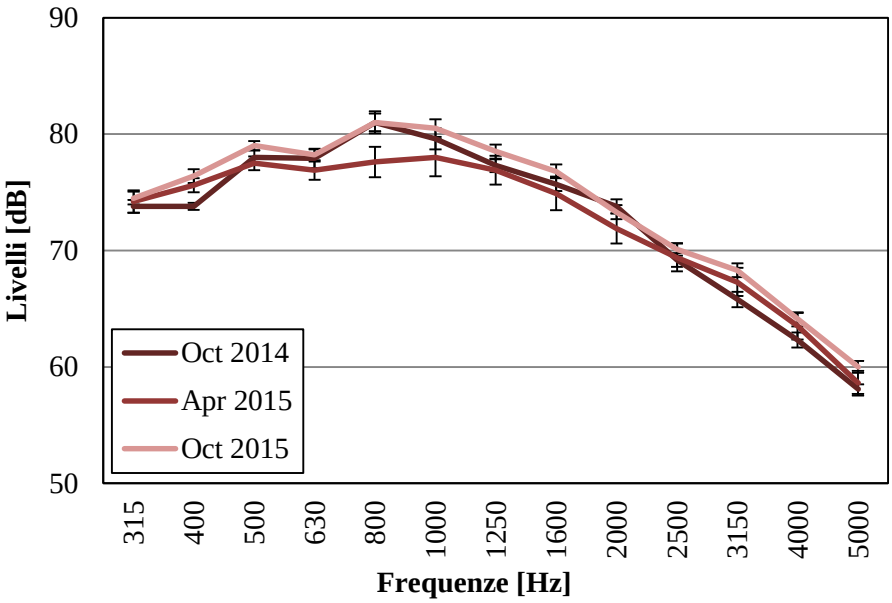

Figure 5.6: Emission spectra for SMA 1.20

Figures 5.7, 5.8 and 5.9 plot the Lcpx evolution, in terms of dB(A), over the different surveys for the three surfaces under investigation at 40 km/h, 50 km/h and 80 km/h respectively. As expected, the registered noise is directly proportional to the speed of measurement.

Figures 5.10 and 5.11 plots shows the differences between the rubberized pavements and the standard SMA pavement at different measuring speeds.

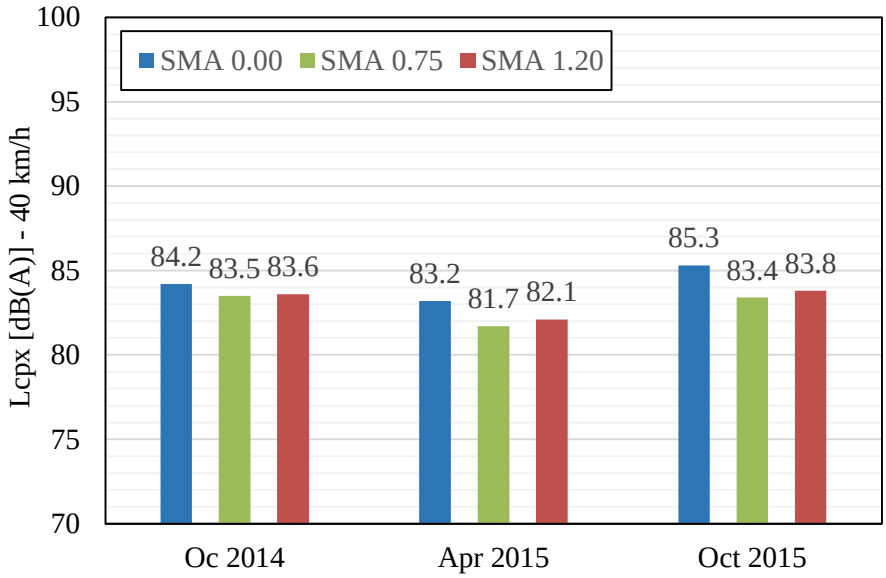

Figure 5.7: Evolution of the average Lcpx measured at 40 km/h

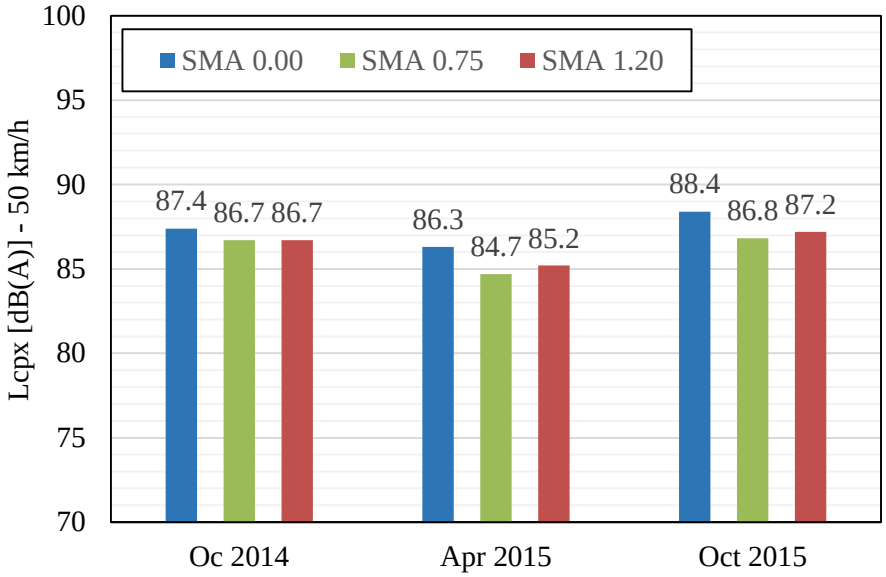

Figure 5.8: Evolution of the average Lcpx measured at 50 km/h

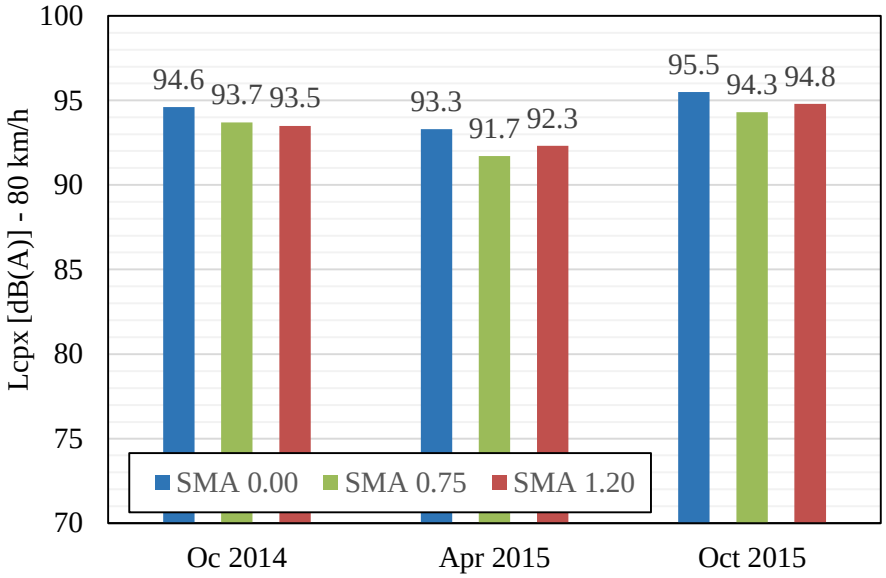

Figure 5.9: Evolution of the average Lcpx measured at 80 km/h

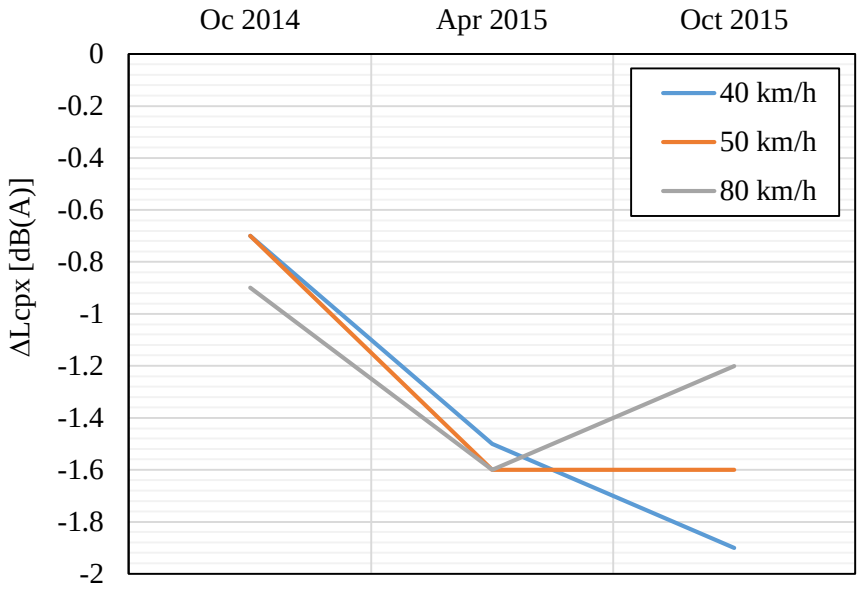

Figure 5.10: Difference between Lcpx of 0.75 SMA and SMA 0.00

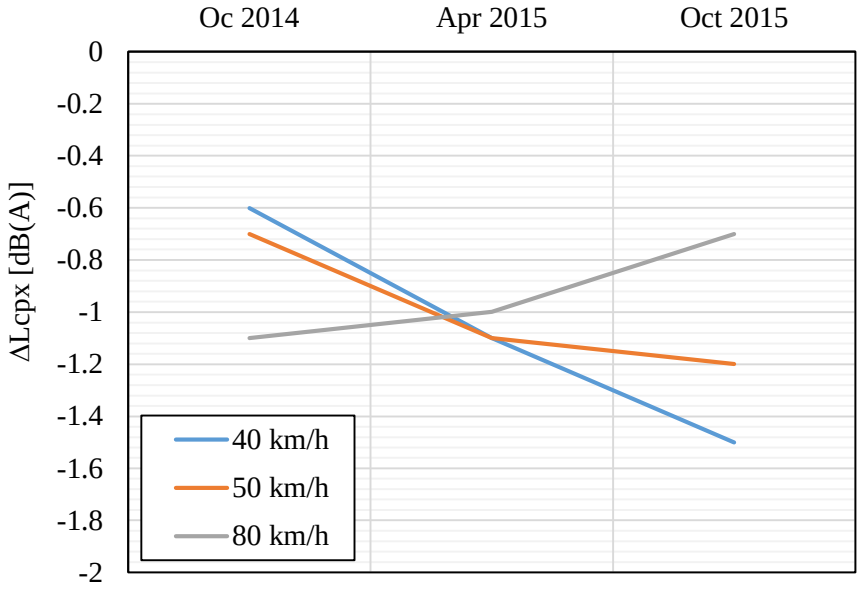

Figure 5.11: Difference between Lcpx of 1.20 SMA and SMA 0.00

After the analysis of the results of the measurement sessions, it is concluded that both pavings containing rubber offer an increasing acoustic benefit over the time in terms of reduced emission of tyre rolling noise compared to the standard SMA pavement taken as the reference.

It should be noted that the reference pavement shows a high spatial variability of the noise levels, which could result from unevenesses and imperfections at the time of laying. Therefore, the uncertainty associated with the average value is high and this is reflected negatively on the uncertainty associated with the differential values calculated for the two rubberized pavements.

This evidence highlights that the acoustic performance of a pavement heavily depends not only on the quality of the materials, but also by the construction method. A spatial dishomogeneity was also found for the rubberized pavements, with the pavement SMA 1.20 presenting higher levels in the initial sections (considering the direction of travel).

The absolute values of LCPX can not be used for a direct comparison between the measurement sessions, as during the first was used a tyre with wearing and hardness levels next to the limits imposed by technical standard, which was replaced with a new tyre for subsequent sessions. Indeed, lower levels of hardness and wearing of the tyre are linked to smaller rolling noise, in accordance to the smaller sound levels found in the second measurement session compared to the first.

The sound levels of the last measurement session are higher for all the investigated pavements, according to the normal evolution of the road pavements in the first year of service. In any case, the two rubberized mixtures exhibits LCPX levels at 50 km/h of 87 dB(A), which is significantly lower than the 93-94 dB(A) of the in service pavements.

5.2 Texture and skid resistance

This section will discuss the results of the measurement of texture and skid resistance on the trial site of Zola Predosa. Both local and continuous measurement were carried out. While the dynamic advanced measurements with Skiddometer and Profilometer covered the entire paved surface, the static measurements of macrotexture and skid resistance were performed at intervals of about 12 ÷ 13 meters for 20 measuring points on each lane, as shown in Figure 5.13. Tests were performed exclusively in the odd points (1 - 19) in the standard SMA lane, while in the rubberized lane tests were performed on each station (referred to as G).

5.2.1 Static measurements

This section presents the results of the skid resistance and the macrotexture investigations at the locations described in Figure 5.13. They consist of ten measurement points each surface. The macrotexture was determined in accordance with EN 13036-1 prior to the measurement of the skid resistance in accordance with EN 13036-4, which requires water.

Figure 5.12: BPN measured at different locations during the surveys for SMA 0

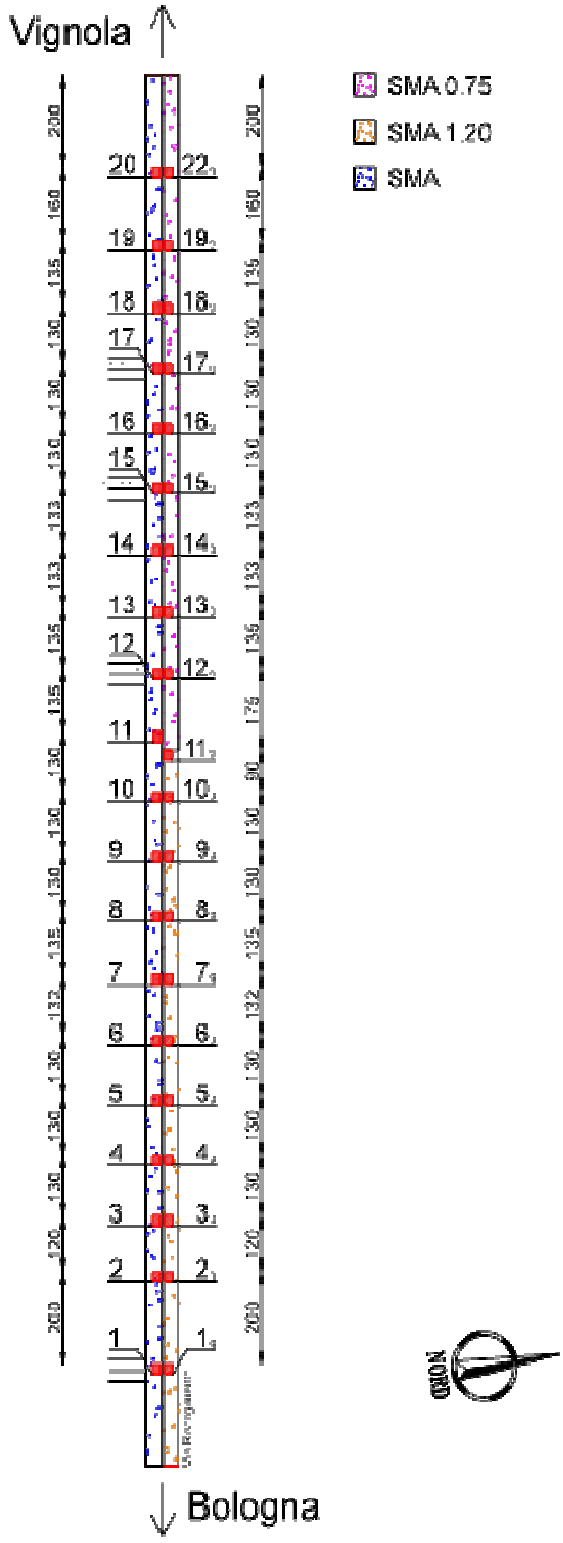

Figure 5.13: Position of the measuring section for the static measurements

5.2.1.1 Skid resistance

This section discusses the PTV values obtained at the different measurement locations, following the numbering indicated in Figure 5.13. Comparisons between the materials and during the surveys will be made, in order to assess the skid resistance during time. For the evaluation of the eligible values of BPN / PTV, different specifications, technical guidelines, scientific papers were taken as reference.

The technical guideline for bituminous pavements of the Province of Bolzano specifies for SMA the following:

"In the period between 6 and 12 months from completion of the paving, the skid resistance must be assessed through a Skid Tester, according to CNR 105/85. Alternatively, the SFC, with the SCRIM equipment according to CNR 147/92, can be determined.
Values of BPN lesser than 60, or alternatively SFC values lesser than 0.60, will result in penalties of 1% of the price for every point of deviation.
Values of BPN lesser than 50, or alternatively SFC values lesser than 0.50, will result in the removal of the layer and the subsequent reconstruction at the Company's expenses..."

The Office for design and execution of road works, Province of Turin specifies for hot mix asphalts made with modified bitumen:

"For the wearing course the skid resistance, measured with the Skid Tester in accordance with EN 13036-4 must provide BPN values equal or greater than 60; the MTD, determined according to EN 13036-1, must be greater than or equal to 0.4 mm. If the average value of BPN or MTD, in a determined section is inferior than the prescribed values, a penalty of the 15% is applied.
If the average value of BPN or MTD is less than or equal to 40 and 0.25 respectively, the layer must be removed completely and a new layer has to be laid. Alternatively, roughening treatments have to be made in order to bring the deficit value above the threshold of acceptability.
If the maintenance is not successful, i.e. the prescribed values are not reached, a 20% of deduction will be applied"

The standard specifications, published by Italian Ministry of Infrastructures and Transports, with regard to surfacings specificies the following:

"In situ are also measured the skid resistance through the skid tester, according to CNR 105/85 and the drainage capacity (except for splittmastix) with portable permeabilimeter, according to EN 12697-19.

The BPN must be greater than

- *50 for porous asphalt course;*
- *55 for hot microsurfacing;*
- *60 for splittmastix asphalt.*

For lower values a deduction of 1% will be applied to the list price for each unit of deviation".

The special tender of Brennero Highways, prescribes for SMA the following lower limits:

- PTV, according to EN 13036-4, greater than 55
- MTD, according to EN 13036-1, greater than 0.35 mm.

Noteworthy is that both the BPN and the PTV values derived from the same tests and differ only for the correction factor applied to the detected value, prescribed in the reference standard (Italian CNR or EN). This correction appears to be more severe in the case of PTV value. Therefore, in order to obtain a "safety" value, the PTV was taken as reference. However, the BPN is also reported.

For the purpose of this research, the following threshold values were adopted:

- PTV> 55 for new paving (reference for the survey of October 2014);
- PTV> 50 for 6-12 months of service (reference for the survey of April 2015);
- PVT> 35 for roads with more than 12 months of service (reference for the survey of October 2015);

Measurement carried out in accordance with EN 13036-4 are plotted in terms of British Portable Number (Figures 5.14, 5.15 and 5.16) and in terms of Pendulum Test Value (Figures 5.18, 5.19 and 5.20).

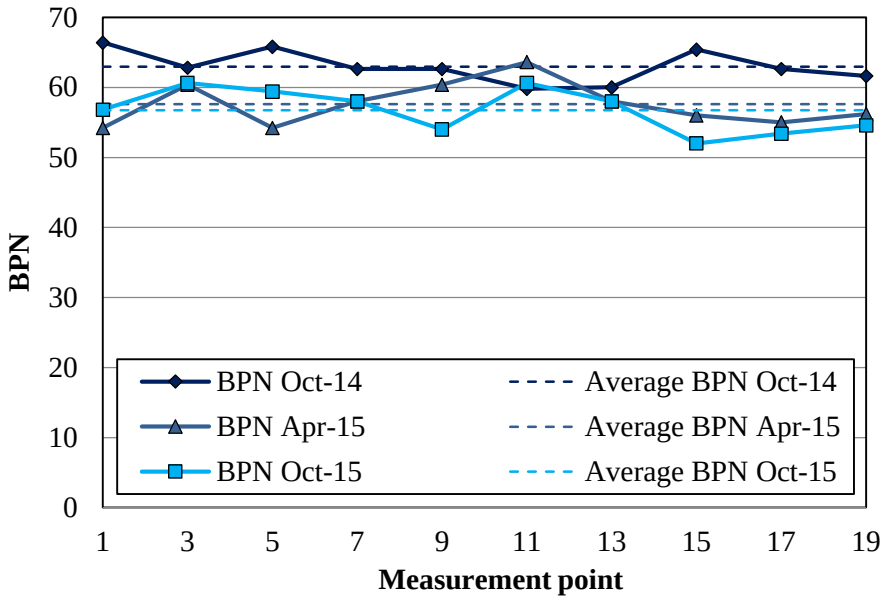

Figure 5.14: BPN measured at different locations during the surveys for SMA 0

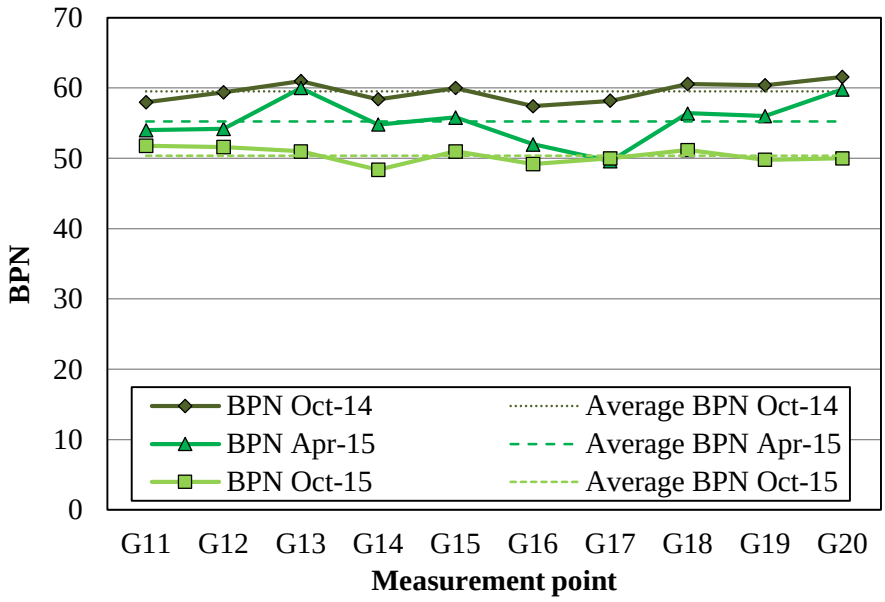

Figure 5.15: BPN measured at different locations during the surveys for SMA 0.75

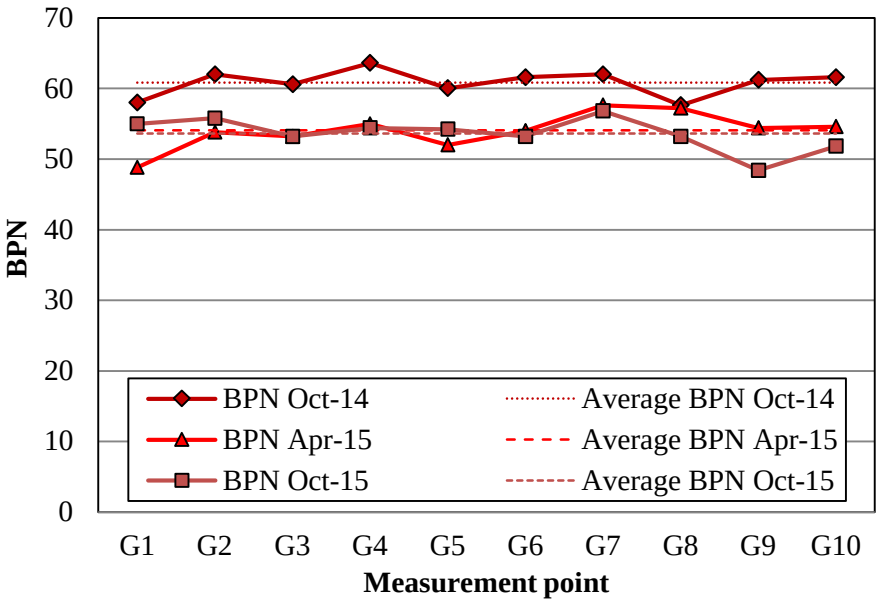

Figure 5.16: BPN measured at different locations during the surveys for SMA 1.20

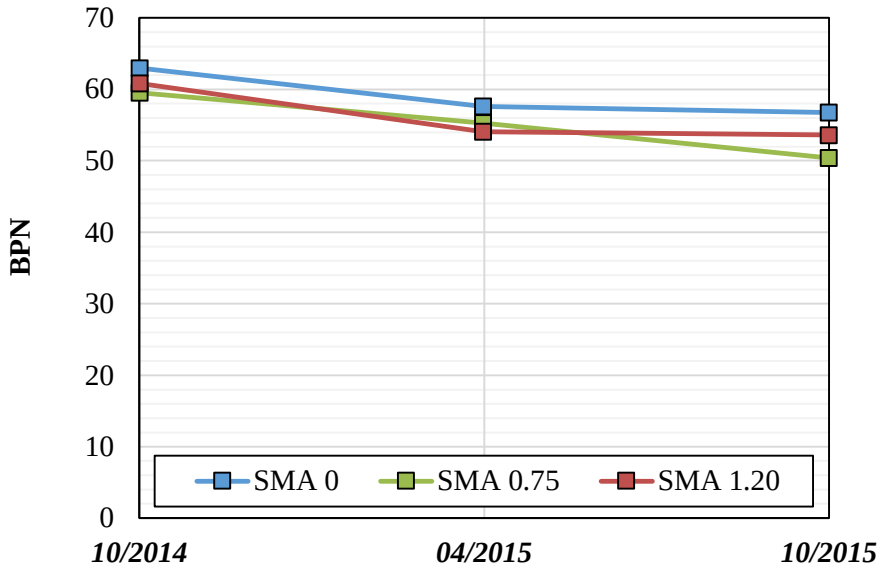

Figure 5.17: Summary of the average BPN measured during the surveys for the three mixtures

The average value of PTV between the ten measurement points is 61.5, 55.8 and 55.5 respectively for the three surveys in chronological order (Table 5.1).

SMA 0 exhibits very uniform PTV values during the first survey, which become higher at the second and third surveys. Ass shown in Table 5.1, the variance increases with time as a clear indication of the surface wear over time. Measurement points 9 and 15 underwent

the greater decrease in the PTV. They are located just in front of side streets, where acceleration, deceleration and shear forces could have polished the surface.

PTV	10/2014	04/2015	10/2015
Average value	61	56	56
Variance	5,93	8,84	10,04
Standard deviation	2,44	2,97	3,17

Table 5.1: PTV statistics for SMA 0

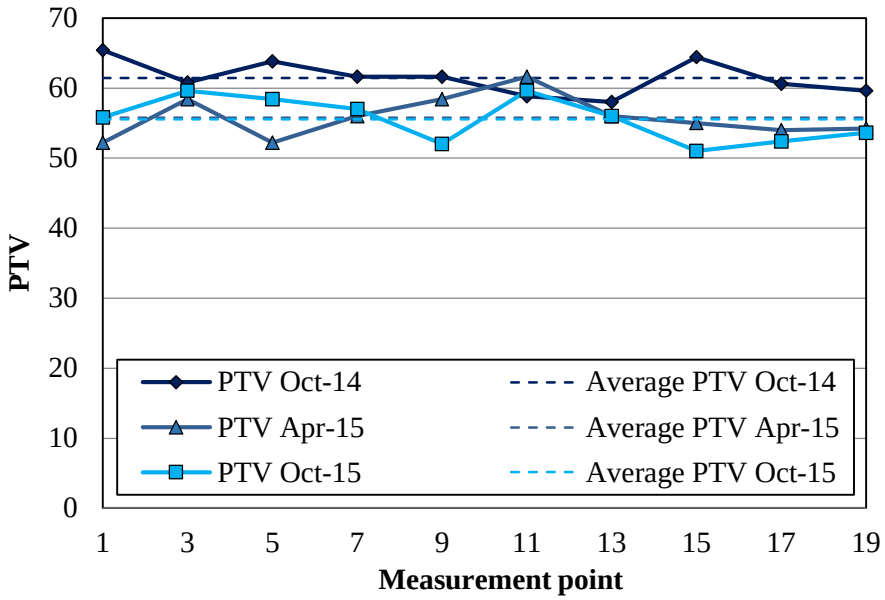

Figure 5.18: PTV measured at different locations during the surveys for SMA 0

SMA 0.75 provides an excellent uniformity of measured PTV values, especially in the first and the third surveys. Outliers were found during the second survey in sections 13 and 20 (higher values), and 16 and 17 (lower values). However, these values were found to be in line with the mean value during the third survey. Values are reduced of 3÷5 points at the second survey and 6÷10 at the third survey.

Being the PTV value one year after laying around 49, the performance of the mixture is above the threshold.

PTV	10/2014	04/2015	10/2015
Average value	58	54	49
Variance	1.57	10.09	1.21
Standard deviation	1.25	3.18	1.10

Table 5.2: PTV statistics for SMA 0.75

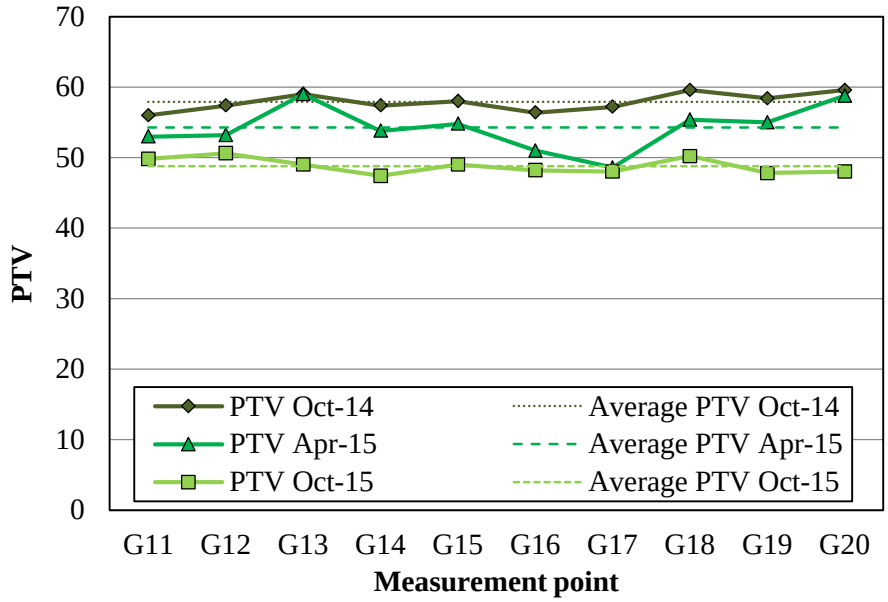

Figure 5.19: PTV measured at different locations during the surveys for SMA 0.75

The rubberized surface SMA 1.20 provides for uniform values which are consistent on the surveys. Variance and standard deviation, shown in Table 6.4 are small.

On October 2015, the lowest value was recorded at the section G9 which is just in front of a supermarket. Car entering its parking could have stressed the pavement, causing polishing of the surface.

Values are reduced of 5÷9 points at the second survey and 6÷10 at the third survey. Being the PTV value one year after laying around 52, the performance of the mixture is above the threshold.

PTV	**10/2014**	**04/2015**	**10/2015**
Average value	59	53	52
Variance	3.16	6.92	5.24
Standard deviation	1.78	2.63	2.29

Table 5.3: PTV statistics for SMA 1.20

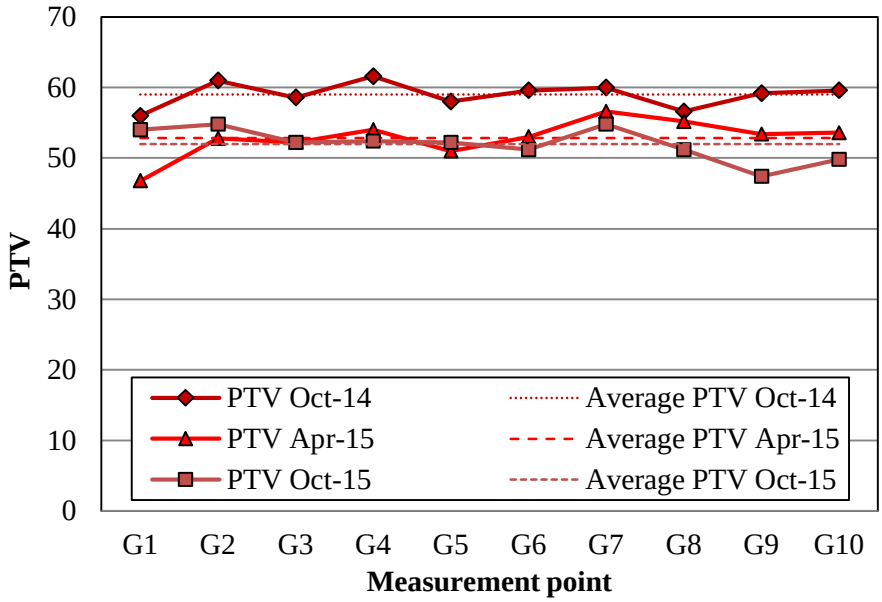

Figure 5.20: PTV measured at different locations during the surveys for SMA 1.20

Figure 5.21 shows a summary of the average values of the PTV for the three surfaces under investigation and during the surveys.

The SMA 0 and SMA 1.20 reveals an almost identical trend. Although SMA 0 keeps a higher PTV value, both surfaces show a reduction of around 10% 6 months after laying. The PTV value keep constant one year after laying with a negligible reduction. The SMA 0.75 exhibits a smaller reduction of the PTV after 6 months and a greater reduction after 12 months, which is around 15%.

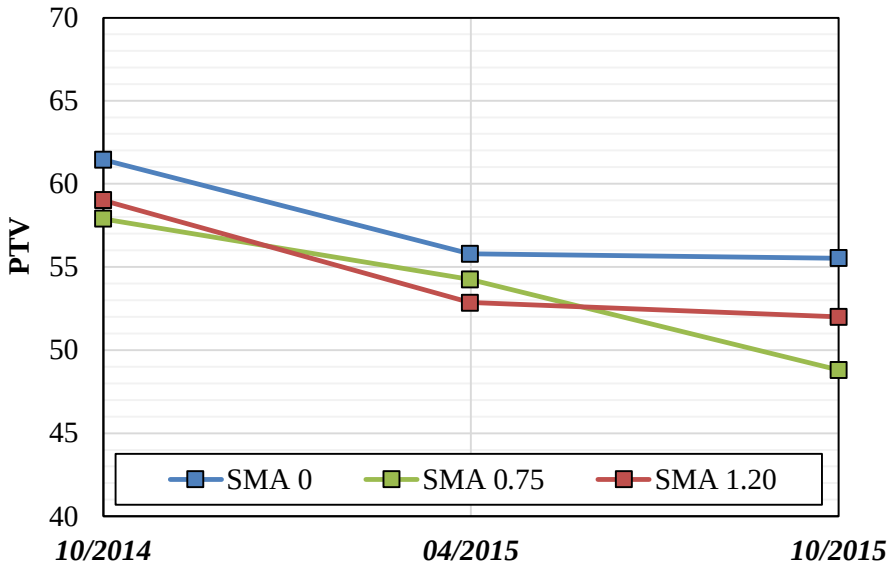

Figure 5.21: Summary of the average PTV measured during the surveys for the three mixtures

5.2.1.2 Macrotexture

The texture of the pavement was firstly measured trough the volumetric patch method, in accordance with EN 13036-1.

For the evaluation of the acceptable values of MTD, different specifications, technical guidelines, scientific papers were taken as references.

The standard specifications, published by Italian Ministry of Infrastructures and Transports, with regard to surfacings, specifies that:

"The MTD, determined according to the CNR 94/83 standard must be greater than:

- *0.8 for porous asphalts;*
- *0.6 for hot microsurfacings;*
- *0.5 for splittmastix asphalts.*

Measures that are performed with a continuous measuring equipment must be referred to MTD with appropriate correlations. The SFC and MTD measurements must be made for each lane, with a measurement step of 10 meters, in a period of time comprised between the 15th and the 180th day after the road had been opened to traffic. In case of occasional and localized inhomogeneities, the measured values can be averaged every 50 m"

The "Brennero Highways" special tender specifications, refers to the measurement of PTV, according to UNI EN 13036-4, and MTD, according to UNI EN 13036-1, pertaining to SMA, prescribing the following lower limits:

- 55 for PTV;

- 0.35 for MTD.

The special tender specifications of the Veneto region states the following:

"SFC values below 40 and/or MTD values below 0.35 will be considered as full responsibility of the contractor, that will have alternatively for free to:

- *Achieve the complete removal of the layer and substitution with a new one;*
- *carry out a roughening treatments in order to restore the parameters above the prescribed thresholds".*

The Special technical standards of ANAS S.p.A indicates that for asphalt mixtures:

"The SFC and MTD indicators should be greater than or equal to 58 and 0.3 respectively. The measures have to be made within a period of time comprised between the 15th and the 180th day from the opening to traffic, with the exception of porous asphalts etc..
Penalties will be applied for homogeneous stretches when their average values of SFC and / or MTD will be assesses lower than the prescribed thresholds; whenever both SFC and MTD average values will be critical, the penalty will be cumulative.
The reduction will be applied in percentage points to the auction of the works of the material involved these points correspond to half of percentage points by which the SFC or the MTD differs from the thresholds. The deduction will cover the entire width of the homogeneous section.
In any case SFC value can be accepted if less than 40. The same applies for MTD values lesser than 0.2".

The document "Maintenance and construction of pavements - technical standards" of the Italian motorway company, "Autostrade per l'Italia" states that:

"The MTD measured through the mini texture meter (WDM - TRRL) or by SCRIM must be greater than or equal to the following values 0.4 mm for normal and special asphalt concretes. The SFC and MTD has to be performed at least on a lane within a period between the 15th and the 180th day from the opening to traffic, except for porous asphalts and high friction surfaces for which the measures are to be carried out between the 60th and the 270th day from the opening to traffic. In any case MTD can fall below 0.25 mm".

Tables 5.4, 5.5 and 5.6 show the statistics of the measured MTD for SMA 0, SMA 0.75 and SMA 1.20 respectively. Figures 5.22, 5.23 and 5.24 plot the MTD values as they were measured on the road. These plots highlight the differences of MTDs between the measurement points and during the surveys. The variance of the data is consistent during the surveys except for the SMA 0, which exhibits a great variance during the last measurement session.

MTD	**10/2014**	**04/2015**	**10/2015**
Average value	0.75	0.75	0.79
Variance	0.002	0.004	0.008
Standard deviation	0.046	0.065	0.090

Table 5.4: MTD statistics for SMA 0

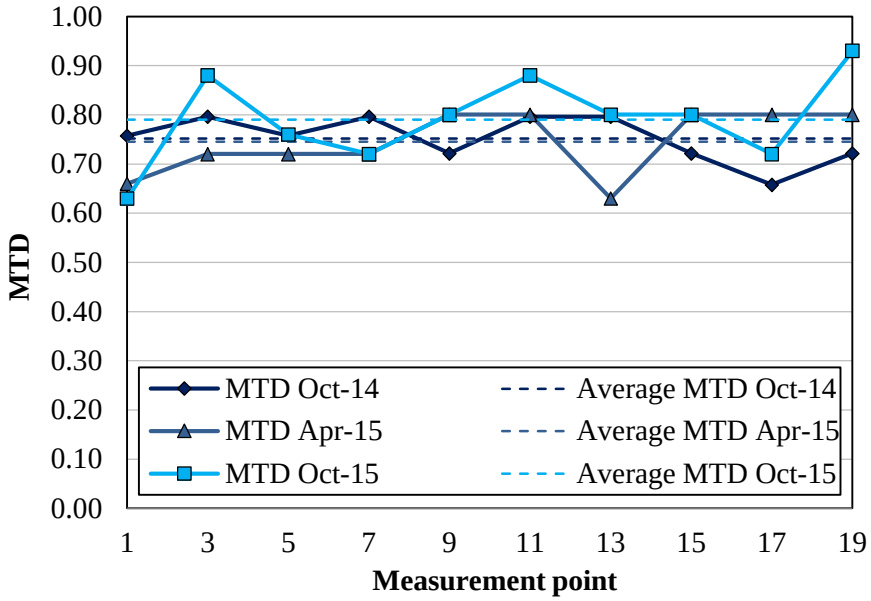

Figure 5.22: MTD measured at different locations during the surveys for SMA 0

MTD	10/2014	04/2015	10/2015
Average value	0.71	0.71	0.74
Variance	0.002	0.004	0.004
Standard deviation	0.043	0.064	0.060

Table 5.5: MTD statistics for SMA 0.75

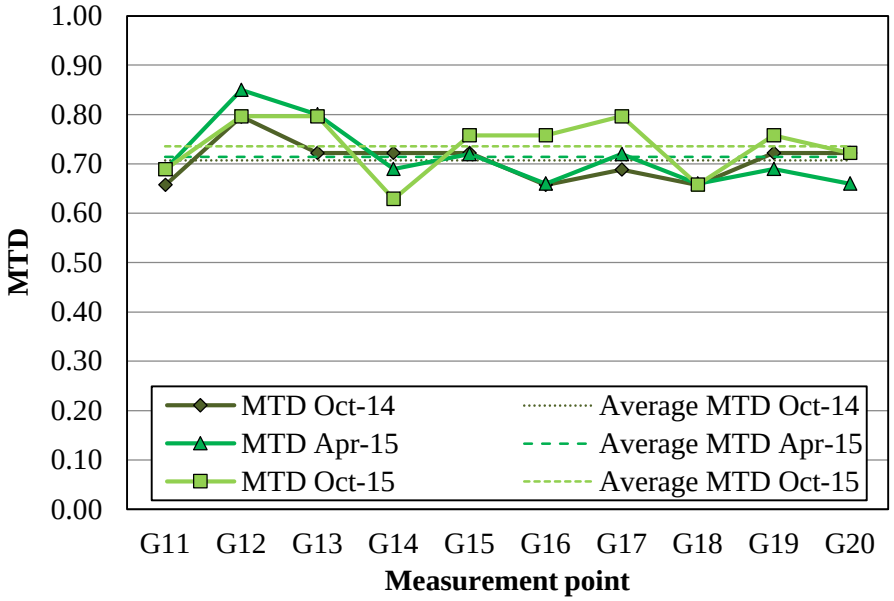

Figure 5.23: MTD measured at different locations during the surveys for SMA 0.75

MTD	10/2014	04/2015	10/2015
Average value	0.70	0.63	0.68
Variance	0.003	0.005	0.002
Standard deviation	0.056	0.069	0.043

Table 5.6: MTD statistics for SMA 1.20

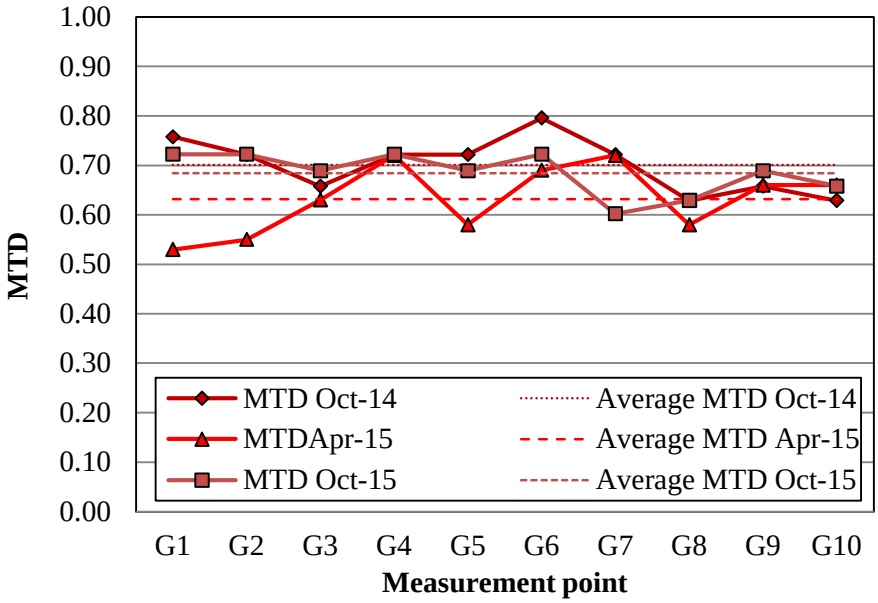

Figure 5.24: MTD measured at different locations during the surveys for SMA 1.20

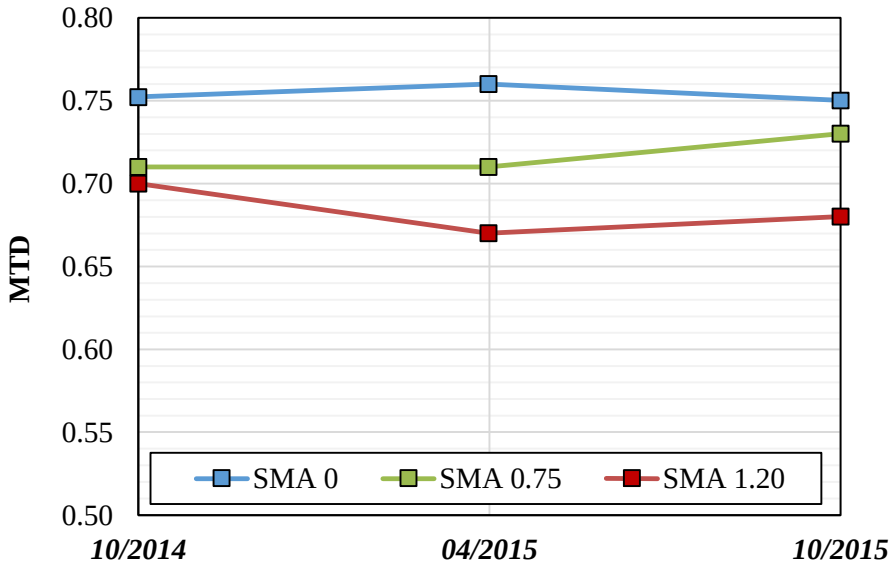

Figure 5.25: Summary of the average MTD measured during the surveys for the three mixtures

Figure 5.25 shows a summary of the average values during the surveys. The data shows that all the surface layers exhibit a substantial high roughness, with the classic SMA having mean values around 0.75 mm and the rubberized surfaces having mean values around 0.70 mm. One year after the laying, MTD is reduced of about 1-5%, which does not affect the performance. The rubberized surfaces exhibit a similar macrotexture with small differences. Overall the classic SMA shows the best macrotexture in terms of MTD. In any case, MTD values of the three surfaces are largely above the thresholds set by the adopted reference standards.

5.2.2 Dynamic advanced measurements

5.2.2.1 Skiddometer

5.2.2.1.1 Equipment and test methods

The Skiddometer BV11 is produced in Sweden, by the Homeland Vammas AEC. It is constituted by a measuring carriage (Figure 5.26), which is towed by a vehicle equipped with an electronic computer for the data acquisition. The sampling intervals is 2 meters. The cart is made from a steel frame supported by two free wheels between which is positioned the measurement wheel for the detection of the friction between the tyre and the surface of the road pavement. The measurement wheel, during the survey, rolls with a predetermined "s" sliding with reference to the side wheels and equal to 17%. The surface is adequately wetted in order to simulate the presence of a water veil of 1 mm thickness. The watering system is constituted by a mechanical pump, connected to one of the outer wheels, which is able to vary the flow of water in function of the survey speed.

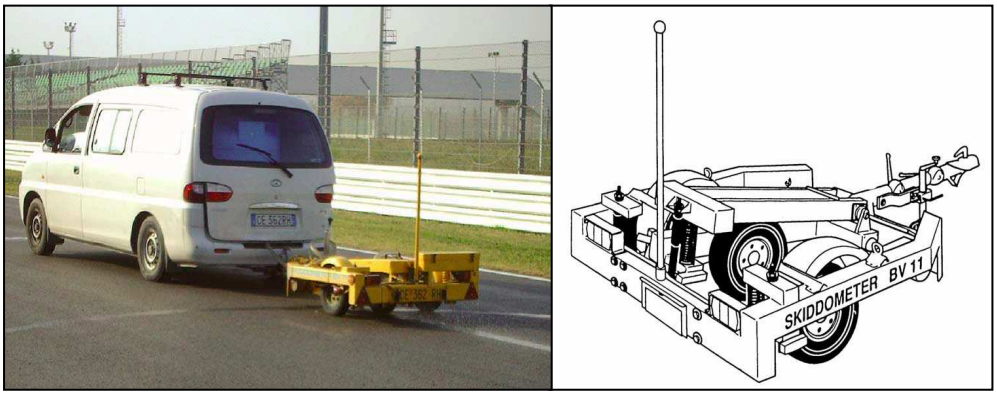

Figure 5.26: Skiddometer BV11

All device functions can be managed inside the towing vehicle using the proprietary electronic processor MI-90, which is able to continuously monitor the following parameters:

- the shear resistance of the carriage towing (*F*);
- the vertical load on the measuring wheel (*P*);
- the measurements speed (km/h);
- the length of the analysed section (m);
- the air temperature (° C).

These parameters are used to calculate the BFC (Braking Force Coefficient) expressed by the equation:

$$BFC = 100 \cdot \frac{F}{P}$$

In order to harmonize the different measurement methods used for the evaluation of friction and texture of road surfaces, the Technical Committee of the Surface characteristics AIRPC organized an international experimentation. It followed the proposal of the IFI index (International Friction Index), which is calculated using relationships obtained from regressions of friction and textural data detected with different types of equipment and is discussed extensively in Chapter 1.

The coefficients for the IFI calculation with reference to the adopted equipment are shown in Table 5.7.

A	B	A	B	C
11.1284	90.906	0.0396	0.85618	-0.01589

Table 5.7: coefficients adopted for IFI calculation

The computation of the data measured during the in-situ campaigns allowed determining the friction parameters BFC with a frequency of 10 m. The parameters measured on the trial site are plotted versus the distance in Figures 5.27, 5.28, 5.30, 5.31, 5.32 and 5.33.

For the evaluation of the reference values for the BFC parameter, the paper "the friction on ordinary asphalt surfaces measured with partially locked wheel devices", written by M. Losa, R. Bacci, P. Leandri was taken as reference. That paper prescribes thresholds for BFC according to the measuring speed:

- BFC > 0.72 for v = 20 km/h;
- BFC > 0.62 for v = 50 km/h;
- BFC > 0.53 for v = 80 km/h.

5.2.2.1.2 Results

This section presents the results of the Laseprof and Skiddometer campaigns on the trial site. The Department of Civil and Industrial Engineering (DICI) of the University of Pisa was appointed to carry out the measurements that will be presented hereafter.
The friction measurements, carried out at speeds of 20km/h, allowed determining the longitudinal friction coefficient every 2 meters.

The measures with the skiddometer at the Zola Predosa trial site were performed at a speed of 20 km/h. Accordingly, it was verified that the measurement provided for BFC values greater than 0.72.

After the first survey, the measured BFC on SMA surface shows a regular trend, with values around 0.82 ÷ 0.83 in the first half and 0.75 in the second half. The average value is 0.80.

The average value of the measured BFC is substantially unchanged after the second survey took place. Values stand around 0.85 in the first half and 0.80 in the second half with an average of 0.81.

One year after laying the BFC provided for the same average value. It can be concluded that the classic SMA presents an overall good skid resistance in terms of BFC values, which are always greater than the set threshold.

The SMA 0.75 shows average BFC values of 0.77, 0.80 and 0.81 for the three surveys in chronological order. This indicates that the BFC tends to grow with time, reaching the same value of SMA one year after laying.

An identical trend and very similar values were found for SMA 1.20, which shows average BFC values of 0.77, 0.81 and 0.82 on October 2014, April 2015 and October 2015 respectively. This indicates that the BFC tends to grow with time, reaching the same value of SMA one year after laying.

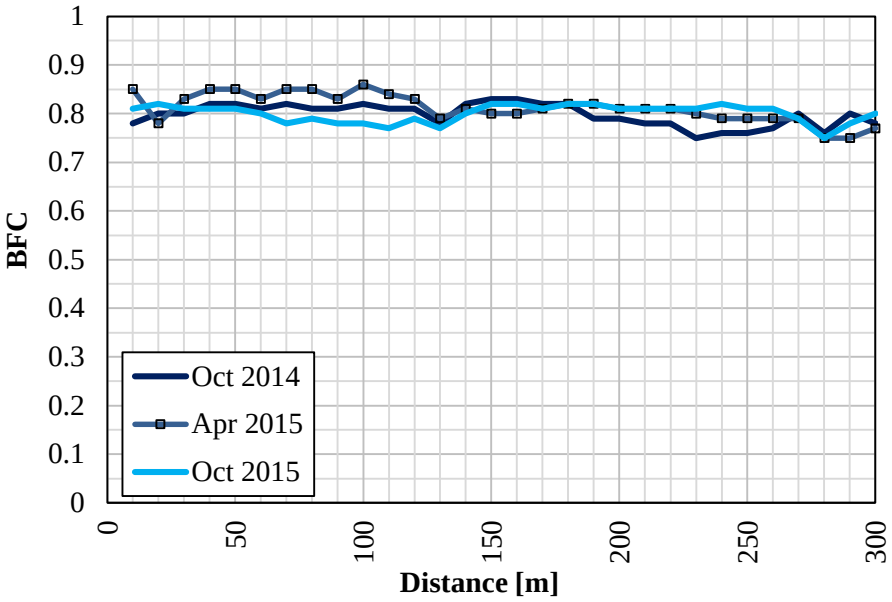

Figure 5.27: BFC for the reference Stone Mastic Asphalt with no rubber

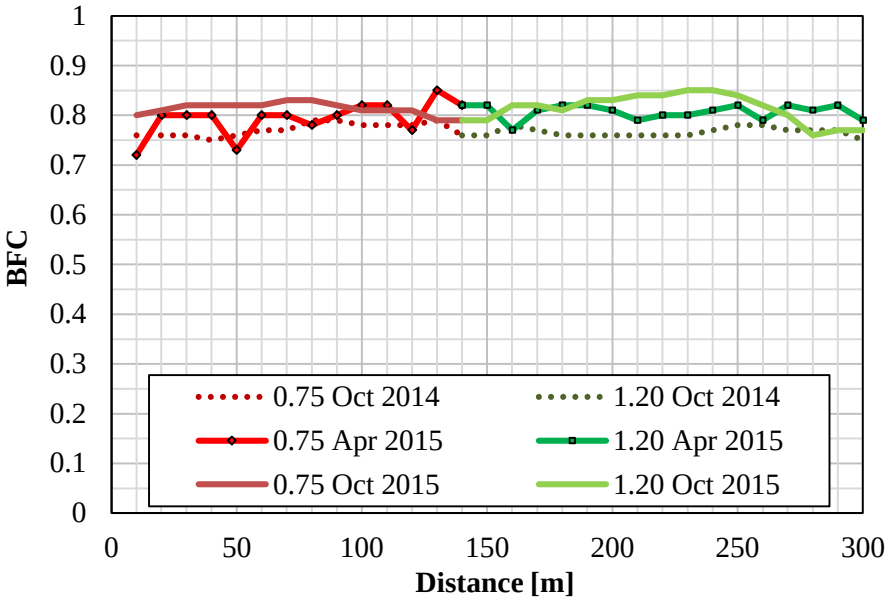

Figure 5.28: BFC for the rubberized SMA surfaces

BFC	10/2014	04/2015	10/2015
SMA 0	0,80	0,81	0,80
SMA 0.75	0,77	0,81	0,82
SMA 1.20	0,77	0,80	0,81

Table 5.8: Summary of BFC during the surveys

5.2.2.2 LaserProf

5.2.2.2.1 Equipment and test methods

The texture of the road trial site, with special regarding to the MPD was determined through the LaserProf. It is a portable system designed for road profiling measurements with no need for permanent installations. The system can be mounted on the trailer hook on a vehicle in a few minutes on-site.

LaserProf is a class I Inertial Profiler designed for quality control and supervision. It complies with ISO 13473-3 (Table 5.9) for devices classified with mobility features "slow".

The equipment enables you to measure longitudinal profiles of any pavement surface. The software supporting LaserProf consists of a real-time recording and calculation module, as well as a module for detailed data selection, calculation and report generation. Among data included in the reports are:

- Raw Longitudinal Profile
- IRI or Inch per Mile

Derived results from the profile, MPD (Mean Profile Depth) and ETD (Estimated Texture Depth) can be calculated.

Reports can utilize the built-in graph generating tools for both 2D and 3D graphs of any of the results.

The high maximum speed capacity allows you to perform measurements while the road is open to the public and with the pace of undisturbed traffic. However, in order to obtain high accuracy data, the survey was made at the speed of 15 km/h with measurement gap of 1 mm.

Device	Classification		Sampling range	Vertical resolution	Laser frequency	Acquisition speed
	Wavelength	*Mobility*				
contactless	D-F	slow	1 mm	0.05 mm	16 kHz	15 km/h

Table 5.9: Laseprof equipment for MPD survey

Figure 5.29: Laseprof equipment for MPD survey

The following paragraph will analyse the values of MPD (Mean Profile Depth) and ETD (Estimated Texture Depth) according to ISO 13473-1/2 standards. MPD is the average value of the depth of the profile points, calculated on a predefined distance of 100 mm, referred to as the "baseline". The baseline is divided in two parts and the Mean Profile Depth (MPD) for each individual profile is determined as the arithmetically averaged two peak levels minus the average (profile) level.
The average level is zero as a result of the highpass filtering or slope suppression procedure as defined by ISO 13473-1.

ETD is the term used to identify the MTD when the first cannot be measured by volumetric method, but rather it is estimated once the MPD is known. This value can be obtained through the application of ETD equation [mm] = 0.2 + 0.8 MPD [mm].
For the evaluation of the eligible values of MPD / ETD, different technical guidelines, scientific papers and standards were taken as reference as usual.

The special tender specifications of the Veneto region specifies for SMA that:
"The surface macrotexture measured through laser instrument according to ISO 13473 in terms of MPD (Mean Profile Depth) or in terms of MTD in accordance with the EN 13036-1, must be greater than 0.8 mm…the SFC MPD (MTD) and IRI have to be measured between the 60th and the 180th day from the opening to traffic".

The "Brennero Highways" special tender specifications, specifies the following:
"The value of the average profile depth (MPD), as a measure of macrotexture according to ISO 13473, will have the following requirements:
(a) asphalt concretes type a: MPD≥0,5
(b) asphalt concretes type b: MPD≥0,6
(c) temporary surface course (binder): MPD≥0,4
(d) porous asphalts: MPD≥1,0
(e) multifunctional asphalts: MPD≥0,8
(f) slurry seals:MPD≥1,0
The survey of SFC and macrotexture has to be made within a period of time comprised between 15th and 180th day from opening to traffic.

In the report *"Experimental survey for the evaluation of macrotexture and skid resistance of a section of the S.P. 569 "Vignola" road in the town of Zola Predosa"*, published by the road experimental laboratory of the department of civil and industrial engineering of the University of PISA, the surface macrotexture is classified by equating ETD to MTD. In this case the table of the CNR 94/1983 standard is applied.

ETD	**Classification**
< 0,20	Very fine
0,20 < ETD < 0,40	Fine
0,40 < ETD < 0,80	Average
0,80 < ETD < 1,20	Coarse
> 1,20	Very coarse

Table 5.10: ETD classification according to CNR 94/1983

For the present discussion, a MPD value in the range between 0.5 mm and 0.8 mm, identified in 0.60 mm, was taken as reference. The two limits are provided by the “Brennero highways specifications" for asphalt mixtures having similar particle size and materials used. The adopted value is justified from the fact that the investigated surfaces do not represent a new construction but a maintenance. Regarding the ETD, the adopted reference is linked to the experiences of the laboratory of the University of Pisa.

5.2.2.2.2 Results

Two months after the opening to traffic, the MPD value of the first half of the SMA lane appears to be oscillating, with values ranging between 0.50 mm and 0.90 mm. In the second half, instead, the MPD is settle in a range between 0.60 mm and 0.65 mm with little significant changes. The average value for the SMA is 0.65 mm.

After the second survey, the MPD of SMA shows a regular pattern around the mean value of 0.60 mm, with a decrease of about 0.15/0.20 mm only in the central section.

The MPD of SMA after the third survey shows a more regular trend compared to the previous test campaigns, demonstrating that all values are settling around the mean value. This less variance is evident looking at Figure 5.30. The average value for the SMA is 0.58 mm, which is 0.07 smaller than the average of the first measurement.

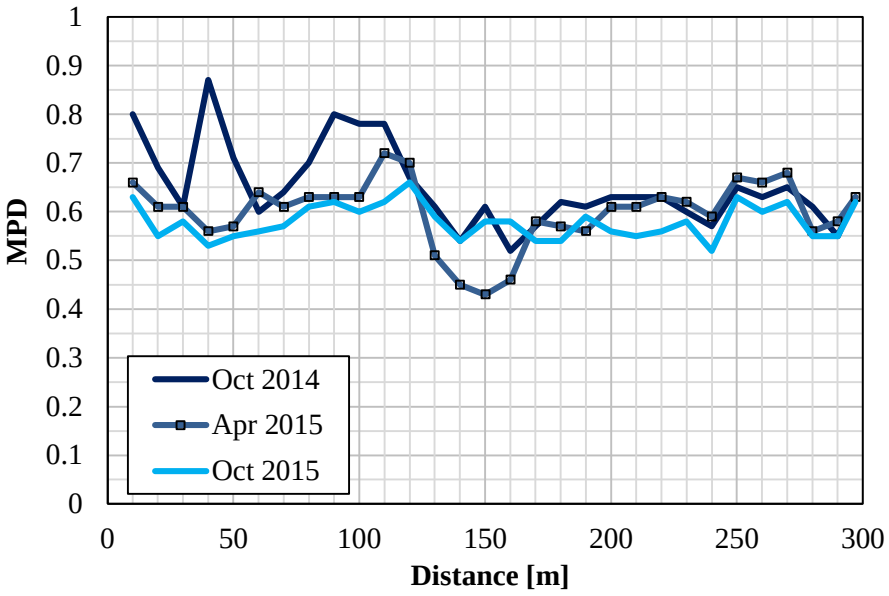

Figure 5.30: MPD for the reference Stone Mastic Asphalt with no rubber

Regarding the SMA 0.75, its MPD value diminishes with a smaller rate compared to the SMA. The average value, in fact, remains constant over the surveys, starting from 0.61 mm and reaching a final value of 0.58 mm, passing from 0.59.

The same can be said for the SMA 1.20. The starting value is 0.62 and an equilibrium is reached at 0.58 after 6 months of trafficking.

All the surfaces meet the adopted requirements, having MPD values above the thresholds over the surveys. Table 5.11 summarizes the mean values of MPD.

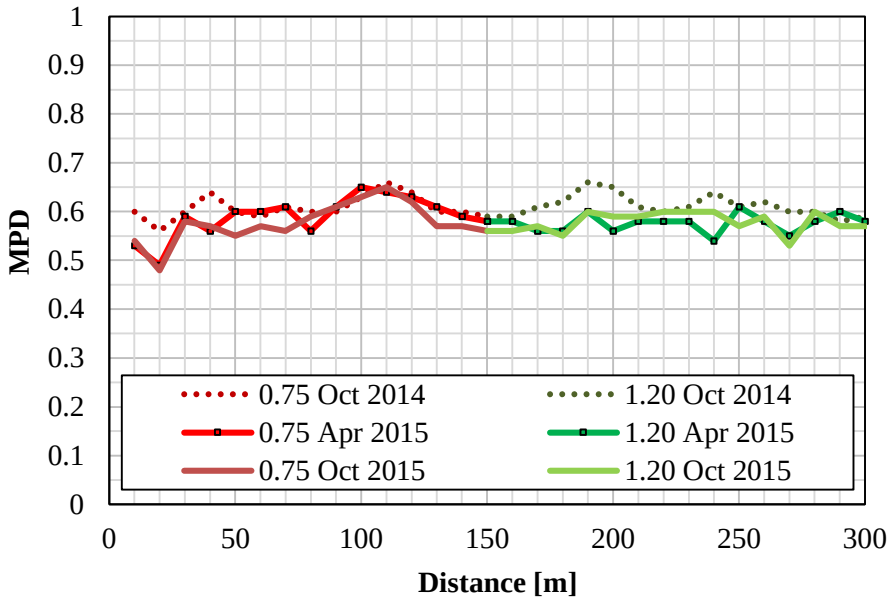

Figure 5.31: MPD for the rubberized SMA surfaces

MPD	10/2014	04/2015	10/2015
SMA 0	0,65	0,60	0,58
SMA 0.75	0,62	0,58	0,58
SMA 1.20	0,61	0,59	0,58

Table 5.11: Summary of MPD over the surveys

The same considerations can be made for the ETD since it is directly proportional to MPD. According to Table 5.10, the macrotexture of the three SMA is classified as *"Average"*. Table 5.12 summarizes the mean values of ETD. Noteworthy is that values are identical one year after laying.

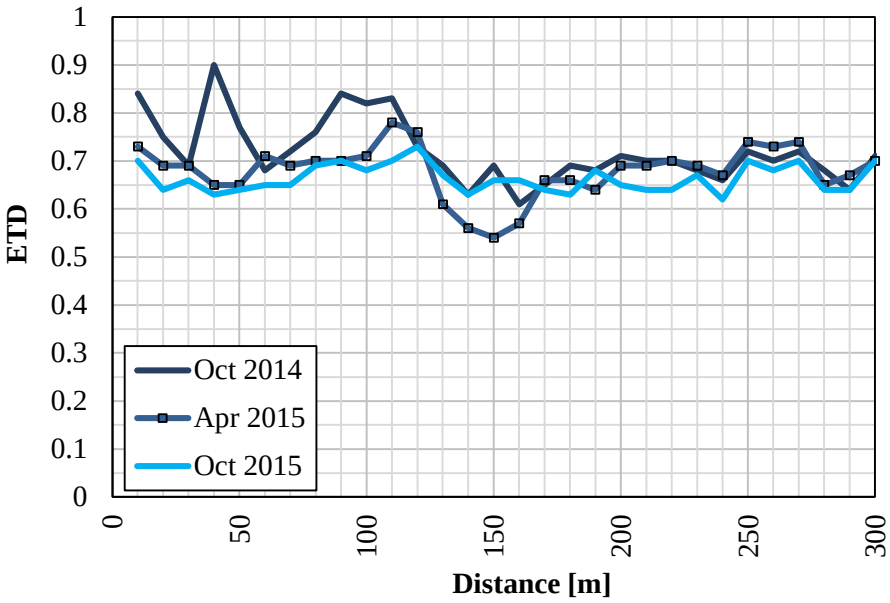

Figure 5.32: ETD for the reference Stone Mastic Asphalt with no rubber

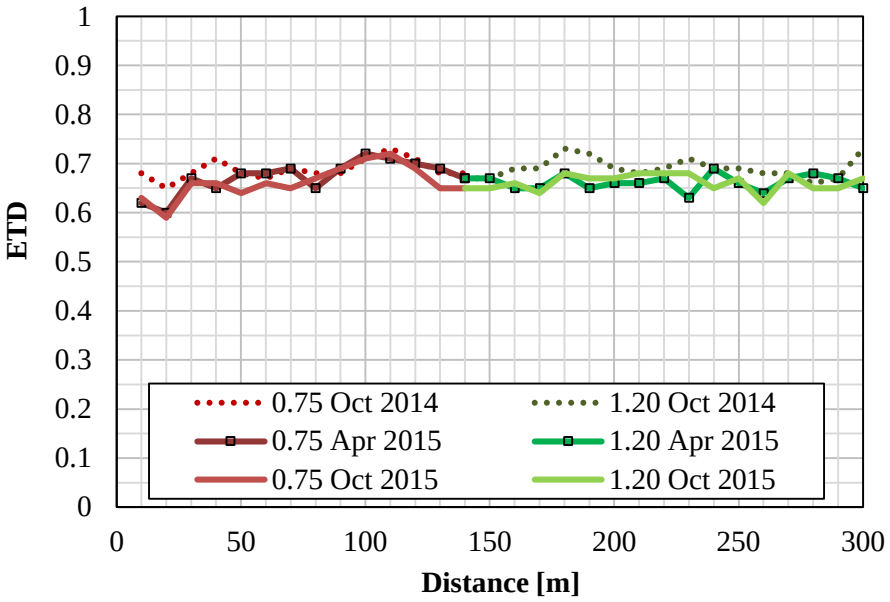

Figure 5.33: ETD for the rubberized SMA surfaces

ETD	10/2014	04/2015	10/2015
SMA 0	0,72	0,68	0,66
SMA 0.75	0,69	0,66	0,66
SMA 1.20	0,69	0,67	0,66

Table 5.12: Summary of ETD over the surveys

Chapter 6

Laboratory simulated trafficking and classic measurements

6.1 Introduction

This section introduces the investigations on the studied rubberized mixtures that were made in laboratory. As seen in previous Chapters, three different surveys were carried out at the Zola Predosa trial site, covering a period of one year after the laying. The surveys allowed for a measurement of the texture and skid resistance on site during the early life of the pavement.

However, they say little about the performance of the mixtures during the years of service.

For this reason, the mixtures sampled during the laying were subjected to simulated trafficking with the Road Test Machine at the University of Belfast, U.K. This allowed measuring a series of parameters related to texture and skid resistance at different stages corresponding to a definite time of pavement service.

Since the aim of the thesis is to analyse the surface characteristics of the rubberized Stone Mastic Asphalts, the mixtures underwent a further trafficking with an old version of Immersion Wheel Track. Accordingly, the resistance to ravelling and the adhesion between bitumen and aggregates were studied with innovative 2D and 3D image analysis. As will be shown in Chapter 7 and 8.

This part of the research was carried out by the Author at the laboratory of Highway Engineering of the University of Belfast, U.K.

6.2 Road Test Machine

The Road Test Machine (RTM) was used to subject test specimen surfaces to slow speed high stress simulated accelerated trafficking conditions. Trafficking was stopped at predetermined intervals to allow assessment of any change in the surface of the test specimen.

Figure 6.1 shows the RTM. It consists of a 2.1 mm diameter table, which can accommodate up to ten specimens of dimension 305 x 305 x 50 mm. The table rotates at 10 revolution per minutes, which equates to 1.1 m/s. New tyres are fitted at the start of each investigation. Two Federal 195/70R14 tyres are positioned vertically above the rotating table to allow transverse trafficking across the width of the test specimen. Each tyre applies a static load of 5 kN onto the surface of a test specimen. The RTM operates in an environmental room with a temperature of 10 + 2 °C.

Nicholls, in the TRL Report 176 (1997), describes how the RTM is used to assess the resistance to wear of High Friction Surfacing test specimens. This involves 100,000 wheel passes, during which the surface of the test specimen reaches a condition known as equilibrium, which is approximately equivalent to 5 to 8 years of actual trafficking, depending on the volume and heaviness of the loads applied to the road.

Friel (2013) considered the addition of water during simulated trafficking. This was sprayed onto the test specimen immediately before contact with the tyres. Although the RTM tyre angle remains constant throughout simulated trafficking, the Author consider the tracking process causing the greatest amount of tyre / test specimen interaction to be slightly off-centre.

Figure 6.1: Road Test Machine

6.3 Immersion wheel track

The immersion wheel track was test was developed in the United Kingdom during the 1950s to look at adhesion of asphalt materials. A line drawing of the original equipment is shown in Figure 7.2.

In the original method a bituminous test specimen was immersed in water at 40°C for 1 hour. A loaded hard rubber tyre moved back and forth across its surface. The combination of soaking in water at an elevated temperature and wheel tracking induced rutting of the test specimen. Test duration could be increased to determine when stripping of the bitumen / aggregate bond occurred leading to cohesive failure of the test specimen. In 1987, McKibben modified the Immersion Wheel Track Test with a one way braking system to increase contact stress during testing with the solid rubber tyre replaced with a steel tyre (Kennedy, 2014). This allows the test wheel to travel freely forward, then lock and dragged back across the test specimen so inducing mechanism that could induce ravelling failure (Mitchell, 2014).

Since the steel tyre was found to damage the aggregates, in this latest version of the test method, the solid rubber tyre has been replaced with a treaded pneumatic tyre. The treaded was chosen in preference to a slick tyre because it better simulates interaction of a tyreblock pattern with the asphalt surface texture. The size of the existing immersion wheel track equipment restricted the choice of test tyre to a MOJO 10 x 4.5/5 go-cart treaded wet tyre. This is a relatively cheap and commonly available solution.
The one way braking system has been retained to increase contact stress and so exploit any weakness or issue that could result in premature durability related failure (Kennedy, 2014).

Figure 7.3 shows the modified tyre assembly with the treaded test tyre. This is 430 mm by 170 mm made from 10 mm thick steel. Weights are fixed at either end to load the test tyre against the asphalt test specimen. During testing the test specimen is immersed in water at the required test temperature.

What makes a latest version of a 60 year old test method innovative is the use of the image analysis to interpret any change in the slab after simulated trafficking.

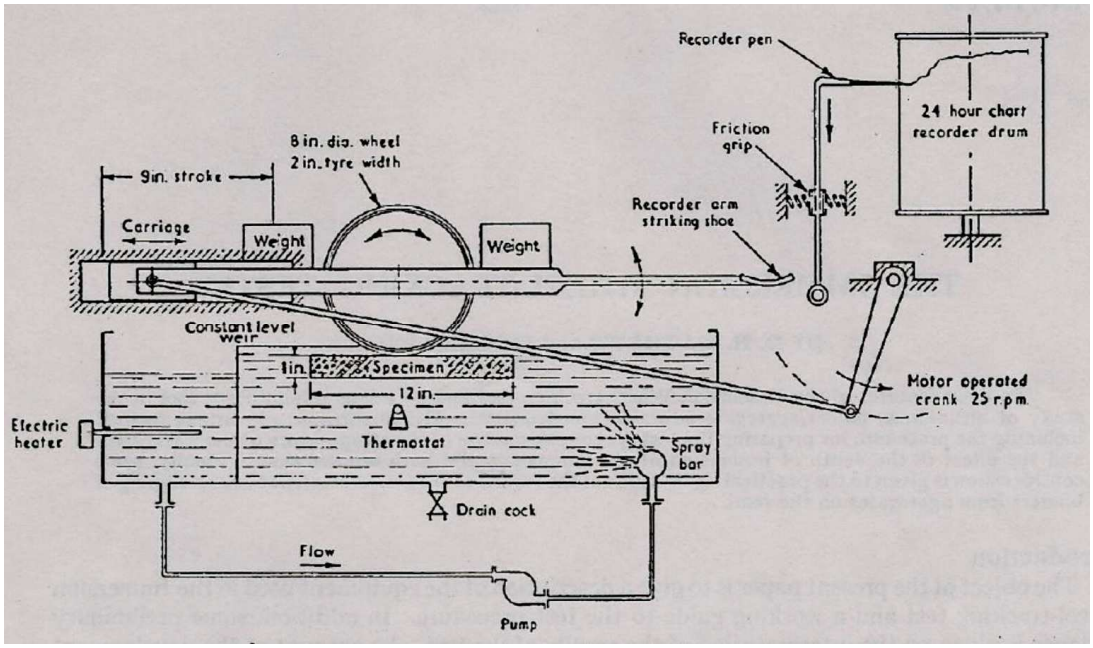

Figure 6.2: Immersion Wheel Track

Figure 6.3: Treaded tyre used for the Immersion Wheel Track

6.4 Mean Texture Depth – EN 13036-1

The volumetric patch technique derived Mean Texture Depth (MTD) is a one dimensional macrotexture classification and calculated in accordance with EN 13036-1:2010.

In order to get a uniform circle of sand spread over the surface that could be inscribed into the slab, a volume of 12.5 ml of sand was used for each test. The volume was obtained by weighing 15.5 grams, based on the sand density, which was 1.24 g/cm^3. The sand was then spread evenly by carefully working the disc with its face kept flat over the surface in a rotary motion. The procedure was complete when no further outward distribution of sand was possible. The diameter of the sand patch was measured to the nearest 1 mm at 4 diameters approximately 45° apart using a ruler.

MTD was calculated as the ratio between the volume of material and the average of the four measured diameter. Results of the test at different trafficking stages the 8 mm SMA are shown in Figures 7.5 and 7.6. No remarkable differences were found between the mixtures that exhibited similar trends.

MTD dropped down rapidly from initial values around 0.70 and reached an equilibrium after 5,000 wheel passes. The texture depth kept constant until the end of trafficking, except of the values corresponding to 75,000 wheel passes which seemed to reflect more an error in the measurement rather than an increase in the texture.

Figure 6.4: Sand placed onto the surface (left) and evenly spread for measuring MTD

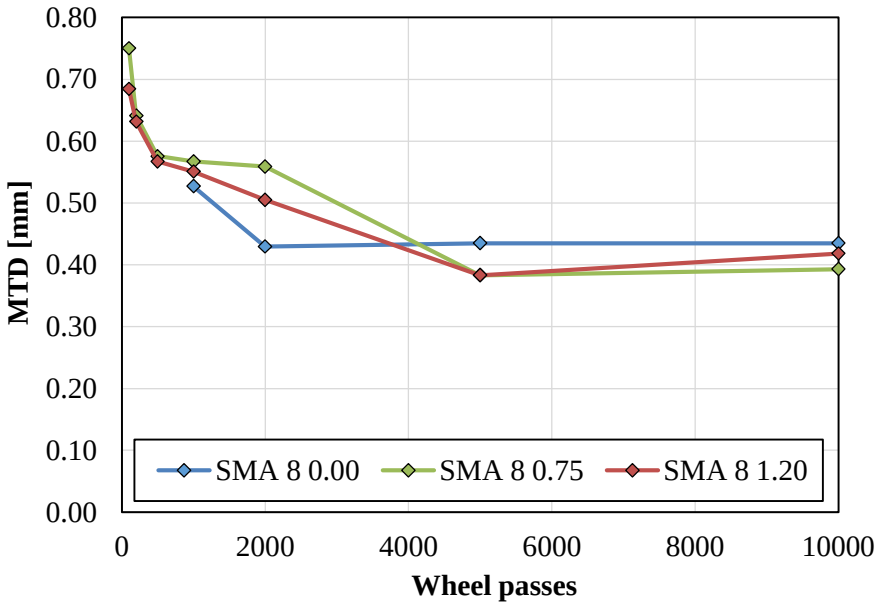

Figure 6.5: MTD versus wheel passes for early 8 mm SMA life

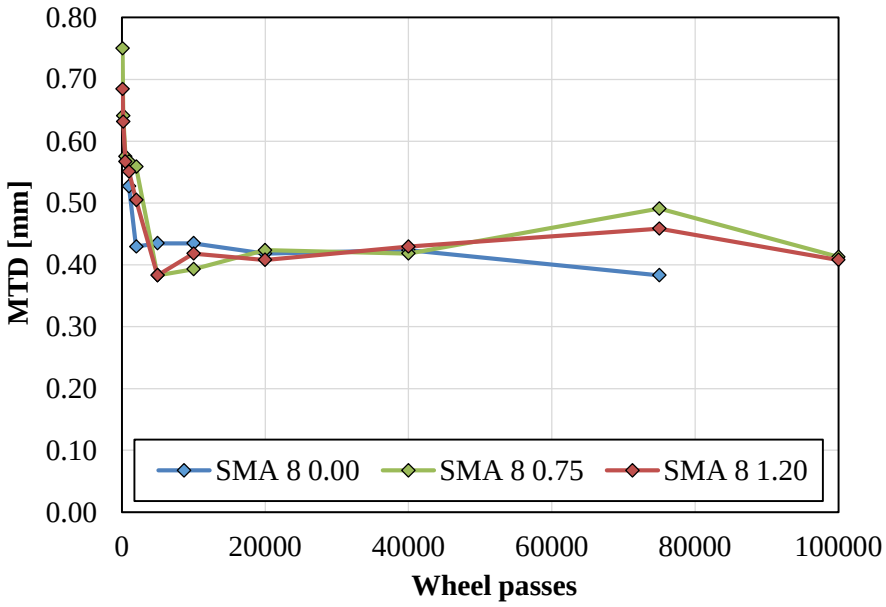

Figure 6.6: MTD versus wheel passes for 8 mm SMA life

6.5 Pendulum Test – EN 13036-4

Pendulum test was carried out according to EN 13036-4. It is known that rubber–road friction evolves during the lifetime of the pavement because of the aggregate polishing and wearing, binder removal and the aging of the binder (Kane et al. 2010). Measurements were made at the same area of the surface at each trafficking stages, which was detected with the help of a steel frame placed onto the surface after placing the slab on the stage and removed before the test.

Before each test the zero level was checked by assuring that the reading were zero while the arm swung freely. The support column of the equipment was set vertical by means of the three levelling screws. The axis of suspension of the pendulum arm was adjusted so that the slider could swing clear of the surface of the specimen and traverse the surface over a fixed length of 126 mm measured with a specific gauge. The surface and the slider were wetted copiously just before releasing the pendulum arm.

Figure 6.7: Steel frame for detecting the area of testing

Since all measurements were made at the constant temperature of 20°C, no corrections were applied to the calculated PTV values. Since first five readings on samples that underwent few wheel passes of trafficking differed by more than three units, the PTV was calculated as the constant value achieved by the final three swings. It was noted that, after a rapid drop down of the reading, the values obtained approached to a constant number with a rate dependent on the trafficking.

The number of swings that were necessary in order to reach three consecutive constant values were recorded and its plot on the number of wheel passes is shown in Figure 7.9. During the early life of the pavement the number of swings necessary to reach a constant

value of PTV are higher compared to the mid-end life, i.e. high wheel passes. This could be linked to the bituplaning phenomenon; since the bitumen content of SMA materials is high, the slider would skid as the bitumen is warmed by the slip during the contact, leading to instable measurements.

Although the bituplaning refers to dry condition it could explain what was observed with these testings. More details can be found in the work of Bullas (2005).

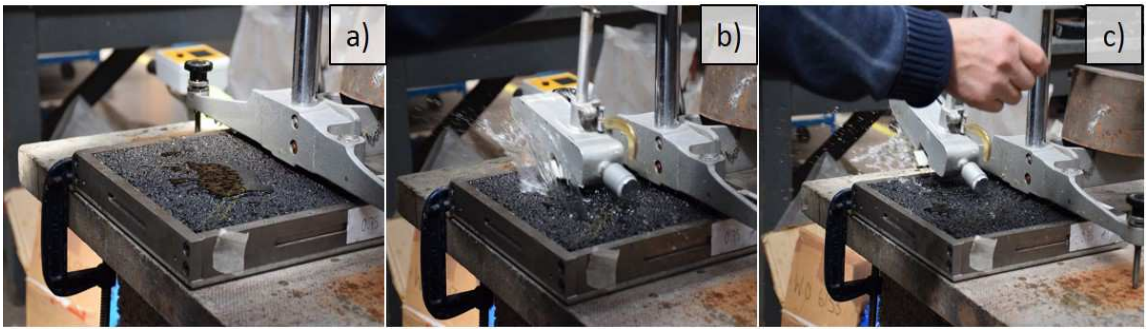

Figure 6.8: Pendulum test. a) the surface is free; b) the slider is in contact with the surface; c) the arm is hold before it swings back to the surface

Figures 7.9 and 7.10 show the PTV values obtained versus the wheel passes of trafficking.

The development of early life skid resistance is not as predictable as the decay in texture depth. This is attributed to complex interactions linked to the aggregate particles re-orientation, under the loads of the simulated trafficking.

Skid resistance achieves a maximum value soon after compaction of the slabs, when the asphalt film on the surface has been worn away and the fresh gritty surface of the aggregate is exposed. This is followed by a gradual reduction.

PTV tends to decrease with trafficking before reaching an equilibrium at 40000 wheel passes. A step in the curves were noted in correspondence of 10000 wp for 0.00 and 1.20 SMAs and 20000 for 0.75 SMA.

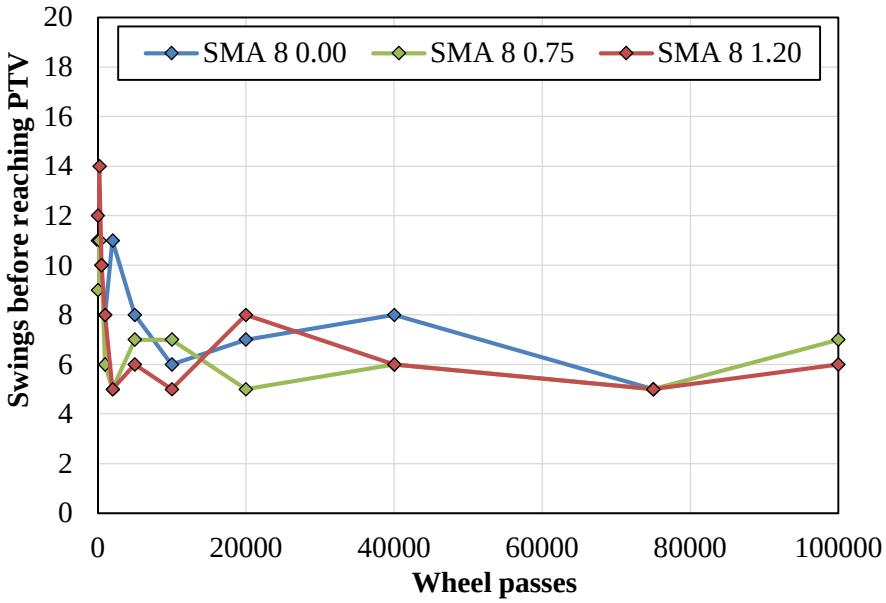

Figure 6.9: Number of Swings before reaching PTV

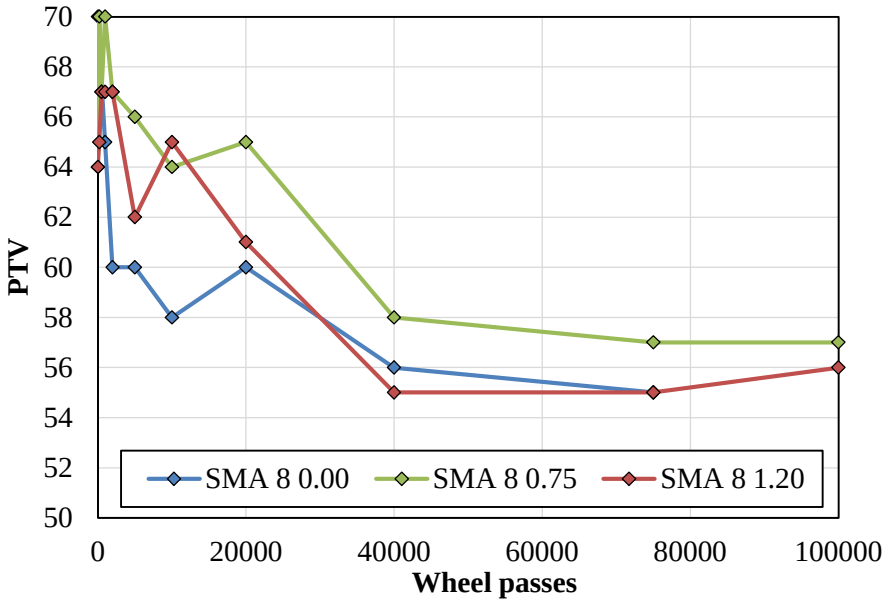

Figure 6.10: PTV versus wheel passes for the different 8 mm SMA

Chapter 7

2D Image analysis

7.1 Introduction

The image analysis is an important tool for the analysis of different parameters in a great fields of research. In the pavement engineering sector, several attempts have been made for both in-situ and laboratory investigations.

Slimane et al. (2008) developed a measurement and characterization method for road microtexture based on image analysis. The first dealt on the image measurement and extraction of roughness information from images. The latter was obtained through a geometrical and frequency based analysis of images, leading to descriptors related to the shape and the density of surface asperities.

A similar work was carried out by Dunford (2011), which is described in Chapter 1. This report investigates whether detailed imaging of the road surface has potential to be applied to the determination of microtexture and then to the measurement of skid resistance.

Cafiso et al. (2006) presented a distress detection procedure which aims at producing a result complying more closely to the distress identification manuals and protocols. The process comprises the automated pavement image collection using a high speed digital acquisition system and the distress detection by way of the pavement distress analyser. a specialised

Lamperti et al. (2015) used the Image analysis to study the adhesion between bitumen and aggregate after rolling bottle test is performed. A pixel inspection is carried out in order to verify the accuracy of the proposed method. Results shows an excellent reliability, suggesting the method could overcome the shortcomings of the visual recognition.

This section is based on the above mentioned work. After the procedure is presented, an example on different coloured aggregates is proposed. Finally, the method is used to assess the bitumen aggregate adhesion at different stages of simulated trafficking and after the ravelling induced by the immersion wheel track.

7.2 ImageJ overview

ImageJ is a public domain Java image processing and analysis program inspired by NIH Image for the Macintosh. It runs, either as an online applet or as a downloadable application, on any computer with a Java 1.5 or later virtual machine. Downloadable distributions are available for Windows, Mac OS X and Linux. It can display, edit, analyze, process, save and print 8–bit, 16–bit and 32–bit images. It can read many image formats including TIFF, GIF, JPEG, BMP, DICOM, FITS and 'raw'. It supports 'stacks' (and hyperstacks), a series of images that share a single window. It is multithreaded, so time-consuming operations such as image file reading can be performed in parallel with other operations.

It can calculate area and pixel value statistics of user-defined selections. It can measure distances and angles. It can create density histograms and line profile plots. It supports standard image processing functions such as contrast manipulation, sharpening, smoothing, edge detection and median filtering. It does geometric transformations such as scaling, rotation and flips. Image can be zoomed up to 32:1 and down to 1:32. All analysis and processing functions are available at any magnification factor. The program supports any number of images simultaneously, limited only by available memory. Spatial calibration is available to provide real world dimensional measurements in units such as millimeters. Density or gray scale calibration is also available (Ferreira, 2012).

7.3 Analysis procedure

ImageJ is proposed in this thesis as an effective image analysis tool to interpret results of different tests on asphalt mixtures. The software was primarily used to identify the percentage of bitumen coverage on the aggregates of an asphalt concrete sample. The aim is to offer an alternative assessment method in order to overcome the potential limits of the visual estimation procedure of the rolling bottle test. In this paragraph the image analysis procedure adopted is presented.

Digital pictures of partially bitumen coated aggregates were taken and processed with ImageJ. This estimation is based on RGB images that are subjected through a series of filters, first deleting the background, and then isolating the only bitumen pixels. The

bitumen coverage estimation is made by computing the areas of the bitumen and of the aggregates on the images.

A specific photographic set was developed (Figure 7.1). The tested blends were put into a plate filled with de-ionized water. The plate had a green background and was irradiated with 2 lamps with an angle of incidence of the light beam of 45° in order to avoid reflections. Picture were taken vertically with a 10 MP camera, with ISO 100, from a distance of 30 cm. Pictures were further processed with ImageJ. Among the different colour spaces available, the YUV was chosen.

The YUV color space separate RGB into luminance and chrominance information (Ford et al., 1998) in terms of one luma (Y) and two chrominance (UV) components. Luma stands for brightness, or lightness, while U and V provide color information and are "color difference" signals of blue minus luma (B-Y) and red minus luma (R-Y). YUV was chosen because of its ability to decouple the luminance and color information where the image can be processed with no effect on the other color components (Ibraheem et al., 2012).

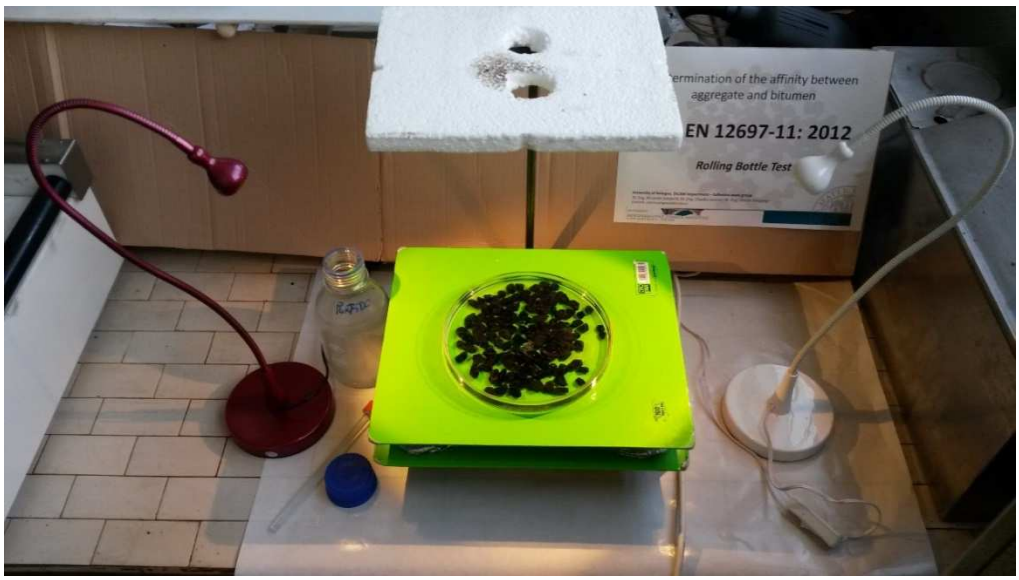

Figure 7.1: Set for digital picturing of tested samples

This peculiarity was confirmed after testing the other available colour spaces (i.e. HSB, RGB and CIE Lab) which gave worse results in terms of quality of the image classifications. The adopted software allows defining a specific threshold for each of the Y, U & V component that compose the image. For this purpose, the plugin “Threshold colour” was downloaded and installed from the company’s website.

After the image was loaded, it was initially cut, in order to focus on a specific Area of Interest (AoI). Therefore, acting on these ranges the image was filtered, leaving out the background. This operation is not perfect and certain black shadows were classified wrongly as belonging to a material. However, as it will be shown later this error is negligible.

Once the image contained only aggregates and bitumen pixels, referred to as non-classified image (Figure 7.2b), the Y, U & V components ranges were further reduced in order to get only the bitumen pixels as shown in the classified image of Figure 7.2c.

Figure 7.2: Image filtering process. a) original image; b) non-classified image; c) classified image

The results at this point are three different images. So the next step was to compute the areas and compare them in order to have a measure of the bitumen coverage of the aggregates. By clicking on “Analyze” and then “Set Measurements”, the “Area” box is ticked.

It is worth to remember that ImageJ allows defining a scale. In other words one can sets how many pixels equal a cm. A ruler, captured with the picture, would help to scale the model. However, the purpose of this investigation was a mere definition of a percentage of area so that the images were not scaled and the software measured the sum of pixels within the specified YUV ranges. The bitumen plus aggregates and the only bitumen areas were automatically computed, enabling the calculation of the percentage of the bitumen coverage of the aggregates with the following equation:

$$Bitumen\ coverage = \frac{A_{bitumen}}{A_{bitumen+aggregates}} \cdot 100\ [\%]$$

The proposed procedure was also validated in order to obtain its degree of accuracy. Pixels colours of samples images were manually checked to understand whether the imaging software classified them correctly (i.e. background, bitumen or aggregate) or not.

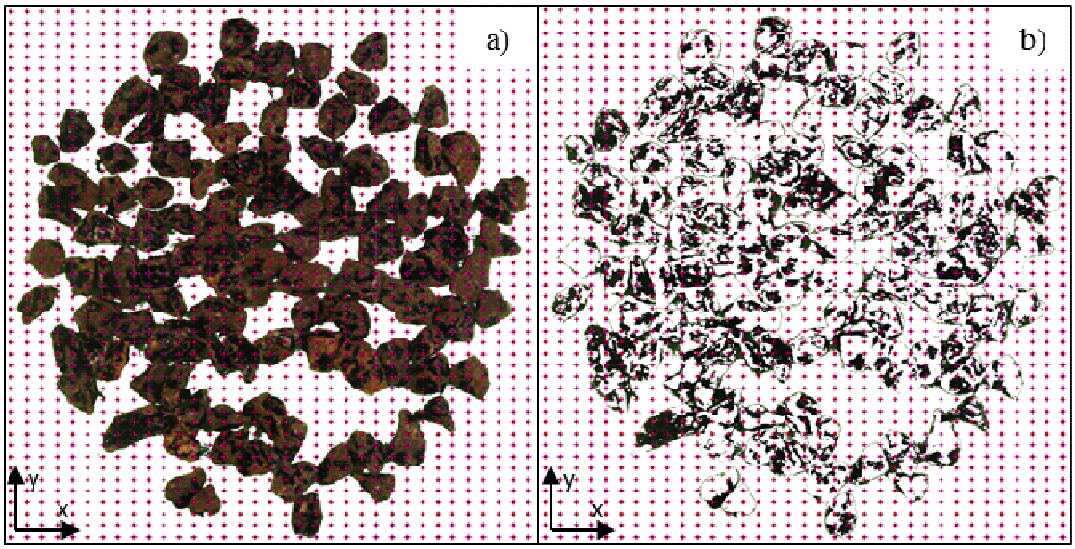

Figure 7.3: Validation of the technique: pixels' color inspection for the non-classified (a) and classified (b) images

For this purpose a specific Java-based code was written, in order to superimpose a 51x51 grid of equidistant points on both the non-classified and the classified image and extract their RGB values and (x,y) coordinates (Figure 7.3).

The selected pixels of both images were grouped in three different classes (aggregate, bitumen and background) based on their RGB values. According to the described procedure of recognition, the passage from the non-classified to the classified image was analysed: if the estimation of the software were correct the bitumen classified pixels would be still classified as bitumen, while the aggregate pixels would be re-classified as background.

The superimposed grid helped in identifying whether the software classification was made correctly or not.

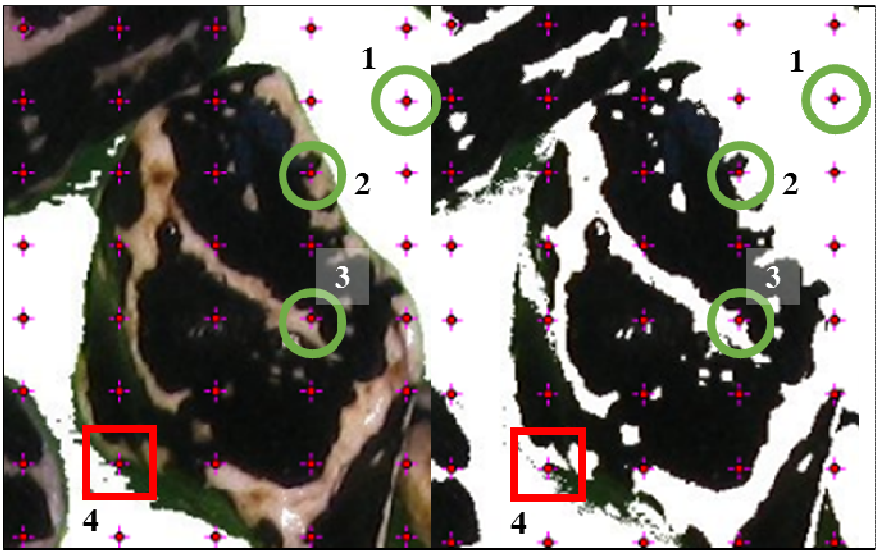

Figure 7.4: Detail of pixels' colour inspection: correct and incorrect classifications

Figure 7.4 shows a detail of the pixels' colour inspection. Circles represent the correctly classified pixels, (1) is background, (2) is bitumen and (3) is aggregate. The square (4) is an example of misclassification; in fact this pixel was classified as bitumen while it was actually a shadow pertaining to the background. However, almost all shadows were classified correctly and represented far less than 1 % of all the background pixels. The adopted procedure validation allowed the generation of confusion matrices, which can be used in a series of descriptive and analytical techniques, such as those based on accuracy indices. In the search for the fundamental characteristics of a generalized confusion matrix for classifications, it is suggested that the matrix should fulfil two characteristics in order to identify a perfect matching case:

- *diagonalization*. The matrix should be diagonal if, and only if, the assessed data match perfectly the reference data;
- *marginal sums*. Marginal sums should match the total grades from the reference and assessed data.

Four different accuracy indexes were computed for each matrix (Table 7.1).

Overall Accuracy OA	Bitumen - Aggregate Accuracy BAA	k-th User Accuracy UA (k)	k-th Producer Accuracy PA (k)
$\frac{\sum_k P_{kk}}{\sum_{kj} P_{kj}}$	$\frac{\sum_{k=1}^{2} P_{kk}}{\sum_{k,j=1}^{2} P_{kj}}$	$\frac{P_{kk}}{\sum_j P_{kj}}$	$\frac{P_{kk}}{\sum_j P_{jk}}$

Table 7.1 Accuracy indexes for a matrix with k classes

Where *Pkj* is the element in row *k* and column *j* and *Pkk* is the element in row *k* and column *k*. An overestimation of the reference pixel membership by the assessed pixel membership leads to errors of commission type (linked to the User accuracy). These commission errors appear in the off-diagonal cells along the row of the class. Conversely, an underestimation of the reference value by the assessed value leads to errors of omission type (linked to the Producer accuracy). These omission errors appear in the off-diagonal cells along the column of the class (Silván-Cárdenas et al., 2008).

7.4 Rolling Bottle test on different coloured aggregates

In order to verify the effectiveness and accuracy of the software, a series of rolling bottle tests was performed. Four different aggregates were tested: porphyry, limestone, basalt and blast furnace slag (Figure 7.5). They were selected in order to cover a broad range of colors.

All aggregates were sieved and washed to obtain a 8-11 mm fraction, according to standard. The adopted base bitumen was a 70/100 pen. Three bottles were tested for each mix for 24 observations. The materials were heated at 160 °C. All the procedures described in EN 12697-11 for mixing and testing were followed. Rolling speed was 60 rpm and the tests were performed at a temperature of 20°C ± 1°C. Visual observation were made after 6 h and 24 h and digital images were taken accordingly.

Table 7.1 shows the YUV ranges found for the image identification of the studied bituminous materials. Y, U & V can vary from 0 to 255. Lower or upper limits vary with different exposure conditions, i.e. with natural light, artificial light only or both. In order to reproduce the analysis of the same materials, an operator could apply these YUV sets

and easily obtain the non-classified and the classified images. For example, for the identification of U parameter of the Limestone in the classified image, the lower limit is chosen between 80 and 100 and the upper limit is 255.

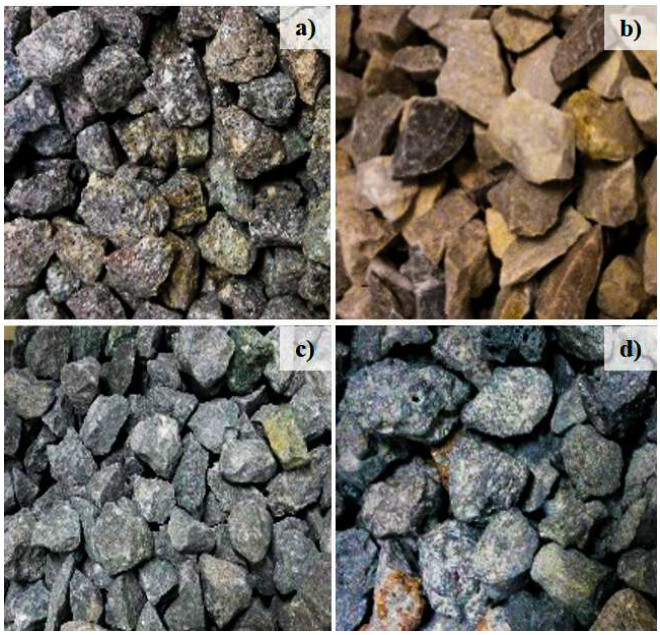

Figure 7.5: Aggregates under investigation: a) porphyry, b) limestone, c) basalt, d) blast furnace slag

		Limestone (L)	Porphyry (P)	Basalt (B)	Blast Furnace Slag (S)
non - classified image	Y	0-195	0-165	0-165	0 - 195
	U	(80÷100) - 255	(80÷90) - 255	(90÷110) - 255	100 - 255
	V	(110÷120) - 255	(115÷120) - 255	(105÷120) - 255	120 - 255
classified image	Y	0 - (55÷85)	0 - (25÷35)	0 - (25÷45)	120 - 255
	U	(80÷100) - 255	(80÷90) - 255	(90÷110) -255	100 - 255
	V	(110÷120) - 255	(110÷120) - 130	(105÷120) - 255	120 - 128

Table 7.2: YUV ranges for materials' recognition

Figure 7.6 shows the results of the tests. The white columns represent the visual estimation carried out by three independent skilled operators, while the dark columns represent the software semi-automatic classification. Results are shown in terms of mean (%) and standard deviation of all the observations, i.e. three for the software and nine for the visual estimations (three bottles and three operators). Considering the software recognition, the limestone exhibited a percentage of coverage at 6 hours of 72.4 ± 1.6 and of 58.4 ± 1.4

after 24 hours. The porphyry was the more prone to stripping (40.6 ± 2.0 after 6 hours and 0.8 ± 0.2 after 24 hours). The basalt showed a higher bitumen coverage after 6 hours 85.2 ± 0.8 and reached a coverage comparable to that of limestone after 24 hours (58.8 ± 2.6). The blast furnace slag gave the best performance compared to the other aggregates (87.91 ± 0.49 after 6 hours and 73.93 ± 1.48 after 24 hours).

Furthermore, Figure 7.6 allows for a comparison between the software and the visual registrations. Regardless of the accuracy, light colored aggregates (L & P) exhibited the higher gap between the visual estimation and the software recognition, with a maximum difference of 22.84 % for the limestone after 24 hours.

On the other hand, differences of recognition for dark aggregates like basalt and blast furnace slag amounted to 5-6%. Standard deviations of the results of the software measurements were smaller compared to those of the visual estimations. As a result, the proposed procedure would give reliable results with less tested bottles, reducing the material needed as well as test and processing time.

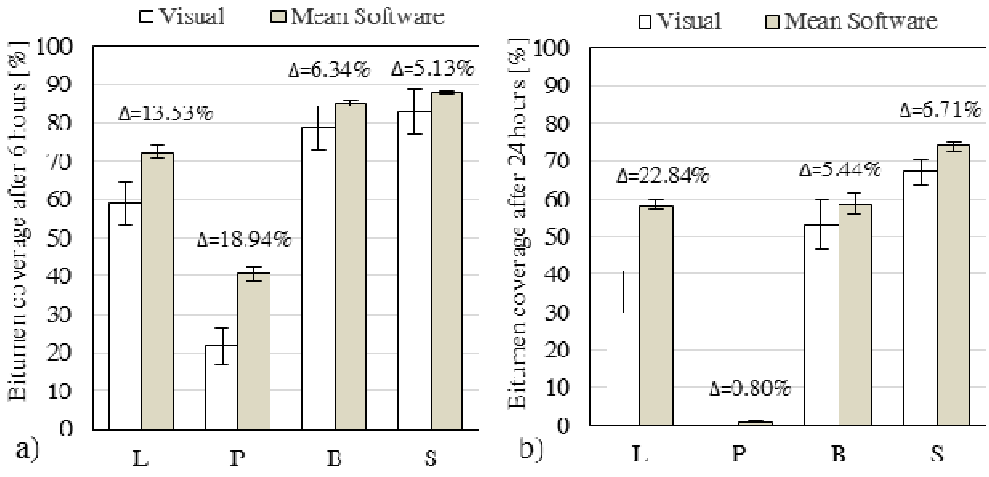

Figure. 7.6: Results of rolling bottle tests after 6 hours (a) and 24 hours testing (b)

Table 7.3, 7.4, 7.5 & 7.6 show the confusion matrices of the tested aggregates and their accuracy indexes. "*bkGD*" stands for background, while "*Bit.*" refers to the bitumen. Results show that the software easily drops out the background, with a producer's accuracy of 100%. The example of Table 3 shows that 5 out of the 208 total pixels of Limestone were classified as bitumen while 17 out of the 222 pixels classified by the software as Limestone actually belongs to bitumen.

		Reference data				
	Class	L	Bit.	bkGD	Sum	*User's Accuracy*
Classified image	L	204	17	2	223	*91.5%*
	Bit.	5	529	8	542	*97.6%*
	bkGD	0	0	1836	1836	*100.0%*
Sum		209	546	1846	2601	
Producer's Accuracy		*97.6%*	*96.9%*	*99.5%*		

Table 7.3: Confusion matrix and accuracy indexes for Limestone

		Reference data				
	Class	P	Bit.	bkGD	Sum	*User's Accuracy*
Classified image	P	421	10	0	431	*97.7%*
	Bit.	15	316	17	348	*90.8%*
	bkGD	0	0	1822	1822	*100.%*
Sum		436	326	1839	2601	
Producer's Accuracy		*96.6%*	*96.9%*	*99.1%*		

Table 7.4: Confusion matrix and accuracy indexes for Porphyry

		Reference data				
	Class	B	Bit.	bkGD	Sum	*User's Accuracy*
Classified image	B	133	16	1	150	*88.7%*
	Bit.	20	568	11	599	*94.8%*
	bkGD	0	0	1852	1852	*100.0%*
Sum		153	584	1864	2601	
Producer's Accuracy		*86.9%*	*97.3%*	*99.4%*		

Table 7.5: Confusion matrix and accuracy indexes for Basalt

		Reference data				
	Class	S	Bit.	bkGD	Sum	*User's Accuracy*
Classified image	S	127	37	0	164	*77.4%*
	Bit.	13	397	10	420	*94.5%*
	bkGD	0	0	2017	2017	*100.0%*
Sum		140	434	2027	2601	
Producer's Accuracy		*90.7%*	*91.5%*	*99.5%*		

Table 7.6: Confusion matrix and accuracy indexes for Blast furnace slag

The software well classified pixels belonging to L and P having a Producer's accuracy of respectively 97.6% and 96.6%. As expected B and S, due to their dark grey color, were by far the most confound with the bitumen. Producer's accuracies were respectively 86.9% and 90.7%.

In the example in table 7.6, 37 out of the total 164 pixels classified as blast furnace slag by the software, actually belonged to bitumen. Table 7.7 shows a summary of the Overall Accuracy (OA) and the Bitumen – Aggregate Accuracy (BAA) indexes for all the adopted aggregates.

Aggregate	**L**	**P**	**B**	**S**
OA [%]	98.8	98.4	98.1	97.7
BAA [%]	97.1	96.7	95.1	91.3

Table 7.7: OA and BAA indexes for the tested aggregates

The OA index shows that the software is highly accurate. The BAA index indicates that the accuracy in recognizing the difference between the bitumen and the aggregate is greater than 95% for L, P and B and greater than 90% for S.

It is concluded that the lighter the colour of the aggregates, the higher the BAA. These results confirmed the validity of the procedure compared to the visual estimation, with a consistent reduction of the errors and of the time for the test execution.

7.5 Effect of rubber on adhesion

7.5.1 Rolling Bottle test

The influence of the rubber on the adhesion was investigated through a rolling bottle test, performed on a 6/8 mm fraction of porphyry. According to 12697-11, the aggregates were sieved, washed and dried at 160°C for three hours; finally they were mixed with a 50/70 pen bitumen. The reference standard recommends the use of 18.0 grams of bitumen for 510 grams of 6/8 mm aggregate fraction. In order to take into account the bitumen content adopted for the SMA slabs under study, which was increased of 1.0% for the 0.75 slab and 2.0% for the 1.20 slab, the samples were composed as shown in Table 7.8.

Sample	***0.00***	***0.75***	***1.20***
Aggregate 6/8 [g]	170	170	170
Bitumen 50/70 [g]	6.0	6.8	7.5
< 420 με Rubber [g]	0	1.3	2.0

Table. 7.8: Composition of the samples for the rolling bottle test

While emptying the bottles at the end of the rolling period, it was noticed the presence of the rubber as loose particles. This followed the adoption of the dry process of rubber inclusion. As the water strips the bitumen from the aggregate, the crumb rubber is pushed away from the surface.

Figure 7.7: Loss of rubber during the Rolling Bottle test

Notwithstanding, results showed a substantial uniformity of the bitumen coverage on three blends tested. Results are shown in Figure 7.8. It is highlighted that the rubber was added to the bitumen – aggregate compound after their mixing, hence once the aggregate was fully coated. Although more tests need to be carried out to fully understand the phenomena, the rubber does not seem to affect the adhesion between the porphyry and the 50/70 bitumen. Further research could vary the proportions and/or the type of materials involved, as well as mix the rubber to the aggregate prior to mixing with the bitumen.

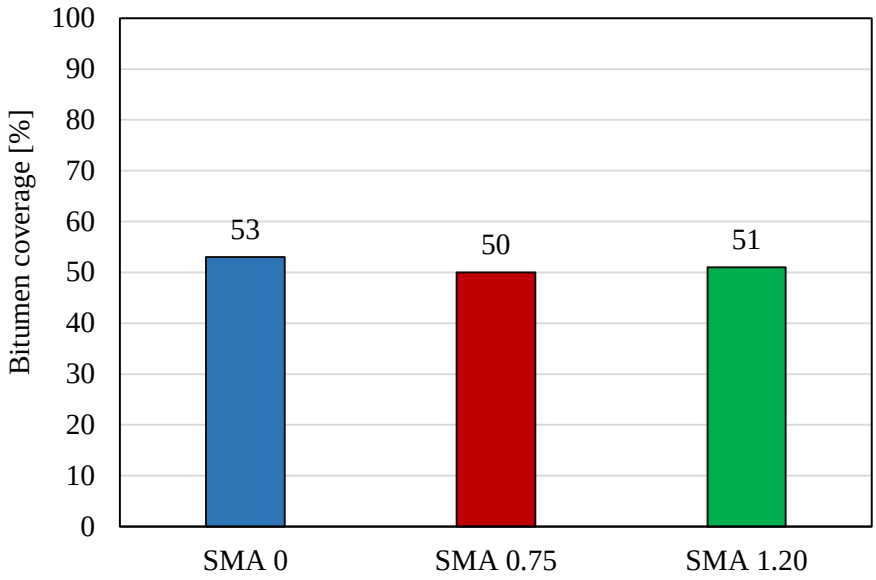

Figure 7.8: Results of the rolling bottle test on bitumen – rubber – aggregate blends

7.5.2 Simulated trafficking – RTM and IWT

ImageJ was also used to evaluate the adhesion of the bitumen to the aggregate mixtures after the slabs underwent the simulated trafficking of Road Test Machine and Immersion Wheel Track.

At the end of each stage, twenty-five pictures of the slab were taken from different orientations, in order to create the 3D model of the sample. This will be discussed better in the next chapter.

The pictures were merged together through the Microsoft Image Compositor Editor (ICE) to create a single high-resolution image of the sample. This software is capable of recognizing similar features between different pictures and performs the alignment and subsequent composition of them to form a single image.

Initially, the pictures were loaded on ImageJ as they were saved from ICE, but this resulted in an excessive computational time for the analysis. For this reason, the pictures underwent an intermediate step analysis into Lightroom®. This allowed cropping the pictures by saving the central square of them, which is one ninth of the slab dimension and approximately 2000 x 2000 pixels.

Lightroom® permitted also to highlight some pictures properties to improve the analysis. For instance, some of them were taken with a high exposure, causing reflections onto the slab surface, especially after the Immersion Wheel Track was performed, when small water droplets appeared as white spots in the picture. By reducing the highlights and the exposure, the noise was reduced.

Indeed, as the slab was not trafficked, it seemed difficult to get the small stripped aggregate as the surface appeared almost exclusively black. By enhancing the saturation of the colour, these parts became more visible, both to human eyes and especially to the software. It is important to highlight that these operations did not altered the colours and then the results of the analysis. On the contrary they made possible an accurate analysis, reducing the noise of the picture and making the photo clearer.

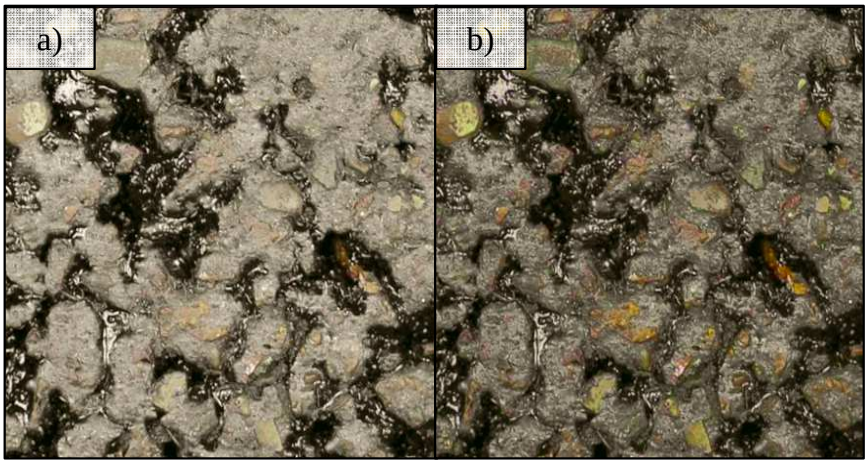

Figure 7.9: Picture improvement through Lightroom®

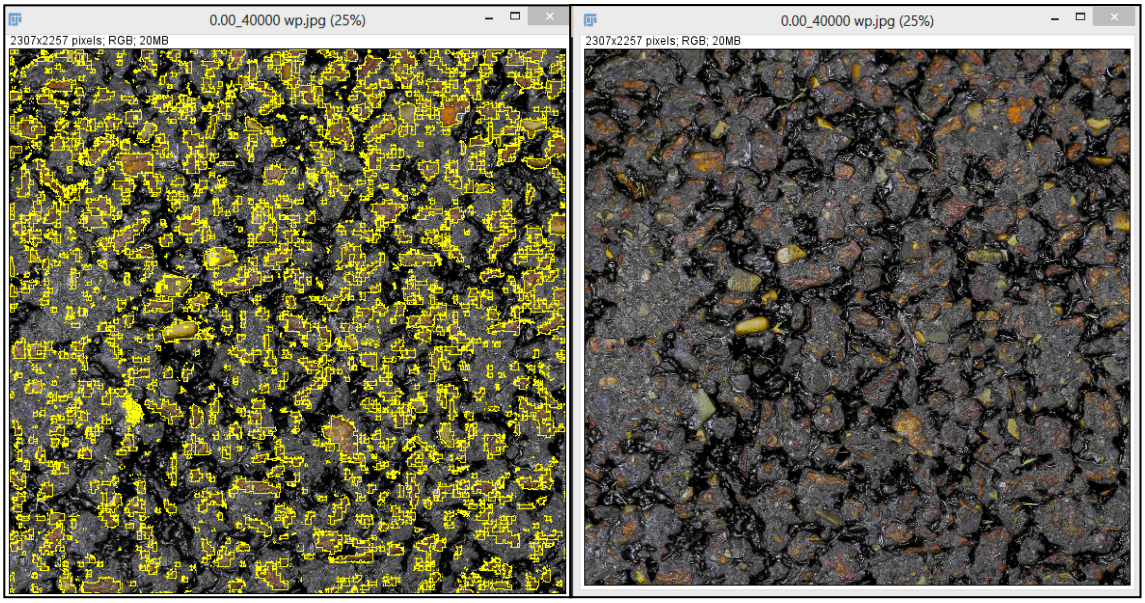

Figure 7.10: Picture analysis with ImageJ

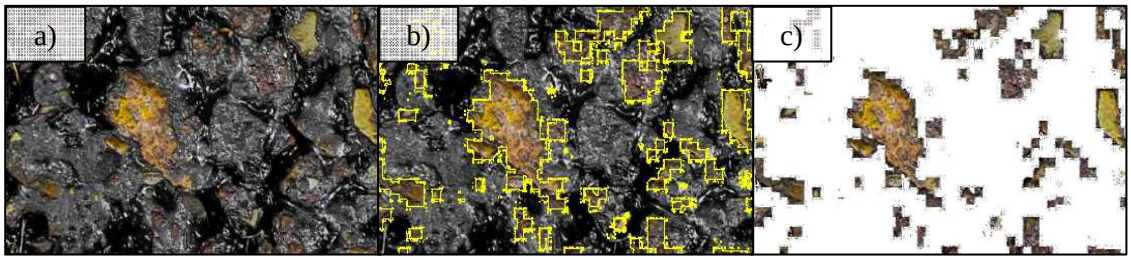

Figure 7.11: Areas selection process with ImageJ

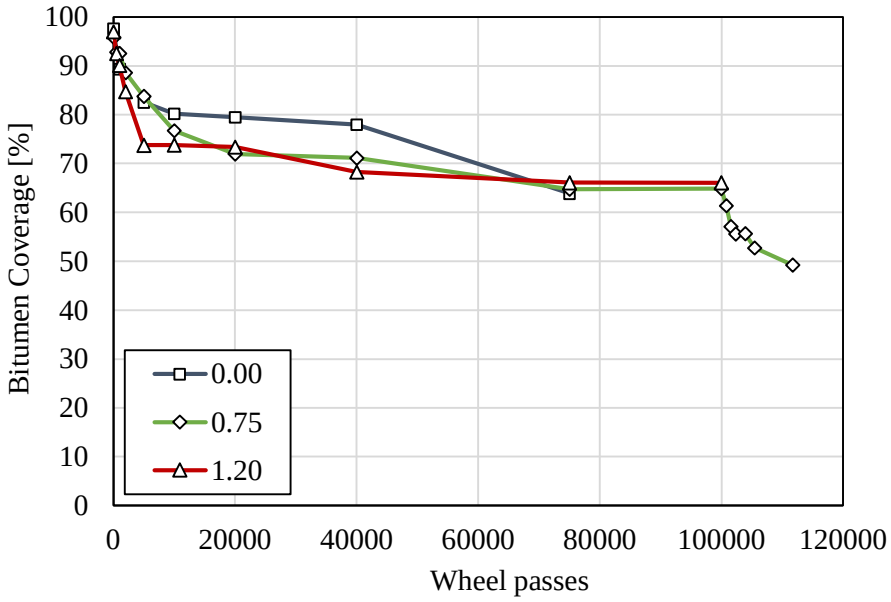

Figure 7.12: Development of the adhesion with trafficking for SMA surfaces

Figures 7.10, 7.11 and 7.12 show the picture improvement through Lightroom® and the slab analysis with ImageJ respectively.

Results of the 2D Image analysis for the trafficked rubberized SMA slabs are shown in Figure 7.12. Initially, the simulated trafficking rapidly wear the surfaces, which appear stripped from the bitumen for almost the 30% at 5000 wheel passes.

The rate of stripping then clearly reduces and the adhesion reaches an equilibrium at 75000 wheel passes. It is interesting to observe that the dropping of the adhesion seems to be accelerated by the presence of the rubber, notwithstanding the bigger amount of bitumen of the rubberized surfaces. Indeed, the classic SMA keep the adhesion at higher level until 40000 wheel passes.

As expected, the Immersion Wheel Track caused a strong stripping of the bitumen of approximately 15% after 225 minutes of testing. The lack of adhesion will certainly make the slab weaker and prone to failure.

Chapter 8

3D Image analysis

8.1 Image capturing technique

Close Range Photogrammetry (CRP) was used as a non-contact method of capture for 3D modelling.

Development of the CRP method considered the main factors that influence the method. Initial calibrations allowed understanding the method of photos acquisition in terms of number of pictures, orientation of the cameras and type of framework. In order to achieve a good accuracy of the models that would not be too detrimental to the computation time, a series of 25 images were taken for 275 x 275 mm slabs, ensuring at least 60 % forward overlap and at least 30 % side overlap. The camera was fixed on the shaft of a trolley and the slab was moved after each picture was taken, so that the camera positions would form a regular 5 by 5 matrix across the slab.

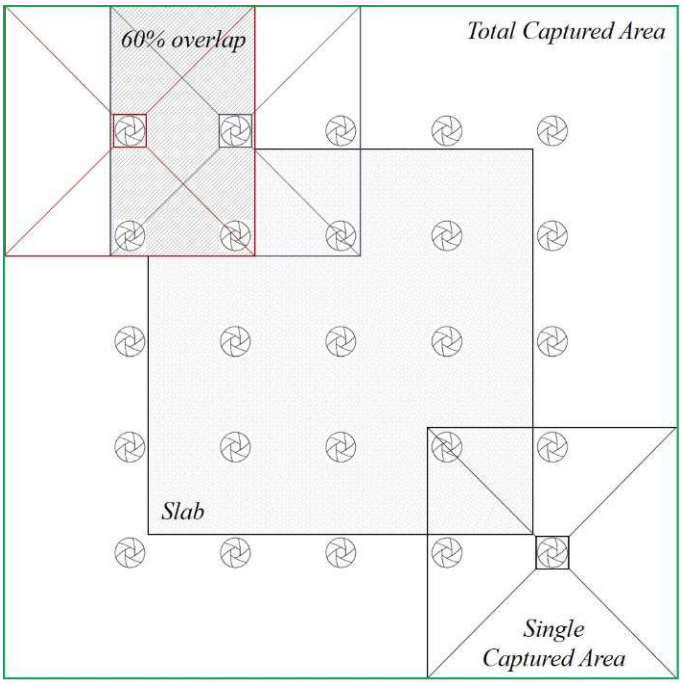

Figure 8.1: CRP acquisition method for slabs

Contextually, a series of 14 images were taken for 10mm diameter cores, moving the slabs so that 2 rows of four picture would be taken across the diameter, and 2 rows of three on the edge of the cores. The acquisition method is shown in Figure 8.1.

CRP photogrammetry requires a specimen coordinate framework (Millar 2013). This was achieved using a reference framework of control points during image capture to allow the recovery of surface elevation. Two methods were tried i.e. a scale rule and a calibrated aluminium framework of control points. Although the use of a scale rule provides recovery of surface elevation, it does not permit orientation of the surface. However, this can be rectified by applying a bi-rotational transformation to the specimen 3D model.

Difficulties emerged in modelling the pins of the calibrated aluminium framework during initial tests. This way would have been impossible to correlate the reference points and consequently apply the scale to the models. The use of the ruler was the preferred method and was used in the totality of laboratory investigations. An angular ruler was then fixed with tape to the slab prior photos acquisition. CRP images were captured using a Canon EOS 6D with 20.2 megapixel full frame sensor and 100 mm Macro lens, which is a high standard SLR camera, ensuring high quality images.

Natural light and two LED lights one in front of each other illuminated the sample during acquisition. No flash was used. A remote shutter release was adopted to minimise camera shake. The accuracy of CRP relies on the quality of images captured. Calibration was not required for the 3DF Zephyr Pro software.

8.2 Model creation – Zephyr, Meshlab

8.2.1 Introduction

Zephyr is a software for the 3D reconstruction of objects from photos. It was developed by 3Dflow, a consultancy company established under in 2011 as a spin-off of the University of Verona. It is based on a Structure from Motion (SfM) pipeline, codename Samantha, which is a range imaging technique. Sfm refers to the process of estimating three-dimensional structures from two-dimensional image sequences, i.e. through a moving camera (the motion). Three-dimensional reconstruction is the process of recovering the properties of the environment and optionally of the sensing instrument from a series of measures.

The first stage of Samantha is devoted to the automatic extraction and matching of keypoints among all the *n* available images. Its output is to be fed into the geometric stage that will perform the actual structure. Good and reliable matches are the key for any geometric computation. The images are organized into a tree with agglomerative clustering, using a measure of overlap as the distance. The reconstruction then follows this tree from the leaves to the root. As a result, the problems is broken into smaller instances, which are then separately solved and combined. The dendrogram produced by the clustering stage imposes a hierarchical organization of the views. After the sparse point cloud is generated, a novel multiview stereo algorithm that fully takes advantage of the output of a structure and motion pipeline is applied to generate a dense point cloud.

The main characteristics of Zephyr can be summarized as follows:

- automatically recovering of the relative cameras positions and orientation along with a sparse reconstruction of the scene directly from a set of casual images;
- Fully automatic camera orientation process;
- Tree-based reconstruction to handle an high number of photos.

An extensively description can be found in the PhD thesis of Toldo (2013).

8.2.2 3D model creation

The 3D modelling method of the samples was carried out through 3DF Zephyr Version 1.020 software. The modelling was in 3 stages:

- reconstruction project: sparse point cloud;
- creation of a dense point cloud;
- scaling, rotating and exporting of the model for the analysis.

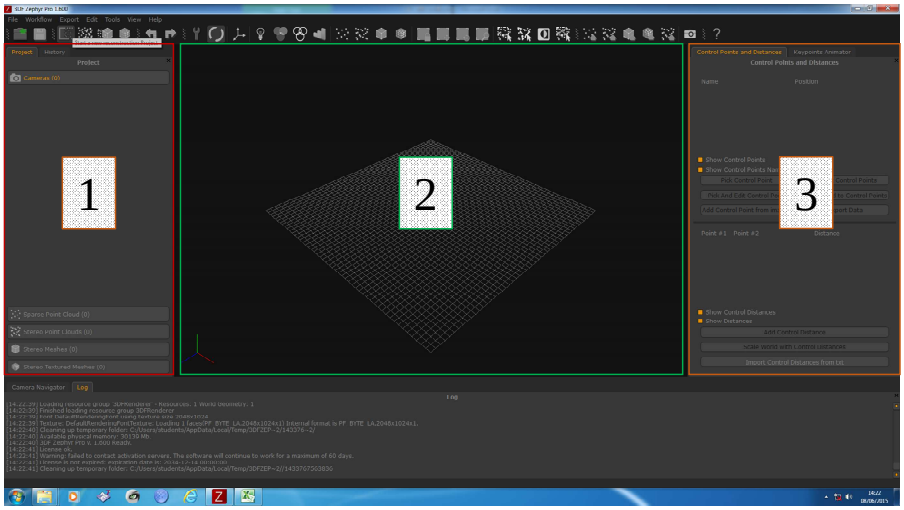

Figure 8.2: Initial Zephyr screen

Zephyr's interface is made of three main windows as shown in Figure 8.2.

On the left there is the project window which summarizes the number of pictures loaded and enlist the mesh reconstruction types. The main window is the workspace, which visualizes the results of the software analysis. The third window is used to manage control points and distances, which help scaling the model to xyz real dimensions. The first step was to use create a sparse point cloud by stitching together the photographs of a sample.

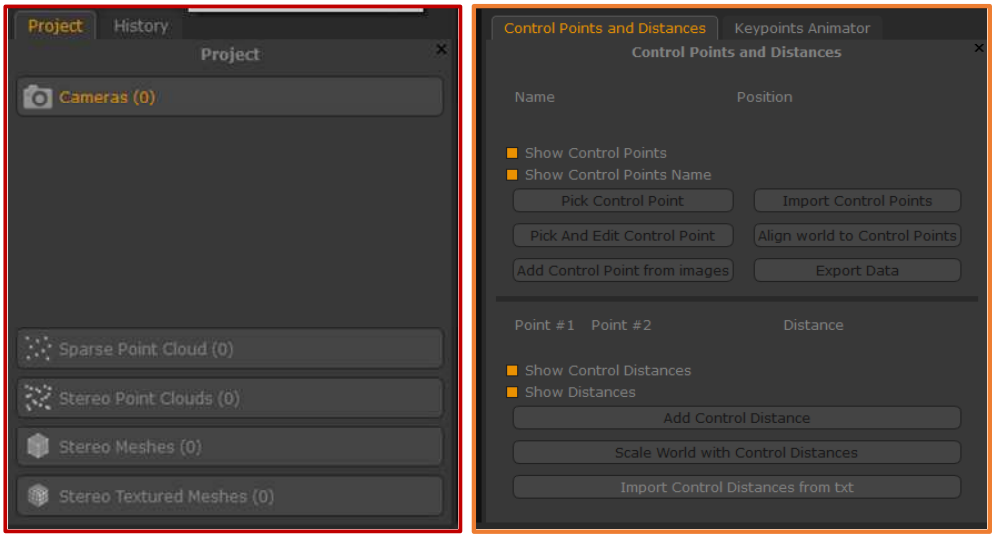

Figure 8.3: Zephyr window 1 and 3 (control points and distances)

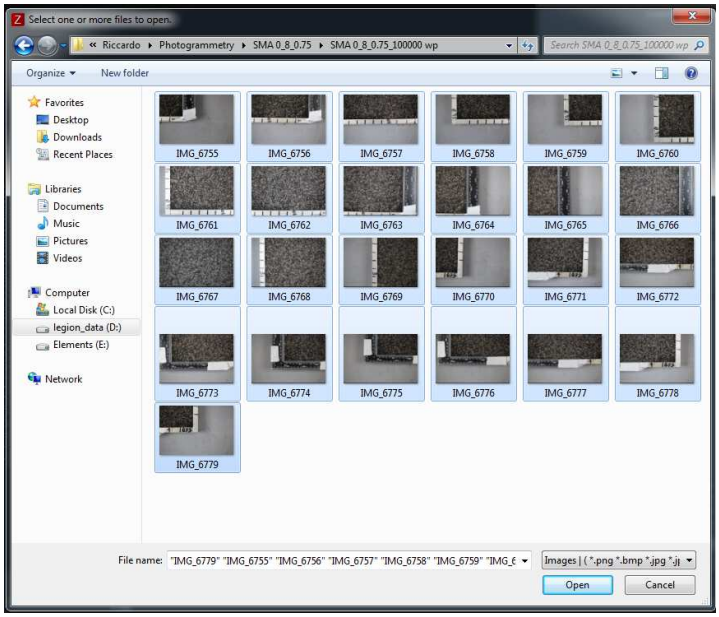

Figure 8.4: Picture loading window

Once the necessary photographs were added to the wizard, a screen displayed calibration, camera and lens information. The settings selected to ensure a higher level of accuracy compared to the default settings, are shown in Table 8.1. This lengthened the process but provided a more accurate model.

Name	Setting	Default
Keypoint Density	High	Medium
Matching Type	Accurate	Fast
Matching Stage Depth	Automatic	Automatic
Reprojection Error Tolerance	Strict	Normal
Bundle Adjustment	Full	Local
Photo Ordering	Unordered	Unordered

Table 8.1: Settings for the sparse point cloud computation

- *Keypoint Density*: let you control the number of keypoints to be extracted for each image. The more keypoints are extracted the more times is required, but the chances to align more images are increased.
- *Matching Detail*: let you control the number of pairwise matching between images. The higher, the more time is required, but the chances to align more images is increased.

- *Matching Type*: let you control the mode the features are matched between images.
- *Error Tolerance*: let you control the maximum reprojection error during the geometric reconstruction. A 'strict' value may lead to more accurate reconstructions while a 'wide' value may increase the chances to align cameras that would otherwise be discarded.
- *Bundle Adjustment Mode*: The bundle adjustment is an internal routine that minimizes the reprojection error at the end of each reconstruction stage. With the 'Full' mode all the cameras and points will be adjusted, while the 'Local' mode is more efficient and uses only the strictly needed points at each stage and the 'Local and Restrained' uses a bounded maximum number of points for each camera
- *Photo Ordering:* 'Sequential' means photos were taken in a sequential way (photo 1 close to photo 2, photo 2 close to photo 3 and so on...), Unordered will result in a longer run time.

Moreover, the software ask for the camera orientation presets, allowing to select from a drop down menu between aerial, human body, urban and close range, which was the selected option. After having summarized the session, it is possible to launch the calculation.

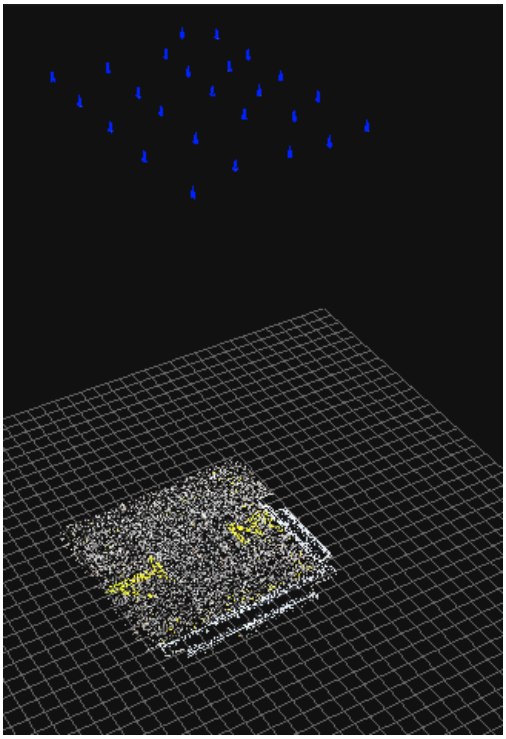

Figure 8.5: Camera orientations

After the computation, the newly created sparse point cloud is loaded on the workspace as shown in Figure 8.6. A pop up menu indicate whether the photos have been oriented and then used for the cloud creation. If the reconstruction has been successful, blue dots show up the camera positions from which photos were taken.

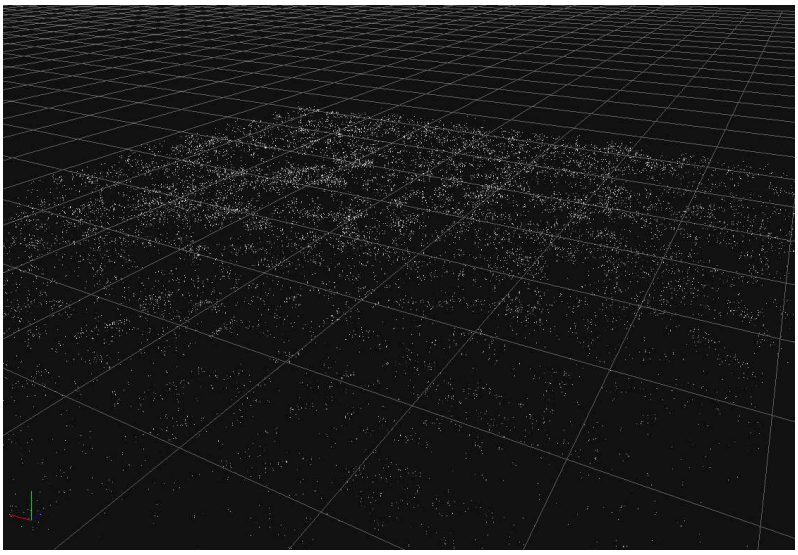

Figure 8.6: Sparse point cloud

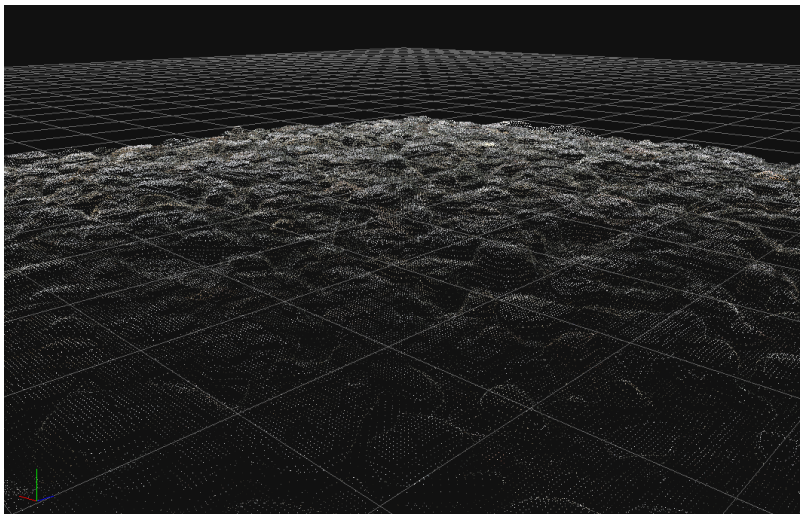

Figure 8.7: Dense point cloud

The next step was to create a dense point cloud. The settings were left as default. The sparse point cloud was cleaned before launching the computation in order to remove any anomalies that could affect the results. Figure 8.7 shows a screenshot of the created dense point cloud.

The next step was to create the mesh. The only setting change was to increase the polygon count to high, giving a more accurate representation of the surface. This controls the number of triangles in the final mesh. Figure 8.8 shows the newly created mesh. The mesh was exported in .PLY format for further processing.

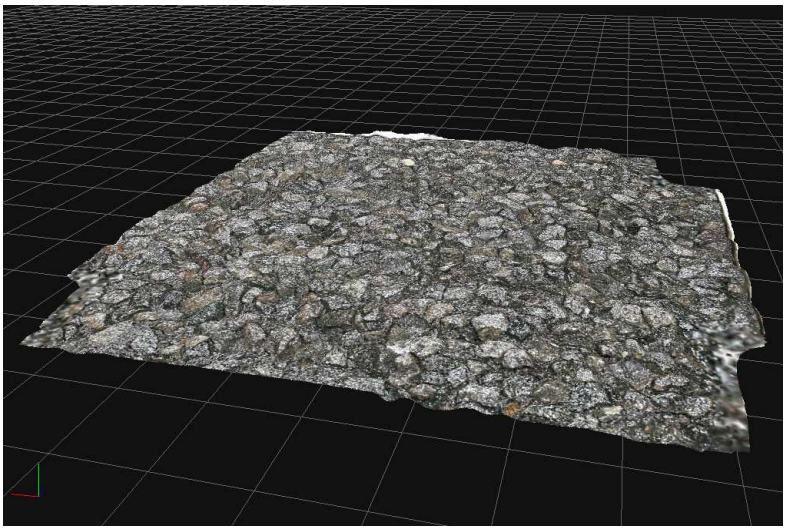

Figure 8.8: Final mesh

Models created in Zephyr must be scaled to the real dimensions of the samples. For this purpose, a series of control points were selected by picking the same point on multiple images so that the software will adapt the mesh accordingly. In order to facilitate the visual recognition, prior to photos acquisition an angular ruler was fixed to the steel frame of the slab so that it was captured together with the sample. Figure 8.9 shows a screenshot taken during the control point acquisition; in this example, the 90 mm mark was selected on seven different images. For each model created, four different control points, i.e. known centimetre markers, were selected.

The final step allowed to proper scale the model. First, two cross distances between the known control points were added for each model, and the real distance set between them. Then, by selecting ‘Scale world with control Distances’, the software scale the model and re-arrange the clouds accordingly.

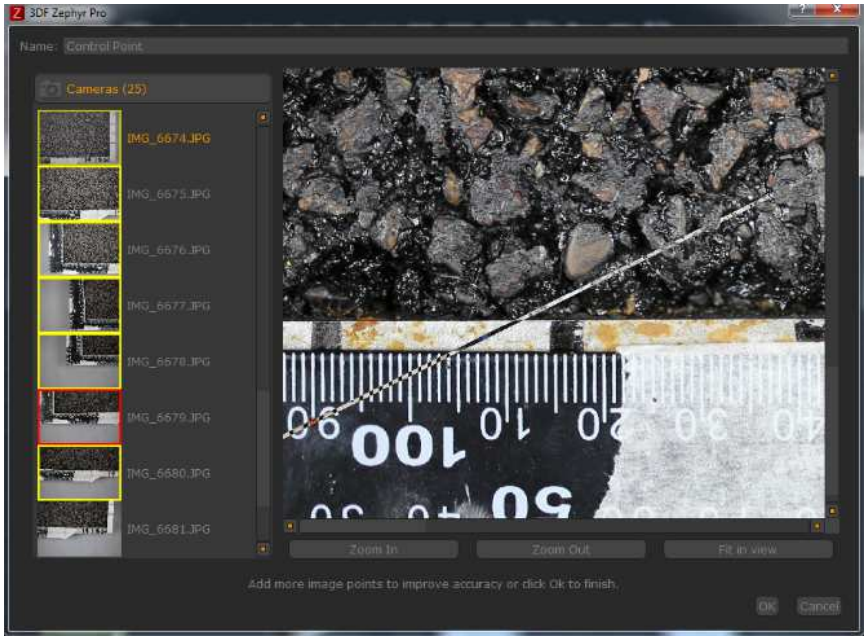

Figure 8.9: Final mesh

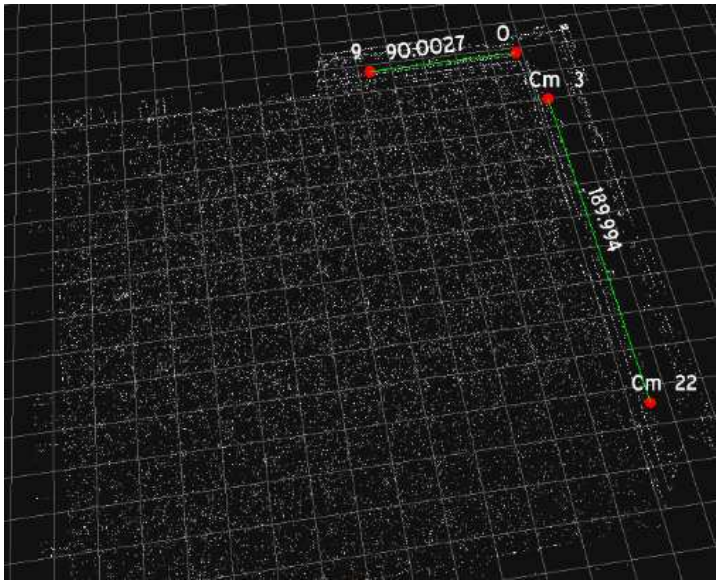

Figure 8.10: Final mesh

A pop up window appear, with a message of the mean residual value. The closer this value to 0 the more accurate the scaling. Achieving a value over 1 translates to a high level of inaccuracy and so the process should be repeated. The residual value was less than 0.01 for each model created.

This process can also be used to check the accuracy of scaling with control points. If the model has already been scaled, the program will give a measurement of the distance

between the two points. The new mesh with the defined control distances is visible on the workspace, as seen in Figure 8.10.

The format of the created mesh is .PLY. Due to restrictions on the software Mountains Map cannot open this type of file. In order to convert the file, Meshlab was used. This program was also used to orientate the sample correctly. When the mesh is imported the display is a side view of the upside down mesh. In order to correct the filter “Transform Flip and/or Swap Axis” was applied.

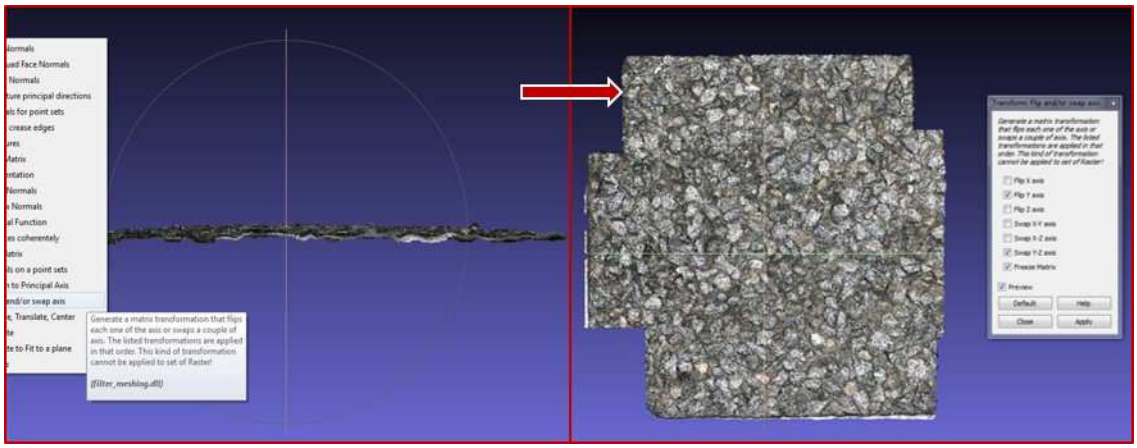

Figure 8.11: Final mesh

There is a notable colour difference when the Y axis is swapped. This present due to the lights during photo acquisition. It helps to identify the correct surface to orientate. The mesh was then exported in .XYZ format so it could be opened in Mountains Map.

8.3 Surface imaging analysis – MountainsMap

All of the 3D models created in this thesis were analysed using Digital Surf MountainsMap Version 7 spatial information software. MountainsMap allows 2D and 3D analysis of areal surface texture (EN ISO 25178). A 3D model file is imported in the .xyz format allowing a studiable to be formed. The term studiable refers to a MountainsMap document that contains a dataset upon which analysis can be carried out.

Prior to the investigations, different operators were applied to prepare the 3D model for analysis:

1. Selection of the Area of Interest for analysis. The slab dimension, i.e. a 275 mm side square, was reduced to a 145 by 225 mm rectangle centred to the longitudinal

axis. This allowed to compare the change in texture induced by the RTM with the wearing induced by the IWT focusing on the same area. Cores, whose diameter was 150 mm were analysed to an extent of 120 mm, leaving out the external 30 mm.

2. Level by using rectangle least squares option in order to make the mean plane within mountains.
3. Remove form
4. Re-level as the mean plane value had changed.
5. Set threshold function to remove top 0.5% of values. This brought the surface much more levelled and reduced surface noise generated by zephyr while trying to compute deep holes.
6. Re-level

This series of operators for the studiable adjusting was applied for each model to ensure the analysis was carried out with appropriate and accurate models, with the least possible noise.

The operators used for the analysis varied according to the different investigations and will detailed prior to showing the results.

8.4 Preliminary analysis

A preliminary study was made to assess the influence of the various parameters extracted from MountainsMap. The three 8 mm slabs were compared with other Stone Mastic Asphalt gradations: a 0/6 150 mm core, a 10 mm 275 x 275 mm slab and a 0/14 150 mm core. The materials are shown in Figure 8.12.

The Volume of Peak Material was investigated by altering the lower limit, p to predetermined areal material bearing ratio (AMBR) values on each Abbott Firestone Curve (Figure 8.13). The upper limit, q was maintained at 80 % AMBR. Figures 8.14, 8.15 and 8.16 show how Vmp, Vmc and Vvv change due to different AMBR sets. As the lower bearing ratio is raised the Vmp increase at the expense of the Volume of Material core. As the lower limit is set at the same value of the upper limit q, i.e. 80%, the Volume of Material Core is zero (Figure 8.15).

As expected, the bigger the aggregate gradations, the bigger are the Vmp and Vmc recorded. The Volume of Void is not affected by a change in the lower limit as it depends upon a change in the upper limit only.

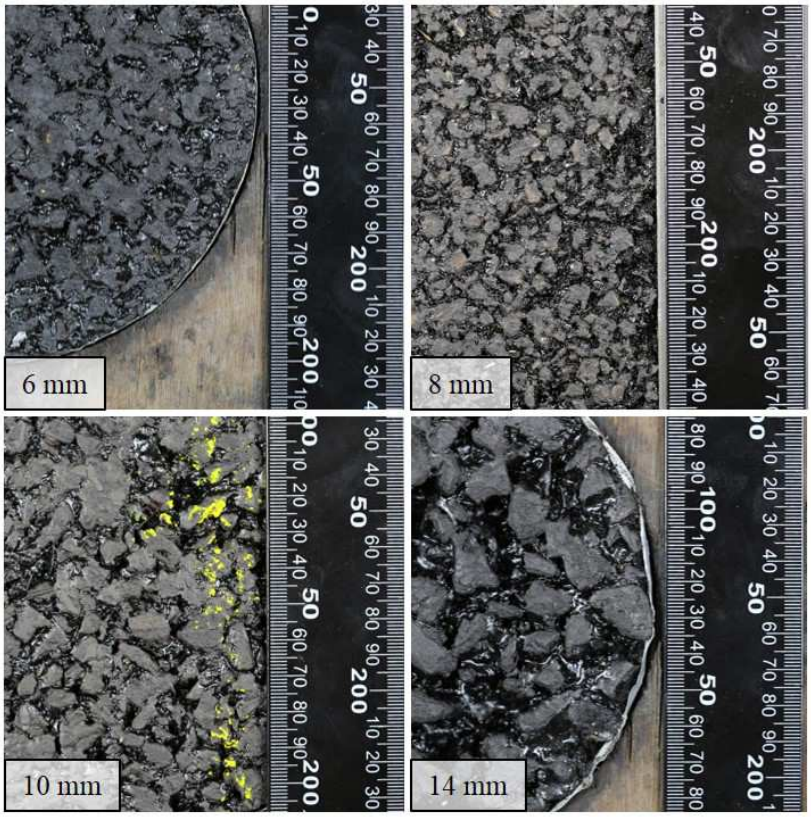

Figure 8.12: different gradations of SMA under study

Figures 8.17 plots Vmp against PTV where the lower limit, p was adjusted to 5%, obtaining Vmp5. The upper AFC limit, q was maintained at 80 %. The Figure plots all data during simulated trafficking, from 0 to 100000 wheel passes. No correlation is evident between Vmp5 and PTV, indicating that the friction is not related with the magnitude of Vmp. This results is in line with McQuaid (2014).

Figure 8.18 plots Vmp80 against Mean Texture Depth, measured with the Sand patch method, throughout simulated trafficking. Data are clustered based on the aggregate gradation. A linear correlation with an R^2 value of 0.94 was found, demonstrating Vmp at 80 % AMBR to increase with increasing MTD. Figure 8.19 plots Sa against Vmp80. The good linear correlations, especially for 6 mm and 8 mm samples suggest Sa could be used to estimate Vmp80 without analysing the AFC.

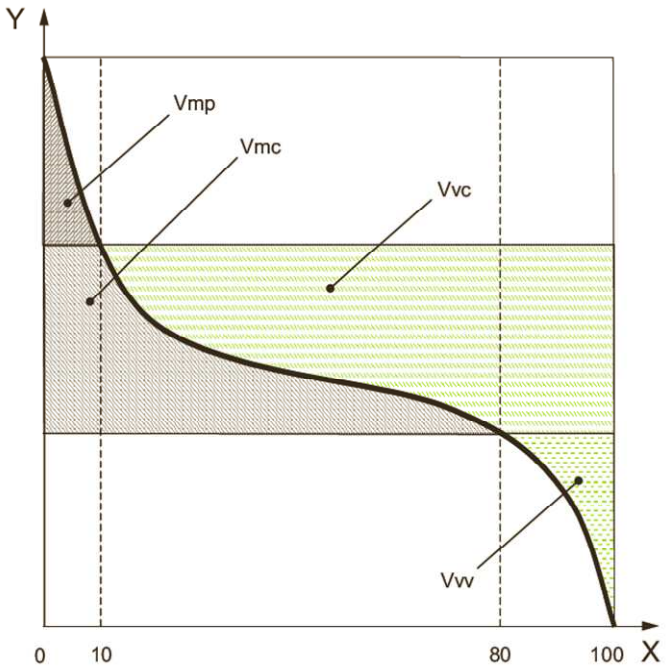

Figure 8.13: Void volume and material volume parameters (EN ISO 25178:2012)

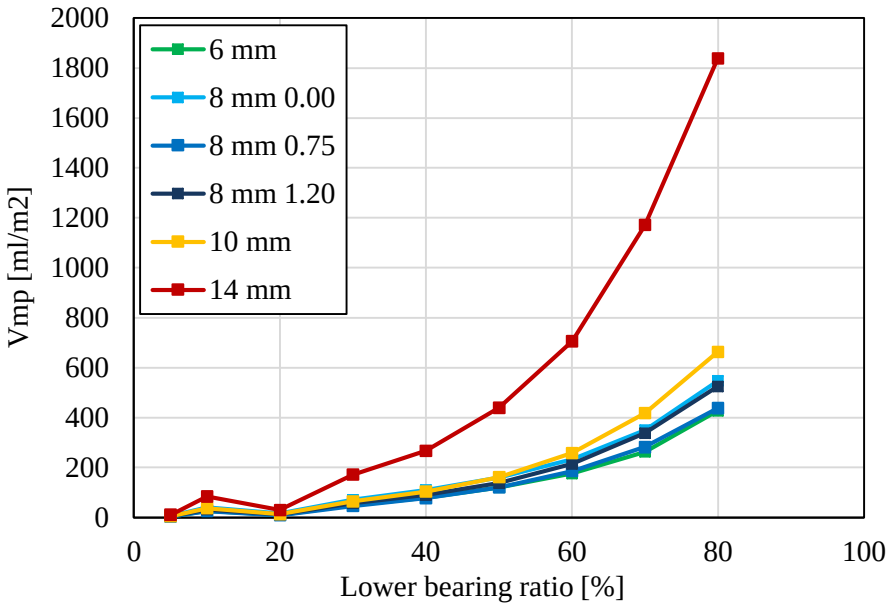

Figure 8.14: Vmp versus lower bearing ratio

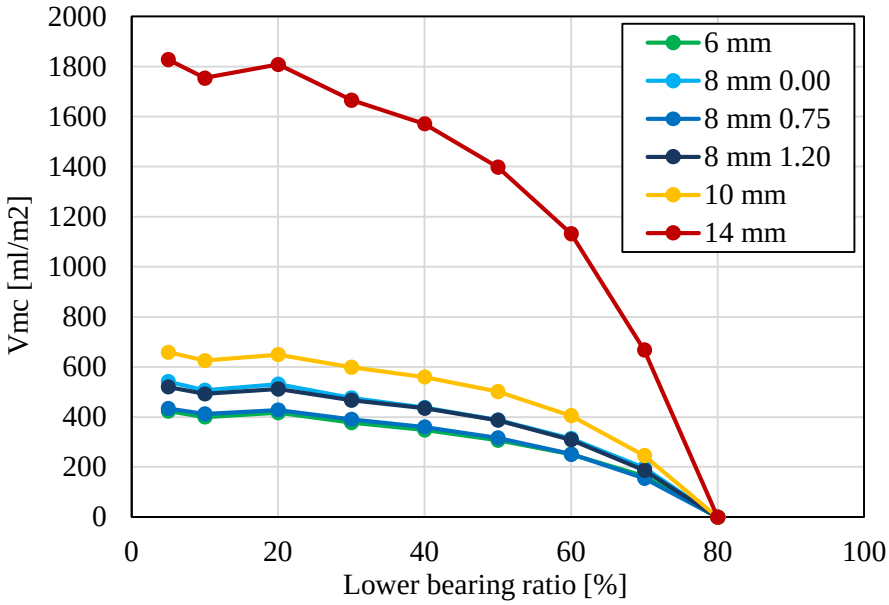

Figure 8.15: Vmc versus lower bearing ratio

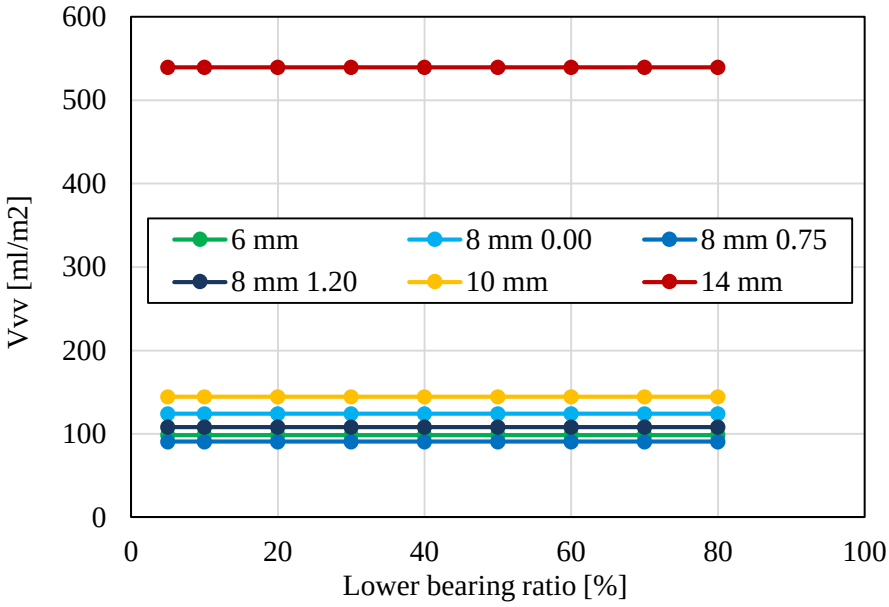

Figure 8.16: Vvv versus lower bearing ratio

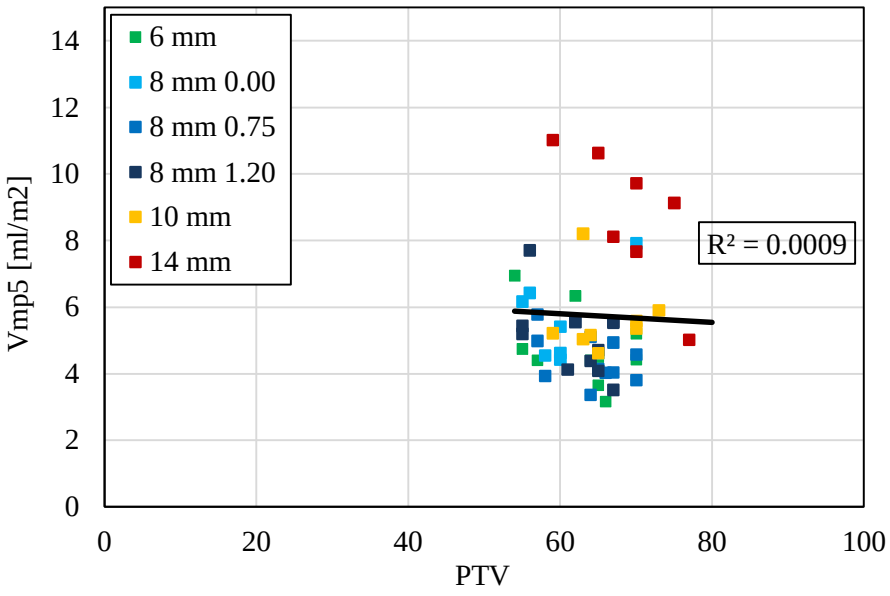

Figure 8.17: Vmp5 versus PTV

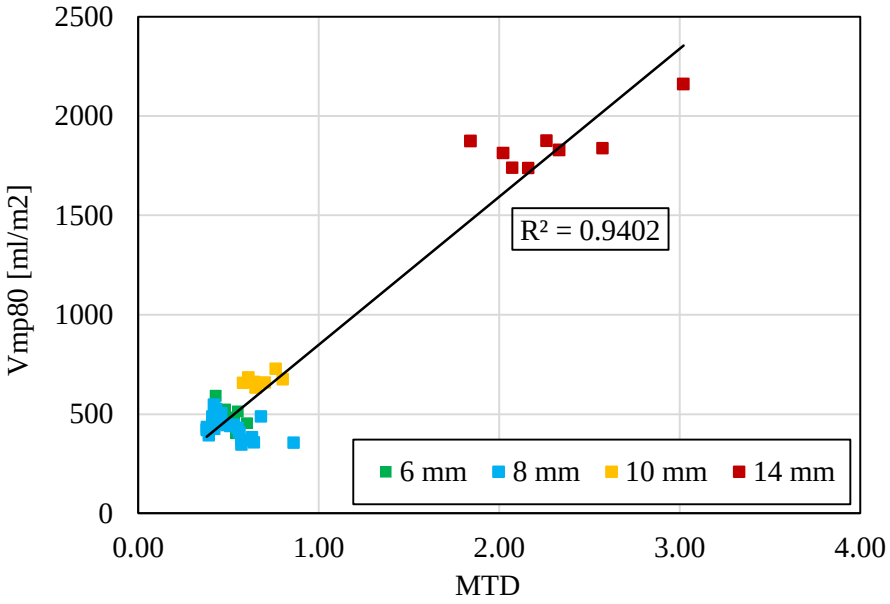

Figure 8.18: Vmp80 versus MTD

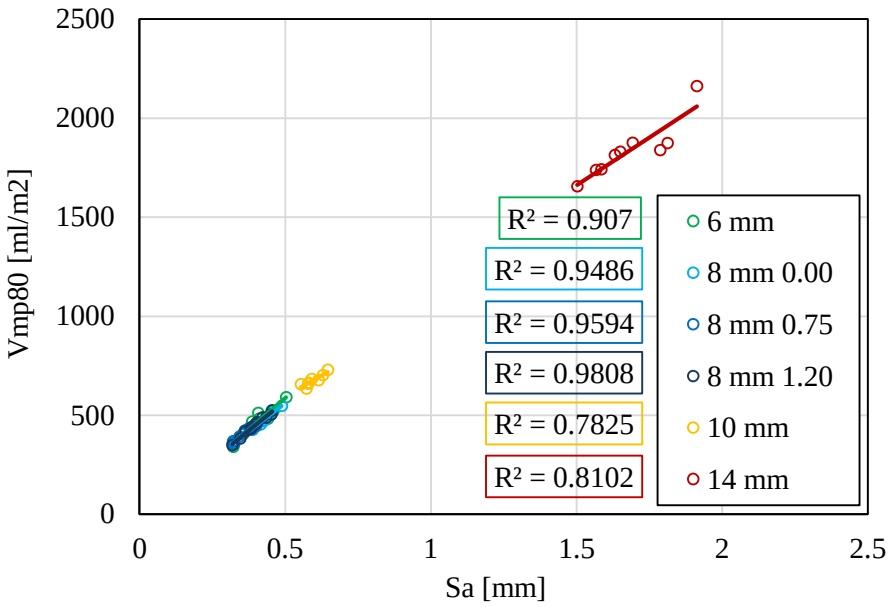

Figure 8.19: Vmp80 versus Sa

8.5 Results - Texture change with trafficking

8.5.1 Abbott-Firestone Curve and surface heights parameters

The most important and famous investigation for 3D models of asphalt surfaces is related to the Abbott Firestone Curve, AFC.

The Areal Material Ratio Curve, i.e. Abbot Firestone Curve, is established by evaluating the material ratio at various levels from the highest peak to the lowest valley. The volumetric parameters were investigated by setting the lower limit, p, to 5% and the upper limit, q, to 80% on each AFC.

The Material Volume parameters Vmp, Vmc, Vvc and Vvv were extracted for each 3D model and plotted versus the wheel passes to understand how they change with the simulated trafficking.

An example of the evolution of 3D models throughout trafficking, magnified on the z axis, is shown in Figures 8.20. They can help understanding the subsequent analysis and plots.

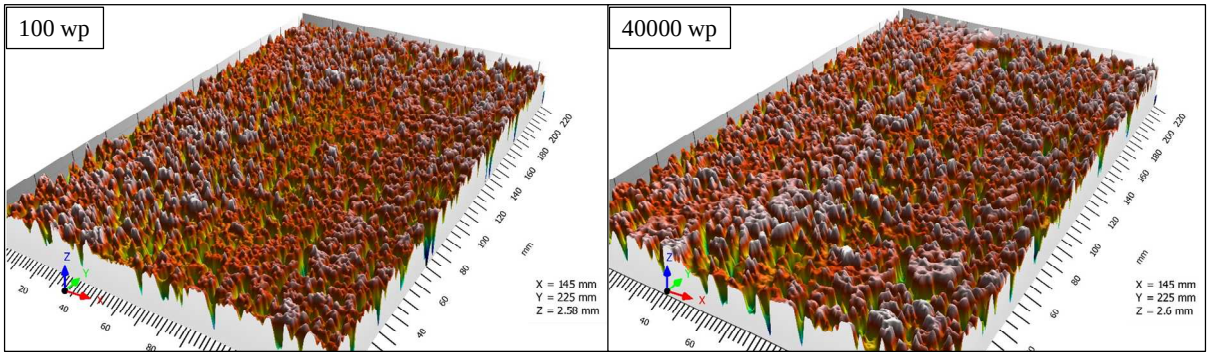

Figure 8.20: 3D Models of the 0.75 slab at different trafficking stages - RTM

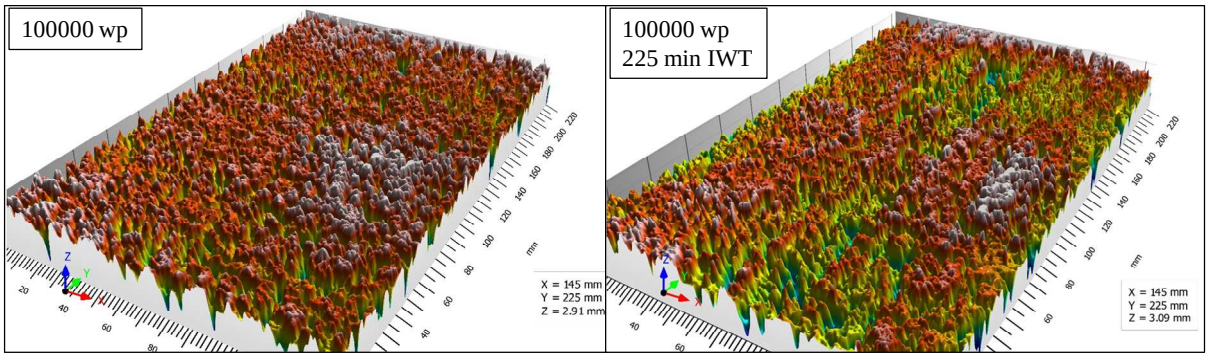

Figure 8.21: 3D Models of the 0.75 slab at different trafficking stages – end of RTM and IWT

8.5.1.1 Comparison between the slabs

Figures 8.22 and 8.23 show the development of Volume of Material Peak. The behaviour of the three slabs is very similar as they are characterized by the same sequence: an initial drop, a rise at 2000 wheel passes (Figure 8.22), another drop followed by a constant increase in Vmp5 starting from 20000 wheel passes (Figure 8.23).

The value of Vmp shows an overall increase with time. As the surface texture is worn, the depth, at which the cross sectional area of the slab surface along a plane represents the 5% of the entire slab cross sectional area, moves down and the volume of peak changes accordingly.

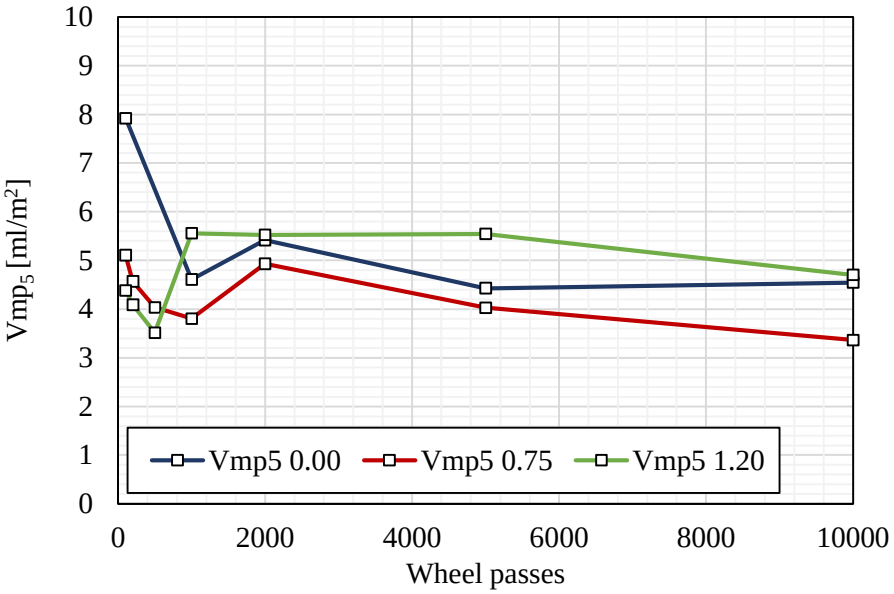

Figure 8.22: Volume of material peak 5% low limits for 8 mm slabs, early life

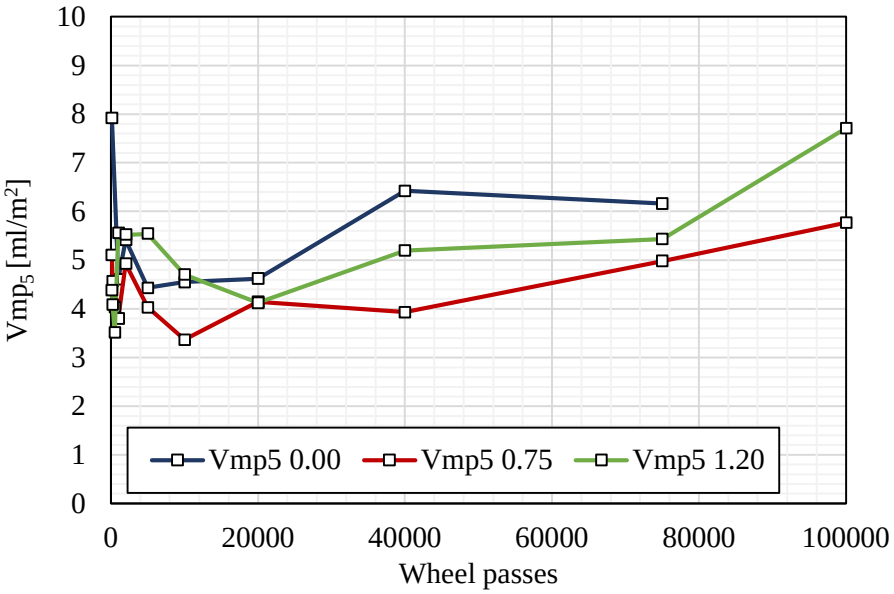

Figure 8.23: Volume of material peak 5% low limits for 8 mm slabs

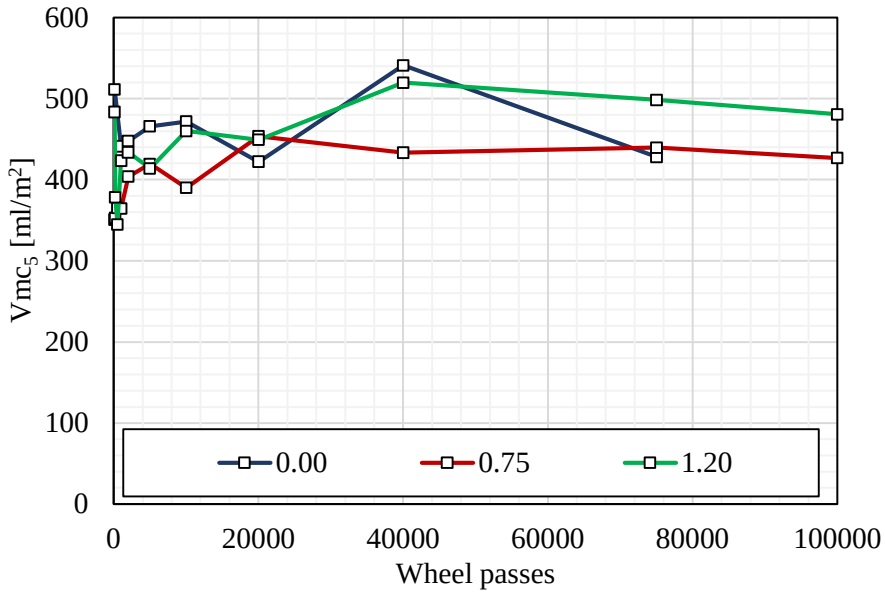

Figure 8.24: Volume of material core 5% low limit for 8 mm SMA

The Dale Void Volume Vvv, is the volume of space bounded by the surface texture from a plane at a height corresponding to 80% material ratio level to the lowest valley. As shown in Figure 8.25, after initial fluctuation the parameter stabilized to a greater value during RTM. An outlier was found for the 0.0 slab. The volume of material core, shown in Figure 8.24, exhibits a trend similar to that of Vmp.

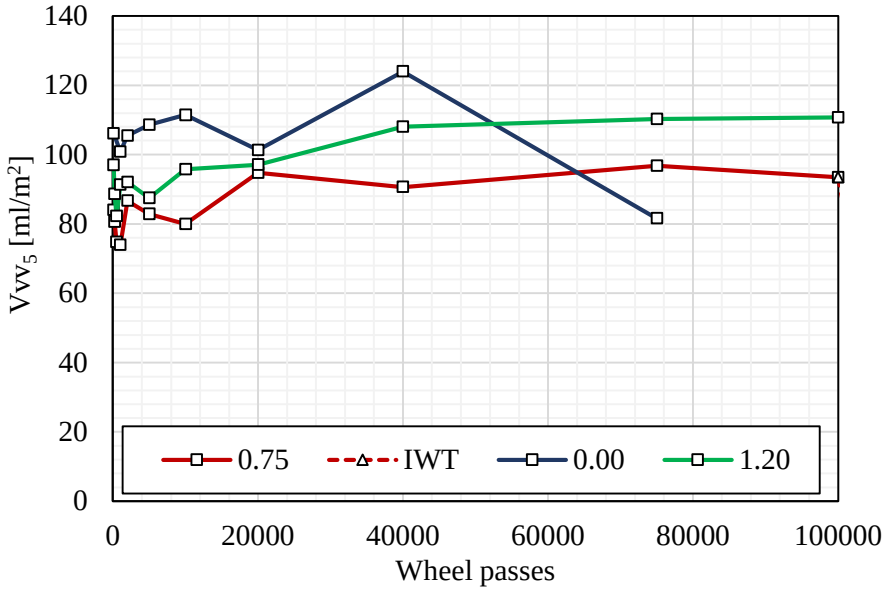

Figure 8.25: Volume of void 5% low limit for 8 mm slabs

Figure 8.26 shows the change of Sk with the simulated trafficking. Sk, which is the distance between the highest and lowest level of the core surface, generally increased with trafficking.

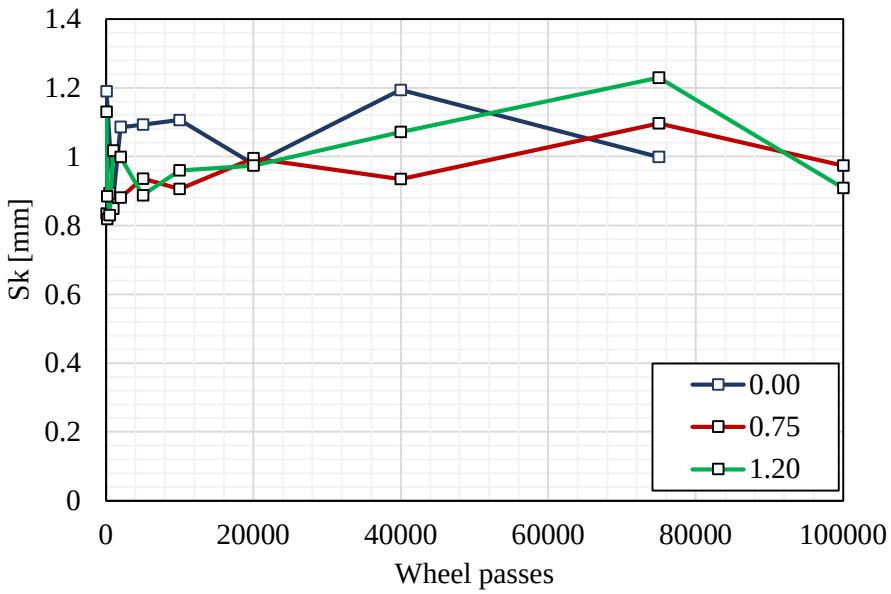

Figure 8.26: Sk for 8 mm slabs

The arithmetical mean height Sa, i.e. the mean surface roughness, as shown in Figures 8.27 and 8.28, was found to be constant during the RTM test. No remarkable differences were found between the three 8 mm slabs.

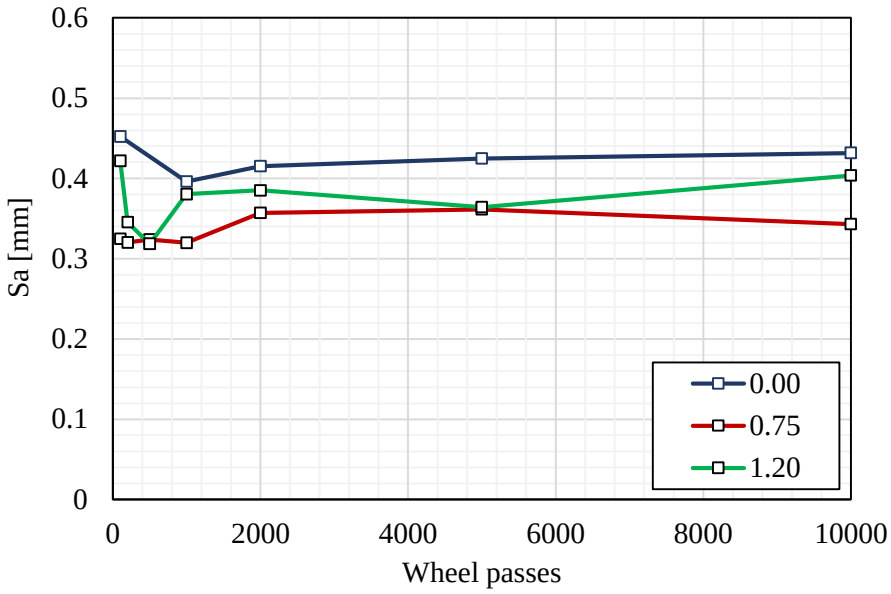

Figure 8.27: Sa for 8 mm slabs, early life

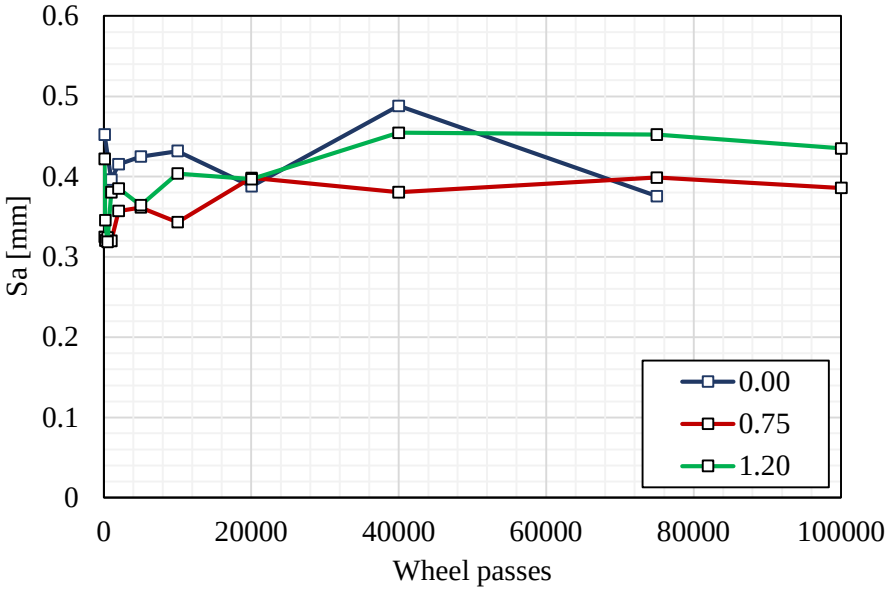

Figure 8.28: Sa for 8 mm slabs

8.5.1.2 RTM versus IWT

Figure 8.29 shows the development of Vmp5 for 0.75 slab after trafficking of RTM and IWT test. The dragging of the test wheel onto the surface wears the texture, creating ruts, which lead to greater Vmp.

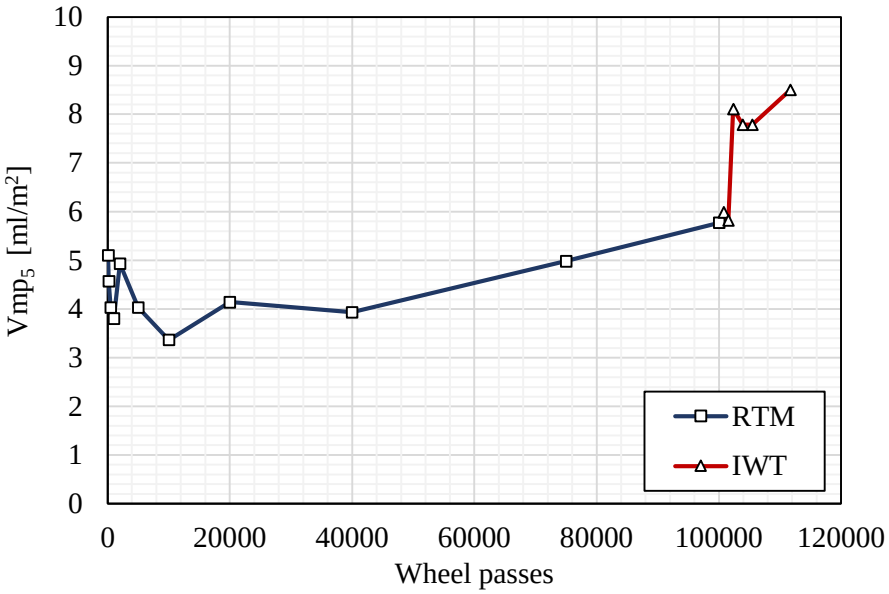

Figure 8.29: Volume of material peak 5% low limits for 0.75 slab

The second parameter analysed is the Core Material Volume Vmc (Figure 8.30), which is the volume of material comprising the texture between heights corresponding to the material ratio values of 5% to 80%. After initial increase, this parameter reaches an equilibrium and keep constant until the end of the simulated trafficking. Similar to the case of Vmp, the IWT induces a consistent increase of Vmc.

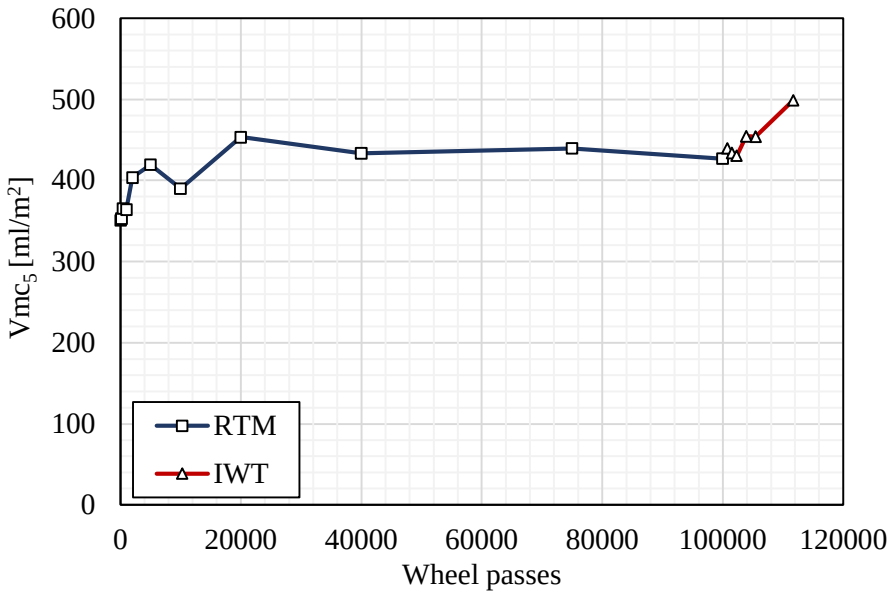

Figure 8.30: Volume of material core 5% low limit for 0.75 slab

After initial fluctuation Vmc stabilized to a greater value during RTM. The IWT caused a decrease which could be related to the dust removed from the surface and infilling the pores during the immersion. The volume of void is shown in Figure 8.31.

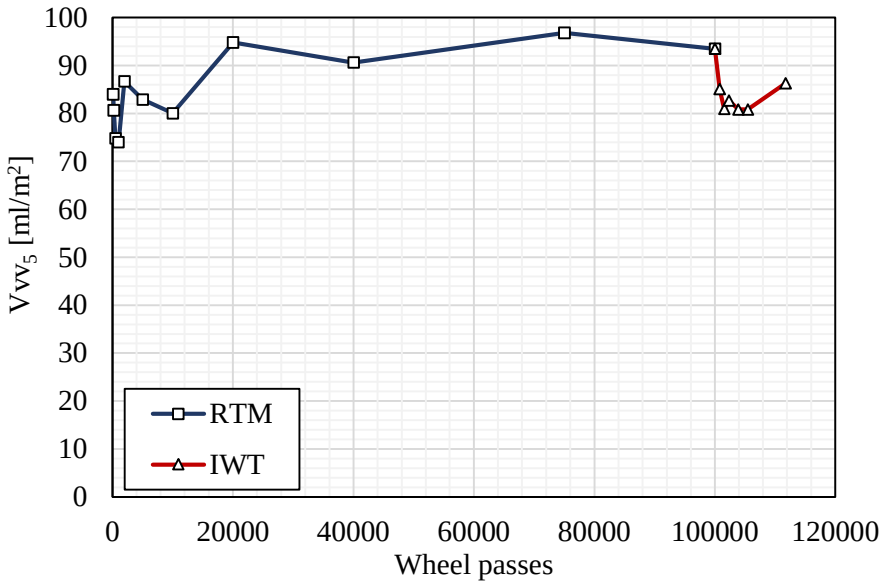

Figure 8.31: Volume of void 5% low limit for 0.75 slab

Figure 8.32 shows the change of Sk with the simulated trafficking. Sk, which is the distance between the highest and lowest level of the core surface, was found to increase with a highest rate observed for the IWT compared to the RTM.

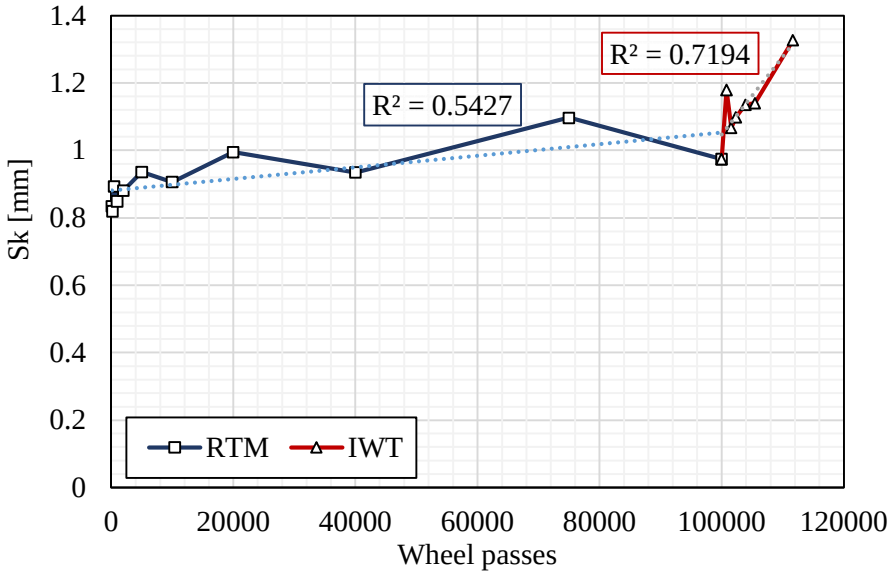

Figure 8.32: Sk for 0.75 slab

The arithmetical mean height Sa was found to be constant during the RTM test. The IWT induced, on the other hand, an increase of this parameter.

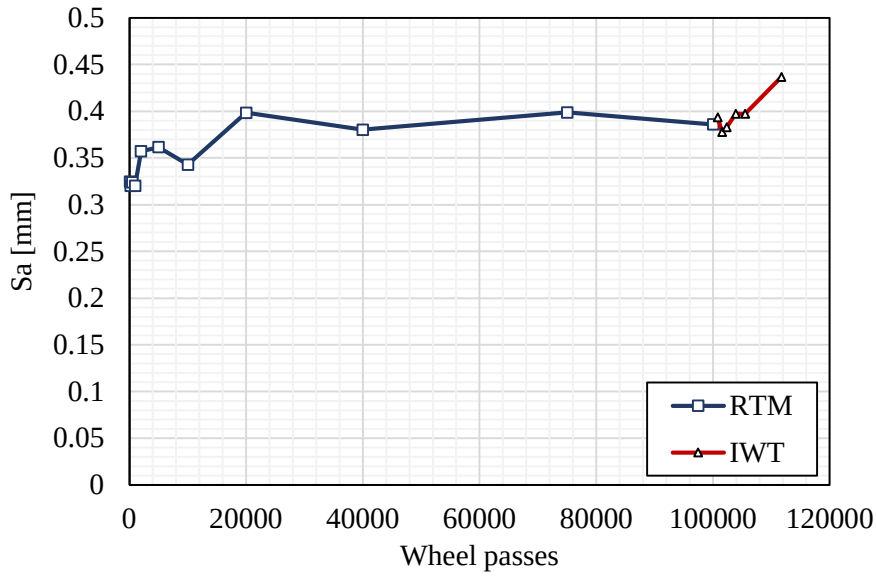

Figure 8.33: Sa for 0.75 slab

The arithmetical mean height Sa exhibits excellent linear correlations with Vmp_{80} both for RTM and IWT, in accordance with what was shown in the preliminary analysis paragraph. Accordingly, Sa could be used to estimate Vmp80 without analysing the Abbott Firestone Curve even after IWT test.

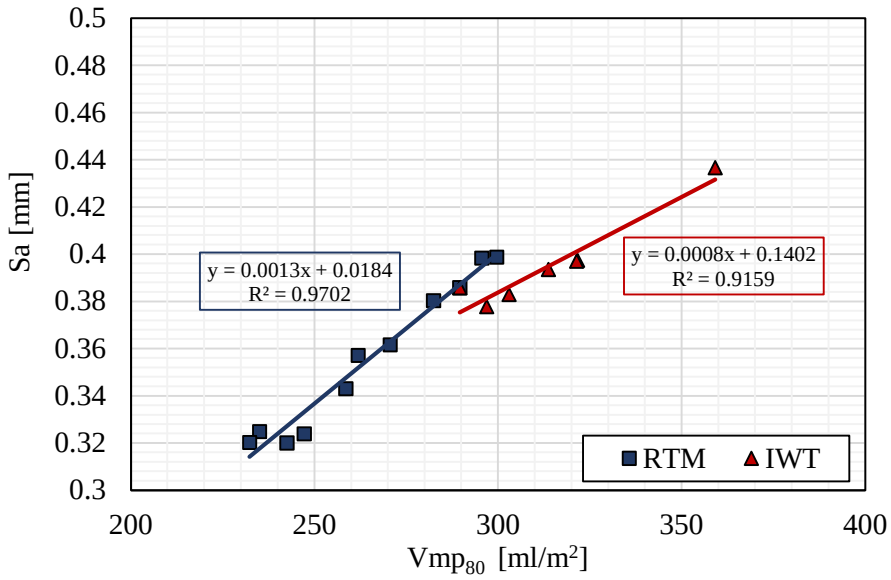

Figure 8.34: Sa versus Vmp80 for 0.75 slab

8.5.2 Void volume and projected Area

This investigation allows determining the volume of void for a slice of the slab above a given depth from the maximum height. In other words, it highlights how the voids are distributed inside the slab. It gives also the opportunity to compare the change in the void distribution during the trafficking.

8.5.2.1 Comparison between the slabs

Figure 8.35 shows the volume of void of the trafficked 0.00 slab. Generally, the different curves exhibit a similar trend: a linear decrease in the volume of void with the depth inside the slab, a change in the curvature around 1 mm height from the highest point and a rapid drop towards zero volume of void at the bottom.

Figure 8.35 shows that the 0.00 slab underwent an important difference in the texture from the 40000 wheel passes. Since the y axis is the height from the highest point of the slab, a

shift of the curve could be related to an elevation of some aggregates. This could be the case of the 40k curve, which is parallel to the bundle, but not the case of the 75k curve which assumed a different curvature.

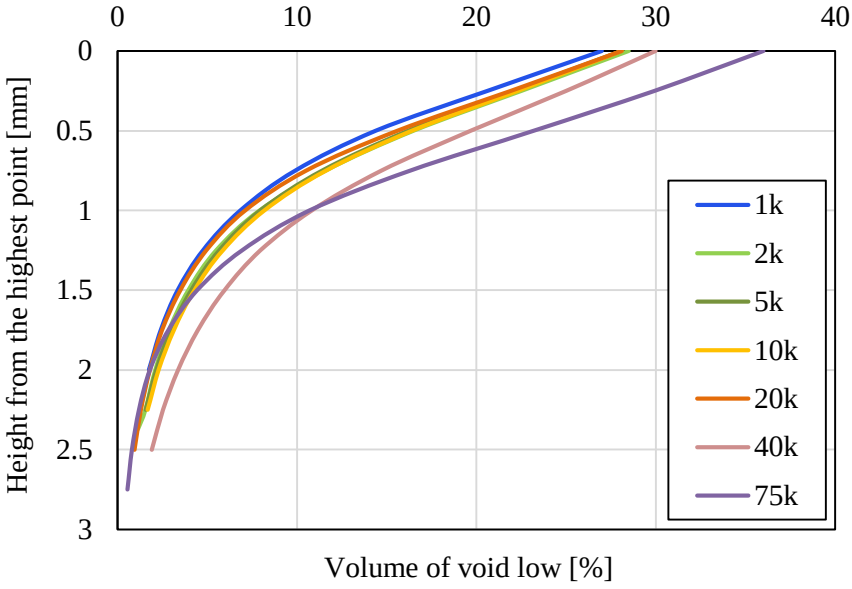

Figure 8.35: Volume of void low for 0.00 slab

The projected area, i.e. the projection of the slab surface which stand below an horizontal plane at a given height s plotted in Figure 8.36. The considerations made for the volume of void can be applied for the projected area.

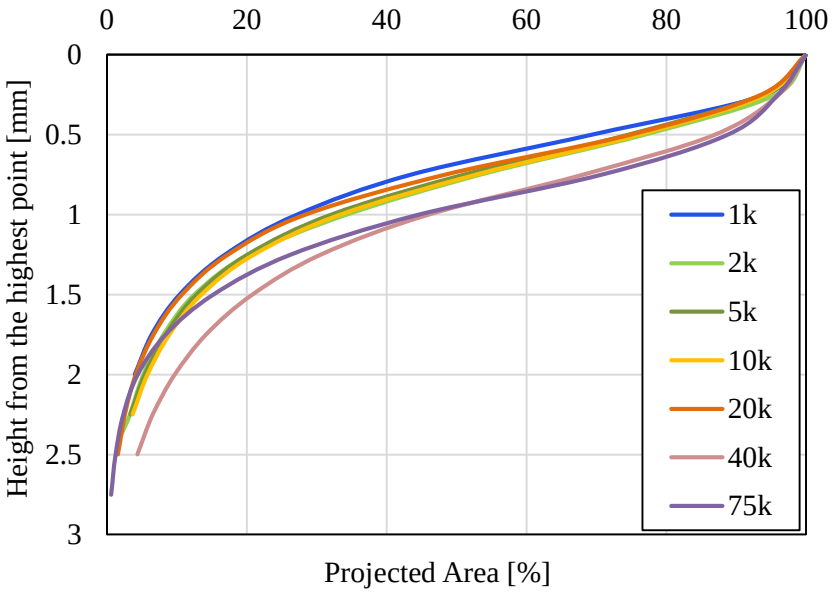

Figure 8.36: Projected Area along height for 0.00 slab

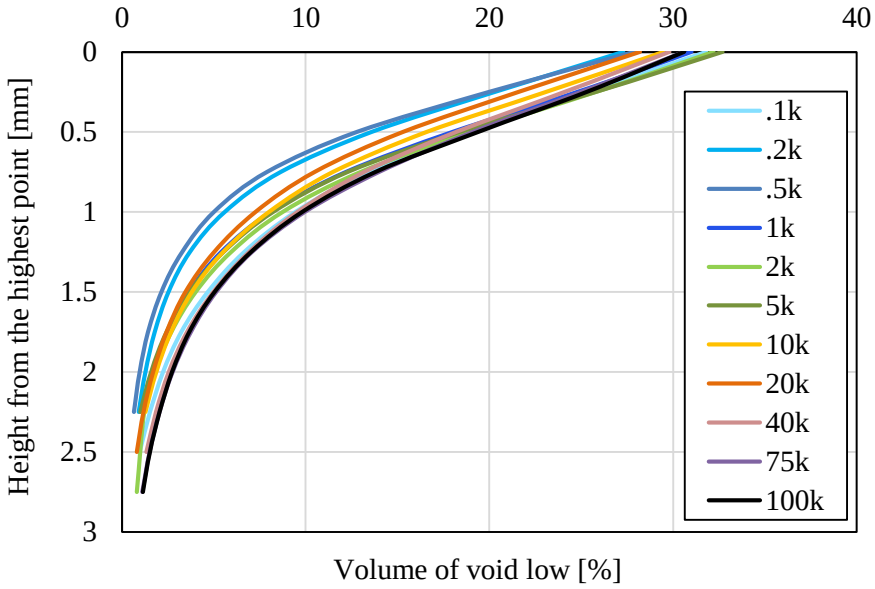

Figure 8.37: Volume of void low for 1.20 slab

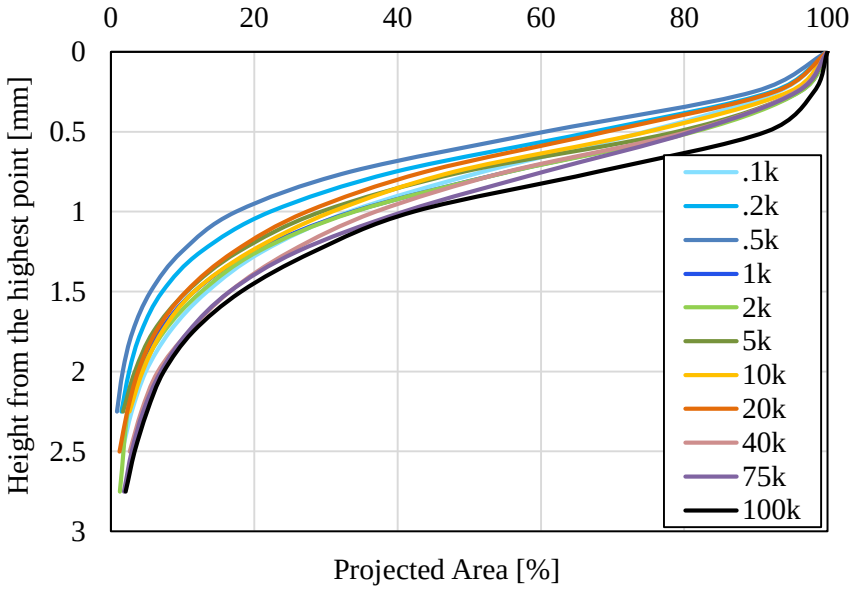

Figure 8.38: Projected Area along height for 1.20 slab

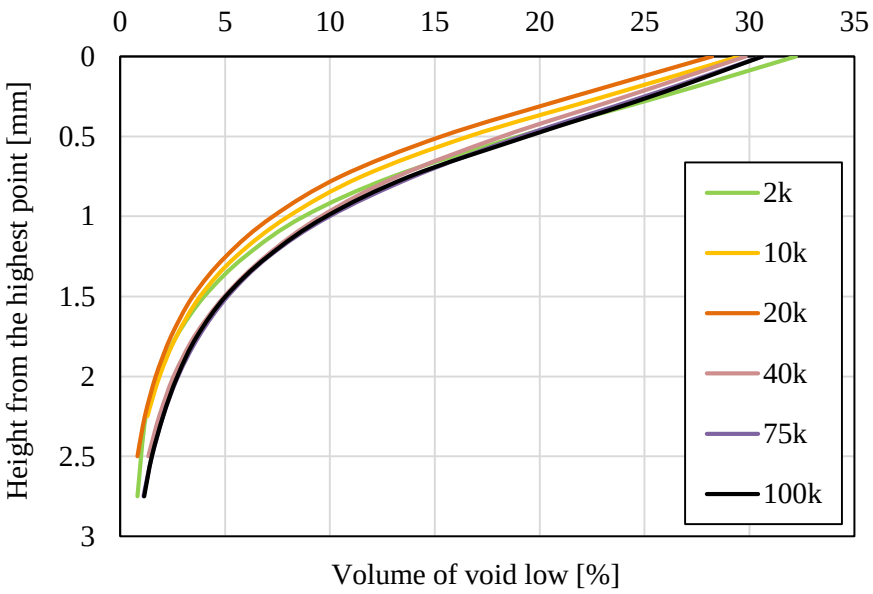

Figure 8.39: Volume of void low for 1.20 slab

8.5.2.2 RTM versus IWT

Figure 8.40 shows the volume of void of the trafficked 0.75 slab. The different curves are very close to each other. It is notable a small deviations between bundles of curves as the curvature change.

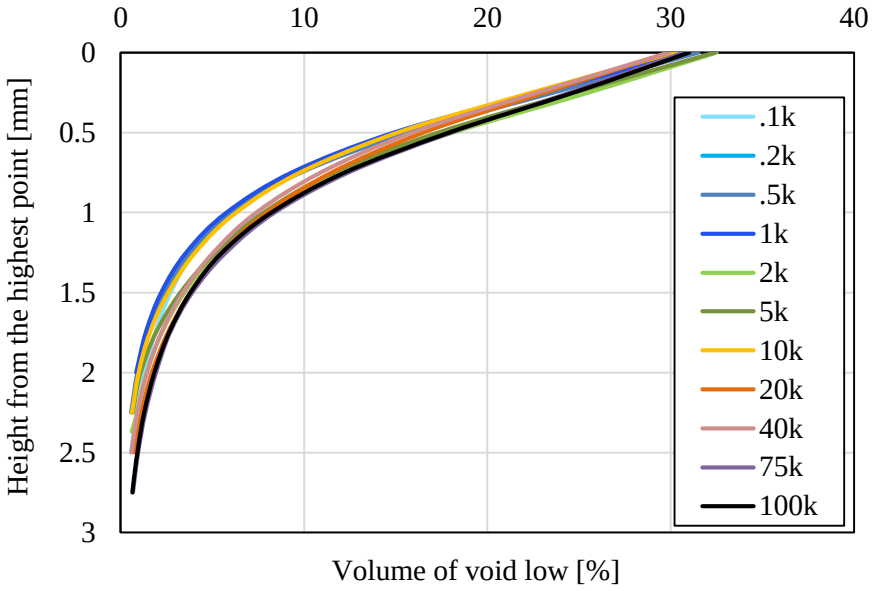

Figure 8.40: Volume of void low for 0.75 slab

Figure 8.41 and 8.42 are a magnification of the Figure 8.40. The first highlight that, during the early life of the pavement, the volume of the void increase as the trafficked curves shift towards the right in the plot.

The latter shows that at 10000 wheel passes the volume of void decrease as it become lower than it was immediately after the compaction of the slab, i.e. at 100 wheel passes. Then the volume of void remains stable up to 40000 wheel passes. At 75000 wheel passes the volume increase again and it reaches a final value (black line in the plot), at the end of RTM trafficking, close to that belonging to 2000 wheel passes. In other words, the slab seems to loose material under the trafficking of RTM until it reaches an equilibrium which is maintained from 10000 to 40000 wheel passes.

The equilibrium value is lower than the previous data, belonging to 5000 wheel passes, from which it can be inferred that the slab underwent a compaction under the simulated trafficking. At high number of wheel passes the volume of void increase again. This change in the texture may be related to a loss of particles and/or wearing, i.e. a damage of the slab.

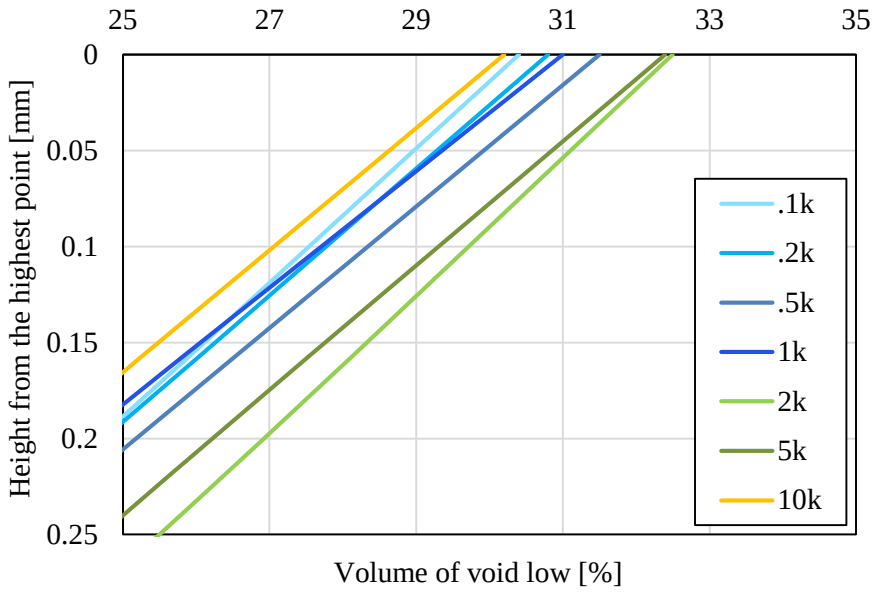

Figure 8.41: Volume of void distribution along height for 0.75 slab, early life

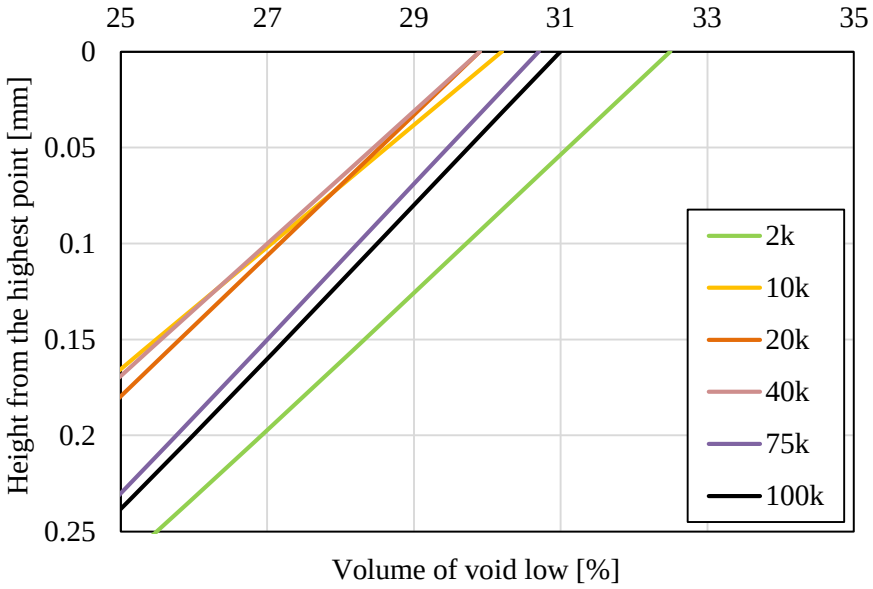

Figure 8.42: Volume of void along height for 0.75 slab

The theory of damage is confirmed looking at the same plot, related to the second trafficking that the 0.75 slab endured, i.e. the immersion wheel track IWT (Figure 8.43). Rutting along the surface was clearly notable with human eyes after 225 minutes of the test. This is confirmed by the plot, which exhibits that, as the time passes, the volume of void increase.

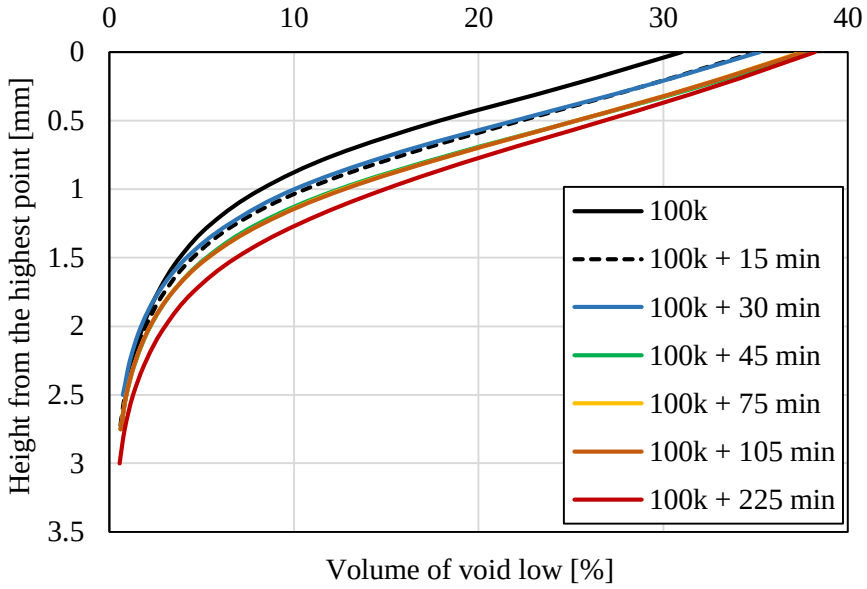

Figure 8.43: Volume of void along height for 0.75 slab during IWT

Figure 8.44 shows that the damage caused by the immersion wheel is far bigger than that induced by the RTM. In fact, the curves belonging to the RTM are very closed to each

other while the curves belonging to IWT, although the slab endured less wheel passes, are more distant.

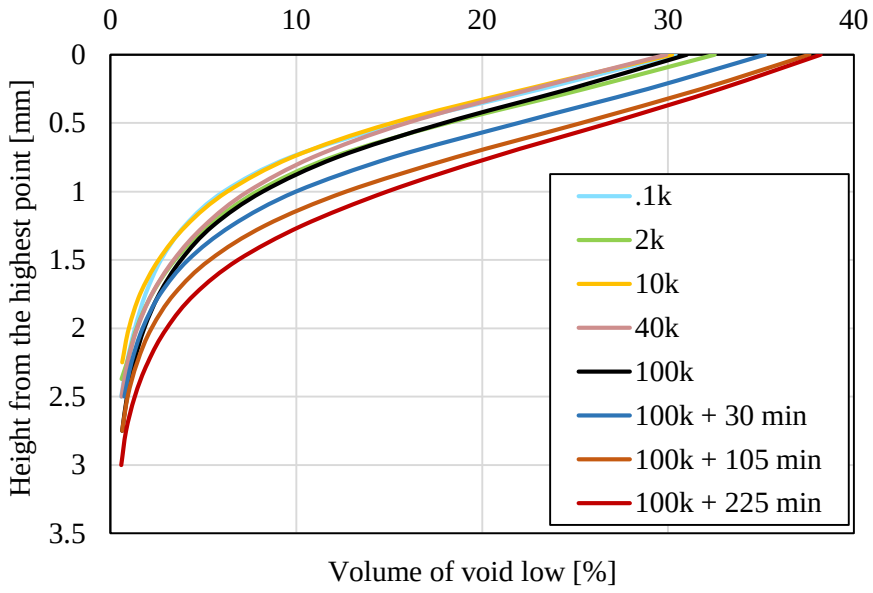

Figure 8.44: Volume of void along height summary for 0.75 slab during RTM and IWT

Figures 8.45 and 8.46 show the projected areas versus the height from the highest point for the trafficked 0.75 slab. No sensible differences were found compared to the volume of void plots. The projected area, is higher at high level of trafficking, compared to the early life. As seen before, at 10000 to 40000 wheel passes a reduction in the projected area was observed, especially for the first millimetre of depth from the highest point.

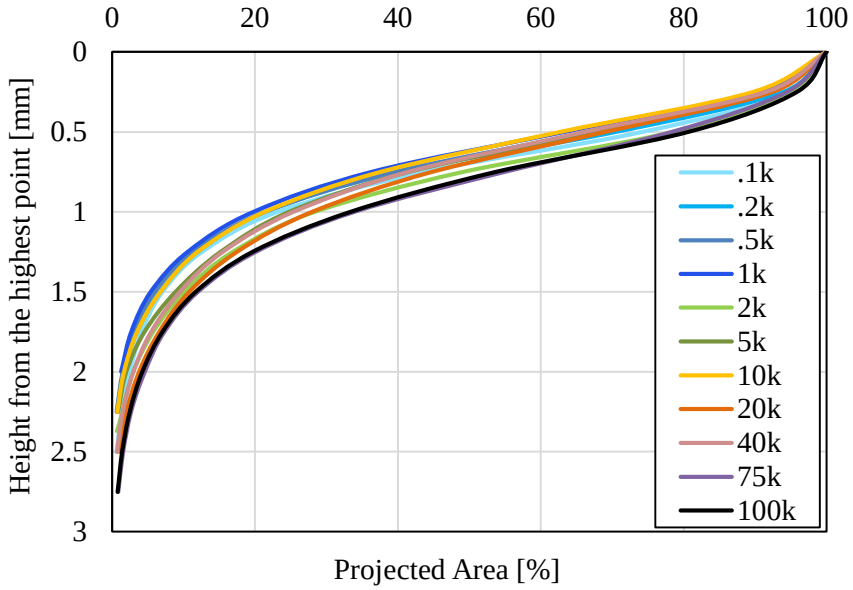

Figure 8.45: Projected Area along height summary for 0.75 slab during RTM

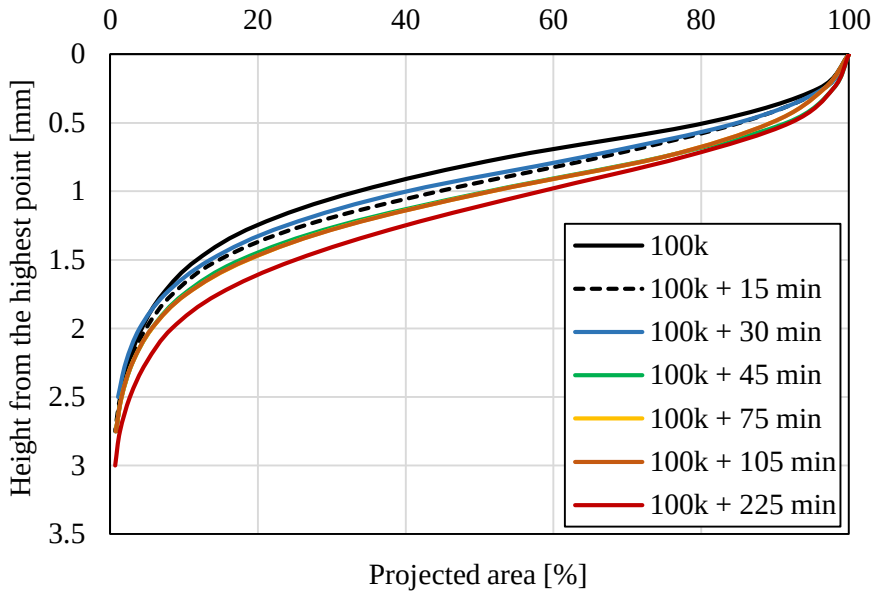

Figure 8.46: Projected Area along height summary for 0.75 slab during IWT

The immersion wheel track caused the projected area to increase at a given depth. This is due to the rutting which created holes onto the surface. These values are plotted in Figure 8.47, which shows the development of the projected area during IWT test. An excellent R^2 was found, increasing with the depth of measurement into the surface.

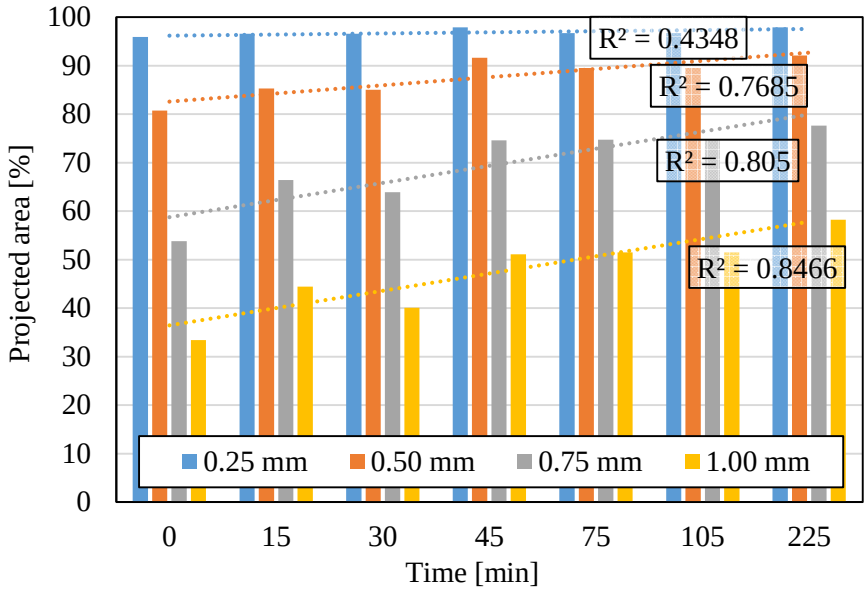

Figure 8.47: Projected Area trend versus time at different depth for IWT test

Figure 8.48 shows a summary of the projected area during the trafficking of the 0.75 slab with both RTM and IWT.

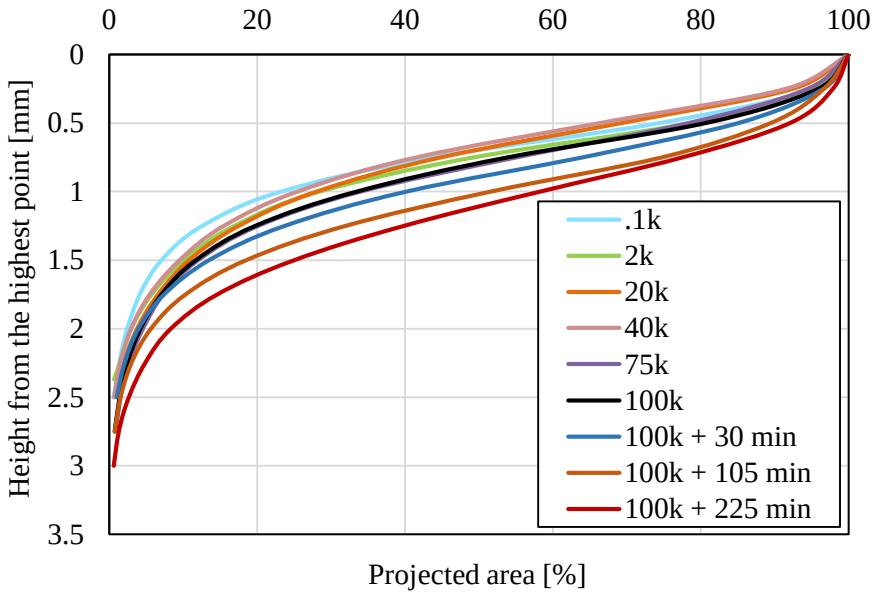

Figure 8.48: Projected Area along height summary for 0.75 slab during RTM and IWT

8.5.3 Slice study

Another interesting way to understand the evolution of material and voids inside the slabs is the slice study. In particular, two different slices were set for each slab, i.e. 1 mm from the top height and 2 mm from the top height, which individuated three regions of the slab. The average volume of material height and the average volume of void height were recorded for the high, median and low volume defined and are plotted in Figures 8.49 to 8.60.

8.5.4.1 Comparison of the three different slabs

The three 8 mm slabs exhibited a very similar trend as can be seen in Figure 8.50. Although the values are slightly different, the initial fluctuation and the decrease of the volume of material high was found in any case. The differences in the absolute values seem to be related to a different level of compaction.

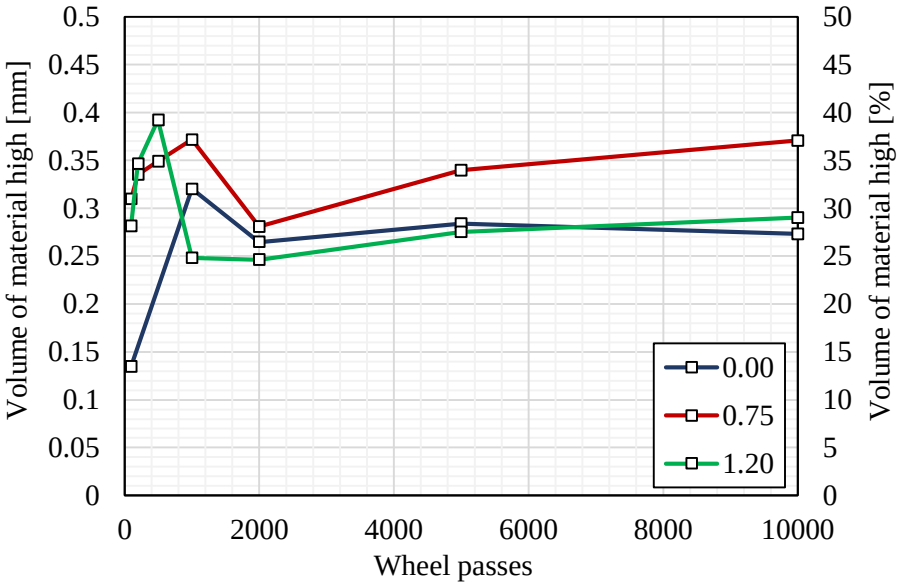

Figure 8.49: Volume of material high for 8 mm slabs, early life

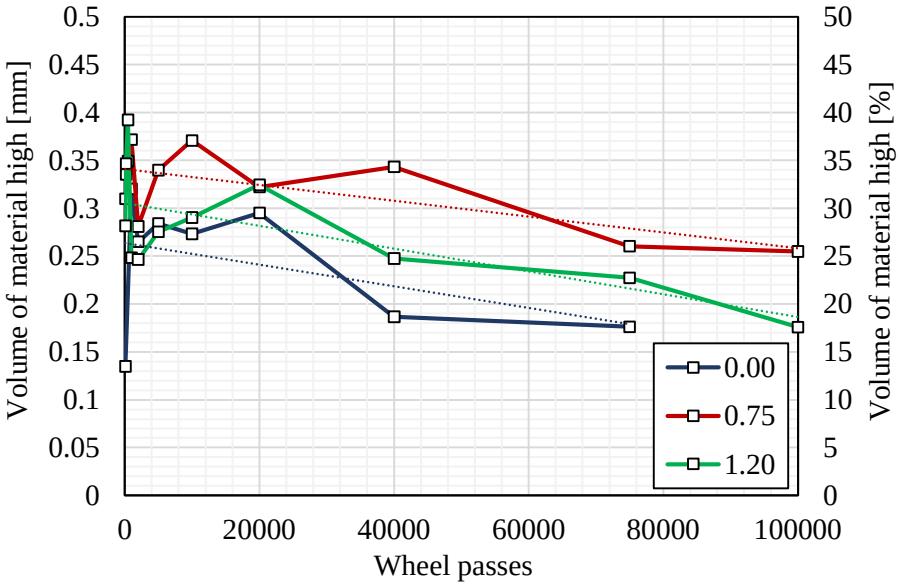

Figure 8.50: Volume of material high for 8 mm slabs

Volumes of void high belonging to 0.00 and 0.75 slabs were found to be very similar during the early life, while the overall trend of the 8 mm slabs is identical (Figure 8.51). It generally decrease with the same ratio, as the trend lines are parallel. This could be related to the stripping of the bitumen or the wearing of the aggregates, leading to a reduction in the material recorded in the first mm of depth.

The volume of void shown in Figures 8.51 and 8.52 are the complementary of what is shown in Figure 8.49 and 8.50 respectively.

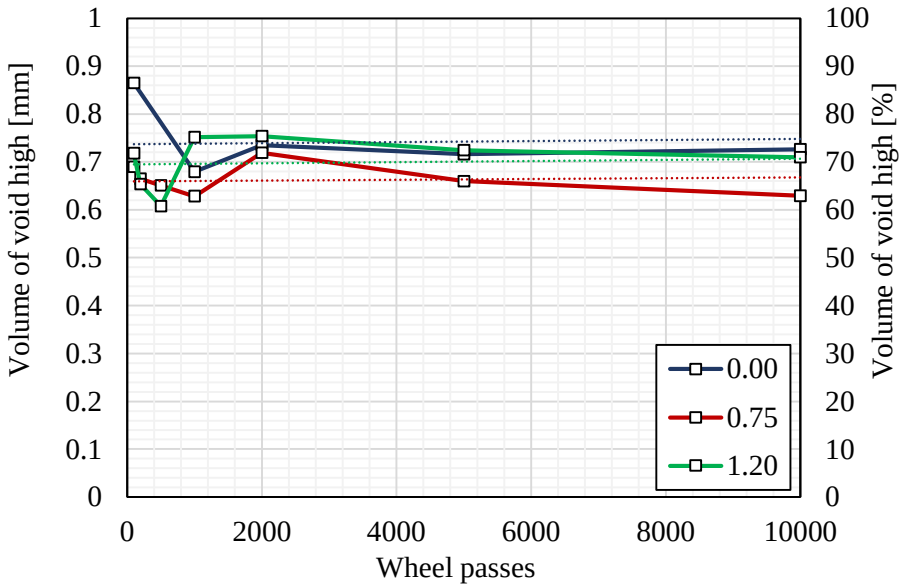

Figure 8.51: Volume of void high for 8 mm slabs, early life

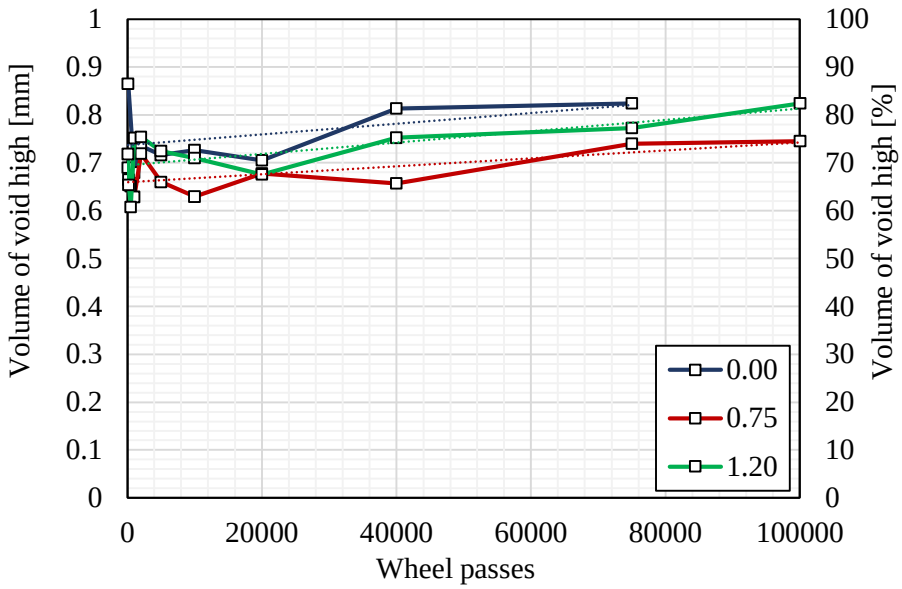

Figure 8.52: Volume of void high for 8 mm slabs

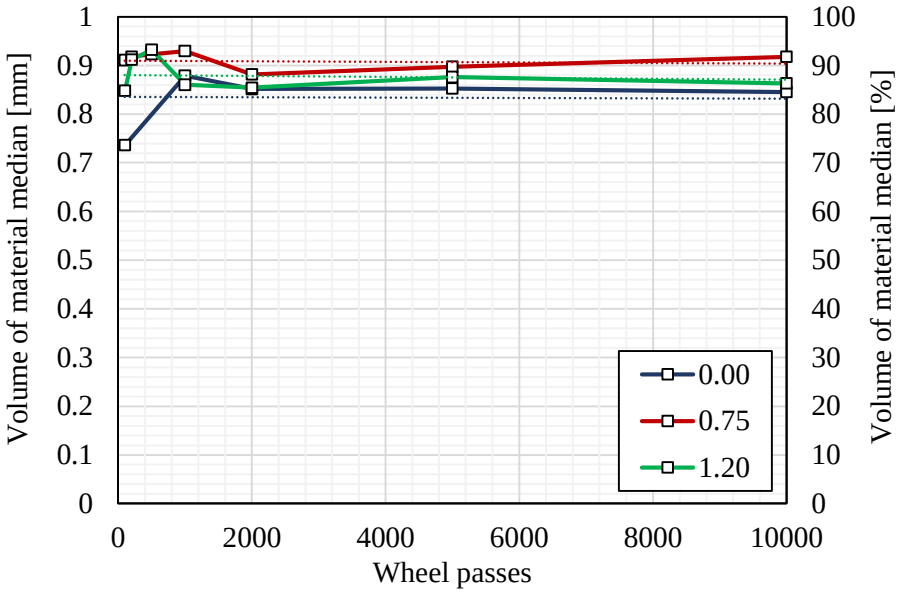

Figure 8.53: Volume of material median for 8 mm slabs, early life

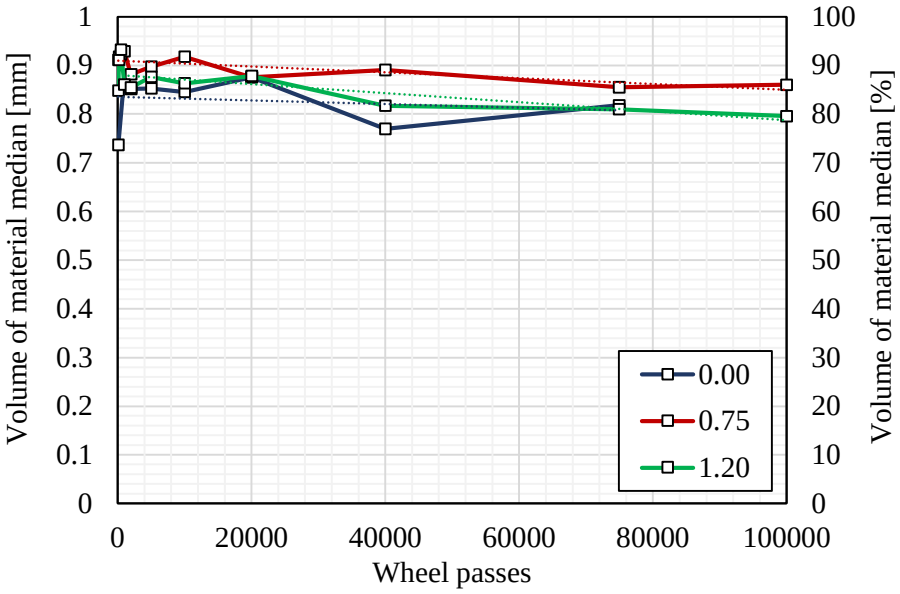

Figure 8.54: Volume of material median for 8 mm slabs

The volume of material in the slice between 1 mm and 2 mm depth, shown in Figure 8.53 and 8.54, was found to be constant during the life of the slabs. Trend lines are almost horizontals.

Volume of void median plots, shows in Figures 8.55 and 8.56 can be read accordingly as for the volume of material.

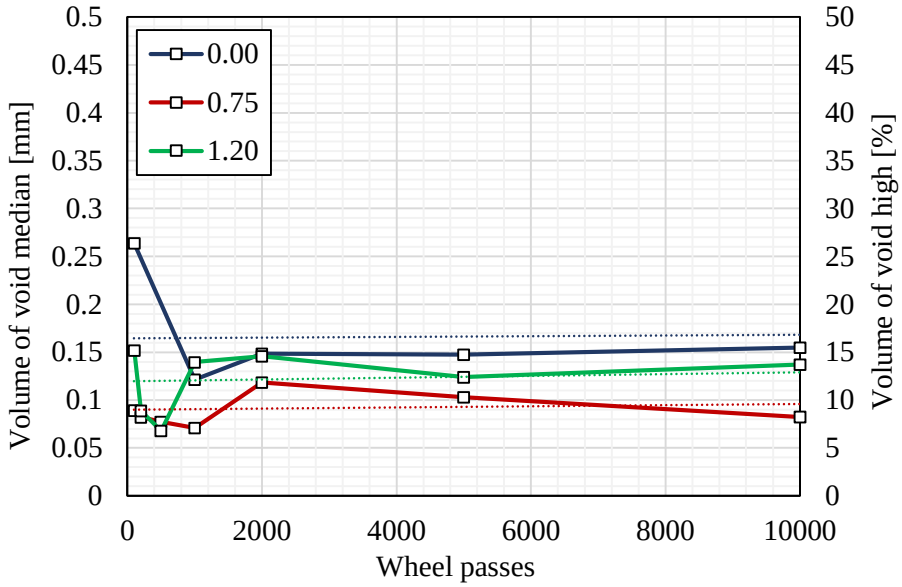

Figure 8.55: Volume of void median for 8 mm slabs, early life

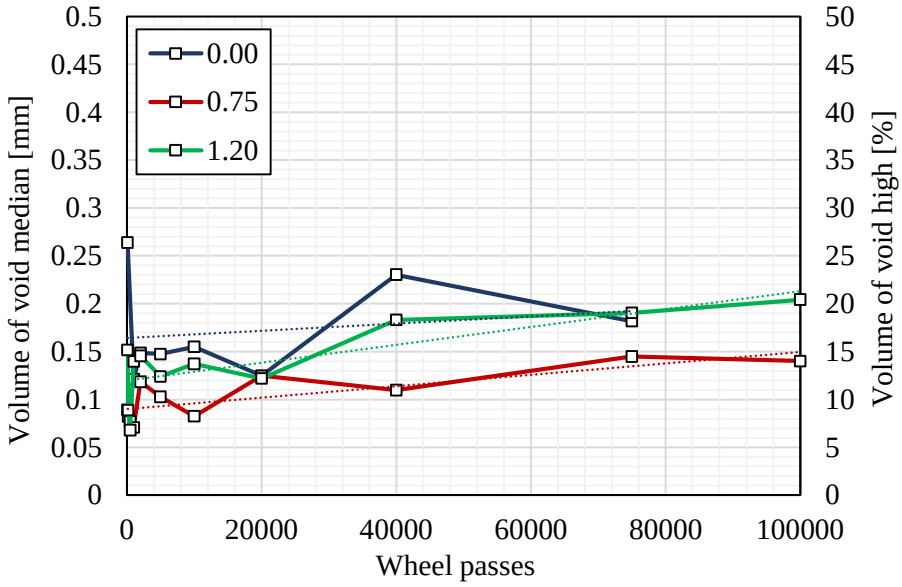

Figure 8.56: Volume of void median for 8 mm slabs

The volume of the material low and its complementary void is presented in percentages in place of millimetre. The heights of the slab pertaining to the models at different

trafficking stages were found to be slightly different. It would have been difficult to compare volumes and voids in absolute terms accordingly.

As shown in Figures 8.59 and 8.60, while there are no differences during the early life, a slightly increase in the voids was found from 10000 to 75000 wheel passes.

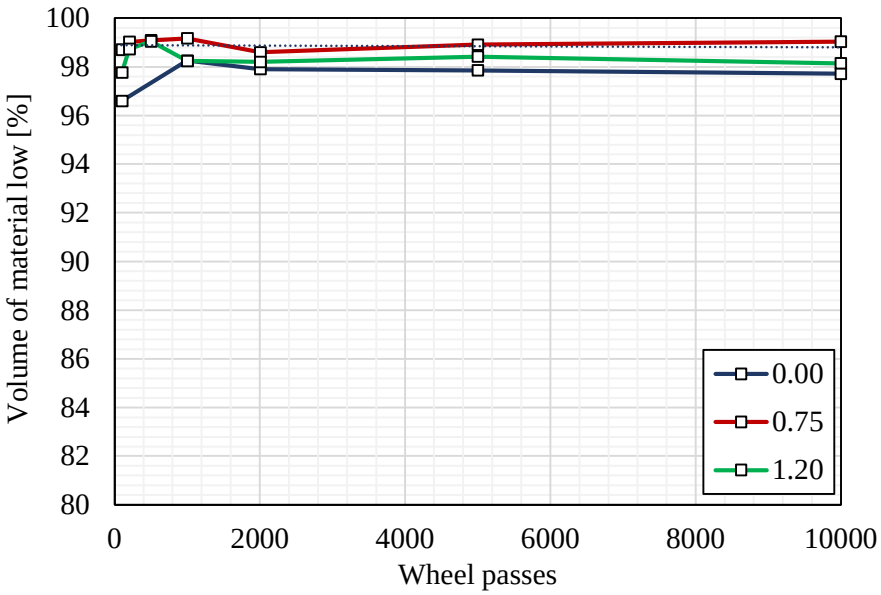

Figure 8.57: Volume of material low for 8 mm slabs, early life

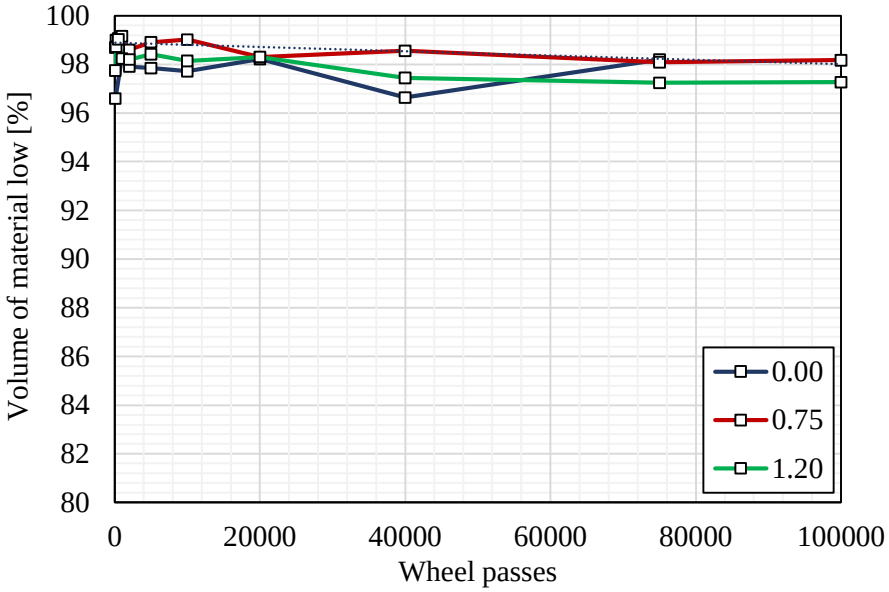

Figure 8.58: Volume of material low for 8 mm slabs

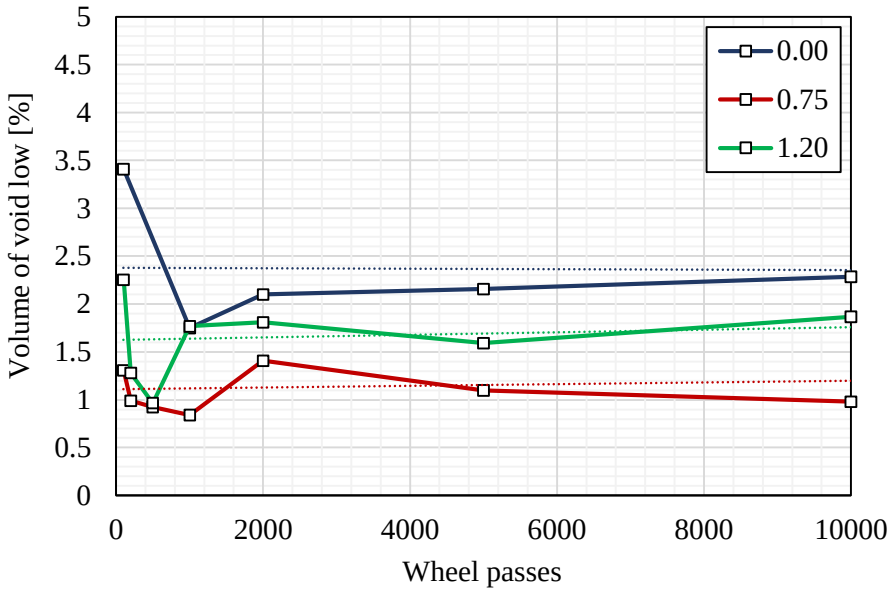

Figure 8.59: Volume of void low for 8 mm slabs, early life

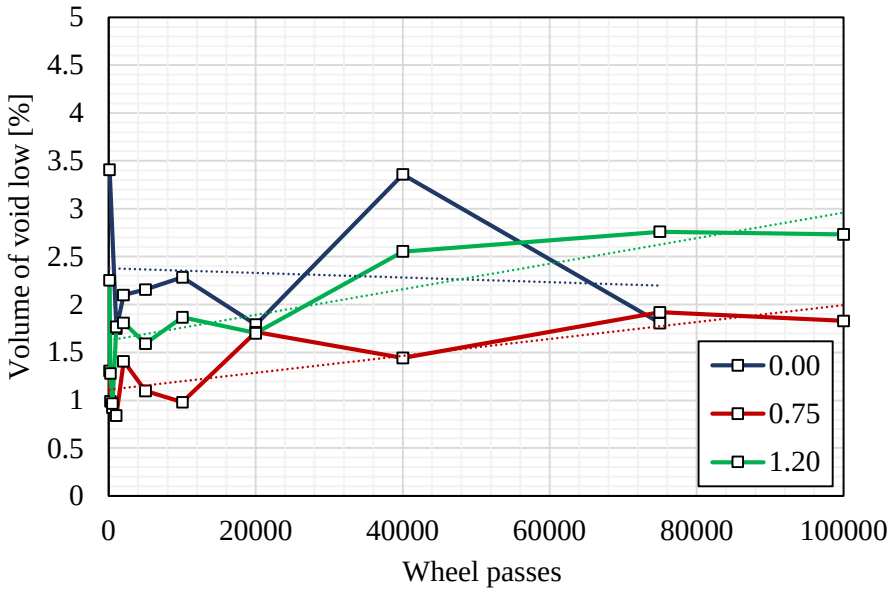

Figure 8.60: Volume of void low for 8 mm slabs

8.5.4.2 RTM versus IWT

The 0.75 slab plot is presented separately to highlight the effect of the trafficking induced by the Immersion Wheel Track test. A good and excellent R^2 was found for each RTM and IWT parameter respectively. In order to better understand the subsequent plots, the

map evolution of this investigation at different trafficking stages is presented in Figures 8.61 and 8.62.

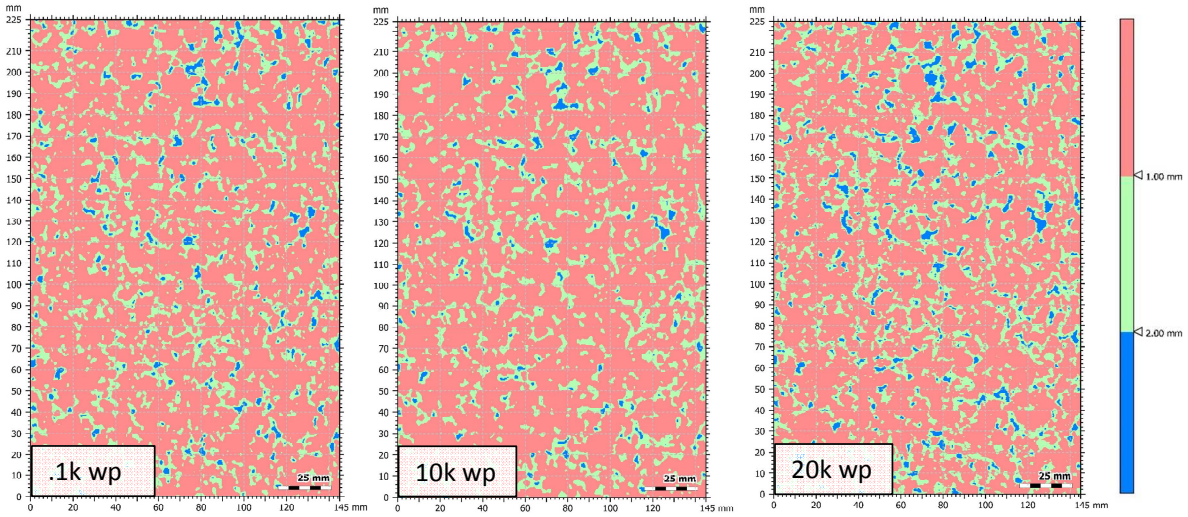

Figure 8.61: Slice study: map evolution for 0.75 slab, RTM

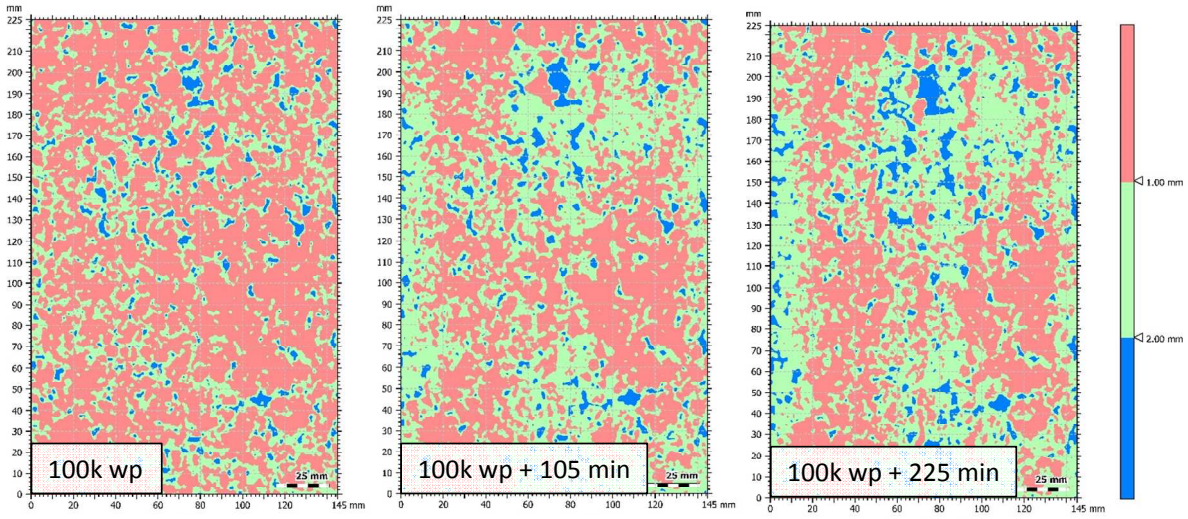

Figure 8.62: Slice study: map evolution for 0.75 slab, IWT

In the first volume, from the top height to one millimetre depth, the average volume of material exhibited an initial fluctuation with a sinusoidal form until equilibrium at 10000 wheel passes, from which it decreased reaching a final value of 0.25 mm after 50000 revolutions of RTM.

The IWT caused the volume of material high to drop down rapidly, reaching a final value after 225 minutes of test that is halved, i.e. 0.13 mm.

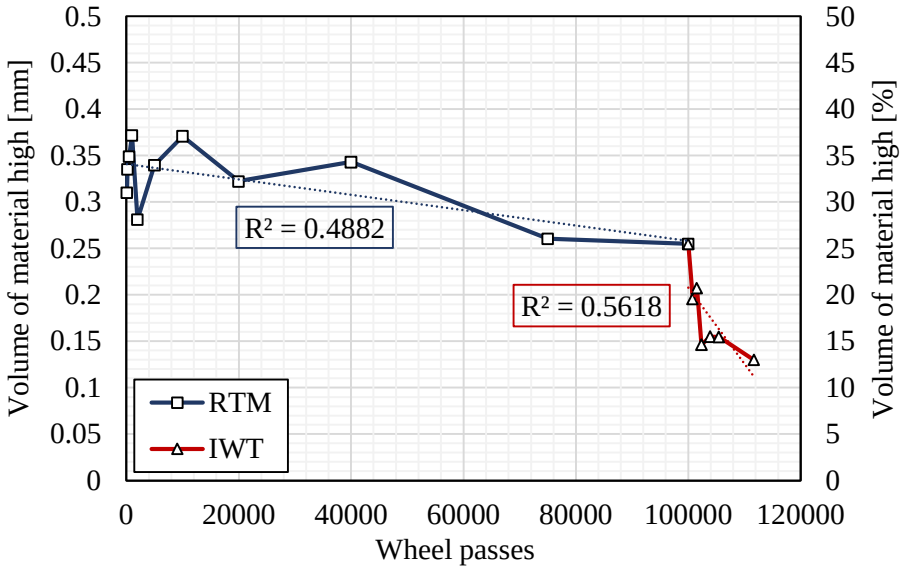

Figure 8.63: Volume of material high for 0.75 slab

On the other hand, the average volume of void high is complementary to the volume of material. An initial fluctuation was observed, decreasing in the first 1000 wheel passes, which is certainly related to the compaction of the slab. After the equilibrium, at 10000 wheel passes, the average volume of void increased reaching a final value of 0.75 mm after 50000 revolutions in the RTM. As seen before, the IWT produced a rapid increase of this parameter compared to that of RTM.

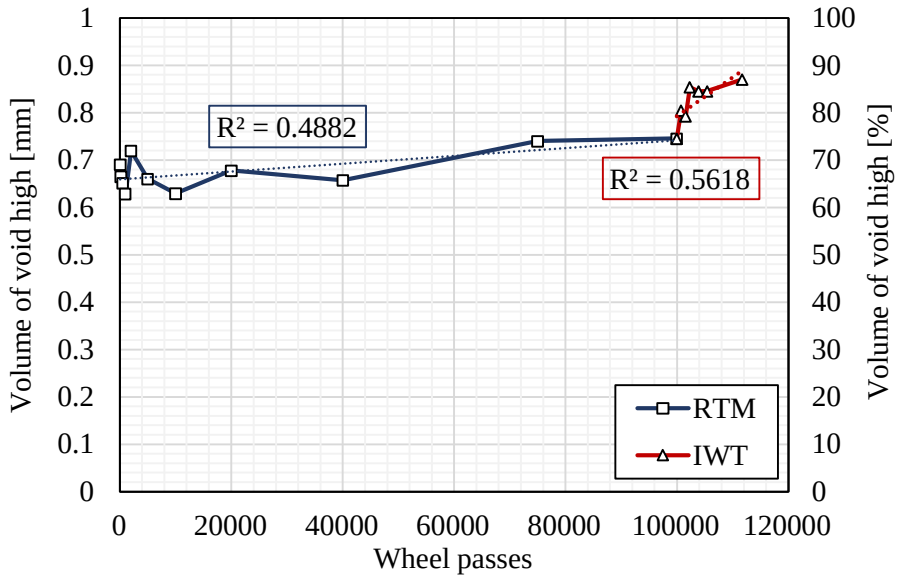

Figure 8.64: Volume of void high for 0.75 slab

In the second volume, from one to two millimetre depth, which represents the core of the slab, the average volume of material is initially the 90% of the total volume of the slice. As the slab undergoes the trafficking, the volume follows an initial fluctuation with a sinusoidal form until equilibrium at 10000 wheel passes, from which it slightly decreases reaching a final value of 0.86 mm at 50000 revolutions of RTM.

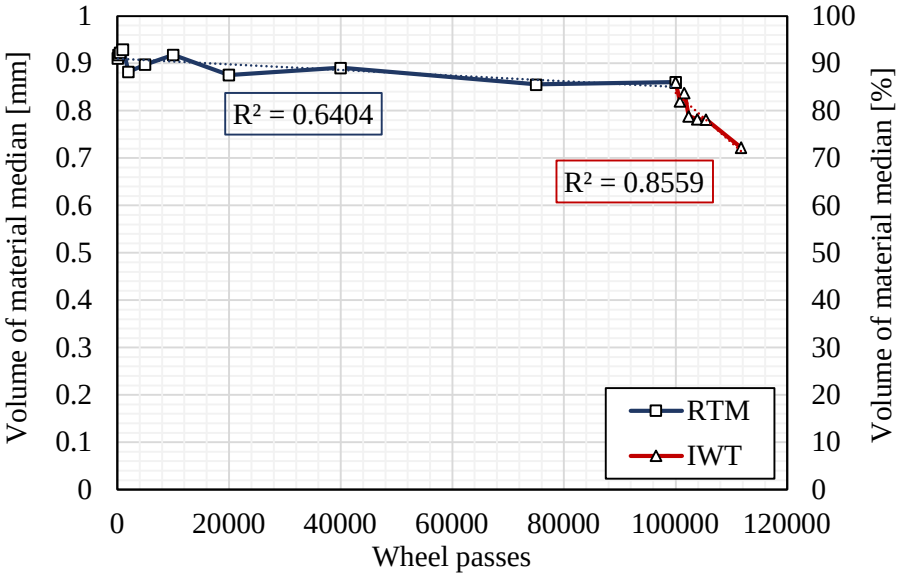

Figure 8.65: Volume of material median for 0.75 slab

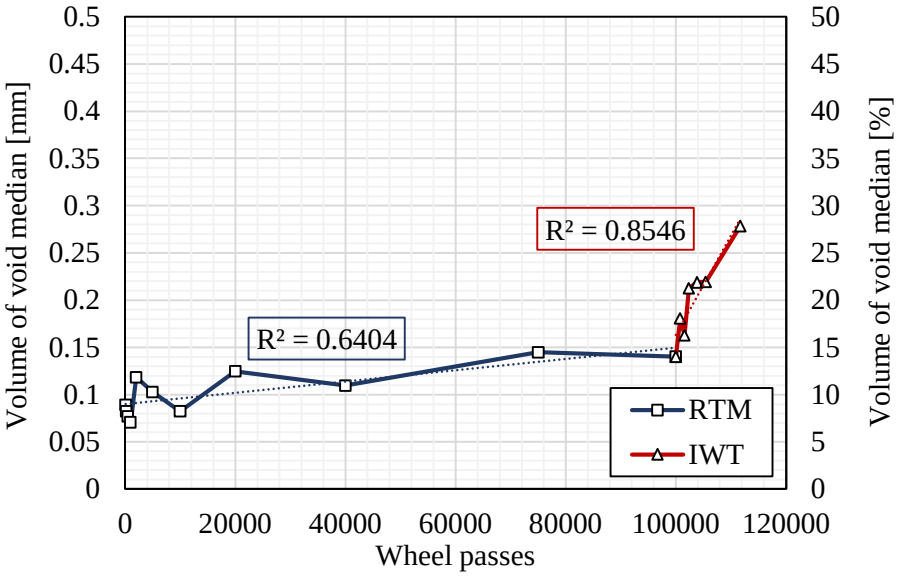

Figure 8.66: Volume of void median for 0.75 slab

Data are always close to the trend line, which exhibits a R^2 equal to 0.6404, higher compared to that belonging to the first volume.

Like the case of the first volume, the IWT causes the volume of material median to drop down rapidly, reaching a final value of 0.72 mm after 225 minutes of test. The R^2 belonging to IWT data is 0.8559 which confirms a good correlation of the data along the linear trend line.

The volume of material low, i.e. the bottom volume, plotted in Figure 8.67, represents almost all the volume of the slice. Notwithstanding this, the trafficking induced a slightly reduction in this parameter also. Starting from 98.8% circa, this value reaches 98% at the end of RTM and 96.8% at the end of IWT.

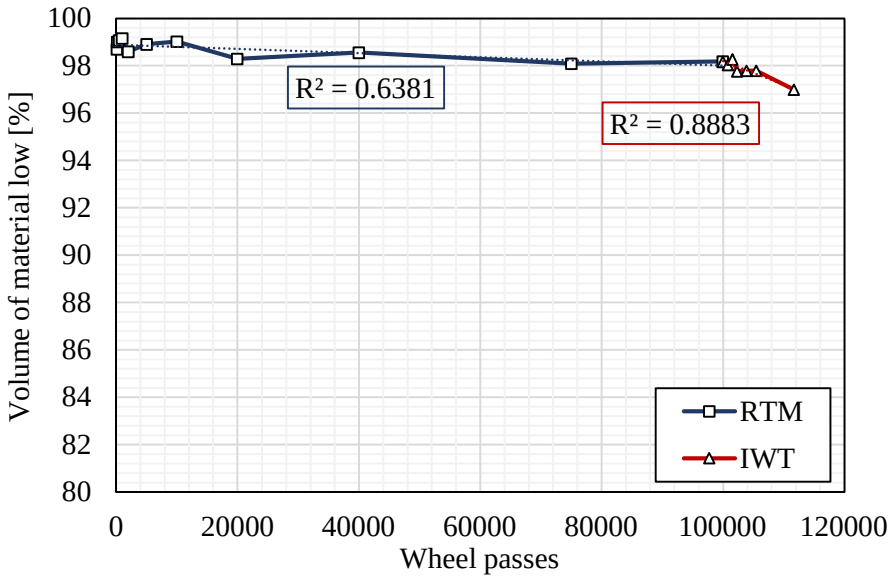

Figure 8.67: Volume of material low for 0.75 slab

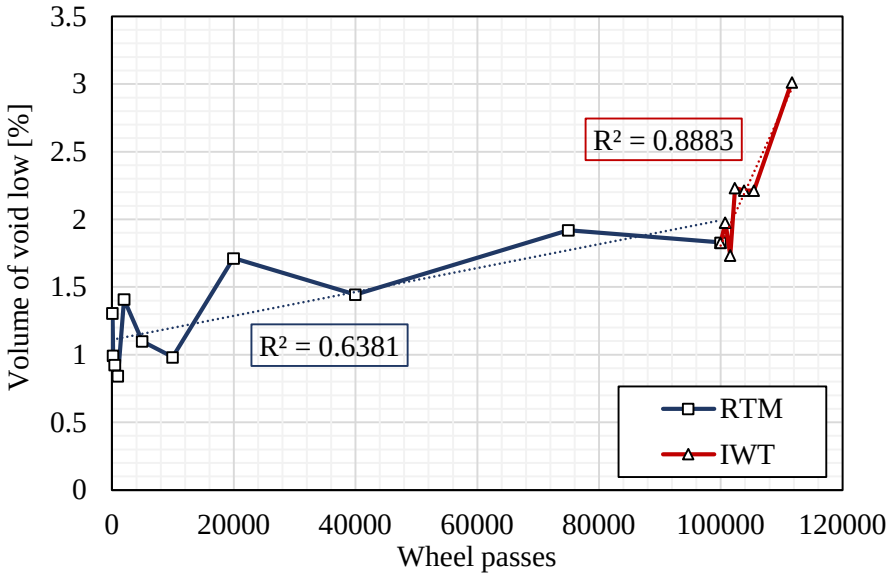

Figure 8.68: Volume of void low for 0.75 slab

Values were plotted looking only at the percentages, leaving out the absolute values of the parameters. This was necessary to compare the values belonging to different trafficking, since the models created with the photogrammetry exhibited slightly different heights, orders of 0.2 ÷ 0.4 millimetres.

The great differences of the effect of Road Test Machine and Immersion Wheel Track on both the volume of material and the volume of void are evident.

After initial fluctuations, the volume of material decreases with different rate during the two different tests. The IWT induces a strong acceleration on the wearing of material, due to the combined action of dragging and high test temperature. This results in a rapid drop down of the volume of material.

On the other hand, the volume of void generally follows the inverse path of the volume of material, with an increase after initial fluctuation.

8.5.5 Use of vinyl material to replicate asphalt surface macrotexture

This chapter investigates the use of vinyl material to replicate asphalt surface macrotexture.

Cast replication facilitates practical and accurate recovery of pavement surface texture. According to McQuaid (2015), the 3D models of the replicate showed capture to greater depth into the surface macrotexture.

Vinyl cast replicates was created of 0.75 asphalt slab test specimen following 100,000 wheel passes of accelerated dry trafficking on the Road Test Machine.

The vinyl material used for the vinyl cast replicate technique was a hot melt compound. This is a red coloured, flexible, durable and non-toxic material (MBFG, 2013). The vinyl compound was cut into small pieces and heated to 150°C. A template was placed around the edges of the slab test specimen to contain the fluid Vinamold. The fluid was poured over the surface ensuring uniform coverage, as shown in Figure 8.69. After cooling for a few minutes the cast was peeled off the surface. Care is required during the removal

process, especially when working with deeply textured slab test specimens. This resulted in a reverse replicate of the slab test specimen texture.

The use of Vinamold on the simulated trafficked asphalt slab test specimens caused localised bitumen staining on the vinyl cast replicates. Although no visible removal of bitumen was noticed on the asphalt surfacing, suggesting that use of this hot material did not change surface texture, it is likely that the bitumen film removed will weaken the adhesion between bitumen and aggregate. For this reason, the cast replicate was created once the slab underwent all the 100000 wheel passes of simulated trafficking.

Figure 8.69: Pouring the hot vinamold onto the slab surface

Figure 8.70: Peeling off the hot vinamold from the slab surface

It is interesting to understand the ability of the photogrammetry technique to replicate the surface texture of the specimen, especially the inner part which seems difficult to capture.

The 3D model of the vinyl replicate was created following the same procedures adopted for the original slabs. Once the model was loaded on MountainsMap, it was mirrored on the z-axis to obtain a perfect replicate of the original slab.

In order to assess the differences between the models, the volume of void low and the projected area along the height of the slab were computed. The plots of the original and the vinyl replicate samples are shown in Figures 8.71 and 8.72.

Results indicates a perfect overlap between the curves, indicating the suitability of the technique for correctly creating the 3D model. It can be stated that, for a 0/8 asphalt concrete, having negative texture like the SMA under investigation, the vinyl replicate does not add valuable information for the 3D modelling.

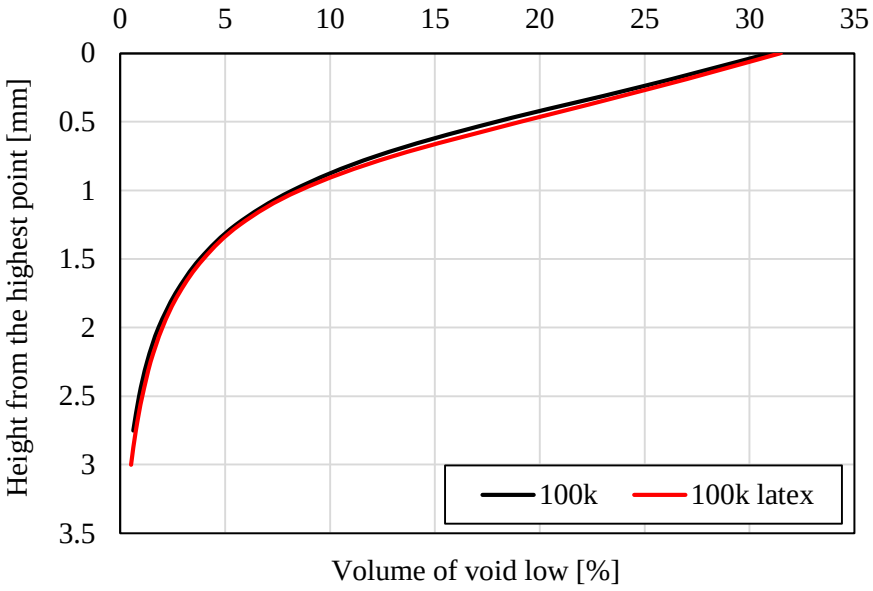

Figure 8.71: Comparison of Volume of void for original and vinyl replicate samples

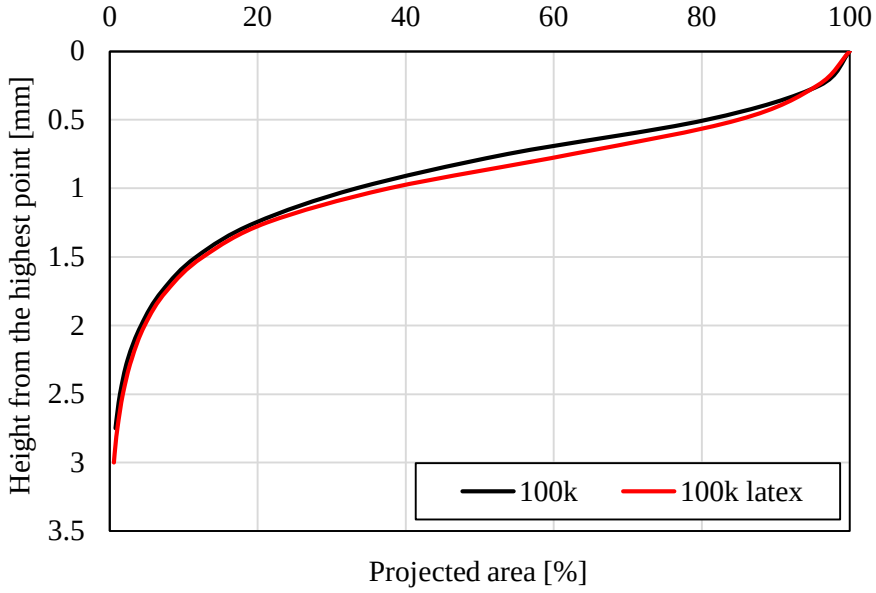

Figure 8.72: Comparison of Projected Area for original and vinyl replicate samples

Chapter 9

The tyre – pavement interaction

9.1 Introduction

This section will discuss the investigation of the tyre/stone mastic asphalt interaction. Contact stress is generated by traffic loading at the tire / asphalt interface and affects asphalt properties such as skid resistance, permanent deformation and resistance to fatigue failure (Woodward et al., 2013).

The investigation consisted in measuring the contact area and the pressure generated by a loaded griptester tyre on the SMA surfaces, at predetermined simulated trafficking stages with RTM.

In order to better comprehend the results, a preliminary analysis on the parameters affecting the measurement is presented, as well as a comparison with other SMA having different grading curves.

9.2 Test description

The test method involve the use of a modified Wessex wheel tracking machine, allowing for both dynamic and static testing. The existing rubber wheel for the machine is replaced with a Findlay Irvine GripTester tyre, which is normally used for friction measurement on roads and runways and standardized in BS 7941-2:2000. The load applied on the GripTester tyre during laboratory testing is equivalent to the load experienced by the tyre during the surface friction measurement of an airport runway using GripTester. This load is simulated by applying a load of 3.34 kg to the end of the modified wheel tracker's level arm (Figure 9.1).

The tyre/asphalt interface is measured using the XSENSOR pressure mapping system. This system includes a flexible pressure imaging sensor mat, which has a 2.54 mm spatial resolution and 3,600 sensing points. Accordingly, the mat is extremely sensitive and therefore, dust and other debris in contact with the mat can cause anomalies to be captured

during recording. The pressure mat is interfaced with XSENSOR X3 Pro Version 6 software, which facilitate quick data acquisition and processing. The system is capable of capturing up to 16 frames per second, i.e. individual contact images, recording the pressure for each of the 3,600 sensors.

Data are visually processed by selecting a frame or merging them together to form a continuous contact patch or alternatively selecting an area of interest. Pressure maps can be viewed in both 2D and 3D formats that can be easily compared selecting the "Multi-view Mode" or the "Frame compare mode". The spatial pressure matrix can be exported into a comma separated valued (CSV) file in order to be analysed with Microsoft Excel.

Figure 9.1: Equipment for the tyre/surface interaction analysis

9.3 Understanding tyre/surface interaction

Tyre/surface interface governs the safety and durability of a particular surface when in contact with a rolling tyre. Therefore, understanding this interface is of vital importance, to pavement engineers.

The aim of this paragraph is to analyse the tyre/surface interface of simple surfaces in order to better understand and interpret the pressure distribution between the tyre and complex surfaces, which is the case of almost any flexible and rigid pavement. Certainly, some pavement surfaces would appear smooth and with consistent texture but they are not. A bituminous or cementitious mixture is a complex and heterogeneous compound formed by different units. The particles orientation, dimension, angularity combined with

small unevenness largely affect the pressure distribution at the interface. This lead to various multi-dimensional forces and stresses developed, which occur as a direct result of the complex interaction between a flexible rubber tyre and a rigid pavement surface (De Beer, 2008). The tyre/surface interface is affected largely by surface texture at different wavelengths, also being affected by tyre properties and vehicle dynamics (Woodward et al., 2013).

Initial tests and calibrations allowed understanding factors that affect the measurement. The first investigation evaluated the static contact patch on a reference smooth glass of four radial positions of a partially worn Finlay Irvine GripTester tyre (Figure 9.2).

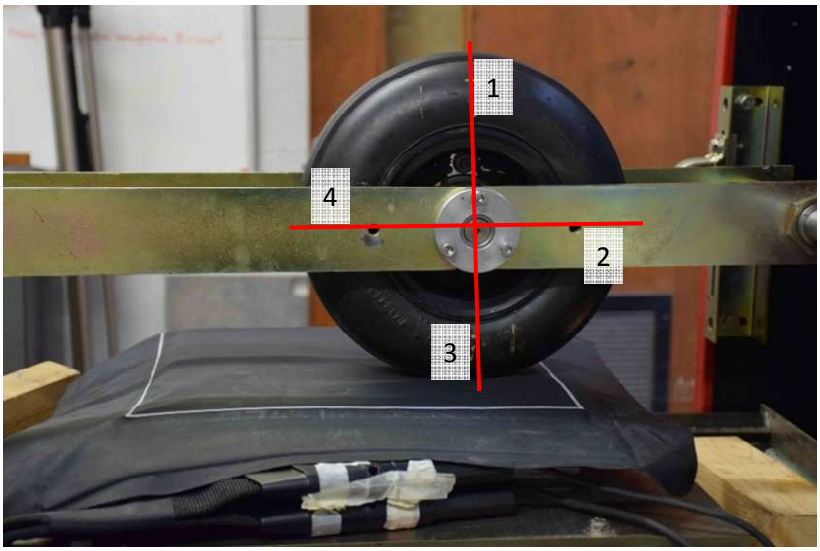

Figure 9.2: Positions of the GripTester tyre for the preliminary assessment

For each position a series of static measurement were done changing the following parameters:

- inflation pressure of the tyre: 10, 20, 30 and 40 psi, corresponding to 69, 138, 207 and 276 kPa;
- load applied to the end of the modified wheel tracker's level arm: 0, 3.265, 5.701 and 7.709 kg.

An example of a contact patch of the tyre on the glass during static measurement is shown in Figure 9.3 Hot colors indicate high contact pressure. It can be observed the cross symmetry of the contact patch and a longitudinal eccentricity caused by the load applied to the end of the level arm. Height and width of the tyre footprint were manually measured while the software automatically gave contact patch area, average and peak pressure.

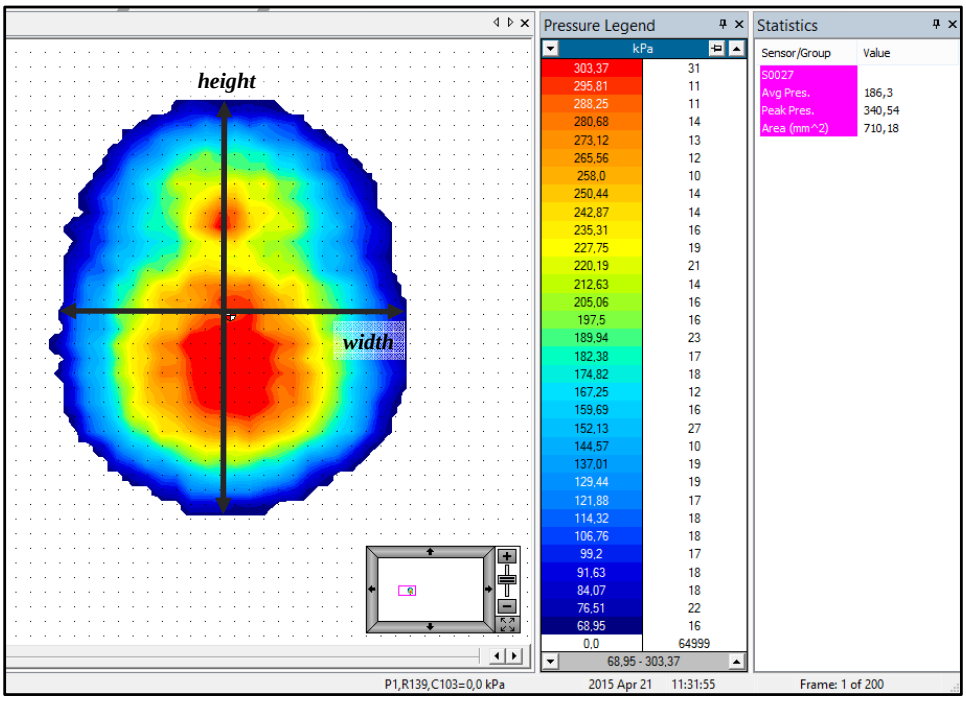

Figure 9.3: Contact patch of a reference smooth glass

Data were exported and subsequently processed on Microsoft Excel, leading to plots in Figures 9.4 to 9.12.

Width and height of the tyre footprint were found to be directly proportional to the load applied exhibiting similar rates for the different inflation pressure values. Width values especially, as shown in Figure 9.4, were very similar, except the 69 kPa pressure inflation case that exhibited an extreme increase with the load.

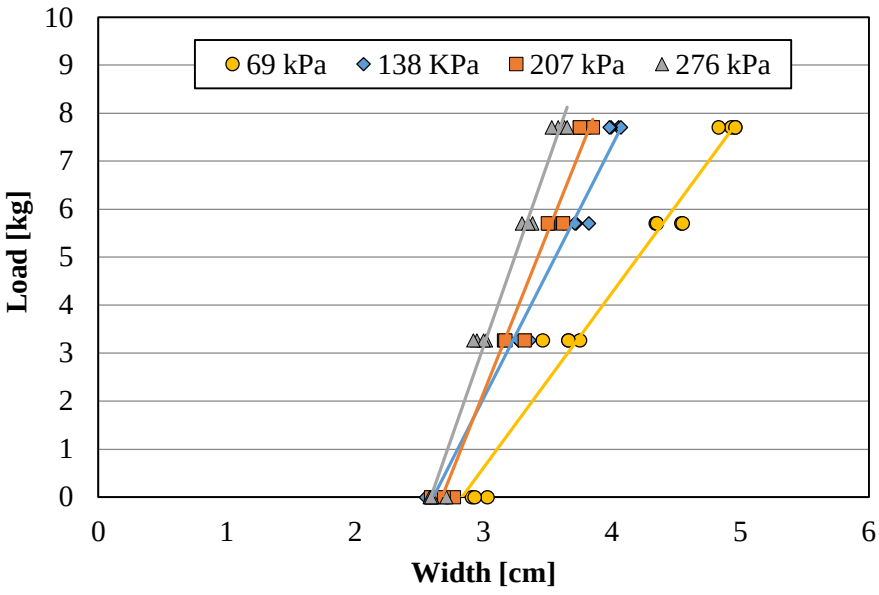

Figure 9.4: Load applied to the end of the level arm versus width of the tyre footprint

Changing the inflation pressure led to greater differences in the height compared to the width of the footprint (Figures 9.4 & 9.5).

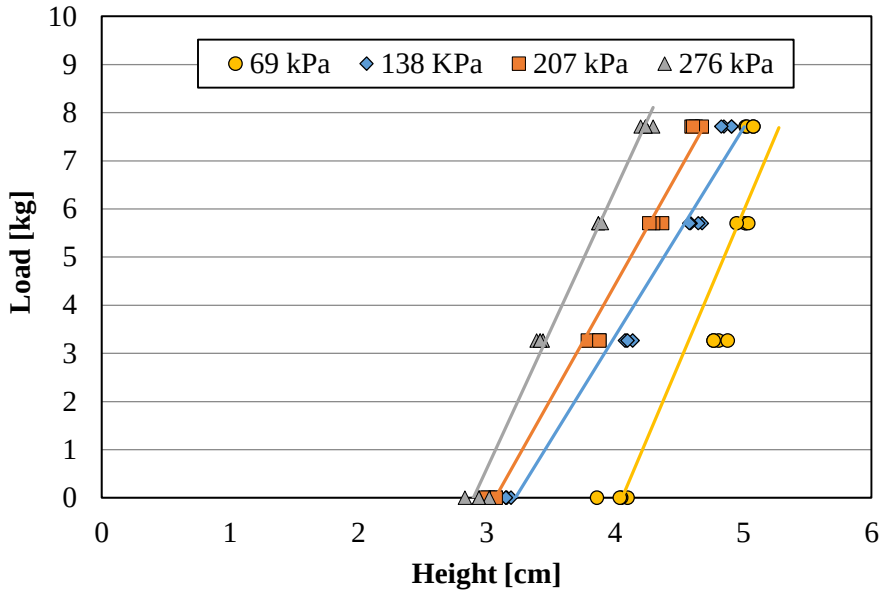

Figure 9.5: Load applied to the end of the level arm versus height of the tyre footprint

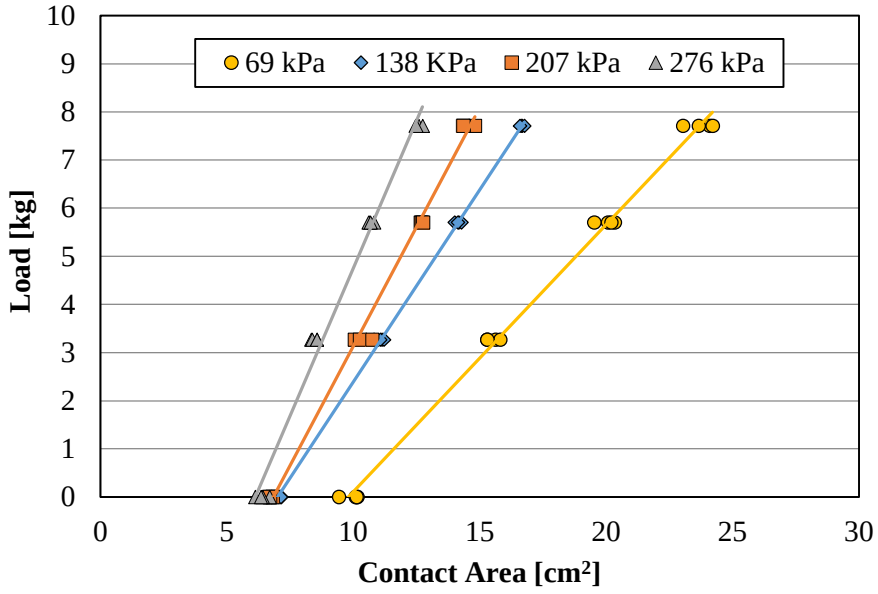

Figure 9.6: Load applied to the end of the level arm versus contact patch area of the tyre

The contact area plotted in Figure 9.6 showed that the more the tyre is inflated the smaller will be its footprint and the bigger the load the greater the differences between the cases.

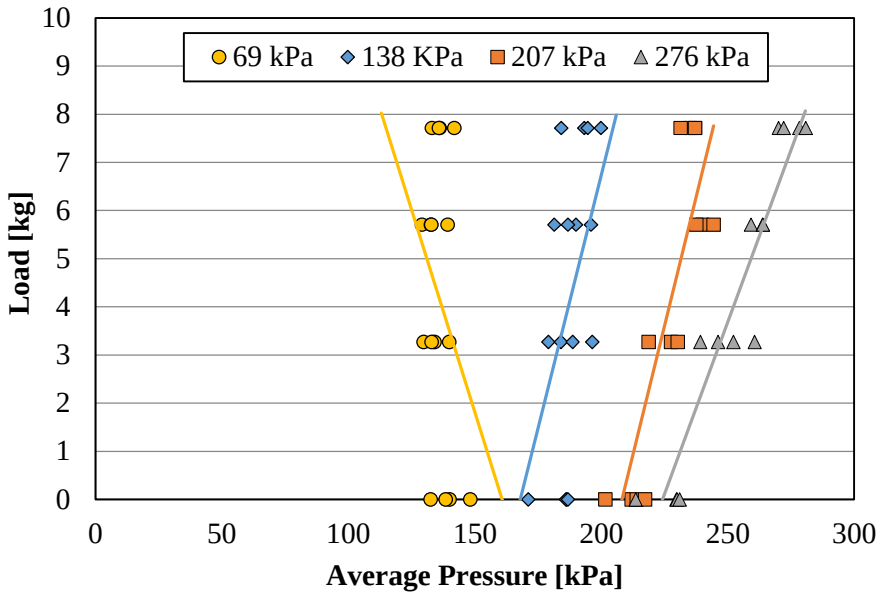

Figure 9.7: Load applied to the end of the level arm versus average pressure

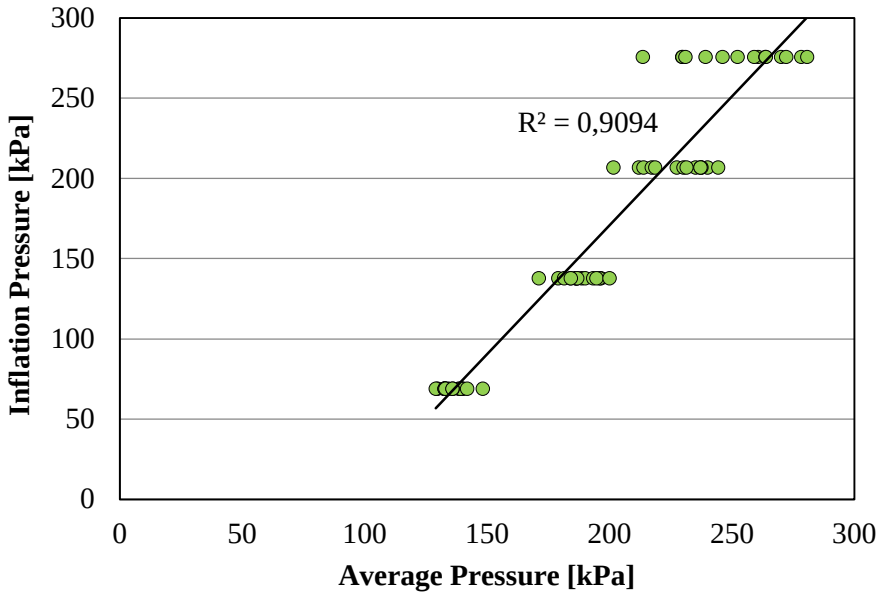

Figure 9.8: Inflation pressure versus average measured pressure

Figure 9.7 and 9.8 show the linear correlation between the average pressure of contact with the load applied and the inflation pressure respectively. Higher inflation pressures caused the variance of the average contact pressure to increase. In other words, the difference between the pressure developed with no load applied and the pressure developed with 7.7 kg applied to the end of the level arm was greater at high inflation pressure.

Figure 9.9 shows the relationship between the average pressure and the contact area. Since a rubber tyre is deformable, these two parameters were directly proportional so that as the tyre was more loaded both the average pressure and the contact area increased.

Lowering the inflation pressure reduced the angular coefficient of the trend line i.e. greater contact area corresponding to the same increase of contact pressure. The 69 kPa inflation pressure was a limit: the average pressure remained constant while the contact area raised.

The opposite would have occurred if the tyre had been infinitely rigid: no contact area growth and average pressure dependent on the load applied. In fact, as the tyre was more inflated, i.e. rigid, the trend lines tended to be vertical.

Figure 9.10 shows the relationship between the inflation pressure and the contact area. It is clear that as the inflation pressure increased, the trend lines corresponding to different loads applied tend to get closer. This is in line with what found by Millar et al. (2011), which demonstrated less differences of contact patch between different tires at higher inflation pressures.

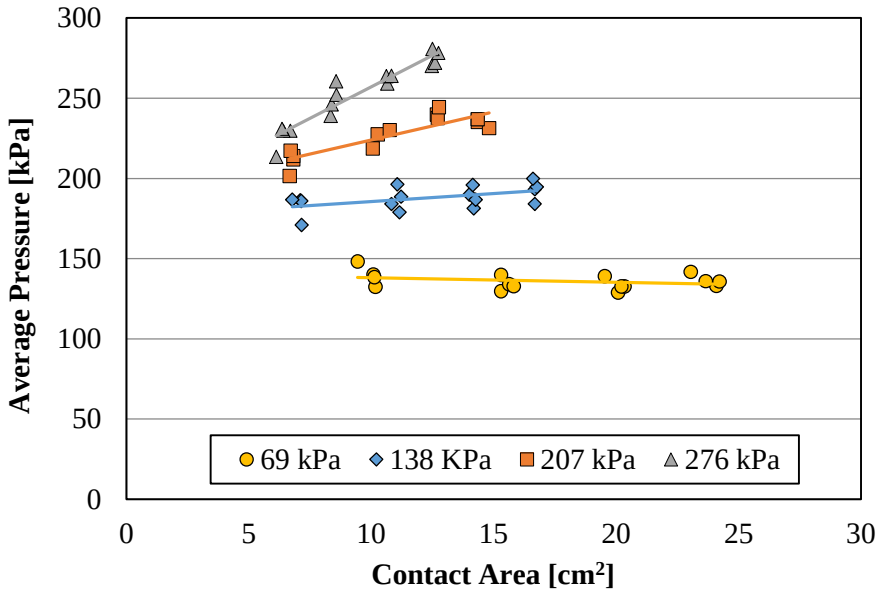

Figure 9.9: Average measured pressure versus contact patch area

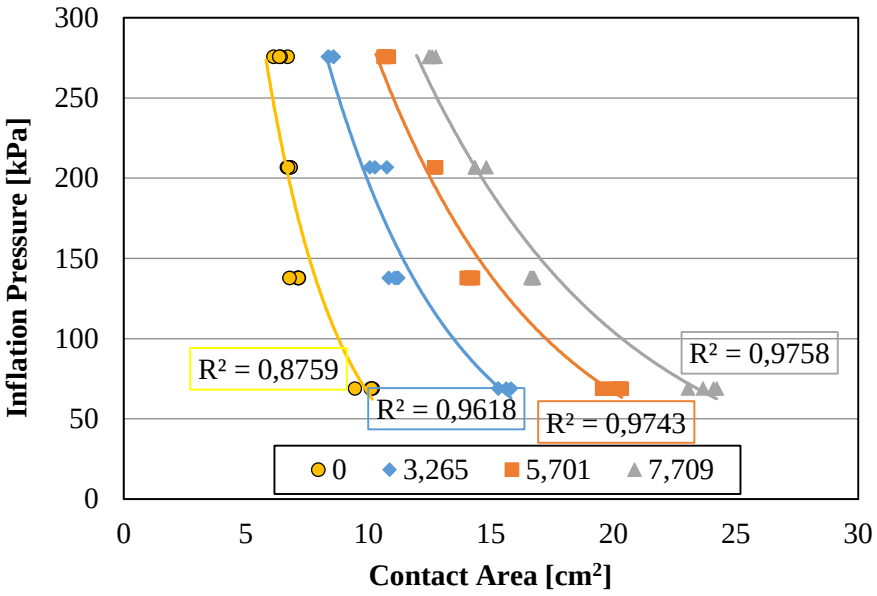

Figure 9.10: Inflation pressure versus contact patch area

In order to verify the reliability of the static measurements, results obtained at the four different positions of the tyre selected for the tests were compared.

A variability in the results arose as shown in Figure 9.11 and 9.12, corresponding to the average pressure and the contact area respectively.

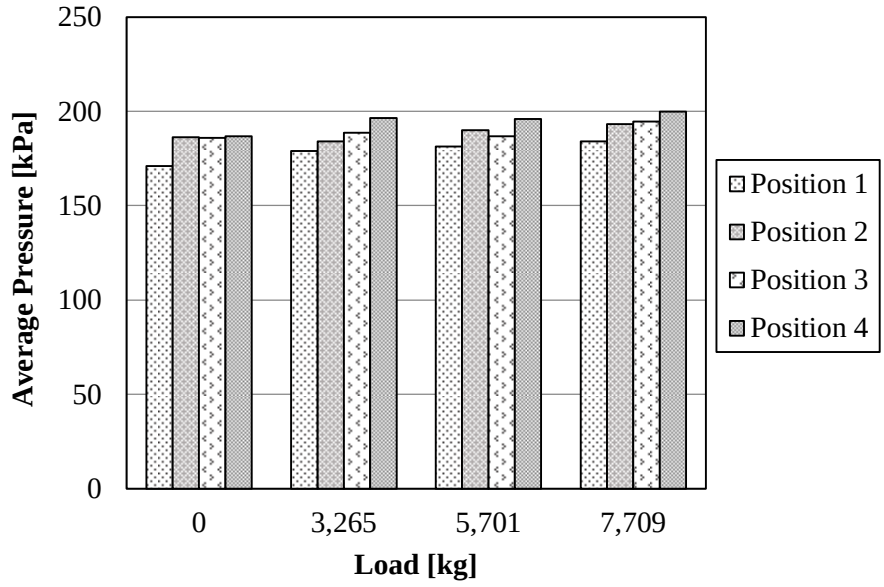

Figure 9.11: Average measured pressure versus load applied

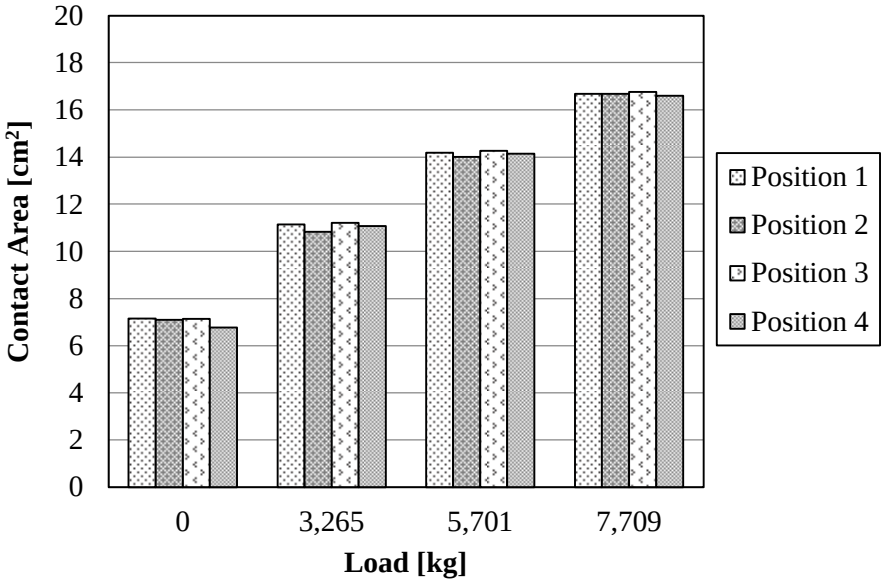

Figure 9.12: Contact area versus load applied

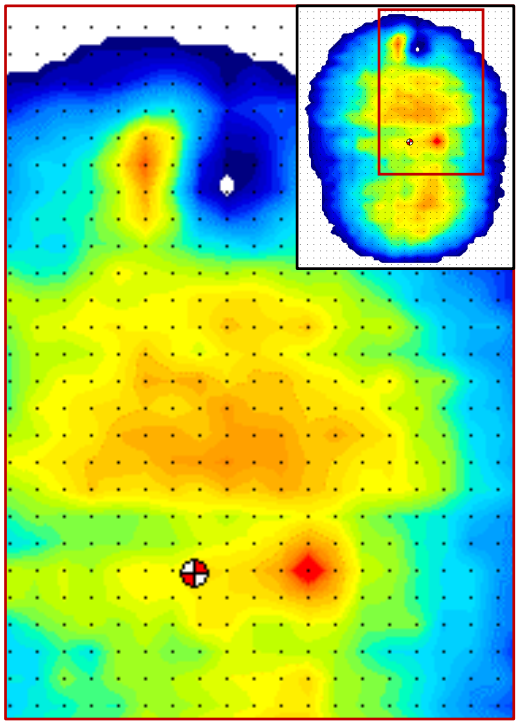

Figure 9.13: Contact patch of a rejected tyre

The contact patch area can also indicate irregularities of the tyre surface as shown in Figure 9.13. Three were the anomalies found out testing this tyre:

- cross asymmetry of the pressure distribution;

- a non-contact point incorporated in the contact area, indicating a local lack of material inside the tyre;
- a hot point, indicating a bulge of the rubber;

While these anomalies had been easily recognized testing the tyre on a reference smooth glass, they would have been confused with surface irregularities during routine pavement/tyre interactions investigations.

It was inferred that the tyre irregularities can affect the measurement so that the results could be compromised. Accordingly, after validation, the same tyre was used for all the analysis.

Furthermore, all the static measurements presented in the next paragraphs were carried out with the validated tyre on the same position.

9.4 Ideal surfaces

Once the relationship between the parameters involved in the tyre/surface interaction were established, ideal surfaces with consistent texture were studied. This was a fundamental step in order to comprehend further analysis on complex surfaces.

The tests were performed in dynamic mode by slowly pushing the stage onto which the Finlay Irvine tyre was supported so that the tyre rolled over accordingly. During every test 200 frames were recorded with a frequency rate of 10 frames/second.

Based on the previous experience, the testing tyre was the same for every test. Furthermore, a permanent mark was made on it so that every test was carried out on the same tyre strip.

Three ideal surfaces were selected for this study (Figure 9.14):

- smooth glass;
- small tiles texture, 1 cm side and rounded corners;
- big tiles texture, 2 cm side and flat corners.

Both the tiles surfaces were tested twice centring the tyre on a groove within the mosaic and on a single row of tiles to better comprehend the effects of the spaces between the

cells. From now on, the first will be referred to as “Groove Centred”, G.C., and the latter “Tile Centred”, T.C.

Figure 9.16, 9.17, 9.18, 9.19, 9.20 show the pressure maps for the tested surfaces. In order to optimize the reading of the maps, different range values were adopted for plotting each surfaces: the colour palette change accordingly, representing low-pressure values with cold colours like blue and high-pressure values with hot colours like red. A low threshold was set at 68.95 kPa so that the software marks as zero the cells that satisfy the criteria.

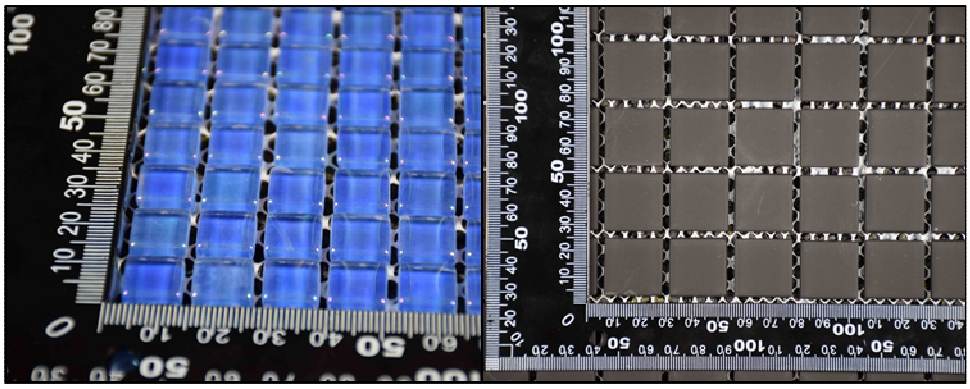

Figure 9.14: Small and big tiles mosaics

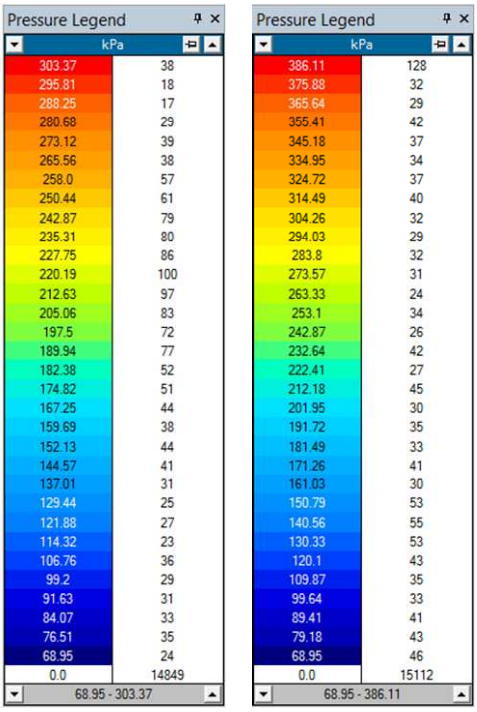

Figure 9.15: Pressure legend for the glass and the big tiles plots (left) and for the small tiles plots (right)

Range values are 68.95 kPa to 303.37 kPa for glass and big tiles surfaces and 68.95 kPa to 386.11 kPa for small tiles surface.

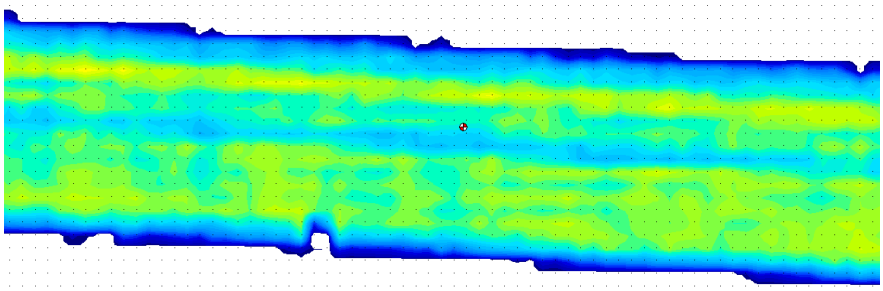

Figure 9.16: Pressure distribution strip for the glass

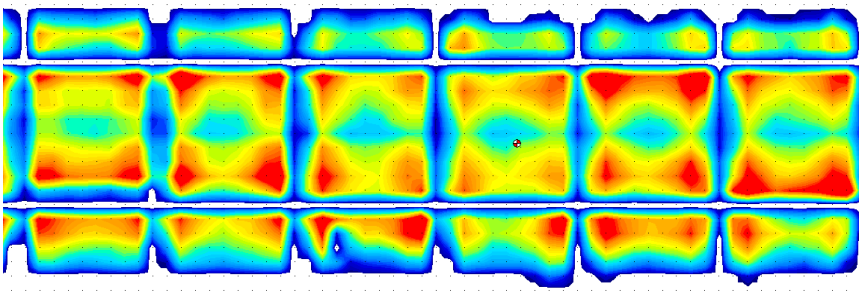

Figure 9.17: Pressure distribution strip for the big tiles. Wheel centred on the tiles (T.C.)

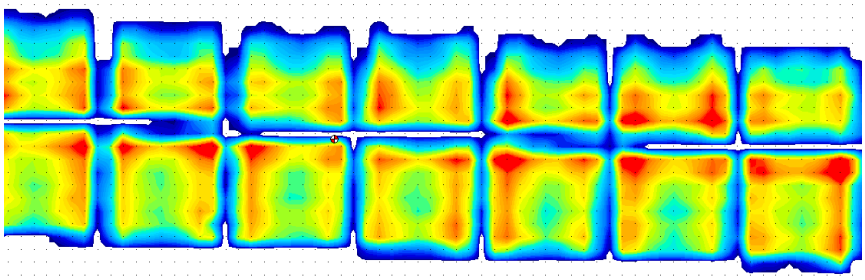

Figure 9.18: Pressure distribution strip for the big tiles. Wheel centred on the groove (G.C.)

The contact patch of the tyre on the glass (Figure 9.16) highlights the smoothness of the surface. The pressure is well distributed over the entire surface and kept constant within a small range of values, less than 300 kPa. Consequently, as the variance is small no peaks were detected.

The contact patches of the tyre on the big tiles mosaics in Figures 9.17 and 9.18 show that the contact primary develop on the corners of the tiles. When the tyre was centred on a row of tiles the pressure observed was minimal on the tyre axle strip and reached the maximum value on the border of the tiles, especially on the corners. No big differences

were observed as the tyre was centred on a groove; even if case the pressure seemed to be slightly better distributed, with less peaks on the corners.

The contact patches of the tyre on the small tiles mosaics are shown in Figures 9.19 and 9.20. The tyre is in contact with more and smaller tiles so that the resulting contact area is reduced compared to the previous case resulting in a higher pressure. Furthermore, the form of this type of tile which is not flat and has got rounded corners imply that the pressure is primary developed on the centre of the tiles. The alignment of the tyre with the tiles did not affect the pressure distributions.

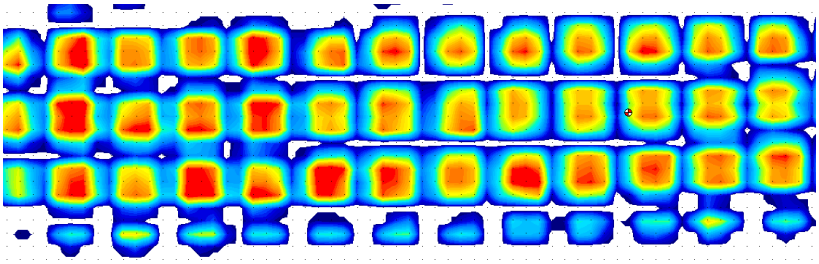

Figure 9.19: Pressure distribution strip for the small tiles. Wheel centred on the tiles (T.C.)

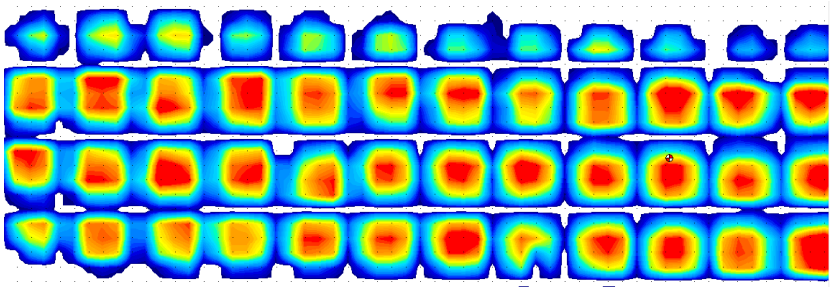

Figure 9.20: Pressure distribution strip for the small tiles. Wheel centred on the groove (G.C.)

Data were also analysed analytically by exporting pressures and contact areas values into an Excel spreadsheet. In particular, two different graphs, allowing for an intuitive comparison between different surfaces, were created :

- average pressure frequency distribution;
- average pressure cumulative frequency distribution.

In order to better represent the results, the first distribution was obtained by classifying every pressure value of the tyre/surface interaction into 68.95 kPa size bins, which is equivalent to the low pressure threshold, while for the latter 10 kPa size bins were adopted.

Figures 9.22 and 9.23 show the frequencies plots for the three ideal surfaces. The glass density curve is very compact, with the central class reaching the 70% of the frequency, indicating that the pressure values, as seen before, are very constant over the interaction surface. The peak pressure is under 300 kPa.

The big tiles surface density curve is more spread and exhibits a higher peak pressure of approximately 400 kPa. The most central class is less frequent compared to the glass with a value of 40%.

Finally, the small tiles surface shows, among the three studied surfaces, the more spread distribution. Three consecutive classes can be considered central as pressure values are equally distributed between 68.95 kPa and 344.75 kPa. The peak pressure is higher compared to glass and big tiles surfaces and is close to 500 kPa.

These cases have shown an inverse proportionality between the peak pressure and the contact area: the smaller the contact area (Figure 9.21) the higher the peak pressure.

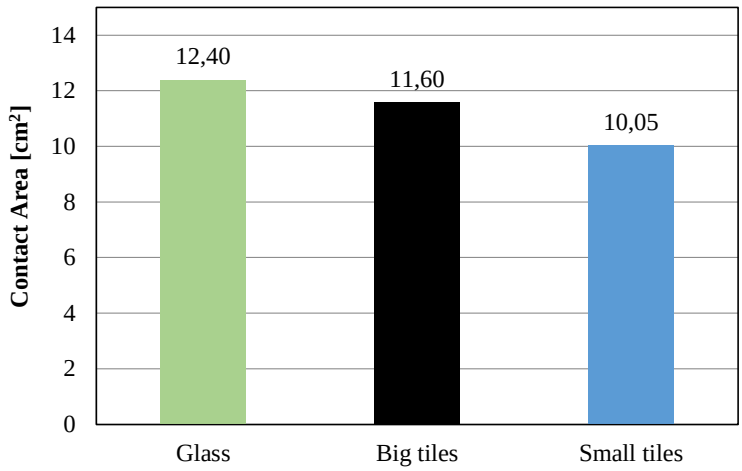

Figure 9.21: Pressure distribution strip for the small tiles. Wheel centred on the groove (G.C.)

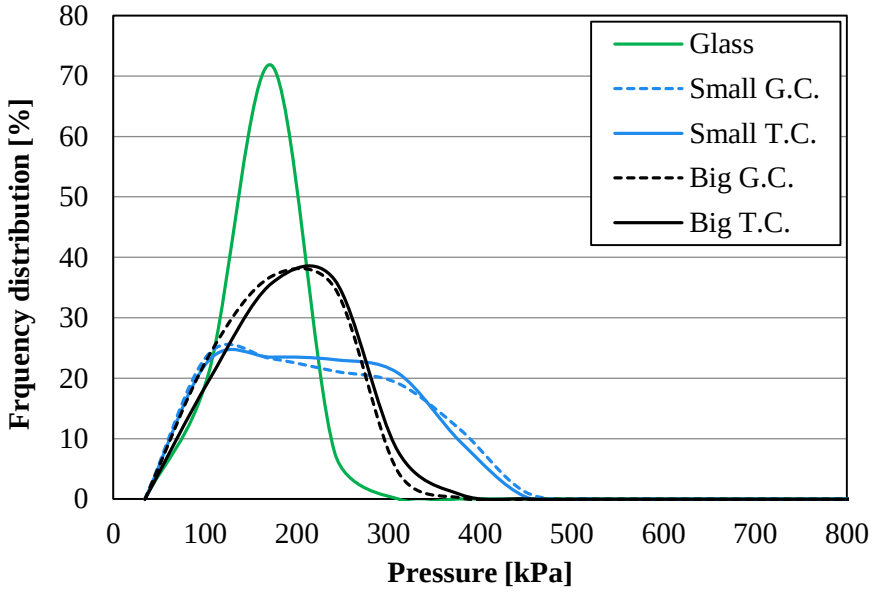

Figure 9.22: Frequency distribution comparison for glass and tiles

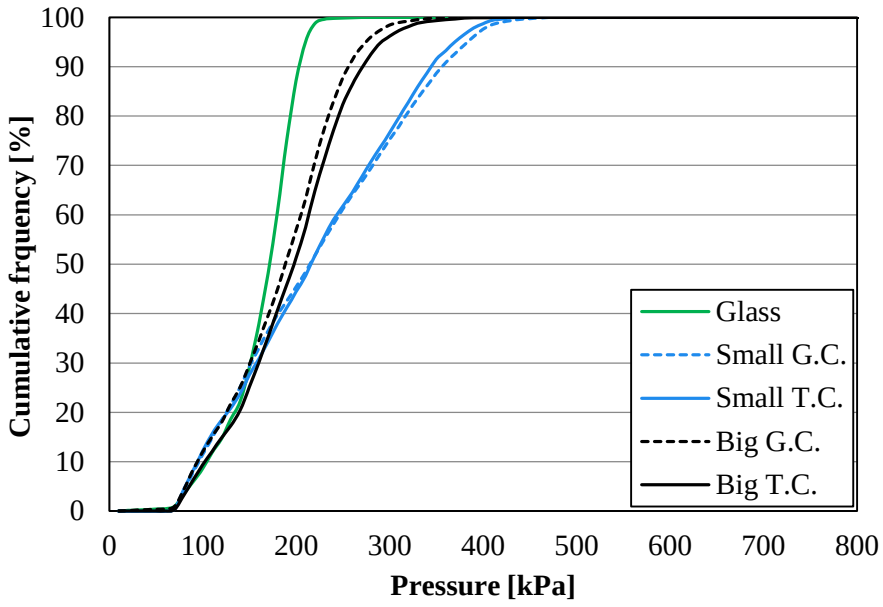

Figure 9.23: Cumulative frequency comparison for glass and tiles

9.5 Different asphalt surfaces

This section deals with the study of different road pavement surfaces, in order to comprehend and compare their interaction with the tyre.

In particular, different gradations of Stone Mastic Asphalt were analysed, i.e. a 0/6 core, a 8 mm slab, a 0/10 m slab and a 0/14 core. Furthermore, a plain surface was taken as reference and two positive texture surfaces were added to the comparison: a high friction surface and a cycle lane surface. The tests were performed in static mode, by applying a load of 3.3 kg to the end of the level arm.

Figure 9.24 shows the relationship between the pressure and the contact area. As stated in the previous section, pressure have shown an inverse proportionality with the contact area: the smaller the contact area the higher the peak and the average pressure.

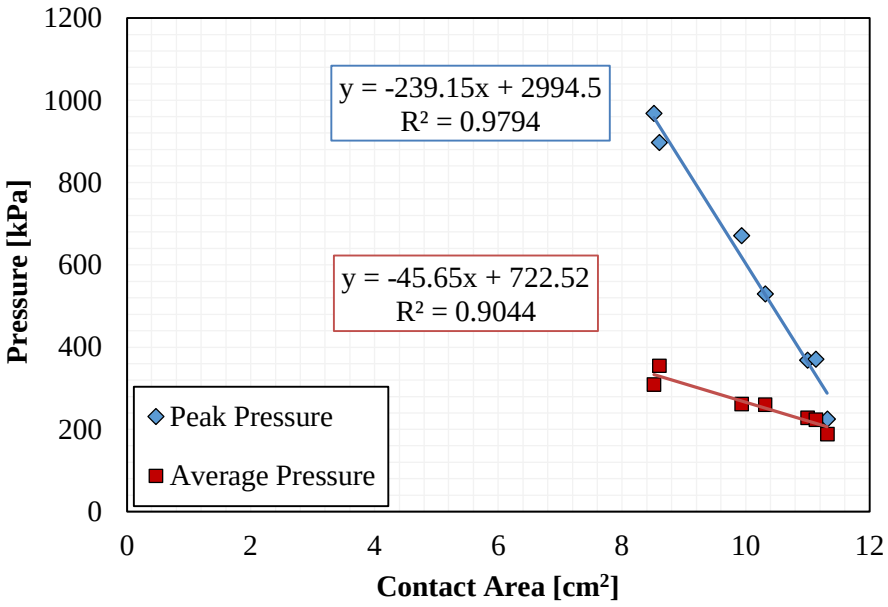

Figure 9.24: Cumulative frequency comparison for different surfaces

Figure 9.25 shows a comparison between average, peak pressure and contact area for the investigated surfaces. They can be grouped in three different couples. SMA 6 and SMA 8 exhibit very similar, having low peak pressures and high contact areas. SMA 10 and the cycle surface show similar contact area of 11 cm^2 circa and intermediate peak pressure. Finally, SMA 14 and the high friction surface, although representing highly pronounced negative and positive texture surfaces respectively, show a similar behaviour with a small contact area and a peak pressure higher than 900 kPa. The bundles are clear in Figure 9.28, which shows the pressure cumulative frequency.

Figure 9.26 shows the pressure frequency distribution. The first bundle, SMA 6 and SMA 8, exhibit uniform and consistent curves along the median, while the second bundle formed by SMA 10 and the cycle surface differ from the first for a tail towards the high-

pressure levels. HFS and SMA 14 curves are asymmetric and spread towards the high-pressure levels, especially the latter that is particularly scattering.

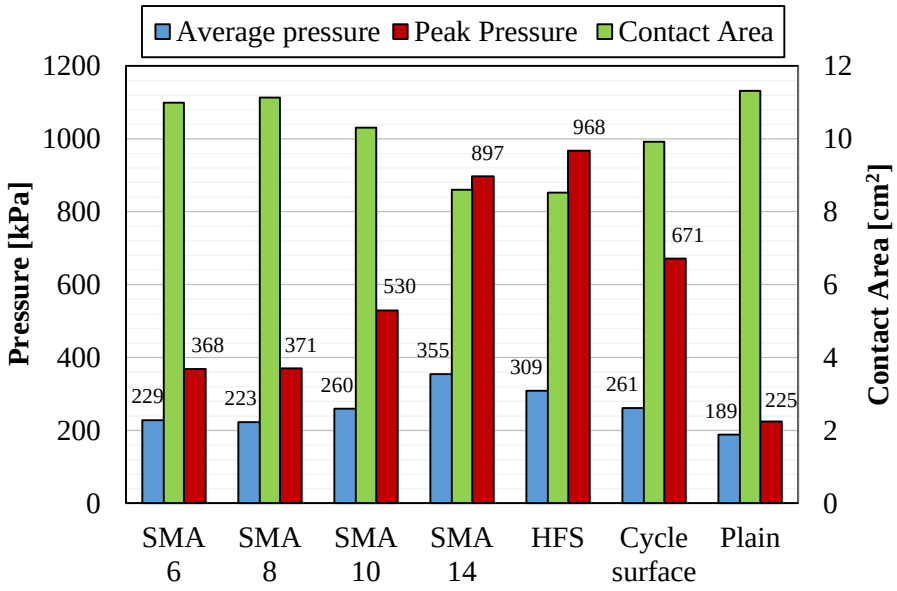

Figure 9.25: Comparison of pressure and contact area for different surfaces

Figure 9.27 shows a magnification of the frequency distribution highlighting the discontinuity of SMA 14 pressure, which fluctuate towards the zero.

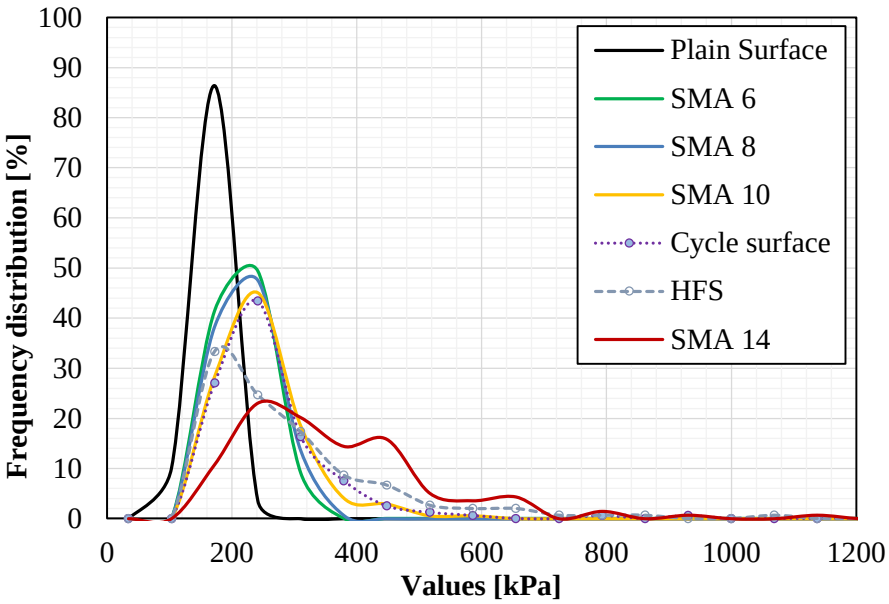

Figure 9.26: Pressure frequency distribution for different surfaces

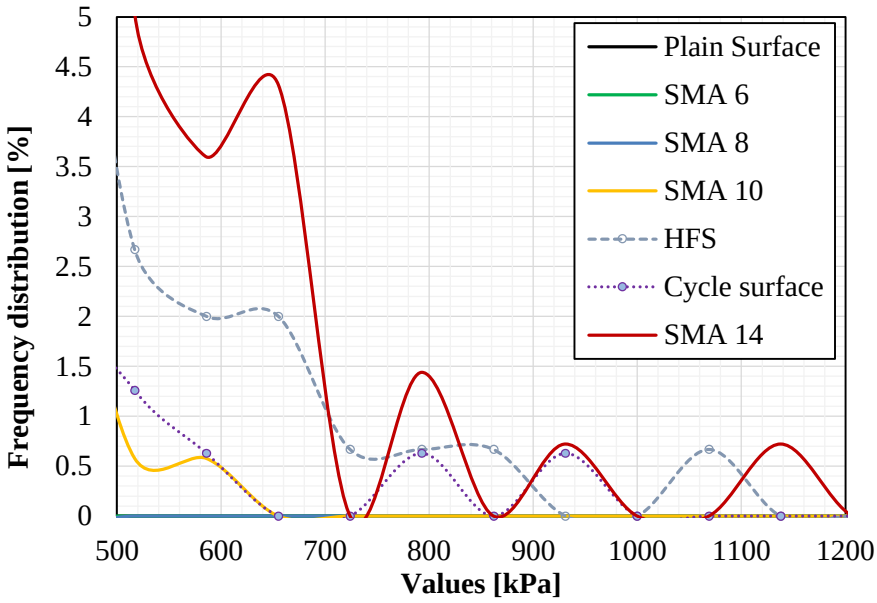

Figure 9.27: High-pressure frequency distribution for different surfaces

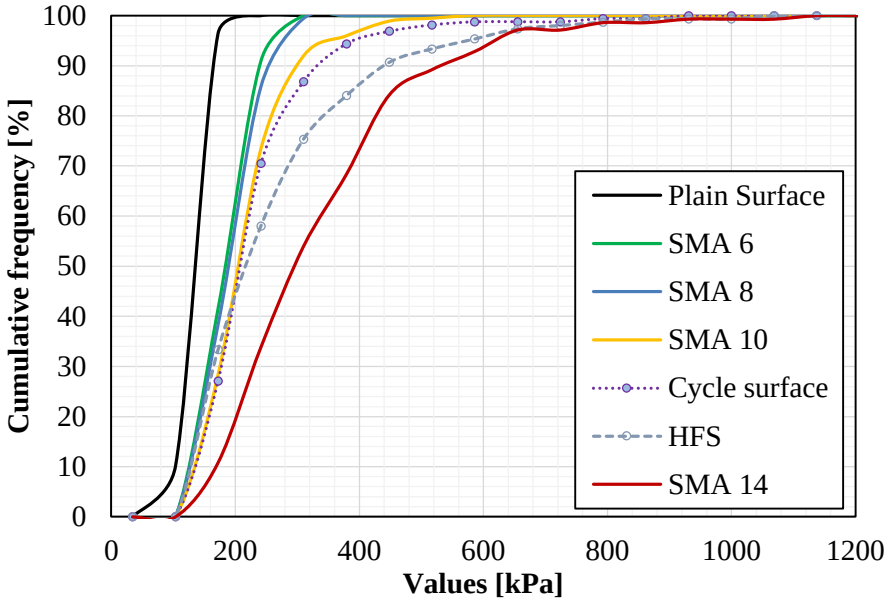

Figure 9.28: Cumulative frequency distribution for different surfaces

9.6 Rubberized 8 mm SMA

This paragraph discusses the tyre/surface interaction for the three 0/8 stone mastic asphalts under investigation. The slab test specimens, after being compacted inside a 275 x 275 mm steel frame with a roller compactor, underwent 100,000 wheel passes of simulated trafficking using the RTM.

Trafficking was stopped at regular intervals to determine the tyre/surface interaction with dynamic measurements in the direction of the trafficking. In order to evaluate the change in the texture the slab was tested on the same strip at every stage. A weight of 3.3 kg was applied at the end of the level arm of the Modified Wessex wheel track and the same strip of the tyre was used for each test.

9.6.1 *mm SMA 0.00*

The 0.00% rubber 0/8 mm SMA slab underwent 0, 200, 500, 1000, 2000, 5000, 10000, 20000, 40000 and 75000 wheel passes of simulated trafficking with RTM.

Figure 9.29 and 9.30 show respectively the frequency and the cumulative frequency distribution of the contact pressure. The density curve is asymmetric, raising rapidly to reach the most frequent values, which are comprised between the range 100 – 250 kPa, and dropping gentler towards the high-pressure values ending up with a tail representing the peak pressure values, attested around 500 kPa. This form was found to be typical, as it came up for each measurement.

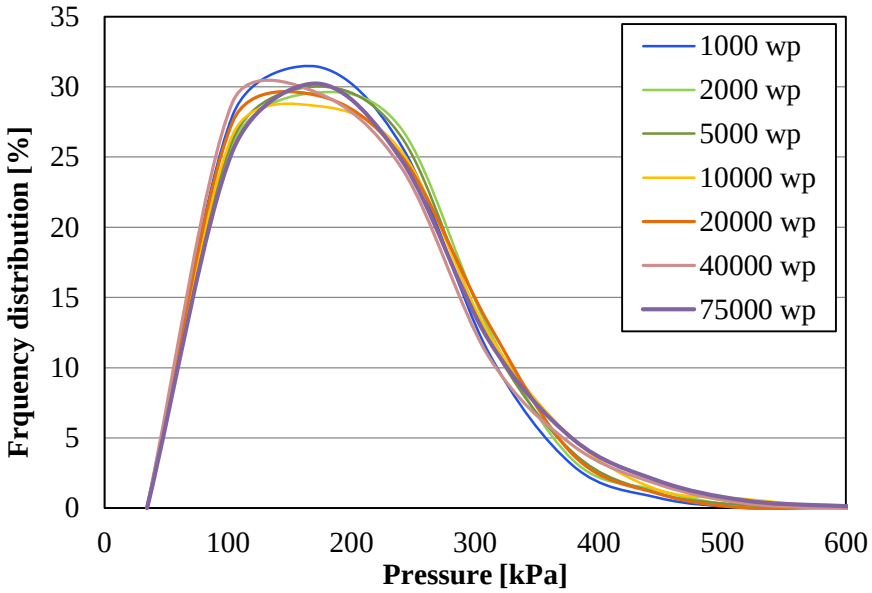

Figure 9.29: Frequency distribution comparison for different trafficked 8 mm 0.00 SMA specimen

At first sight, no sensible differences are evident induced by the simulated trafficking with the pressure maintaining very similar density and cumulative frequency curves. The

interaction, in terms of contact pressures, between the tyre and the surface is substantially the same notwithstanding the trafficking the slab underwent.

However, by applying a magnification on the high-pressure area of the frequency distributions, Figure 9.31, it is possible to appreciate that, as the slab start to be high trafficked, the contact pressure increase, indicating a change in the texture of the slab.

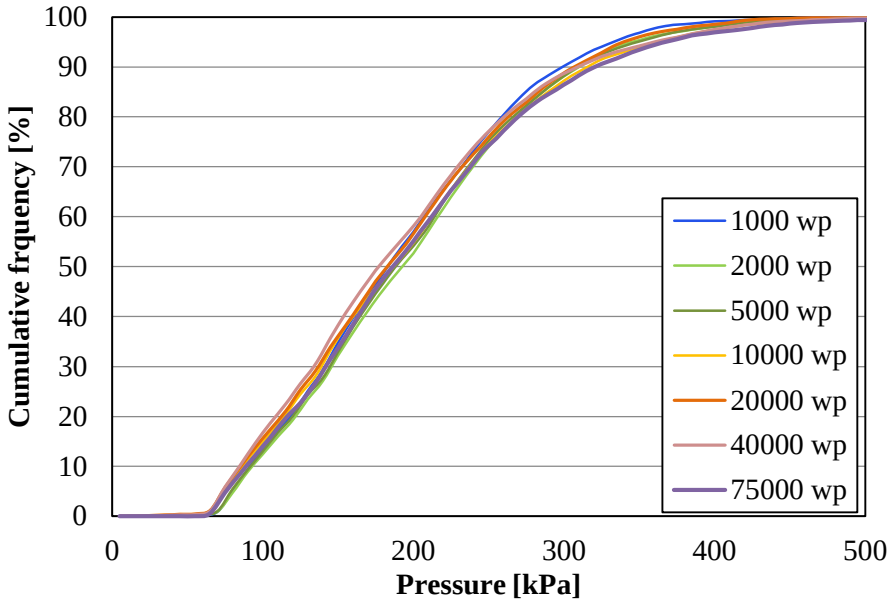

Figure 9.30: Cumulative frequency comparison for different trafficked 8 mm 0.00 SMA specimens

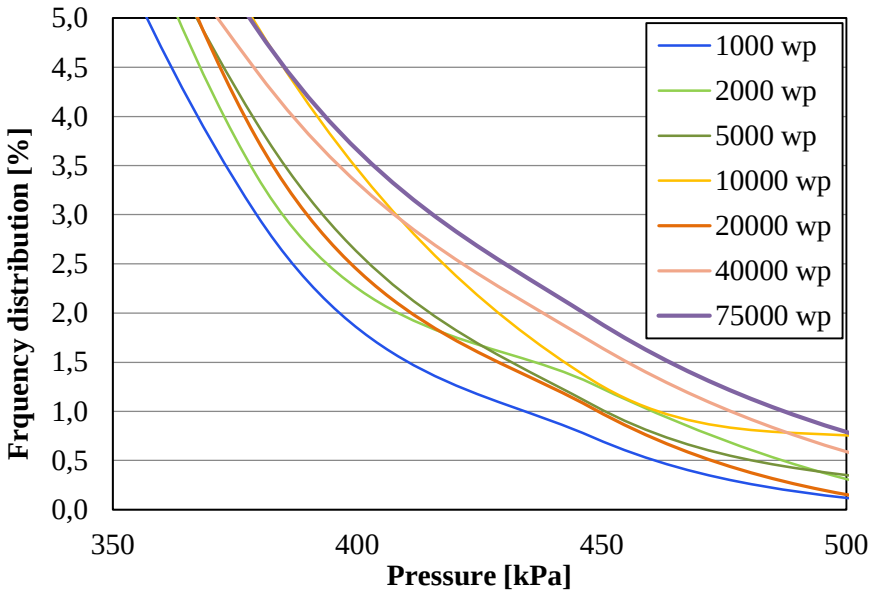

Figure 9.31: Magnification of the density distribution tail for 8 mm 0.00 SMA specimen

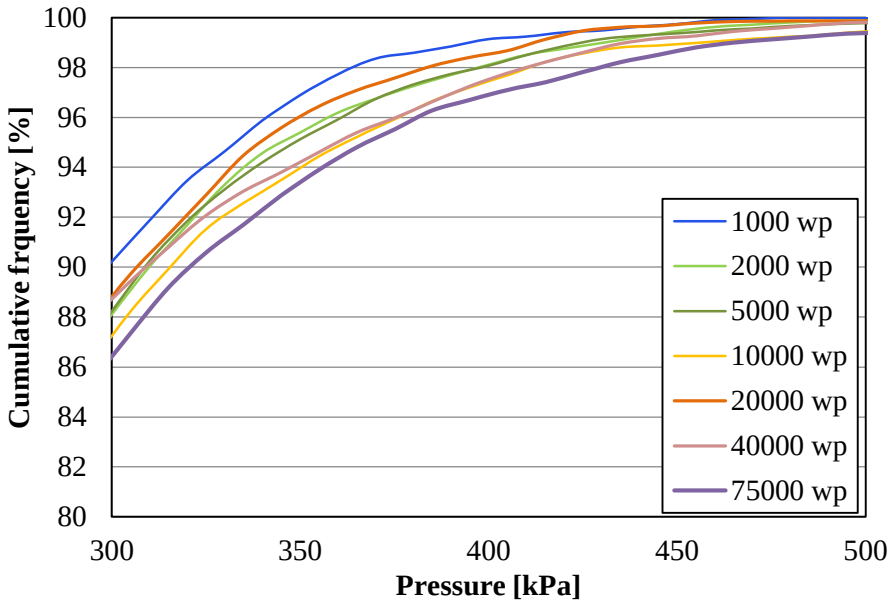

Figure 9.32: Magnification of the high-pressure area for 8 mm 0.00 SMA specimens

9.6.2 *8 mm SMA 0.75*

Having noticed a change in the texture with the trafficking of the first tested slab, the 0.75% rubber 0/8 mm SMA slab underwent 0 to 100000 wheel passes of simulated trafficking, while the investigation was deepened by stopping the trafficking at 200, 500, 1000, 2000, 5000, 10000, 20000, 40000, 75000 and 100000 wheel passes.

Figures 9.33 and 9.34 show the pressure map evolution at the different stages. The range values of representation is 68.95 to 358.53 kPa. Pressure maps are very similar up to 5000 wheel passes. From 10000 wheel passes, it is possible to observe a change in the contact area, with the creation of small non-contact holes, which shape change with the trafficking. From 40000 wheel passes the pressure raise definitely, as highlighted by the red hot spots on the maps, which indicate high-contact pressure points.

Figure 9.35 and 9.37 show the frequency and the cumulative frequency distributions. These curves assumed the typical forms described in the previous paragraph. Here the change in the pressure is clear and evident.

Blue and green indicators, which designate the early life of the pavement (200 to 5000 wp), are very close to each other and the variance is minimum.

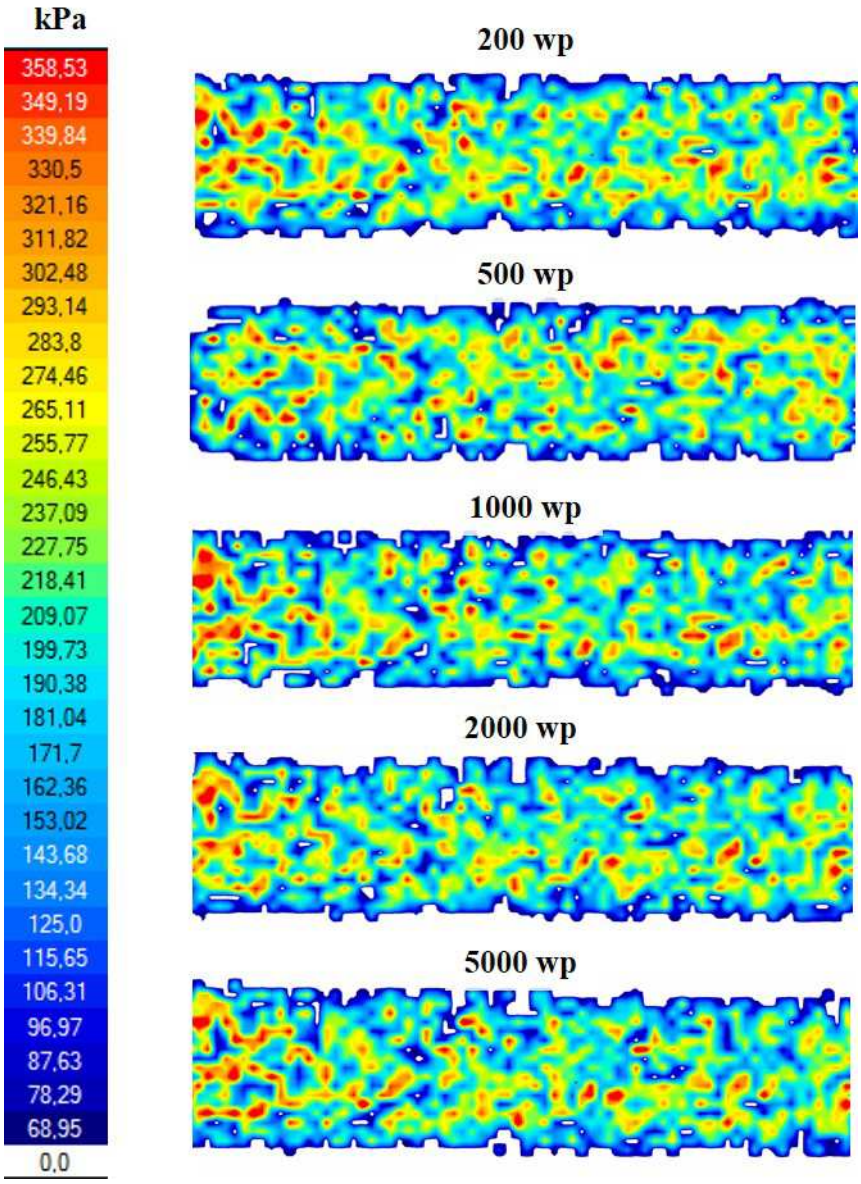

Figure 9.33: Early life pressure maps evolution for 0.75 SMA

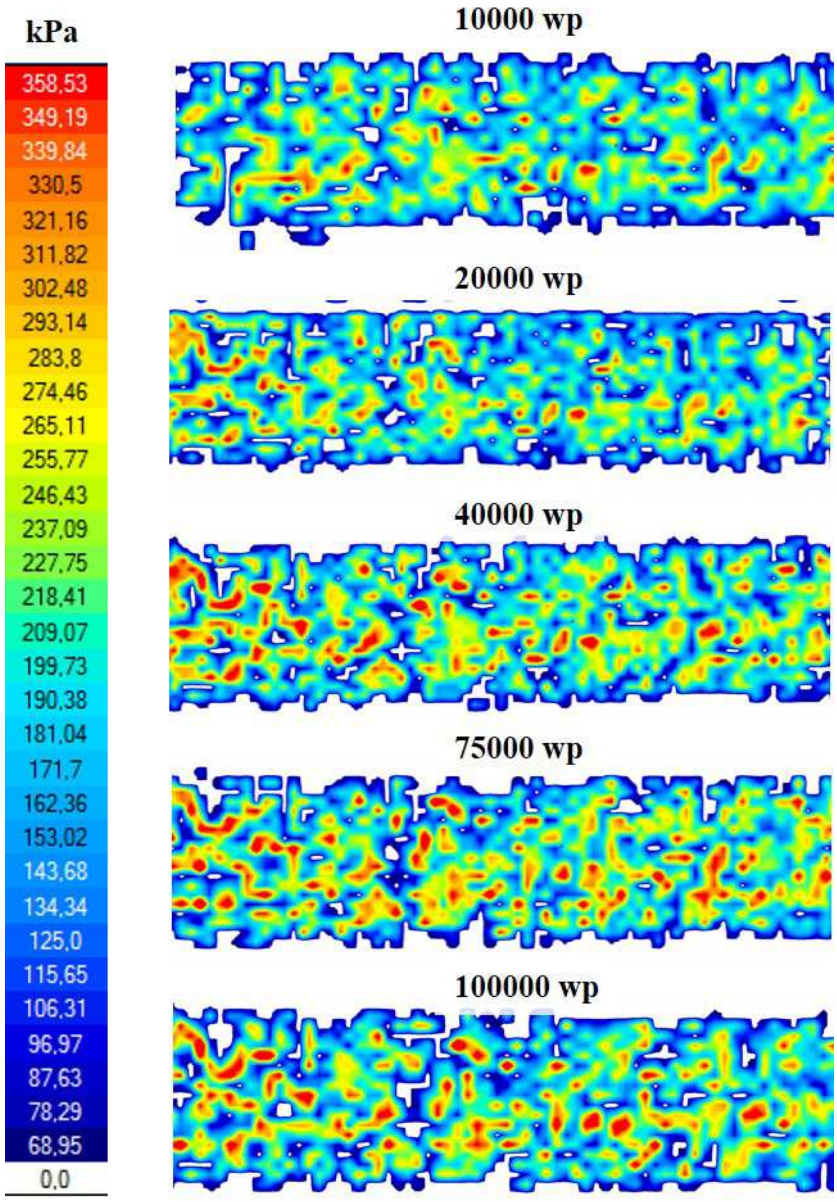

Figure 9.34: Pressure maps evolution for 0.75 SMA

Yellow and orange lines (10000 and 20000 respectively), which stand for the first years of service of the pavement, are slightly shifted to the left side of the graphs, and the density distribution is more centred on the median value, with even less variance. This might indicate that the slab underwent a better compaction under traffic so that the particles have been rearranged causing the average and the peak pressure to reduce. The shifting is even more evident in the density distribution graph and in its magnification in Figure 9.36.

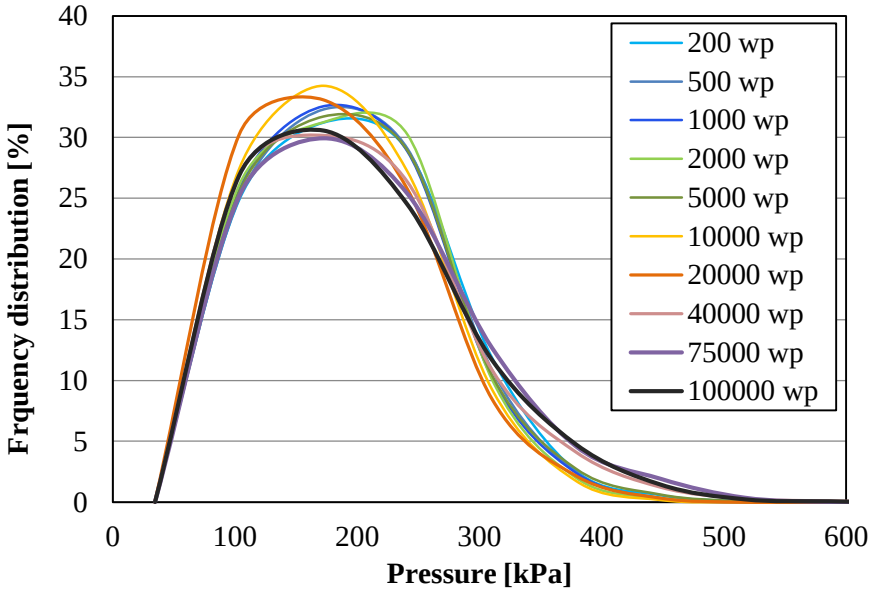

Figure 9.35: Frequency distribution comparison for different trafficked 8 mm 0.75 SMA specimens

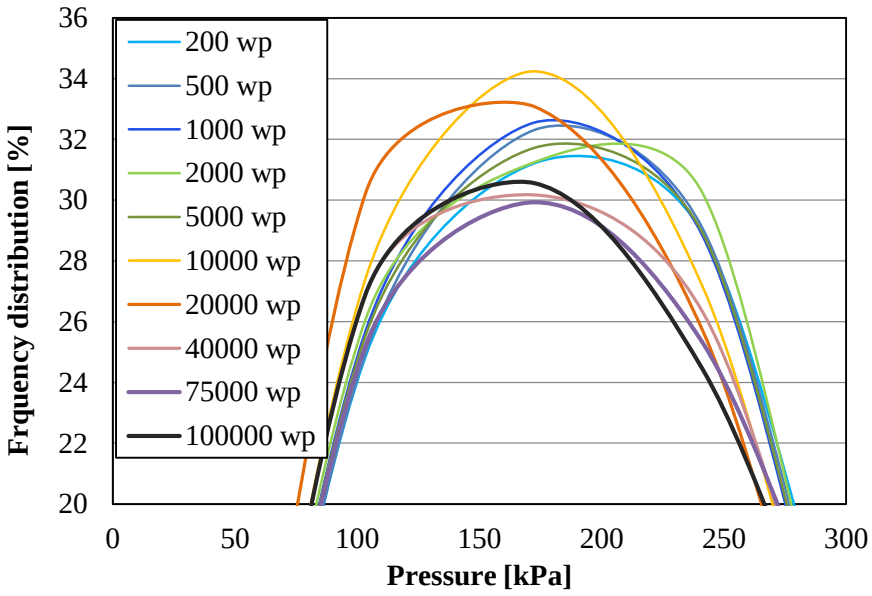

Figure 9.36: Magnification of the most frequent pressure area for 8 mm 0.75 SMA specimens

While the slab underwent the last three cycles of trafficking, its texture changed accordingly. The pink, purple and black curves, which indicate 40000, 75000 and 100000 wheel passes respectively, represent the third bundle of curves of these graphs. Here the median value drop while the tail raise, indicating a spread of the pressure over a wider range of values and simultaneously an increase in the peak pressure value.

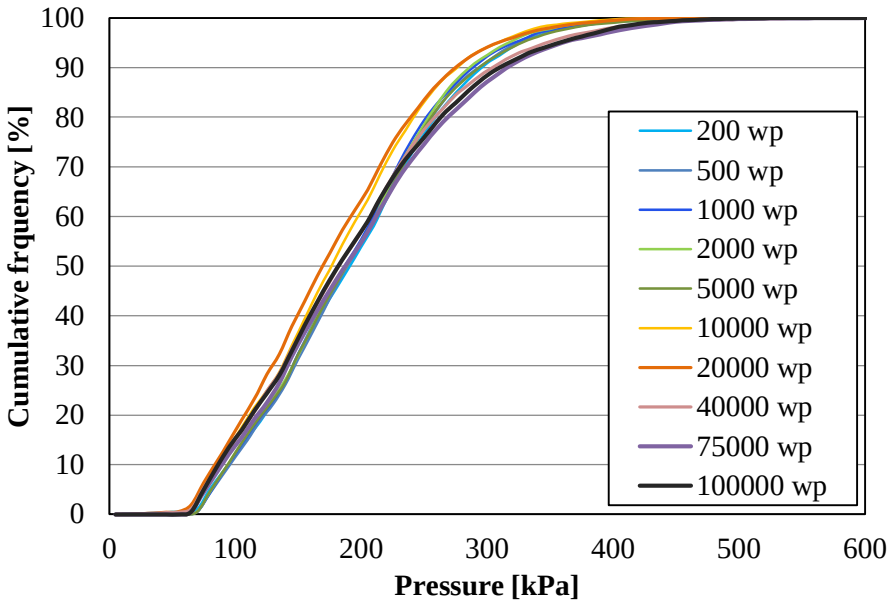

Figure 9.37: Cumulative frequency comparison for different trafficked 8 mm 0.75 SMA specimens

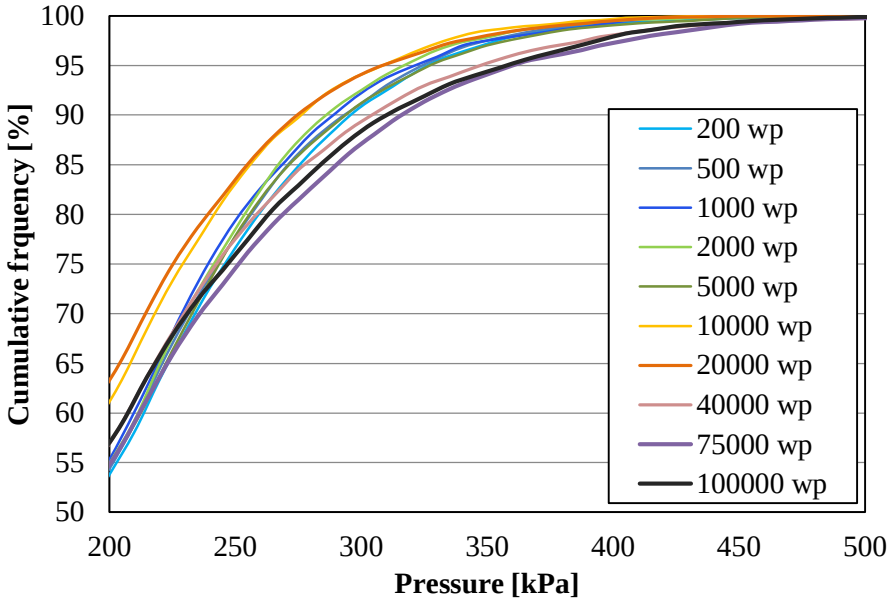

Figure 9.38: Magnification of the high-pressure area for 8 mm 0.75 SMA specimens

9.6.3 *8 mm SMA 1.20*

The 1.20% rubber 0/8 mm SMA slab underwent 0 to 100000 wheel passes of simulated trafficking, stopped for measurement at 200, 500, 1000, 2000, 5000, 10000, 20000, 40000, 75000 and 100000 wheel passes. Figure 9.39 and 9.41 show the frequency and the cumulative frequency distributions.

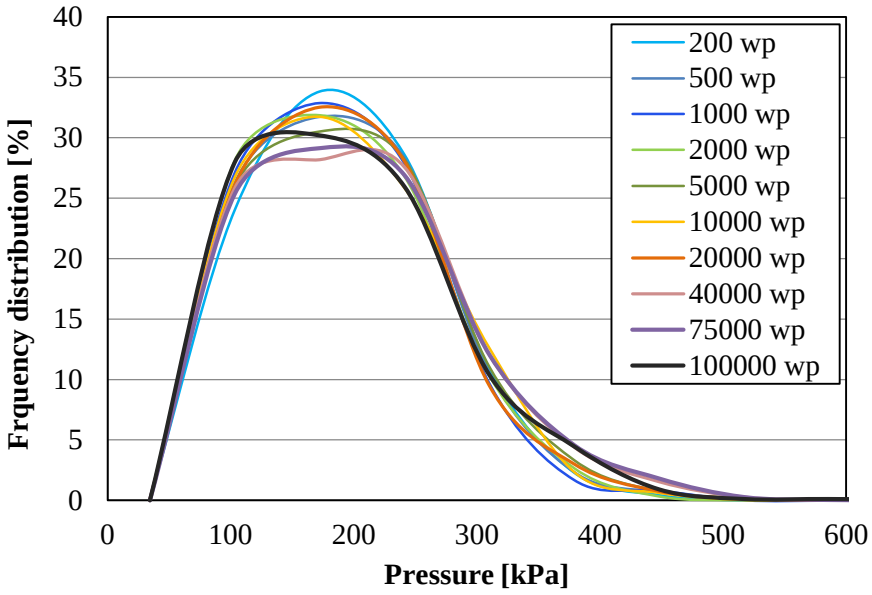

Figure 9.39: Frequency distribution comparison for different trafficked 8 mm 1.20 SMA specimens

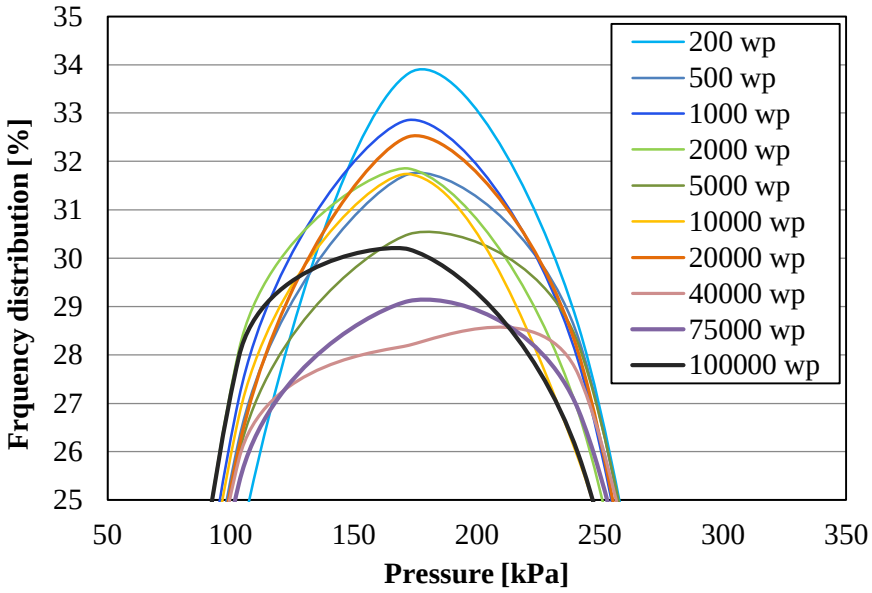

Figure 9.40: Magnification of the most frequent pressure area for 8 mm 1.20 SMA specimens

The same considerations made for the other rubberized slabs can be applied here.

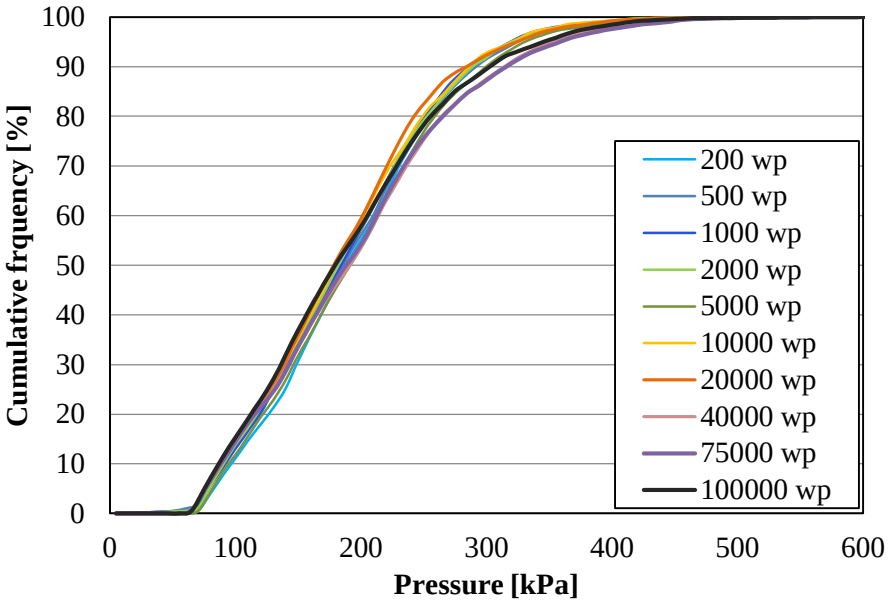

Figure 9.41: Cumulative frequency comparison for different trafficked 8 mm 1.20 SMA specimens

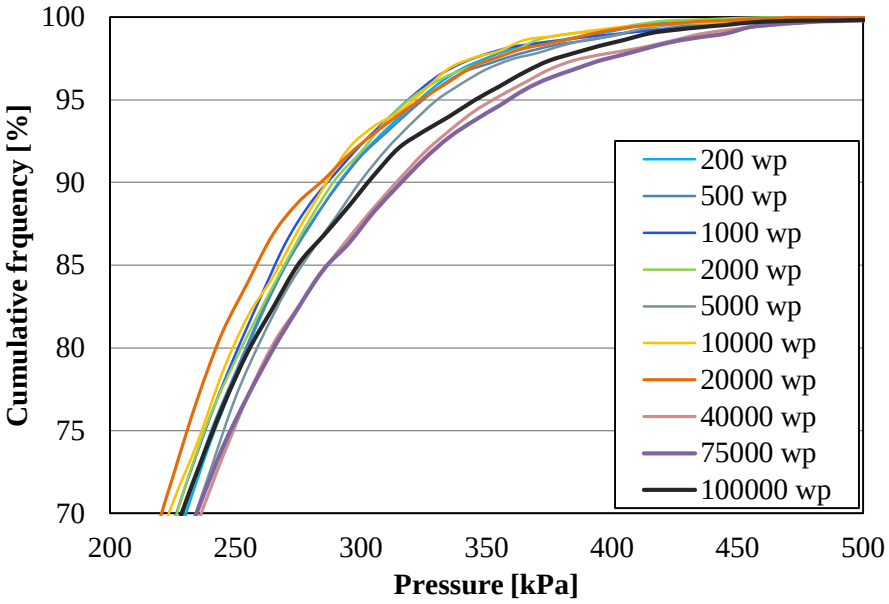

Figure 9.42: Magnification of the high-pressure area for 8 mm 1.20 SMA specimens

Chapter 10

Discussion

10.1 Introduction

This thesis deals with the characterization of texture and skid resistance of rubberized Stone Mastic Asphalts mixtures. These fundamental properties of surface courses were assessed both in situ and in laboratory, as seen in previous sections. In particular, the image analysis and the measurement of contact pressures belong to an innovative framework, which is next to flank, if not replace, the classic measurements so far employed.
Accordingly, this Chapter aims to discuss the results obtained, looking for comparison between parameters and giving interpretations to them.

10.2 Texture evolution

The texture change of the experimental laying during the first year of service has been shown in Chapter 5 in terms of MTD, MPD and ETD. Results underline a substantial uniformity of the parameters between the three materials, bringing to the conclusion that the rubber did not influence the texture. As expected, a uniform reduction in the profile depth took place during the pavement service.

The laboratory investigation allowed measuring the texture over a greater simulated in-service period. The texture evolution was examined under different point of views, as shown in Chapter 8. In order to give an overview on these aspects, results are summarized here in terms of skewness *Ssk* and kurtosis *Sku*.

The skewness represents the degree of symmetry of the surface heights about the mean plane. It is derived from the amplitude distribution curve and represents the degree of bias, either in the upward or downward direction. Since it is normalised by *Sq*, it is unit-less and can assume positive values, indicating the predominance of peaks, or negative values, indicating valley structures comprising the surface. However, this parameter cannot distinguish if profile spikes are evenly distributed above or below the mean line and it is

strongly influenced by any isolated peaks or valleys (Leach, 2010). A graphical explanation is shown in Figure 10.1.

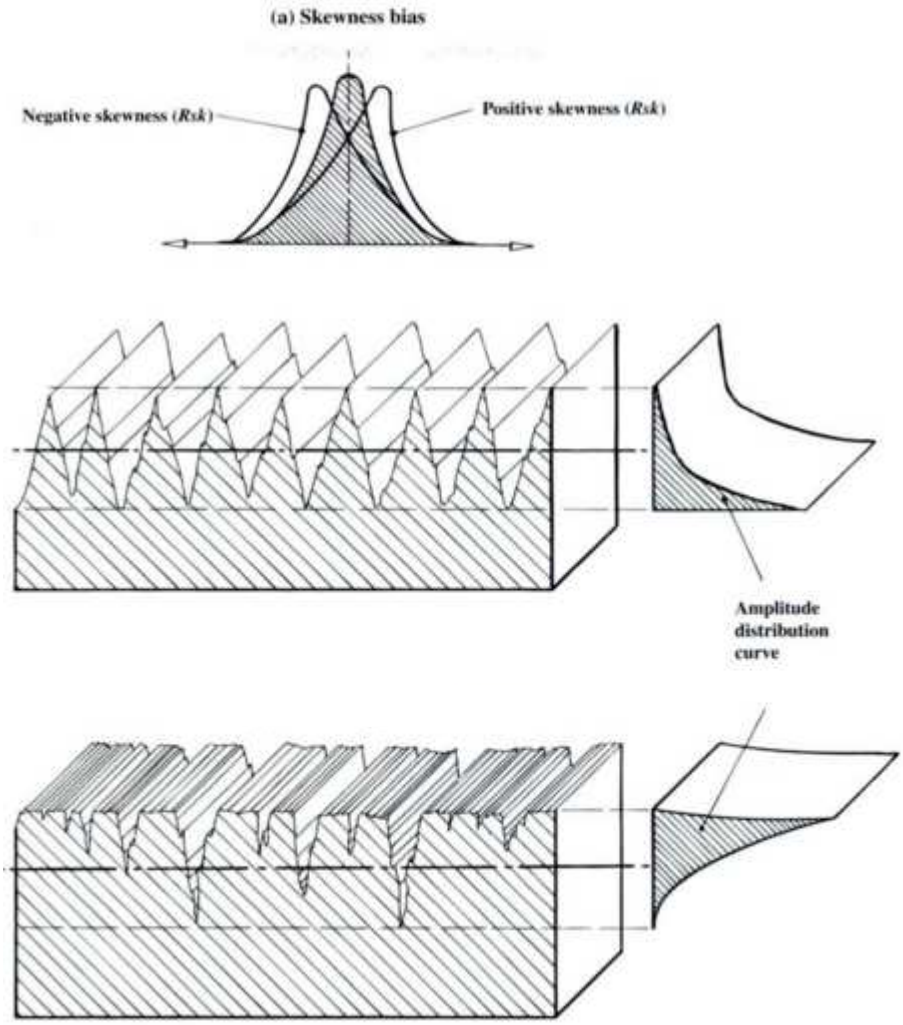

Figure 10.1: Skewness of a surface (Smith, 2002)

Unlike the skewness, the kurtosis *Sku* can detect if the profile peaks are distributed in an even manner across the sampling length trace, as well as providing information on the spikiness of the area. The presence of inordinately high peaks or deep valleys results in high kurtosis, Sku>3.00, while a bumpy surface topography exhbits a small kurtosis, Sku<3.00.

A surface with a Gaussian height distribution has a skewness of zero and a kurtosis of three. Surfaces described as gradually varying, free of extreme peaks or valley features, will tend to have Sku <3.00. Ssk is useful in specifying honed surfaces and monitoring for different types of wear conditions. Sku is useful for indicating the presence of either

peak or valley defects which may occur on a surface (Michigan metrology®). Different textures, having opposite Ssk and Sku values are shown in Figures 10.2 and 10.3.

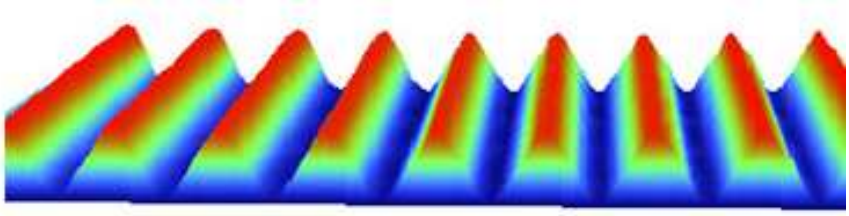

Figure 10.2: Example of a periodic texture, with *Ssk* value 0.16, *Sku* value 1.63 (Michigan metrology®)

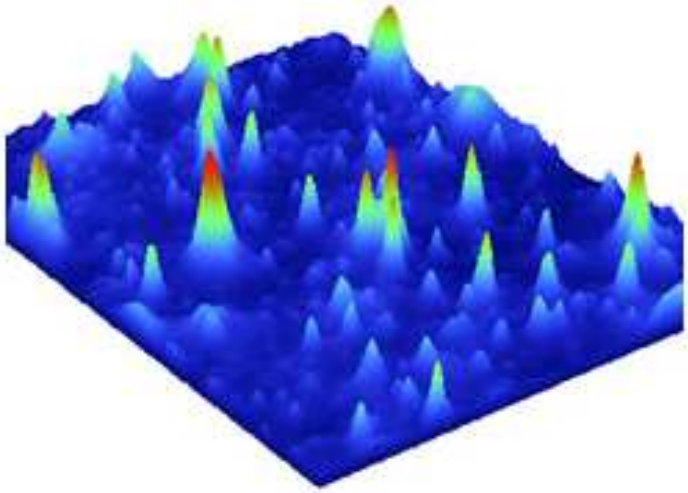

Figure 10.3: Example of a spiky texture, with *Ssk* value 3.20, *Sku* value 18.71 (Michigan metrology®)

The texture evolution is explained by considering three different stages of the slab lifetime:

- the early life, equivalent to approximately the first 5000 ÷ 10000 wheel passes of simulated trafficking;
- the mid-life, under which the slabs undergo 10000 to 75000 wheel passes;
- the end of life, which is reached after 75000 wheel passes and/or especially after the immersion wheel track test.

10.2.1 Early life evolution

Figures 10.4 and 10.5 show the skewness and the kurtosis trend respectively, over the first ten thousands wheel passes of simulated trafficking. Results exhibit an initial fluctuation,

i.e. the skewness drop from “-1.0” to “-1.5” and then rise again, until it reaches an equilibrium, while the opposite was found for the kurtosis, with values in the range 4 ÷ 6.

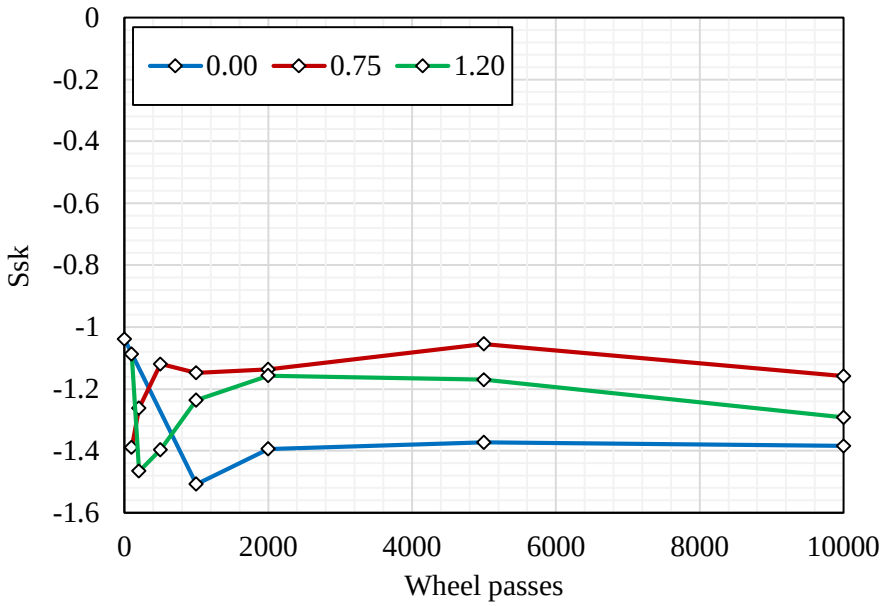

Figure 10.4: Skewness versus wheel passes, early life

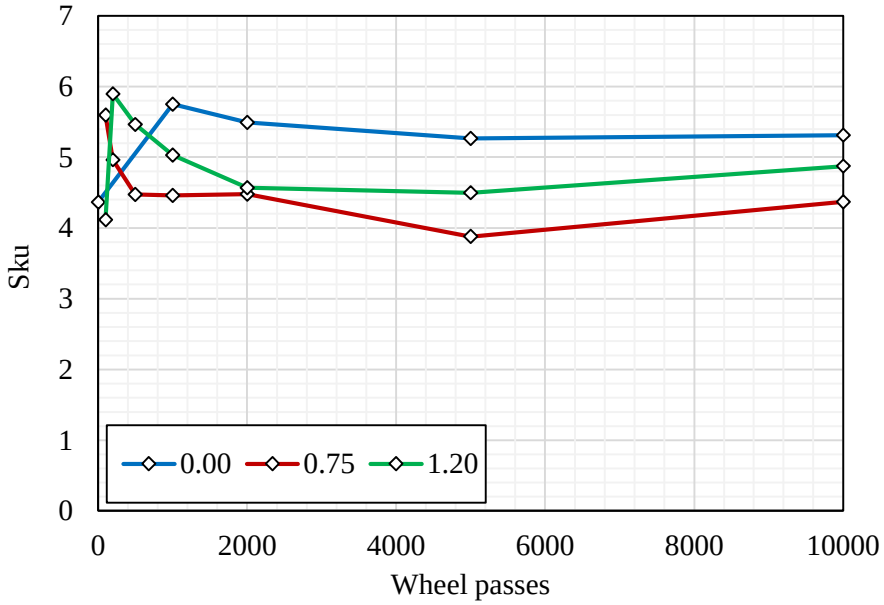

Figure 10.5: Kurtosis versus wheel passes, early life

During this early stage the increasing of the absolute value of the skewness and the decreasing of kurtosis is related to the stripping of the bitumen mortar, which lead to less material to be recorded above the mean plane and to the re-orientation of the particles under the loads as the slab keep compacting. Indeed, Figure 7.12 shows that the stripping of the bitumen mortar from the top of the surface take place in a greater extent during the

early life. In order to show this, the picture of the SMA 0.75 slab after 100 and 5000 wheel passes are shown in Figure 10.6.

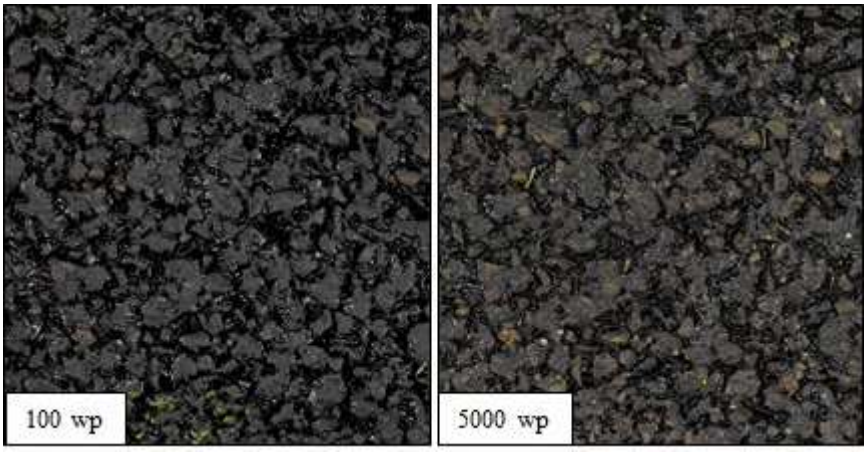

Figure 10.6: Pictures of the 0.75 SMA surface after 100 and 5000 wheel passes

This could also be the explanation of the diminishing of the contact area during the early life, as shown in Figure 10.7. As a matter of fact, as the bitumen is worn away, the tyre relies on a lesser area of contact.

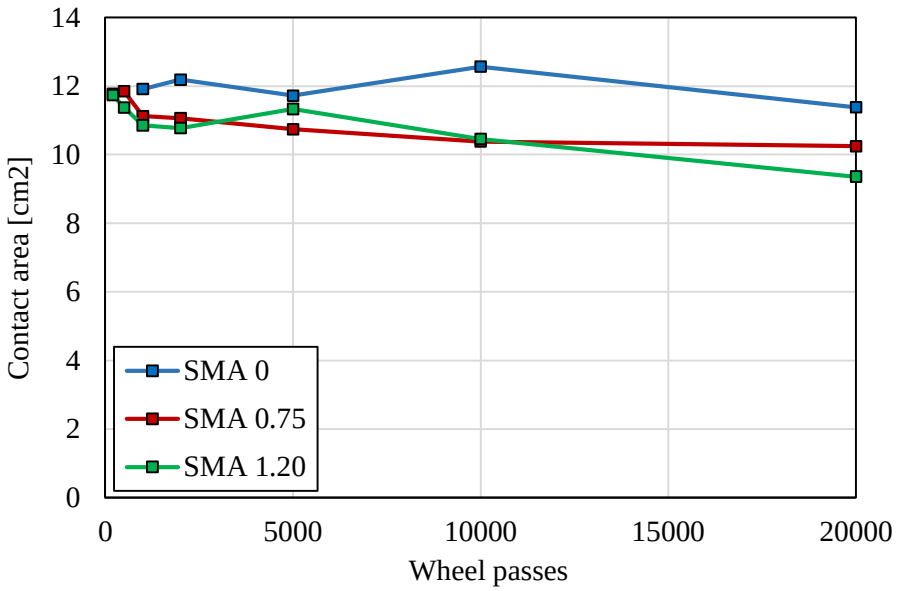

Figure 10.7: Contact area versus wheel passes

As for the pressures beneath the tyre, Chapter 9 highlighted that they evolve very slowly. In particular, Figure 9.34 showed that pressures during the early stage stand within a bundle, which is uniform without any peaks.

Indeed, Figure 8.22 showed a reduction of the recorded Volume of peak material in the early life.

Figure 10.8 explains the initial peak of the kurtosis for the SMA 1.20. A subsidence occurred at 500 wheel passes, making the remained texture peaks more isolated.

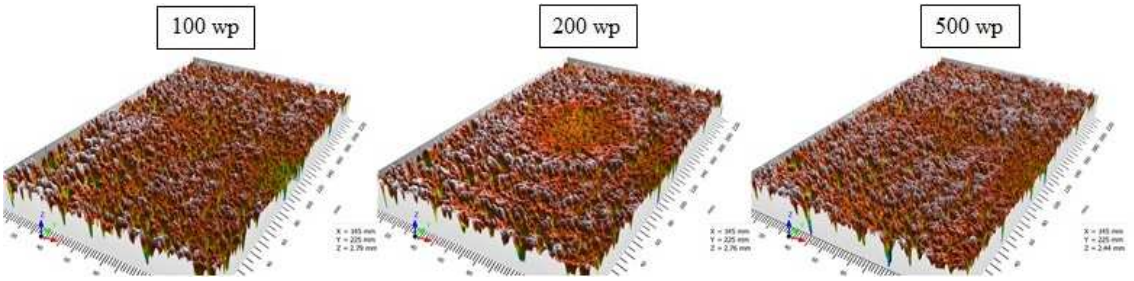

Figure 10.8: Early life 3D models of SMA 1.20 slab

10.2.2 Mid-life

During the mid-life most of the investigated parameters appear to have reached an equilibrium, while others still evolve.

Skewness and kurtosis evolution during trafficking are shown in Figure 10.9 and 10.10.

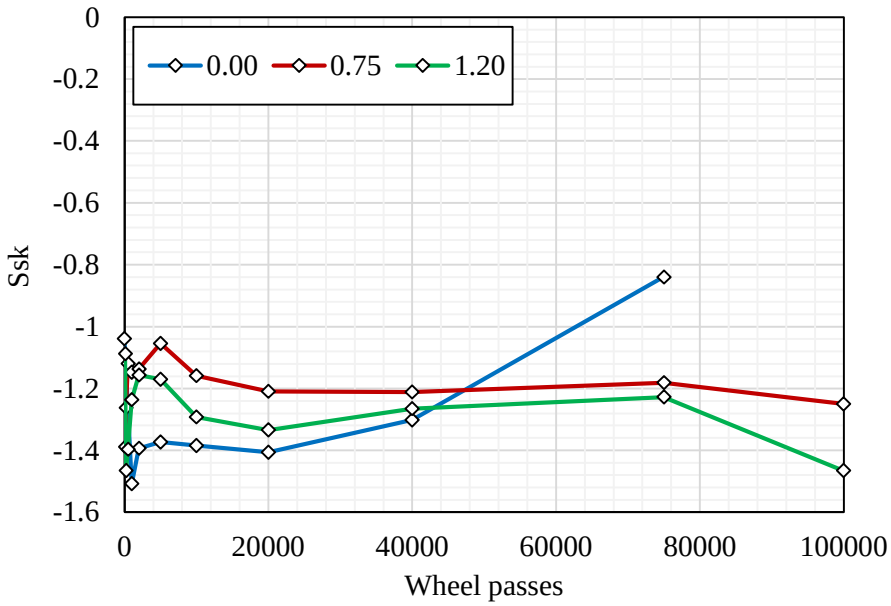

Figure 10.9: Skewness versus wheel passes

Both remain almost constant, with the first exhibiting a small increase with the wheel passes. This mean that the distribution of the bulk of the material does not change with reference to the mean plane and the surfaces keep their negative texture.

The SMA 0 value corresponding to 75000 wheel passes could be an outlier.

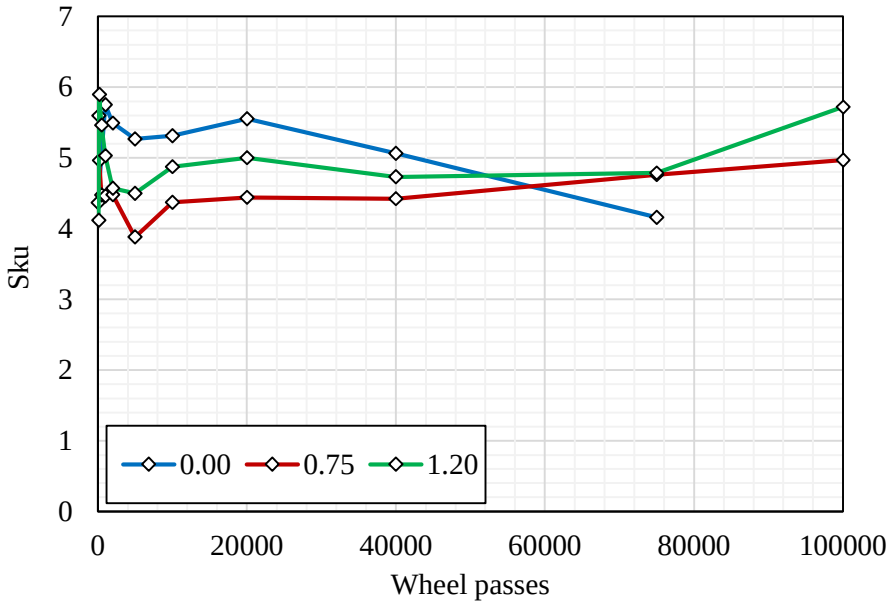

Figure 10.10: Kurtosis versus wheel passes

The contact area continues to evolve during the lifetime with a consistent trend between the three surfaces, as shown in Figure 10.11. The interaction decrease continuously, reaching a minimum at 20000 wheel passes, after which a peak in the contact area was observed.

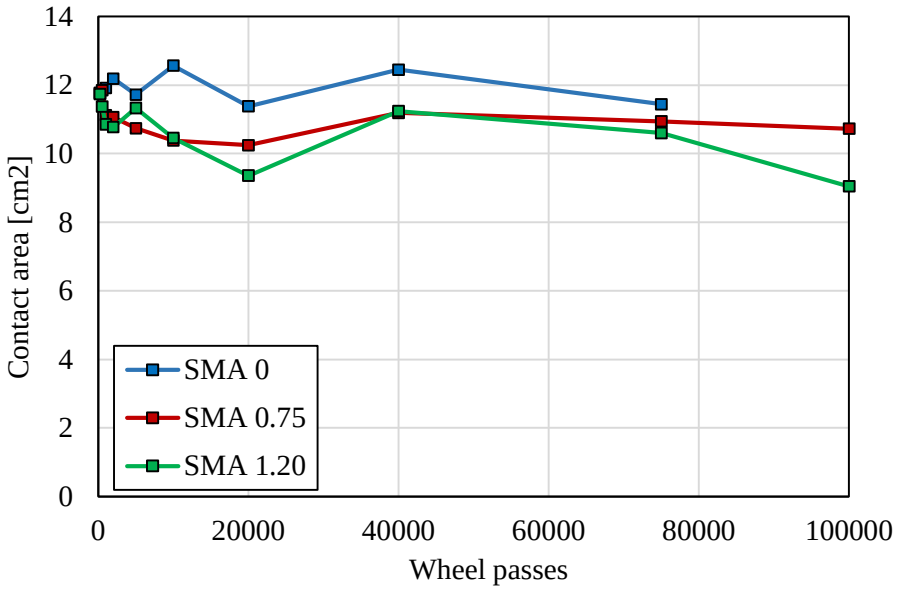

Figure 10.11: Contact area versus wheel passes

While the decrease is linked to the wearing of material on the top of the surface, the peak, which is common to the three mixtures, may be associated to a particular polishing state, which flatten the surface, and less likely to a particle re-orientation.

As for the pressures beneath the tyre, a change take place after 10000 wheel passes. As seen in Chapter 9, after the early stage the pressure exhibit a decrease in the range 10000 ÷ 20000 wheel passes again, before raising again and showing peaks of high pressures towards the end of life. This reduction corresponds to the drop of the contact area.

Figure 8.23 highlighted an increase of the volume of peak material during time, while Figure 8.24 showed that the Volume of material core reached an equilibrium only after 40000 wheel passes.

This part of the life is characterized by a continuous polishing of the surface. As the volume of peak is related to the areal material bearing ratio, this means the plane that intersects the 5% of area moved down increasing the recorded volume, as it would have been disjointed with the polishing of material.

The maximum stripping of the surface is reached after approximately 75000 wheel passes of simulated trafficking, as shown in Figure 10.12

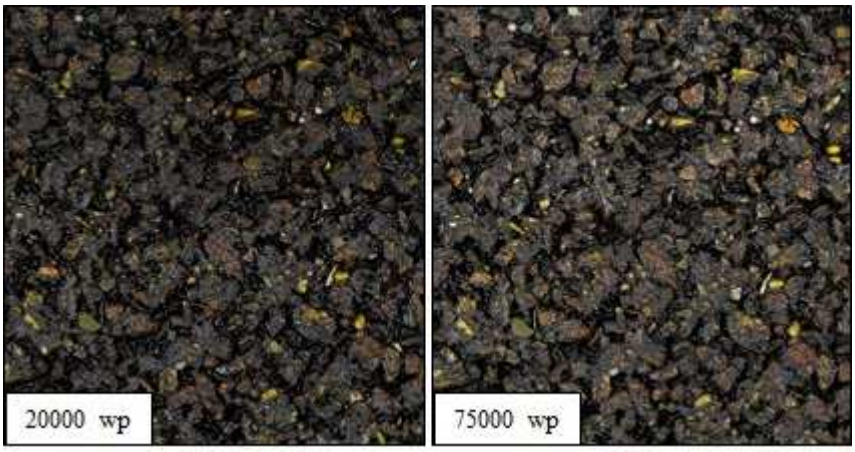

Figure 10.12: Picture of the 0.75 SMA slab after 20000 and 75000 wheel passes

A good correlation was found between MTD and the contact area, as shown in Figure 10.13. Although there would not be a reason why a change in one of them would influence the other, this relationship is proposed as these parameters evolve similarly under the simulated trafficking. In fact, while the macrotexture is reduced as a consequence of the

compaction of the surface, the contact area is reduced as the bitumen removal and the polishing of the surface take place.

The relationship is especially true during the early life, when these parameters behave very similarly.

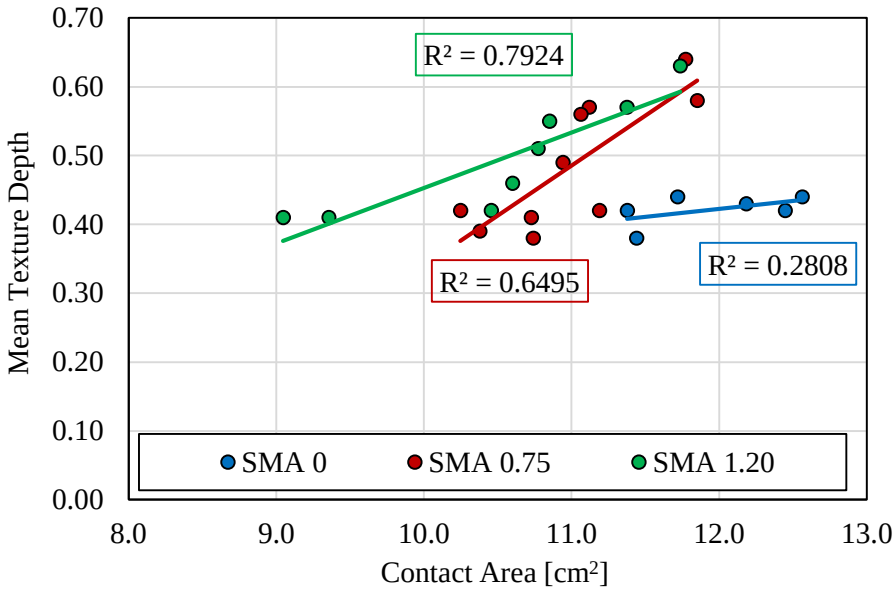

Figure 10.13: MTD versus Contact area

10.2.3 End of life – distress

The simulated trafficking with the RTM was stopped at 100000 wheel passes. According to Nicholls (1997) at this stage the surface of the test specimen reaches a condition known as equilibrium, which is approximately equivalent to 5 to 8 years of actual trafficking. However, the plots in the previous paragraphs highlighted that, at the end of the RTM test, the texture is still changing. In particular, Figure 10.9 shows the skewness to diminish, while Figure 10.10 shows the kurtosis to increase, which is an indication of the presence of new inordinately peaks. This can be confirmed by the continuous decrease of the contact area, which indicates that the interaction relies even more on the few spikes.

In order to accelerate the decay and investigate the texture change of a distressed pavement, the SMA 0.75 slab was subjected to the immersion wheel track test. As shown in Chapter 8, the most notable effect of the IWT is a sudden change in the parameter under investigation. Figure 10.14 shows the skewness and the kurtosis of a the SMA 0.75 slab during RTM and IWT. The skewness raises considerably towards the zero value, while

the kurtosis approaches the value of three, which is the case of a periodic texture. Conversely, the real surface is far away from having a periodic texture.

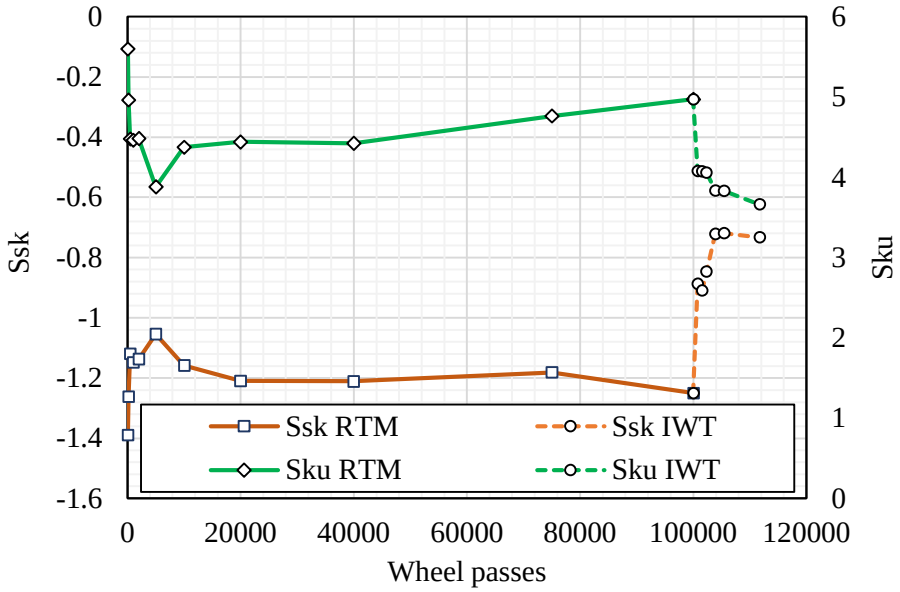

Figure 10.14: Skewness and kurtosis for the SMA 0.75

Figure 10.15 shows the 3D model of the SMA 0.75 slab at the end of the IWT test. The ruts induced by the dragging action across the surface are clearly visible. The original texture is maintained on the side of the slab. Although not regular, the surface at this stage has lost its original negative texture.

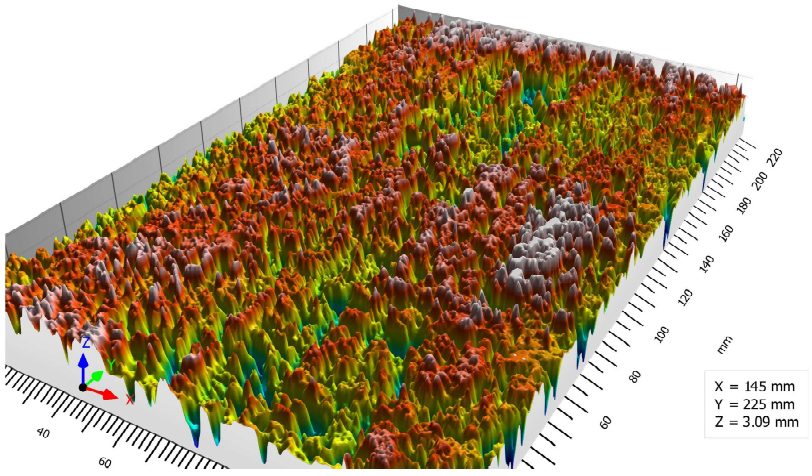

Figure 10.15: 3D model of the SMA 0.75 after 225 minutes of IWT

As for the tyre - surface interaction, the measurements made on the SMA 0.75 slab are shown in Figure 10.16 and 10.17 in terms of frequency and cumulative distribution respectively. A significant change was found between the 20000 and the 40000 wheel

passes. The contact pressure increased, exhibiting more values of high pressure, which could be linked to some stones that rose up as a consequence of the shear action of the tyres.

However, a more prominent change took place at the end of the IWT. Not only the values having high pressure are more likely, but the peak pressures are also higher compared to the case of the RTM. The average contact area of the strip, which is not indicated in the plots, is in line with the other measurements and equal to 11.30 cm^2.

Figure 10.18 shows the pressure map belonging to the SMA 0.75 slab at the end of the simulated trafficking with RTM and at the end of IWT test. The maps, plotted with the same pressure legend, underline the differences of the magnitude of pressures. Figure 10.19, which plots the map after IWT with a greater legend, makes it clear that the contact occurs at the side of the ruts, on which alignment are positioned the hot spots.

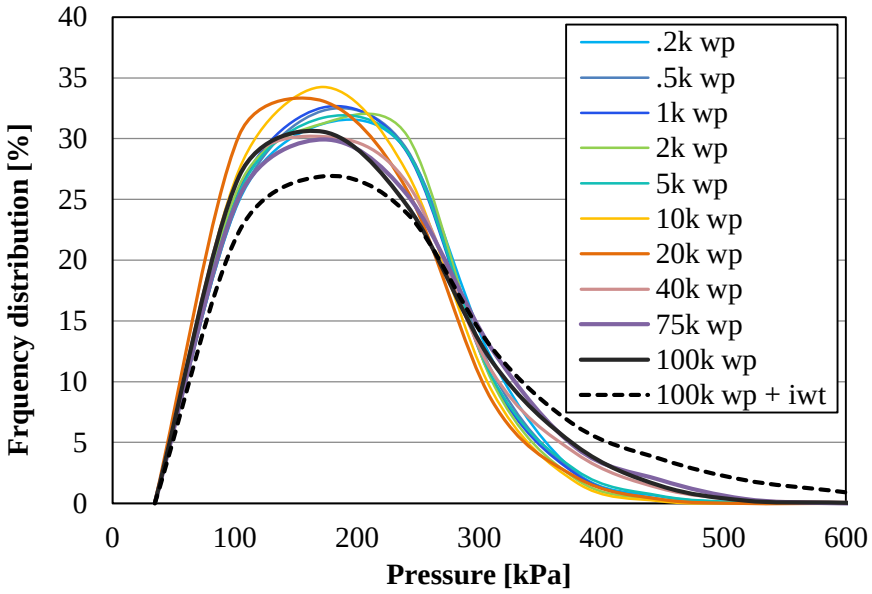

Figure 10.16: Frequency distribution of the tyre pavement interaction pressure for the SMA 0.75

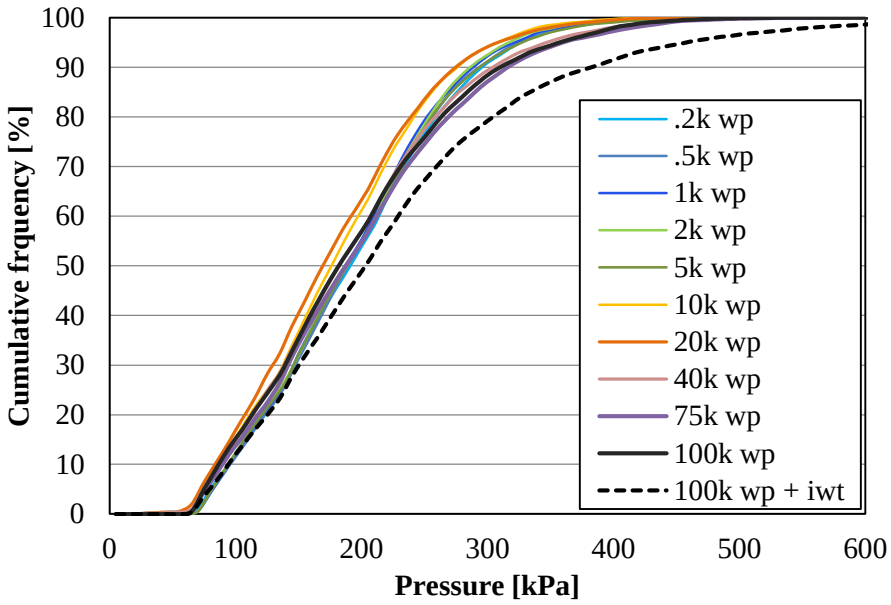

Figure 10.17: Cumulative frequency of the tyre pavement interaction pressure for the SMA 0.75

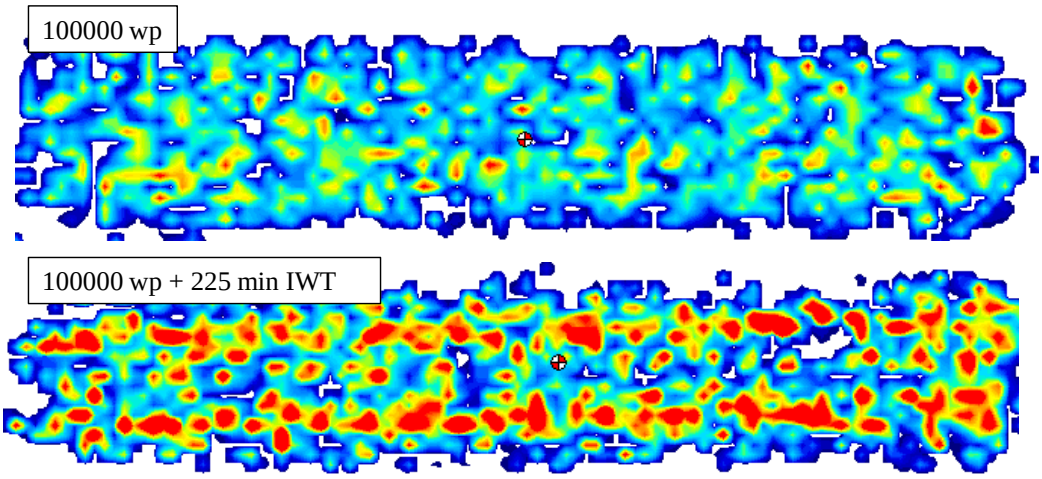

Figure 10.18: Pressure map of the SMA 0.75 slab at the end of RTM and IWT test (pressure legend: 68.95 ÷ 399.9 kPa)

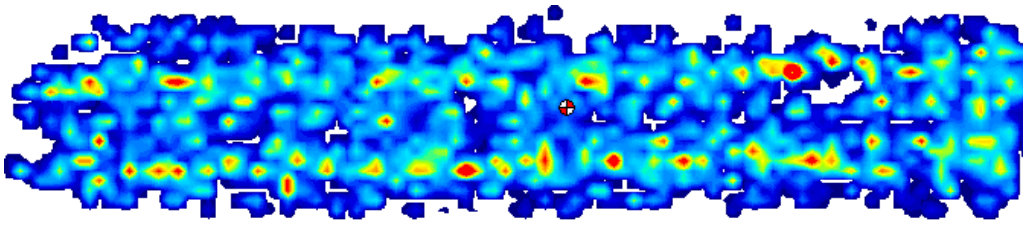

Figure 10.19: Pressure map of the SMA 0.75 slab at the end of IWT test (pressure legend: 68.95 ÷ 703.26 kPa)

Although no direct correlations were found so far, all the parameters presented can be adopted for the prediction of the texture evolution of an asphalt surfaces.

Conclusions

This thesis proposes the use of new technologies for the analysis of surface characteristics of rubberized stone mastic asphalts. Accordingly, two important themes are dealt, i.e. the sustainability and the use of new technologies.

As for the employ of the crumb rubber into road mixtures, results confirmed that this solution is suitable for surface course as it is not detrimental for the skid resistance and it does not imply changes in the macrotexture. This was confirmed both in situ and in laboratory. Moreover the rubber allows for a reduction of the tyre rolling noise levels, especially in the early life of the pavements.

Although in-service performances are not affected, particular attention must be paid during the manufacturing and laying phases. However, as shown in this thesis, by containing the temperatures the environmental and workers exposures to fumes are reduced.

As for the new technologies, the in-situ measurements confirmed that dynamic measurements represent extraordinary tools for the survey of surface properties of pavements, while classic outdated solutions like the volumetric patch technique and skid tester could be left apart in the near future.

However, the in-situ measurements say little about the development of the parameters during the in-service life.

For this reason, when studying new mixes for medium-large scale production, the prediction of textural properties is fundamental, in order to optimize the mix design and/or planning proper maintenance, for time saving and economizing the investment and, above everything, maximize the safety of users.

The work at the base of this thesis combined the use of two different simulated trafficking machines, i.e. the TRL Road Test Machine and an old version of an Immersion Wheel Track. What makes the research innovative is the use of the image analysis and of the Close Range Photogrammetry for the assessment of the texture changes of the asphalt

samples. These techniques showed potential for being permanently included in advanced analysis of pavements performances, offering great and new insights for the studies.

Moreover, a very interesting phenomena that is proposed for the analysis is the investigation of the tyre/surface interactions. Indeed, pressures and areas of contact are strictly linked to texture and skid resistance. Once a mixture has been characterized in laboratory, the measurement of these factors on a similar surface laid on site, would allow to understand the level of distress of the pavement and, based on the traffic, to predict how the surface will behave in the next future.

Some recommendations can be made for future works.

The way the texture change over time is strictly dependent from the manufacturing process. Even if the mixtures is sampled during the laying, as in the case of this work, the compaction method should be as close as possible to that adopted on site. Non-properly compacted asphalt mixtures could behave differently compared to well compacted samples, and accordingly not reflecting the reality, especially in the early life.

Although it is quite impossible, new research is needed in order to improve the capability of reproducing the same site conditions in laboratory. As the behaviour of asphalt mixtures is temperature dependent, a simulated trafficking machine should consider this factor.

While the proposed parameters are capable for predicting the behaviour of a pavement during its lifetime, new efforts need to be addressed to find correlations among parameters. As many of them were found to be fluctuating, especially in the early life, a strong attention to details and separate treatments for the different life stages could help.

References

3DFLOW. ZEPHYR®. http://www.3dflow.net/3df-zephyr-pro-3d-models-from-photos/

AASHTO TP 76-15 (2015). *Standard method of test for measurement of tire/pavement noise using the on-board sound intensity (OBSI) method*. Standard by American Association of State and Highway Transportation Officials

Abreu, L.P.F., Oliveira, J.R.M., Silva, H.M.R.D., Fonseca, P.V. (2015). *Recycled asphalt mixtures produced with high percentage of different waste materials.* Construction and Building Materials, Volume 84, 1 June 2015, Pages 230-238

Ahammed, M.A., Tighe, S. L. (2012). *Asphalt pavements surface texture and skid resistance - exploring the reality*. Canadian Journal of Civil Engineering 39(1): 1-9, 10.1139/l11-109

ANAS S.p.A. (2010). *Capitolato speciale d'appalto. Norme tecniche.*

ASTM E274 / E274M-15. *Standard Test Method for Skid Resistance of Paved Surfaces Using a Full-Scale Tire.*

ASTM E1337 – 90 (2012). *Standard test method for determining longitudinal peak braking coefficient of paved surfaces using standard reference test tire*

ASTM E2157 – 09. Standard Test Method for Measuring Pavement Macrotexture Properties Using the Circular Track Meter

Autostrada del Brennero S.p.A. *Capitolato speciale d'appalto*

Bitelli, G., Simone, A., Girardi, F., Lantieri, C., (2012). *Laser Scanning on Road Pavements: A New Approach for Characterizing Surface Texture*. Sensors. Volume 12, Issue 7. Pages 9110-9128

BS 7941-2:2000. Methods for measuring the skid resistance of pavement surfaces. *Test method for measurement of surface skid resistance using the GripTester braked wheel fixed slip device*

Buncher, M.S., (1995). *Evaluating the effects of the wet and dry processes for including crumb rubber modifier in hot mix asphalt*. PhD thesis. National Center for Asphalt Technology. Auburn University, Alabama, U.S.A.

Bullas, J.C. (2006). – *Bituplaning: a low dry friction phenomenon of new bituminous road surfaces.* PhD Thesis. University of Southampton

Cafiso, S., Di Graziano, A., Battiato, S. (2006). *Evaluation of pavement surface distress using digital image collection and analysis*. International congress on advances in Civil Engineering, October 11-13, Yildiz Technical University, Istanbul, Turkey.

Concessioni autostradali Venete. *Capitolato speciale d'appalto. Norme tecniche*

Concise International Chemical Assessment Document 59 (2004). World Health Organization

CNR B.U. - 105/85. Norme per la misura delle caratteristiche superficiali delle pavimentazioni. *Metodo di prova per la misura della resistenza di attrito radente con l'apparecchio portatile a pendolo.*

CNR B.U. - 147/92. Norme per la misura delle caratteristiche superficiali delle pavimentazioni. *Metodo di prova per la misura del coefficiente di aderenza con l'apparecchio S.C.R.I.M.*

Digital Surf. *MountainsMap® 7*. http://www.digitalsurf.com/en/index.html

Dondi, G., Mazzotta, F., Sangiorgi, C., Pettinari, M., Simone, A., Vignali, V., Tataranni, P. (2014). *Influence of cement and limestone filler on the rheological properties of mastic in cold bituminous recycled mixtures*. Proceeding of 3rd International Conference on Transportation Infrastructures – ICTI 2014, April 22–25, Pisa, Italy, 2014

Dunford, A. (2011). *Measuring skid resistance without contact.* TRL report. ISBN: 978-1-84608-911-4

EN 1097-6. Tests for mechanical and physical properties of aggregates. Determination of particle density and water absorption

EN 1097-8. Tests for mechanical and physical properties of aggregates - Part 8: *Determination of the polished stone value*

EN 12697-5. Bituminous mixtures - Test methods for hot mix asphalt - Part 5: *Determination of the maximum density*

EN 12697-11. Bituminous mixtures - Test Methods for hot mix Asphalt - Part 11: *Determination of the affinity between aggregate and bitumen*

EN 12697-12. Bituminous Mixtures - Test Methods For Hot Mix Asphalt - Part 12: *Determination of the water sensitivity of bituminous specimens*

EN 12697-17. Bituminous mixtures. Test methods for hot mix asphalt. *Particle loss of porous asphalt specimen*

EN 12697-23. Bituminous mixtures. Test methods for hot mix asphalt. *Determination of the indirect tensile strength of bituminous specimens*

EN 12697-26. Bituminous mixtures — Test methods for hot mix asphalt. *Stiffness*

EN 12697-31. Bituminous mixtures. Test methods for hot mix asphalt. *Specimen preparation by gyratory compactor*

EN 12697-34.Bituminous mixtures. Test methods for hot mix asphalt. *Marshall test*

EN 12697-49:2014. Bituminous mixtures. Test methods for hot mix asphalt. Determination of friction after polishing

EN 13036-1. Road and airfield surface characteristics - Test methods - Part 1*: Measurement of pavement surface macrotexture depth using a volumetric patch technique*

EN 13036-3. Road and airfield surface characteristics - Test methods - Part 3*: Measurement of pavement surface horizontal drainability*

EN 13036-4. Road and airfield surface characteristics - Test methods - Part 4*: Method for measurement of slip/skid resistance of a surface: The pendulum test*

Ferreira, T., Rasband, W. (2012). *ImageJ User Guide, IJ 1.46r revised edition.* https://imagej.nih.gov/ij/docs/guide/user-guide.pdf

Findlay Irvine GripTester. http://www.findlayirvine.com/

Flintsch, G., de León, E., McGhee, K., AI-Qadi, I. (2003). *Pavement Surface Macrotexture Measurement and Applications.* Transportation research board 1860(1):168-177

Fornai, D., Persici, V., Lupi, C. (2015). *Occupational health risk assessment for the workers exposed to rubberized asphalt fumes; a comparative study based on monitoring campaigns.*

Friel, S. (2013).Variation of the friction characteristics of road surfacing materials with time. PhD thesis. University of Ulster, U.K.

Gómez-Meijide, B., Pérez, I., Airey, G., Thom, N. (2015). *Stiffness of cold asphalt mixtures with recycled aggregates from construction and demolition waste*. Construction and Building Materials, Volume 77, 15 February 2015, Pages 168-178

Greenwood engineering. https://www.greenwood.dk/laserprof.php

Hasan, M.R.M., Colbert, B., You, Z., Jamshidi, A., Heiden, P.A., Hamzah, M.O. (2016). *A simple treatment of electronic-waste plastics to produce asphalt binder additives with improved properties*. Construction and Building Materials, Volume 110, 1 May 2016, Pages 79-88

Henry. J.J. (2000). *Evaluation of Pavement Friction Characteristics*. NCHRP synthesis 291. Transportation Research Board

Highways England. *Design Manual for Roads and Bridges*. (2006). https://www.gov.uk/guidance/standards-for-highways-online-resources

Ibraheem N.A., Hasan, M.M., Khan, R.Z., Mishra, P.K. (2012). *Understanding Color Models: A Re-view*. ARPN Journal of Science and Technology Volume 2, Issue 3. Pages 265-275

ISO 25178-2:2012. Geometrical product specifications (GPS) -- Surface texture: Areal - Part *2: Terms, definitions and surface texture parameters*

ISO 13473-1:1997. Characterization of pavement texture by use of surface profiles - Part 1: *Determination of Mean Profile Depth*

ISO 13473-2:2002. Characterization of pavement texture by use of surface profiles - Part 2: *Terminology and basic requirements related to pavement texture profile analysis*

ISO 13473-3:2002. Characterization of pavement texture by use of surface profiles -- Part 3: *Specification and classification of profilometers*

ISO 13473-5:2009. Characterization of pavement texture by use of surface profiles -- Part 5: *Determination of megatexture*

ISO 11819-1:1997. Acoustics - *Measurement of the influence of road surfaces on traffic noise - Part 1: Statistical Pass-By method*

ISO/DIS 11819-2. Acoustics - *Measurement of the influence of road surfaces on traffic noise - Part 2: The close-proximity method*

Kane, M., Artamendi, I., Scarpas, T. (2013). *Long-term skid resistance of asphalt surfacings: correlation between Wehner–Schulze friction values and the mineralogical composition of the aggregates.* Wear, Volume 303, Issues 1–2. Pages 235-243

Kane, M., Zhao, D., Do, M.T., Chailleux, E., de Larrard, F. (2010). *Exploring the ageing effect of binder on skid resistance evolution of asphalt pavement*. Road Mater. Pavement Des.11, pages 543–557.

Kim, K.-H., Jahan, S.A., Kabir, E., Brown, R.J.C. (2013). A review of airborne polycyclic aromatic hydrocarbons (PAHs) and their human health effects. Environment International. Volume 60. Pages 71-80.

Kuosmanen, A., Pellinen, T., Hartikainen, L., Petry, F., Westermann, S. (2014). *Durable laboratory rubber friction test countersurfaces that replicate the roughness of asphalt pavements*. Wear. Volume 321. Pages 38-45

Kuttesch, J.S. (2004). *Quantifying the Relationship between Skid Resistance and Wet Weather Accidents for Virginia Data.* Master of Science Thesis. Virginia Polytechnic Institute and State University

Lamperti, R., Lantieri, C., Sangiorgi, C., Bitelli, G., Simone, A. (2015). *Semi-automatic evaluation of the degree of bitumen coverage on bitumen-coated aggregates.* RILEM Bookseries, 8th RILEM International symposium on testing and characterization of sustainable and innovative bituminous materials. Pages 15 - 24

Lantieri, C., Lamperti, R., Simone, A., Vignali, V., Sangiorgi, C. Dondi, G. (2015). *Mobile laser scanning system for assessment of the rainwater runoff and drainage conditions on road pavements.* International Journal of Pavement Research and Technology. Volume: 8, Number: 1. Pages 1-9

Leach, R.K. (2010). Fundamental Principles of Engineering Nanometrology. ISBN: 978-0-08-096454-6 2010

Leandri, P., Losa, M. (2015). *Peak Friction Prediction Model Based on Surface Texture Characteristics.* Transportation Research Board, Volume 2525. Pages 91–99

LEOPOLDO. Tuscany Region LEOPOLDO project. Preparation of guidelines for the design and the monitoring of road paving for ordinary roads. http://leopoldo.pjxp.com (last accessed 31 March 2016)

Li, L., Wang, K.C.P., Li, Q. (2016). *Geometric texture indicators for safety on AC pavements with 1 mm 3D laser texture data.* International Journal of Pavement Research and Technology. Volume 9, Issue 1, Pages 49-62

Liao, G., Sakhaeifar, M.S., Heitzman, M., West, R., Waller, B., Wang, S., Ding, Y. (2014). *The effects of pavement surface characteristics on tire/pavement noise.* Applied Acoustics. Volume 76. Pages 14-23

Licitra, G., Cerchiai, M., Teti, L., Ascari, E., Fredianelli, L. (2015). *Durability and variability of the acoustical performance of rubberized road surfaces*. Applied Acoustics. Volume 94. Pages 20-28

Licitra, G., Teti, L., Cerchiai, M. (2014). A modified Close Proximity method to evaluate the time trends of road pavements acoustical performances. Applied Acoustics. Volume 76. Pages 169-179

Losa, M., Leandri, P., (2011). *The reliability of tests and data processing procedures for pavement macrotexture evaluation.* International Journal of Pavement Engineering Vol. 12, No. 1, Pages 59–73

Losa, M., Leandri, P., Cerchiai, M. (2012). *Improvement of Pavement Sustainability by the Use of Crumb Rubber Modified Asphalt Concrete for Wearing Courses*. International Journal of Pavement Research and Technology. Volume 5. Issue 6. Pages 395-404

MB Fibreglass. VINAMOLD®. www.mbfg.co.uk

McQuaid (2015). *Development of non-contact 3D measurement of areal pavement texture parameters.* PhD Thesis, School of Built Environment, University of Ulster, U.K.

McQuaid, G., Millar, P., Woodward, D. (2014). *A Comparison of Techniques to Determine Surface Texture Data* – Civil engineering research in Ireland. Queen's University Belfast. 28-29 August 2014.

Michigan Metrology, LLC. http://www.michmet.com/

Millar, P., Woodward, D., Friel, S., Woodside, A. (2011). *An Investigation of the Variation of Contact Area with Inflation Pressure.* International conference bituminous mixtures and pavements. Thessaloniki, Greece.

Millar, P. (2013). *Non-Contact Evaluation of the Geometric Properties of Highway Surfacing Textures Using Close Range Photogrammetry*. PhD Thesis, School of Built Environment, University of Ulster, U.K.

Mitchell, R., Woodward, D., Maguire, C. (2014). *Development of an asphalt durability raveling test.* Sustainability, Eco-efficiency and Conservation in Transportation Infrastructure Asset Management. International Conference on Transportation Infrastructure ICTI 2014, Pisa, April 22-25, 2014.

Mitchell, R. (2014). *An investigation on the durability of warm mix asphalt*. PhD Thesis, School of Built Environment, University of Ulster, U.K.

Ministero delle Infrastrutture e dei Trasporti – CIRS (2001). *Norme tecniche di tipo prestazionale per capitolati speciali d'appalto*, Roma

Moghaddam, T.B., Karim, M.R., Syammaun, T. (2012). *Dynamic properties of stone mastic asphalt mixtures containing waste plastic bottles.* Construction and Building Materials, Volume 34, September 2012, Pages 236-242.

Moghaddam, T. B, Karim, M.R. (2012). *Properties of SMA mixtures containing waste polyethylene terephthalate.* World Academy of Science, Engineering and Technology, vol. 6. Pages 612–622

Mohd Hasan, M.R. Colbert, B., You, Z., Jamshidi, A., Heiden, P.A., Hamzah, M.O. (2016*). A simple treatment of electronic-waste plastics to produce asphalt binder additives with improved properties*. Construction and Building Materials, Volume 110. Pages 79-88

Moreno, F., Rubio, M.C., Martinez-Echevarria, M.J. (2012). *The mechanical performance of dry-process crumb rubber modified hot bituminous mixes: The influence of digestion time and crumb rubber percentage.* Construction and Building Materials. Volume 26, Issue 1. Pages 466-474

Morova, N., Serin, S., Terzi, S., Saltan, M., Kucukcapraz, D.O., Karahancer, S.S., Eriskin, E. (2016). *Utility of polyparaphenylene terephtalamide fiber in hot mix asphalt as a fiber*. Construction and Building Materials, Volume 107, 15 March 2016, Pages 87-94

Nicholls, J.C. (1997). TRL Report 176. *Laboratory tests on high friction surfaces for highways*

Paje, S.E., Luong, J., Vázquez, V.F., Bueno, M., Miró, R. (2013). *Road pavement rehabilitation using a binder with a high content of crumb rubber: Influence on noise reduction*. Construction and Building Materials. Volume 47. Pages 789-798

Pasandín, A.R., Pérez, I., Ramírez, A., Cano, M.M. (2016). *Moisture damage resistance of hot-mix asphalt made with paper industry wastes as filler.* Journal of Cleaner Production, Volume 112, Part 1. Pages 853-862

Pardillo Mayora, J.M., Piña, R.J., (2009*). An assessment of the skid resistance effect on traffic safety under wet-pavement conditions.* Accident Analysis & Prevention, Volume 41, Issue 4. Pages 881-886

Parvez, M.A., Al-Abdul Wahhab, H.I., Shawabkeh, R.A., Hussein, I.A. (2014). *Asphalt modification using acid treated waste oil fly ash*. Construction and Building Materials, Volume 70, 15 November 2014, Pages 201-209

Pasandín, A.R., Pérez, I., Ramírez, A., Cano, M.M. (2016). *Moisture damage resistance of hot-mix asphalt made with paper industry wastes as filler*. Journal of Cleaner Production, Volume 112, Part 1. Pages 853–862

Provincia autonoma di Bolzano (2016). *Direttive tecniche per pavimentazioni bituminose*

Sangiorgi, C., Bitelli, G., Lantieri, C., Irali, F., Girardi, F. (2012). *A study on texture and acoustic properties of cold laid microsurfacings.* SIIV - 5th International Congress - Sustainability of Road Infrastructures

Sangiorgi, C., Tataranni, P., Simone, A., Vignali, V., Lantieri, C., Dondi, G. (2016). *Assessment of waste bleaching clay as alternative filler for the production of porous asphalts*. Construction and Building Materials, Volume 109. Pages 1-7

Silván-Cárdenas, J.L., Wang, L. (2008). *Sub-pixel confusion–uncertainty matrix for assessing soft classifications*. Remote Sensing of Environment, Volume 112, Issue 3. Pages 1081-1095

Slimane, A.B., Khoudeir, M., Brochard, J., Do, M.-T. (2008). *Characterization of road microtexture by means of image analysis.* Wear, Volume 264, Issues 5–6. Pages 464-468

Skiddometer BV11. http://moventor.com/en/skiddometer-bv-11

Smith, G. (2012). Industrial Metrology: surfaces and roundness. Springer-Verlag London. DOI: 10.1007/978-1-4471-3814-3

Technical Committee 1 Surface Characteristics (1995). *International Experiment to Compare and Harmonize Skid Resistance and Texture Measurements.* PIARC publication sheet. Ref. 01.04.TEN

Tehrani, F.M. (2015). *Noise Abatement of Rubberized Hot Mix Asphalt: A Brief Review*. International Journal of Pavement Research and Technology. Volume 8, Issue 1. Pages 58-61

Toldo, R. (2013). *Towards automatic acquisition of high-level 3D models from images.* Ph.D. Thesis. Università degli Studi di Verona.

Ueckermann, A., Wang, D., Oeser, M., Steinauer, B. (2015). Calculation of skid resistance from texture measurements. Journal of Traffic and Transportation Engineering. Volume 2, Issue 1. Pages 3-16

Woodward, D., Millar, P., Friel, S., Waddell, C. (2013). *Measuring grip and the contact patch.* Airfield and Highway Pavement 2013, Los Angeles. American society of Civil Engineers. Pages 841-854

Woodward, D., Kennedy, K., Mitchell, R., Ryan, D., Millar, P. (2014). *Predicting the durability of warm mix asphalt.* Green technologies - Innovation to implementation and evaluation (B) Session of the 2014 Conference of the Transportation Association of Canada Montreal, Quebec.

Woodward, D., Millar, P., Lantieri, C., Sangiorgi, C., Vignali, V. (2016). *The wear of Stone Mastic Asphalt due to slow speed high stress simulated laboratory trafficking*. Construction and Building Materials, Volume 110. Pages 270-277

XSENSORS Technology Corporation. http://www.xsensor.com/

Yan, K., Xu, H., You, L. (2015). *Rheological properties of asphalts modified by waste tire rubber and reclaimed low density polyethylene*. Construction and Building Materials, Volume 83. Pages 143-149

Yaacob, H., Woodward, D., Woodside, A., Hainin, M., R. (2008). *Changes of surface dressing texture as related to time and chipping size.* Malaysian Journal of Civil Engineering, Volume 20 (1). Pages 1-11